11 De Mayerne

Binding medium, pigments and metal soaps
characterised and localised in paint cross-sections

Katrien Keune
2005

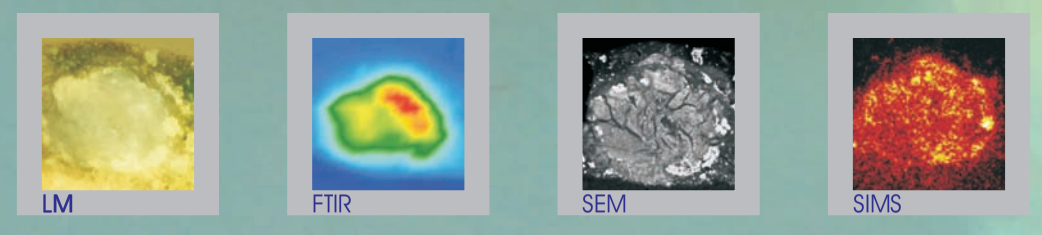

Binding medium, pigments and metal soaps characterised and localised in paint cross-sections

Katrien Keune
2005

Binding medium, pigments and metal soaps characterised and localised in paint cross-sections

Katrien Keune

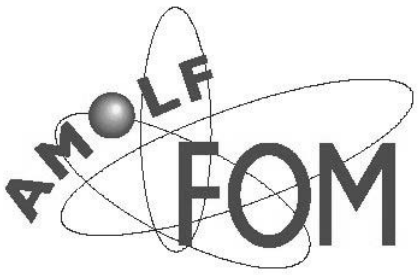

The work described in this thesis was performed at AMOLF (FOM Institute for Atomic and Molecular Physics), Kruislaan 407, 1098 SJ, Amsterdam, The Netherlands. The research at AMOLF is embedded in the FOM research program nr. 49 "Mass spectrometric imaging and structural analysis of biomacromolecules". It is part of the 'De Mayerne' programme funded by the Dutch Organisation for Scientific Research (NWO) and the Foundation for Fundamental Research on Matter (FOM), a subsidiary of the Dutch Organisation for Scientific Research (NWO).

© Katrien Keune

ISBN 90-77209-10-7

Cover: UV microscopic image of paint cross-section CIA 1577 RS06 taken from ‘The Sherborne Triptych’ (see p. 137-141).

Binding medium, pigments and metal soaps characterised and localised in paint cross-sections

ACADEMISCH PROEFSCHRIFT

ter verkrijging van de graad van doctor aan de Universiteit van Amsterdam op gezag van Rector Magnificus prof. dr. P.F. van der Heijden ten overstaan van een door het college voor promoties ingestelde commissie, in het openbaar te verdedigen in de Aula der Universiteit op woensdag 22 juni 2005, te 12.00 uur

door

Katrien Keune

geboren te Mijdrecht

Promotiecommissie

Promotor:	Prof. dr. J.J. Boon
Overige commissieleden:	Prof. Dr. A. Adriaens Prof. Dr. C.J. Elsevier Dr. C.L. Higgitt Prof. Dr. C.G. de Koster Prof. Dr. P.J. Schoenmakers Prof. Dr. J.W. Verhoeven

Faculteit der Natuurwetenschappen, Wiskunde en Informatica

MOLART Reports

This report is the eleventh in the series of MOLART reports. The MOLART reports summarise research results obtained in the course of the MOLART and De Mayerne Research Programmes supported by NWO (Dutch Organisaition for Scientific Research). Information about the MOLART reports can be obtained from Prof. Dr. J.J. Boon, FOM-Institute for Atomic and Molecular Physics, Kruislaan 407, 1098 SJ Amsterdam, The Netherlands, boon@amolf.nl.

1. Molecular studies of fresh and aged triterpenoid varnishes, Gisela A. van der Doelen, 1999. ISBN 90-801704-3-7
2. A mathematical study on craquelure and other mechanical damage in paintings, Petri de Willigen, 1999. ISBN 90-407-1946-2
3. Solvent extractable components of oil paint films, Kenneth R. Sutherland, 2001. ISBN 90-801704-4-5
4. Molecular changes in egg tempera paint dosimeters as tools to monitor the museum environment, Oscar F. van den Brink, 2001. ISBN 90-801704-6-1
5. Discoloration in Renaissance and Baroque oil paintings, Margriet van Eikema Hommes, 2004. Archetype Publications, London.
6. Analytical chemical studies on traditional linseed oil paints, Jorrit D.J. van den Berg, 2002. ISBN 90-801704-7-X
7. Microspectroscopic analysis of traditional oil paint, Jaap van der Weerd, 2002. ISBN 90-801704-8-8
8: Laser Desorption Mass Spectrometric Studies of Artists' Organic Pigments, Nicolas Wyplosz, 2003. ISBN 90-77209-02-6
9. Molecular studies of Asphalt, Mummy and Kassel earth pigments: their characterisation, identification and effect on the drying of traditional oil paint, Georgiana M. Languri, 2004. ISBN 90-77209-07-7
10: Analysis of diterpenoid resins and polymers in paint media and varnishes; with an attached atlas of mass spectra, Klaas Jan van den Berg (forthcoming).
11: Binding medium, pigments and metal soaps characterised and localised in paint cross-sections, Katrien Keune, 2005. ISBN 90-77209-10-7

Published MOLART reports can be ordered from Archetype Publications, 6 Fitzroy Square, London W1T 5HJ, England, Tel: +44 207 380 0800 Fax: +44 207 380 0500, info@archetype.co.uk.

Contents

Chapter 1

Introduction

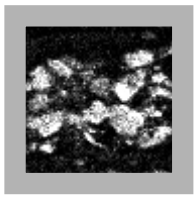

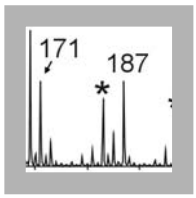

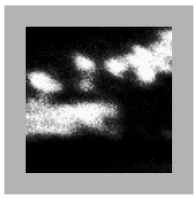

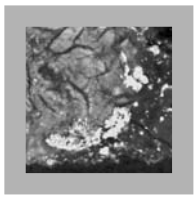

1.1 Studies of paint cross-sections

Paintings are composed of heterogeneous mixtures of organic and inorganic compounds with an often complex multi-layered build-up. Analytical studies of paintings performed on the microscopic and molecular level are the focus of this thesis. The relevance of such an investigation of paintings is the identification of materials to solve art technical historical questions, the deduction of the original appearance and the establishment of the chemical and physical condition before restoration and conservation. Microscopic and molecular studies are carried out on tiny paint samples derived from the painting. These tiny samples are unique and in limited supply. Assuming that such tiny samples are representative for an area under study, valuable general information about the painting can be deduced. The information can be maximized by sequential analyses using different complimentary techniques.

Paint scrapings are used for micro-chemical tests and polarized light microscopy to identify pigments.[1-4] Mineral phase composition of the pigment is determined with X-ray diffraction (XRD). High performance liquid chromatography (HPLC) is now common for the identification of organic pigments.[5] Analysis of paint scrapings with conventional mass spectrometric techniques, such as direct temperature resolved mass spectrometry (DTMS) and gas chromatography/mass spectrometry (GC/MS), gives detailed information on lipids, proteins and resins as constituents of binding medium and varnish.[6-11] The disadvantages of these types of methods are, however, that positional information is lost, and that the valuable paint sample must be sacrificed.

Since the mid 20th century paint samples are embedded in a resin and polished until a flat cross-section of the multi-layered system, the so-called paint cross-section, is visible.[1, 12] In this manner the stratification of the painting and the distribution of the pigment and medium within the layers are preserved. Chemical tests applied *in situ* on paint cross-sections will give some pigment information.[1] However, spot tests are hard to carry out accurately; and the sample is modified after testing. Furthermore, chemical spot tests applied to a paint cross-section are limited to the identification of only a few components. Distributional information has to be obtained by extrapolation. Spot analysis with a scanning electron microscope (SEM) combined with energy dispersive X-rays analysis (EDX) provides information on the elemental composition of pigments. The elemental composition obtained is indicative for certain pigments, but pigments with different mineral phases, but the same elemental composition, like lead carbonate or lead hydroxycarbonate cannot be discriminated nor is it possible to identify pigments with an organic composition, like red lakes of madder or cochineal, in

this manner. Additional analytical techniques have to be applied to the paint cross-section in order to obtain this information. Mineral phases can be determined with XRD and in paint cross-sections, imaging-XRD could be done with electron back-scatter diffraction (EBSD), but this technique has not yet been applied successfully for paint cross-sections, because the surface cannot be made flat enough with the present polishing techniques. So in contrast to rock samples, the various mineral phases present in paint cross-sections cannot be visualised up to now. So far, the elemental composition is used as indicator for the inorganic pigments in paint cross-sections. For identification of organic pigments the combined information from colour, fluorescence, particle shape and elemental composition (for instance elements representative for their substrates) is indicative.

Information on the molecular composition cannot be obtained easily from paint cross-sections. The organic chemical composition of paint cross-sections, *e.g.* the demonstration of proteinaceous and oleaginous binding media, can be visualised with staining techniques.[13-16] However, factors like heterogeneous chemical composition of the medium, ageing processes, the interference with certain pigments, the infiltration of the stain in the cracks or porous layers can easily contribute to a false positive or negative staining results. Furthermore, staining tests are irreversible. Staining is an indirect method to identify the organic composition and the outcome is limited to the selected stain. The exact molecular organic composition and unexpected organic compounds cannot be identified in this way. Potential molecular identification techniques are imaging Fourier transform infrared spectroscopy (FTIR) and the mass spectrometric imaging technique of secondary ion mass spectrometry (SIMS). These imaging techniques are not generally accessible in conservation studios or museums. The advantages and limitations of these techniques for painting studies will be addressed in the forthcoming paragraphs.

The disadvantage of several of the methods addressed above is that the results are limited to the characterisation of the materials while positional information is missing. Besides, in most cases only a single analysis can be carried out on the paint sample, because the precious sample is damaged or lost in the process. To identify painting materials on a molecular and elemental level, these advanced analytical imaging techniques are required. Since there is no single technique, which is informative about all aspects of pigments and binding media, several analytical imaging techniques have to be applied together to reveal "all" aspects of the paint composition. In our laboratory the surface of the paint cross-section is investigated with FTIR, SIMS and SEM/EDX. SIMS is introduced as a new technique for painting research and its usefulness is explored in this thesis. The strength of the combination of these tech-

niques is that they result in different types of chemical information, which makes them complementary. The techniques are superficial, non-destructive and the same paint cross-section can be investigated with more than one imaging technique. The molecular and elemental images obtained can be overlaid and the combined information results in a rather unique and complete picture of the molecular and chemical composition of the paint layers. For a good comparison of the obtained images the paint cross-section is first subjected to FTIR-imaging and SIMS before SEM/EDX, as this latter technique requires a thin carbon coating. The carbon coating can be polished off for subsequent analyses, but this will change the distribution of materials at the surface. Other imaging techniques relevant for painting studies, like imaging Raman spectroscopy and imaging UV/VIS spectroscopy, are not employed in this thesis, but can be very useful in certain cases.

1.2 Analytical imaging techniques

FTIR-imaging gives information on the distribution of specific chemical functional groups. For example, carbonates (derived from pigments) and carbon-hydrogen bonds (derived from medium or varnish) can be characterised and localised in paint cross-sections. Every measurement in FTIR-imaging yields a completely independent IR-spectrum for every spot on the surface of the paint cross-section with a fast IR-camera. The spatial resolution is limited to about 7 µm and the detection of the camera ranges between 4000 – 1000 cm^{-1}, which implies that characteristic features below 1000 cm^{-1}, such as lead chromate (at 856 cm^{-1}) cannot be identified and imaged. Basic lead carbonate cannot be distinguish from lead carbonate due to the detection range (characteristic peaks are found for lead carbonate at 838 cm^{-1} and for basic lead carbonate at 778 and 680 cm^{-1}).[17] FTIR-imaging of paint cross-sections as such is restricted to a specular reflectance approach due to the thickness of the sample.[18] The reflectance intensity is determined by the difference in refractive index between two materials (n_2/n_1) described by Fresnell's law.[19] Minerals or other inorganic materials in paints have a high refractive index ratio, which leads to intense specular reflections (25% with n = 2) and an intense signal in the FTIR reflectance spectra. The opposite is true for organic materials, which results in low intensity signals (4% with n = 1.5) in the spectra. FTIR is able to image pure organic compositions, but the surface must be totally planar in order to obtain good reflections. Unfortunately, when organic compounds are mixed with large amounts of inorganic matter, like chalk or lead white, the peaks representative for the inorganic composition

predominate in the FTIR spectrum. Often, the organic constituent in, for instance a chalk layer, is not visualised with FTIR, as its reflectance and relative concentration are low. Besides in a heterogeneous layer the signal is reduced due to scattering of the infrared light within the sample. Kramer-Krönig transformation is applied to the specular reflectance spectrum to transform it into an absorbance like spectrum, which is more workable and easier to interpret.[20]

SEM is an established technique in technical painting studies. Separate layers, pigment particles and organic constituents can be visualised well in paint cross-sections. The backscattered electrons (BSE) enable a good compositional contrast within the paint cross-section, because heavy elements with high atomic numbers result in higher electron back scattering than lighter elements. Electron beam induced X-rays analysed with an energy dispersive detector (EDX) results in a semi-quantitative spectrum of the elements in the paint cross-section. Elemental mapping gives information on the distribution of these elements in and between the particles in the paint layers. Not all elements can be detected with EDX, because the detection threshold is relatively high and the X-ray energies of several elements overlap. In general, light elements, for example nitrogen, in low concentrations are hard to detect with EDX. EDX is not a suitable technique for detection of trace elements in pigments and media, because their concentration is often below the detection limit (the detection limit is approximately 0.1 wt% for pure materials[21] and is dependent on the element, matrix composition and instrumental settings). Besides, the chance that the generated X-ray radiation is absorbed by lighter elements positioned in the sample is rather large. This is one of the main reasons why quantitative analysis of these very heterogeneous paint samples is barely possible. Elements with overlapping X-ray energies are for instance the *K*-shell of sulphur with the *M*-shell of lead. Lead can be identified by its *L*-shell X-rays. Plotting a theoretical fit by selection of certain elements (an option in the EDAX Genesis soft program) over the acquired spectrum makes it possible to deduce the presence and absence of overlapping elements.

The surface quality of the paint cross-section determines the quality of the BSE-images. A highly flat surface results in better contrast in the images and a sharper visualisation of pigment features at high magnification. The spatial resolution of SEM equipped with a field emission source is about 1-5 nm,[22] this resolution is however rarely required for the study of paint cross-sections. The penetration depth of the beam is determined by the composition of the materials. The dimensions of the interaction volume (volume created by interaction of the primary electron beam with the sample surface) for a low-density and low atomic number specimen are larger (*i.e.* more pear shaped) than for a specimen with high-density and high atomic numbers.

So the depth resolution for the back scattered electrons is between 10-1000 nm (dependent on the acceleration voltage of the electron beam), whereas the X-rays are generated in the bottom part of the interaction volume.[23] As the interaction volume is dependent on the composition under study and the beam settings, the correct interpretation of the BSE and X-ray images is very critical. The information deduced from BSE images can be derived from regions positioned below the surface. Elemental information acquired from a particle or area can be mixed with elemental information from its environment. Selecting the proper beam settings for the paint cross-section under study, like low acceleration voltage or small spot sizes, can help interpretation. The paint cross-sections are charge compensated by covering the surface with an ultrathin carbon coating.

SIMS is a surface sensitive technique that uses a high-energy primary ion beam to generate secondary ions from the surface.[24] Elemental, small and larger molecular information can be obtained in this way. Hence, the size and distribution of pigment particles, the position of organic constituents and the interaction between both can be studied in detail in this manner. Scanning of the focussed beam over the surface generates an image. An entire mass spectrum is acquired for every pixel in the image. By selecting a mass of interest, this information can be plotted into an image illustrating the spatial distribution of that mass peak. The advantage of SIMS applied to paint cross-sections is that the distribution of pigment and binding medium can be studied at the same time in a single sample. The spectral mass information obtained can be highly informative about the material composition in the cross-section. The lateral resolution in an image is, depending on the image size, about 1 μm. The depth probing in SIMS is restricted to the upper atomic layers of the sample. SIMS applied to paint cross-sections has some restrictions. The binding medium in paint is a random three-dimensional cross-linked network, which means that ionisation with the primary ion beam leads to fragmentation of the network. The smaller hydrocarbon fragments (< 100 amu) are the most abundant peaks in the spectrum, but they are too common and cannot be used as markers for the binding medium. Ion yields of characteristic fragments of the medium, like fatty acids derived from an oil binding medium, can be low. This can be explained by the fact that only a small fraction of the analysed surface area contains binding medium constituents while the binding medium itself contains only a small fraction of fatty acids. Besides the ionisation and emission efficiency of fatty acids is low. The absence of peaks characteristic for medium can also be explained by instability under the ionisation conditions, which is the case for dicarboxylic acids, an important major constituent of the oil network. Elements like lead, silver and gold not only enhance the ionisation of organic compounds, but also

suppress the fragmentation of *e.g.* the dicarboxylic acids (see chapter 3.3). This implies that fatty acids are often detected in relative high yields in lead white-containing layers, on lead white particles or near the gold leaf of gildings. The presence of fatty acids in lead deficient layers can therefore not be excluded. This problem can be overcome by homogenizing the surface with an ultrathin metal coating. The benefit of a metal coating is that the ion yields from organic constituent are enhanced, but a disadvantage is that the ion yields from inorganic elements are suppressed, which results in poor quality images.

The advantage of SIMS applied to paint cross-sections is that trace elements, which cannot detected by EDX due to their low concentration, are often detected by SIMS. SIMS has been shown to be able to detect 0.001 wt% of calcium in a lead white matrix, whereas the detection limit of EDX was 0.1 wt% for the same sample (unpublished results). The detection limit of elements in SIMS is depending on their ionisation potential and possible matrix effects. For example, chlorine ionises relatively well, while the ionisation potential of mercury is rather high. The quality of the surface of the paint cross-section is very crucial. SIMS is very sensitive to unevenness of the surface. Uneven sample surfaces result in poor mass and spatial resolution of the SIMS data. The sample preparation must be as clean as possible. Surface contamination with poly-di(methyl)siloxanes and di-iso-octylphthalate must be prevented. Threfore, the samples are rinsed with hexane prior to analysis.

The analytical imaging techniques require a flatter surface of the paint cross-section than what is made available by museums and private restorers. An optimized systematic dry-polishing method was developed to overcome this problem in which the surface is planar; scratches, smearing and holes are minimised and higher quality analytical data are obtained.[25] The sample is fixed in a homemade polishing holder to provide an even pressure on the sample during polishing. The surface area around the sample is decreased to reduce the risk of smearing the embedding medium or certain fractions from the paint itself over the sample. Very short straight movements prevent possible friction, smearing and heating. After each polishing movement the holder is turned by 90°.[25]

During and after sample preparation, contamination is prevented as chemical information must be retained on/in the surface. No liquid to saturate the surface and to reduce the light scattering with the object to improve light microscopic investigation is used on the surface of paint cross-sections.[26] The sample surface is never touched, as fingerprints are a source for fatty acids that are constituent of the oil binding media. A silicone-based putty often used to attach the sample to an objective glass for light microscopic investigations is not used.

1.3 Chemical changes in paintings

The chemical information obtained with analytical imaging techniques gives information about the current composition of the paint sample. It is important to understand that paintings are not static objects, but undergo many chemical and physical changes over time. Original components may be reacting away and new compounds can form. In the past, the conditions for keeping the paintings were not always optimal. Paintings were exposed to fluctuating temperatures, direct sunlight and extremes in humidity, which influenced and promoted chemical aging and degradation reactions in paints. Besides, the various restoration treatments might have influenced the chemical and physical condition of the painting. Spatially resolved analyses of paint cross-sections are expected to give more insight into the time frozen chemical and physical processes, which have taken place.

Many degradation phenomena of pigments are investigated and elucidated via paint cross-sections. Light sensitive pigments degrade on the surface of the painting, but in cross-section a degraded and intact part is visible. As the paint cross-section reveals degraded and intact pigments, the degradation phenomena can be studied in this manner. Examples of pigments which degraded on the surface of the painting are:

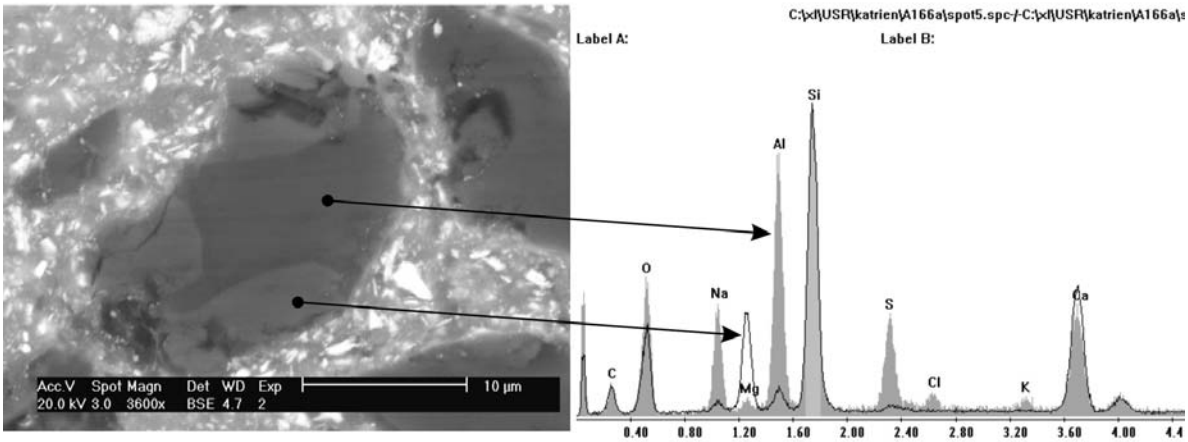

Fig 1.1 Backscattered electron image revealing an ultramarine particle embedded in a lead white oil paint matrix. The ultramarine is part of a paint cross-section (A166/1b) taken from the virgin's blue robe in the panel painting 'The Descent from the Cross' by Rogier van der Weyden (1399/1400-1464). The particle has a heterogeneous composition, where its centre has a lower backscattering intensity compared to the edges of the particle. EDX spot analyses reveal a different elemental composition for the centre and edges of the particle. Natural ultramarine $(Na,Ca)_8(AlSiO_4)_6(SO_4,S,Cl)_2$ is shown in the centre while the edges are proposed to be diopside (monoclinic pyroxene, $MgCaSi_2O_6$), a mineral associated with lazulite.

the fading of red and yellow lakes,[27] indigo[28], the whitening of bone black[29], blackening of vermilion (see chapter 4), colour changes of chrome and cadmium yellow[30, 31] and the decomposition of orpiment and realgar.[32, 33] Pigments that degrade under the influence of their local external environment can only be visualised in paint cross-section. For example, analytical imaging studies on a partially degraded smalt particle (a blue potash glass) containing a discoloured rim and an intact blue core, indicate that an elemental exchange between the particle and surrounded medium occurred.[34]

The type of binding medium constituents detected in a paint cross-section gives information about the condition of the oil. For example, oil paint with a relatively large amount of metal soaps and a relatively small amounts of free and ester-bound fatty acids is indicative for a mature oil paint.[35] The ratio between two fatty acids - palmitic and stearic acid - can be indicative for the type of oil used in the paint. This ratio is determined from paint scrapings with GC/MS.[36] For a meaningful identification of the type of oil paint, the various layers of the paint sample have to be separated, which is not easy at all or simply impossible. SIMS offers the opportunity to measure this ratio from a paint cross-section (see chapter 3.2). The analytical imaging studies of paint cross-sections result in compositional data on single paint layers in a multi-layered paint system.

From the defects observed in paintings it is clear that pigment and binding medium cannot be seen as two separate components in paint. Certain pigments, like smalt, degrade in an oil medium while they are stable in other media.[37] Small crater-like holes filled with a whitish and opaque material, so-called protrusions, are observed on the surface of many paintings.[38] A protrusion is an aggregate of metal soaps, a reaction product from pigment and oil medium. The process of formation of this defect is deduced from detailed studies of paint cross-sections, as many stages of this phenomenon are often observed (see chapter 5).

In general, the particle, molecular and elemental composition within a paint layer is not homogeneous. This heterogeneous composition within and between layers is informative for alteration and degradation processes that have taken place in the paint. Fig. 1.1-1.3 illustrate that not only paint layers are heterogeneous, but that also pigments can be impure and can have a variable morphology. The figure captions explain the phenomena observed.

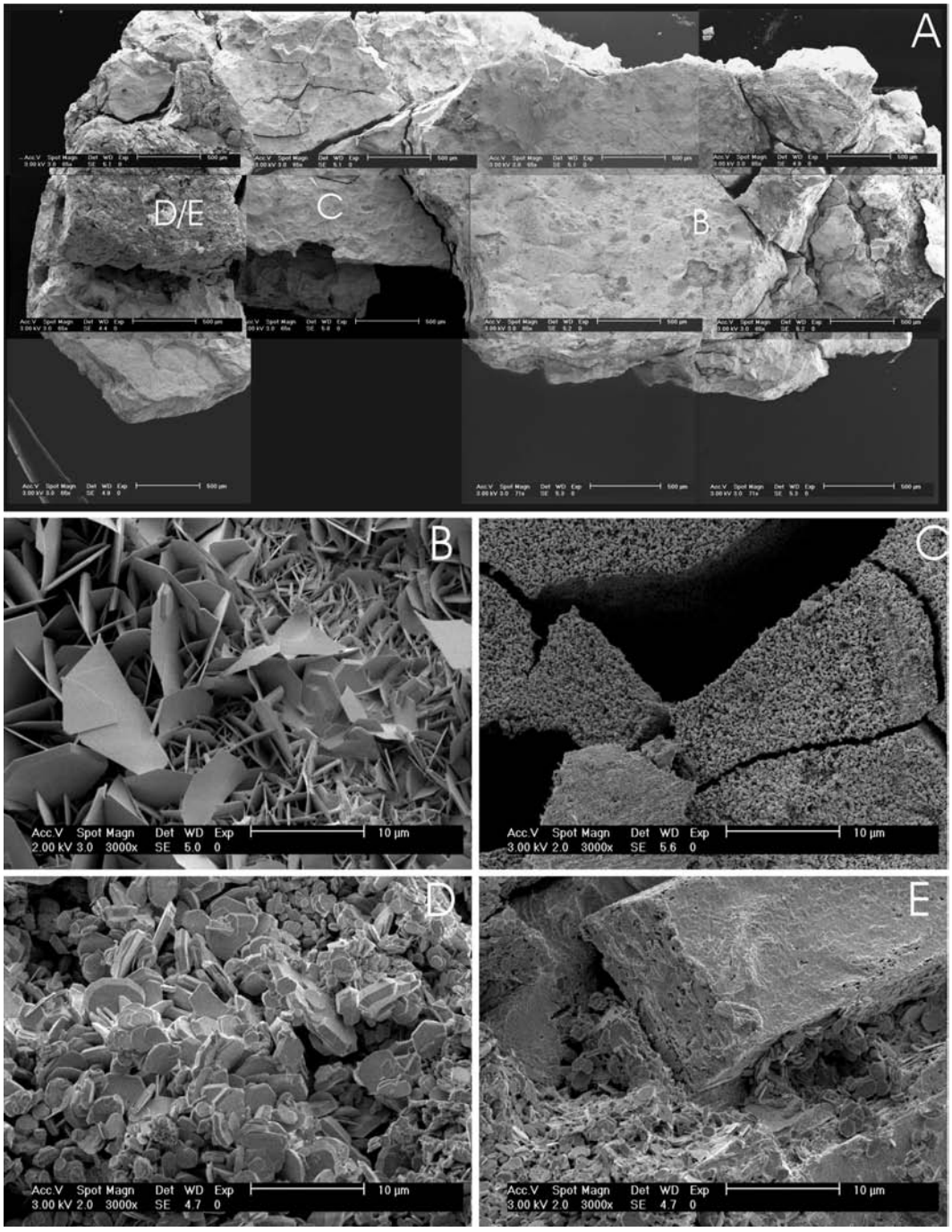

Fig 1.2 Backscattered electron images (A) of a slightly corroded lead piece from a ceramic pot (labeled "C") in possession of Old Holland Paint Company (sample nr. OH.10; provided by Dr. L Carlyle). Traditionally prepared lead white was using the stack process, or "Dutch" method.[39, 40, 41] *A sheet of metallic lead in a ceramic pot is exposed to vinegar, carbon dioxide, oxygen, humidity and high temperatures in a pile of horse manure. The metallic lead is converted into lead acetate and subsequently in lead hydroxycarbonate, which is scraped off. The higher magnified backscattered electron images B-E illustrate the different morphologies in different locations on the lead pieces (different levels in the corrosion). The position of images B-E is indicated in image A. The crystals in image C are probably positioned closer to the metallic lead, whereas the crystals in image B derive from the outer surface of the corroded piece. Traditional lead white pigment is clearly not a pure homogenous compound.*

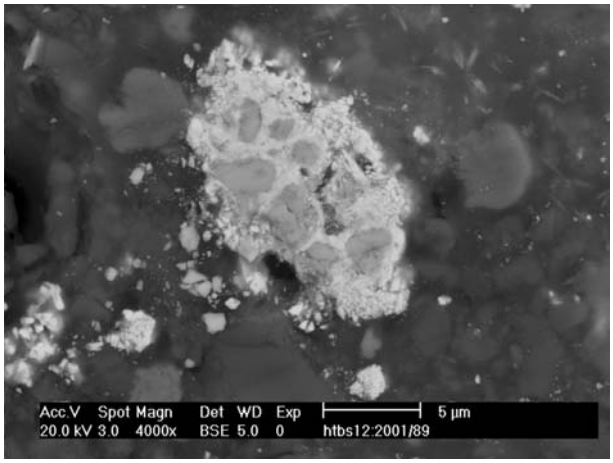

Fig1.3 Backscattered electron image of a lead-tin yellow particle (higher backscattering intensities of tiny lead stannate particles) with tin oxide inclusions (lower backscattering intensity) present in paint cross-section HSTB 12:2001/89. The paint cross-section is taken from a 'Green Leaf of Allegory on the Marriage of Frederick Hendrik and Amalia van Solms' by Gerard van Honthorst (1651), Oranjezaal of the Royal Palace Huis ten Bosch (The Hague, The Netherlands) The tin oxide is probably an unreacted residue in the lead-tin yellow pigment as a result of a poorly designed production process. To get a complete conversion of the lead and tin oxides to lead stannate (lead-tin yellow pigment type I) the conditions in the melt are crucial.[42] *(backscattered electron image: Annelies van Loon, AMOLF).*

1.4 Scope of this thesis

The scope of the thesis is to characterise and localise the constituents of traditional oil paints in paint cross-sections. Oil-containing paint is selected as focal point, because oil is one of the most used binding media in paintings. Besides, the defects described in chapter 5 are associated with the oil medium. The various analytical imaging techniques are used to map characteristics of the oil medium, pigments and their interactions with a high spatial resolution. The analytical imaging techniques are complementary. Examination performed with the various imaging techniques leads to a better understanding of the chemical composition and distribution in paint layers.

In chapter 2, SIMS is introduced as an analytical technique for technical research of paintings. SIMS was performed on a paint cross-section taken from the virgin's blue robe in the panel painting *The Descent from the Cross* (Museo del Prado, Madrid) of the Early Netherlandish artist Rogier van der Weyden (1399/1400-1464). This 15th century panel painting is in a very good condition, which makes it an interesting sample for a detailed study of the binding medium, the pigments and their interaction. The SIMS results are supported by and in agreement with the results obtained with light microscopy, imaging FTIR and SEM/EDX. The interpretation of

the secondary ion peaks that are characteristic for the binding medium is verified with the spectrum of reference materials.

Chapter 3 addresses the oil binding medium in paint cross-sections studied by SIMS. Three aspects of SIMS applied to paint systems are presented in this chapter: the identification of mass spectral data, the localisation of characteristic spectral data and improvement of ion yields from organic substances. In the first part of chapter 3, the mass spectral data of SIMS obtained from an oil model system is compared with information obtained with conventional mass spectrometric techniques, like DTMS and GC/MS. In the second part, the spatial distribution of oil paint characteristics, like fatty acids, is presented. The type of fragment ions detected gives information about the chemical condition of the oil paint. The ratio between palmitic and stearic acid can be indicative for the type of oil. The third part addresses a gold-coating method to enhance the ion yields, which are necessary to improve the quality of the images representative for the oil derived components.

Chapter 4 sheds new light on the well-known phenomenon of the blackening of vermilion. The combination of light microscopic images from SIMS and SEM/EDX elucidates the light induced degradation of vermilion. SIMS and SEM/EDX give complementary elemental information and SIMS has the benefit that fragments of inorganic complexes can be detected. This information leads to a proposal for a mechanism of the chloride induced degradation of vermilion.

The interaction between lead- and zinc-containing pigments and the oil medium, which leads to serious defects in the paint film is presented in chapter 5. Many paintings are found to be affected by metal soap formation, which leads to aggregate formation in the paint film and changes in the appearance of the painting. In this chapter, ten case studies are performed using light microscopy, imaging FTIR, SEM/EDX and SIMS. The analytical imaging results give a better understanding of important reactive compounds, paint compositions and external factors relevant for the formation of the metal soap aggregates.

1.5 Publication list

This thesis is based on the following publications:

Chapter 2

K. Keune and J.J. Boon, *Imaging secondary ion mass spectrometry of a paint cross-section taken from an early Netherlandish painting by Rogier van der Weyden,* Analytical Chemistry, 76, 2004, p. 1374-1385.

Chapter 3.1

K. Keune, E. Ferreira and J.J. Boon, *SIMS characterisation of traditional oil paint: comparative studies with DTMS and GC/MS*, in preparation

Chapter 3.2

K. Keune, E. Ferreira and J.J. Boon, *Characterisation and localisation of the oil binding medium in paint cross-sections using imaging secondary ion mass spectrometry,* In: Conference Proceedings 14th Triennial Meeting of the ICOM Committee for Conservation in the Hague, September 12-16, 2005

Chapter 3.3

K. Keune and J.J. Boon, *Enhancement of the static-SIMS secondary ion yields of lipid moieties by ultrathin gold coating of aged oil paint surfaces*, Surface and Interface Analysis, 36, 2004, p. 1620-1628.

Chapter 4

K. Keune and J. J. Boon, *Analytical imaging studies clarifying the process of the darkening of vermilion*, accepted for publication in Analytical Chemistry, 2005.

Chapter 5

K. Keune, P. Noble and J.J. Boon, *Chemical changes in lead-pigmented oil paints: on the early stage of formation of protrusions*, In: Proceedings of ART 2002, the 7th international conference on non-destructive testing and microanalysis for the diagnostics and conservation of the cultural and environmental heritage, R. van Grieken, K. Janssens, L. Van' t dack and G. Meersman (Eds.), Antwerp, Belgium, 2002, 9 pages

J.J. Boon, J. van der Weerd, K. Keune and P. Noble, *Chemical changes in Old Master paintings: dissolution, metal soap formation and remineralization processes in lead pigmented paint layers of 17th century painting,* ICOM-CC Working Groups Painting 1 & 2 and Painting section, UKIC, Deterioration of Artists Paints: Effects and Analysis Extended abstracts, September, 2001, p. 19-20.

J.J. Boon, J. van der Weerd, K. Keune, P. Noble and J. Wadum, *Mechanical and chemical changes in Old Master paintings: dissolution, metal soap formation and remineralization processes in lead pigmented ground/intermediate paint layers of 17th century paintings.* In: Vontobel, R (Ed.) In ICOM-CC Preprints of the 13th Triennial Meeting, Rio de Janeiro, 1, James and James, London, 2002, p. 401-406.

J.J. Boon, E. Gore, K. Keune and A. Burnstock, *Image analytical studies of lead soap aggregates and their relationship to lead and tin in 15th century lead tin yellow paints from the Sherbourne Triptych*, Infrared and Raman Users Group (IRUG) meeting, 29 March – 1 April, M. Picollo (Ed.), Il Prato, Padova, Florence, Italy, 2004, p. 66-74.

G. Osmond, K. Keune and J.J. Boon, A study of zinc soaps found in paintings at the Queensland Art Gallery, submitted to AICCM Bulletin.

Other publications

J.J. Boon, K. Keune, J. van der Weerd, M. Geldof, and J.R.J. van Asperen de Boer, *Imaging microspectroscopic, secondary ion mass spectrometric and electron microscopic studies on discoloured and partially discoloured smalt in cross-sections of 16th century paintings.* Chimia, 55, 2001, p. 952-960.

J.J. Boon, K. Keune, T. Learner, *Identification of pigments and media from a paint cross-section by direct mass spectrometry and high-resolution imaging mass spectrometric and microspectroscopic techniques*, In: Vontobel, R (Ed.) In ICOM-CC Preprints of the 13th Triennial Meeting, Rio de Janeiro, 1, James and James, London, 2002, p. 223-230.

J. Boon, N. Wyplosz, F. Hoogland, M. Duursma, K. Keune, T. Learner, *Molecular characterization and mapping of 20th century synthetic organic pigments and additives in paints* In: 20th international ICC congress on Modern Art, New Museums in Bilbao, Bilbao Spain, 2004.

A. van Loon, J.J. Boon, K. Keune and J. v.d. Horst, *Binding medium analysis of blue colored glazes on silver gildings on 17th and 18th century German Polychrome Sculpture*, In: Historische Polychromie, Skulpturenfassung in Deutschland und Japan= Historical Polychromy, Polychrome Sculpture in Germany and Japan, K.M.a.M. S., Editor. Hirmer Verlag: München. 2004, p. 352-379.

K. Keune, *Der Farbmann*, kM 37, 2001, p. 16-17.

K. Keune, *Lapis Lazuli tussen kantsteen en legger*, kM 34, 2000.

In Press

B. Leone, A. Burnstock, C. Jones, P. Hallebeek, J. Boon, K. Keune, *The Deterioration of Cadmium Sulphide Yellow Artists' Pigments*, In: Conference Proceedings 14th Triennial Meeting of the ICOM Committee for Conservation in the Hague, September 12-16, 2005.

J. J. Boon, K. Keune and J. Zucker, *Imaging analytical studies of lead soaps aggregating in preprimed canvas used by the Hudson River School painter F.E. Church*, Microscopy and Microanalysis 2005

J.J. Boon, E.S.B. Ferreira and K. Keune, *Imaging analytical studies of Old Master paints using FTIR, SIMS and SEMEDX of embedded paint cross-sections*, Microscopy and Microanalysis 2005

A.van Loon, K. Keune and J.J. Boon, *Improving the surface quality of paint cross-sections for imaging analytical studies with specular reflection FTIR and Static-SIMS*, Conference Proceedings Art 2005, Lecce 16-19 may, 2005

B. Marino, K. Keune, E. Hendriks and J.J. Boon, *SIMS Studies of the Material Aspects in Grounds and Paints in Paintings by Van Gogh*, Conference Proceedings Art 2005, Lecce 16-19 may, 2005

1.6 References

1 J. Plesters, *Cross-sections and chemical analysis of paint samples,* Studies in Conservation, 2, 1965, p. 110-157.

2 R.J. Gettens and G.L. Stout, *Painting materials, a short encyclopaedia,* Dover Publications Inc., New York, 1966

3 M. Chaptal, *Sur quelques couleurs trouvées à Pompeia,* Annales de Chemie, LXX, 1809, p. 22.

4 W. McCrone, L. McCrone, and J. Delly, *Polarized light microscopy*, McCrone Research Institute, Chicago, Illinois, 1984.

5 J. Kirby, *A spectrophotometric method for the identification of lake pigment dyestuff*, National Gallery Technical Bulletin, London, 1997, p. 35-45.

6 J.S. Mills and R. White*, Analyses of paint media*, National Gallery Technical Bulletin, 4, 1980, p. 65-68.

7 J.S. Mills, *The gas chromatography examination of paint media. Part I. fatty acid composition and identification of dried oil films*, Studies in Conservation, 11, 1966, p. 92-108.

8 J.D.J. van den Berg, K.J. van den Berg and J.J. Boon, *Determination of the degree of*

hydrolysis of oil paint samples using a two-step derivatisation method and on-colomn GC/MS, Progress in Organic Coatings, 41, 2001, p. 143-155.
9 J.J. Boon, *Analytical pyrolysis mass-spectrometry - new vistas opened by temperature-resolved in-source py-MS*, International Journal of Mass Spectrometry and Ion Processes, 118, 1992, p. 755-787.
10 J.D.J. van den Berg, *Analytical chemical studies on traditional linseed oil paints.* PhD Thesis, University of Amsterdam, 2002 (http//www.amolf.nl/publications/theses/).
11 G.A. van der Doelen, K.J. van den Berg and J.J. Boon, *Comparative chromatographic and mass spectrometric studies of triterpenoid varnishes: fresh and aged samples from paintings,* Studies in Conservation, 43, 1998, p. 249-264.
12 R.J. Gettens, *A microsectioner for paint films*, Technical Studies in the Field of the Fine Arts 1, 1, 1932, p. 20-28.
13 W. Oswald, *Ikonoskopische studien. 1. mikroskopischer nachweis der einfachen bindmittel*, Sitzungsberichte der Königlich Preussischen Akademie der Wissenschaften, 1905, 167-174.
14 M. Johnson and E. Packard, *Methods used for the identification of binding media in Italian paintings of the fifteenth and sixteenth centuries*, Studies in Conservation, 16 (1971), 145-164.
15 M. C. Gay, *Essais d'identification et de localisation des liants picturaux par des colorations spécifiques sur coupes minces,* Annales Laboratoire de Recherche des Musées de France, 1970, p. 8-24. (Report in English: *Application of the staining method to cross-sections in the study of the media of various Italian paintings of the fourteenth and fifteenth centuries,* Conservation and Restoration of Pictorial Art (Ed. N. Brommelle and P. Smidt), Butterworths, London, 1976, 78-83).
16 R. Wolbers and G. Landrey, *The use of direct reactive fluorescent dyes for the characteriza tion of binding media in cross sectional examinations*, In: Preprints of papers presented at the fifteenth annual meeting of the American Institute for Conservation of Historic and Artistic Works, May 20-24, The American Institute for Conservation of Historic and Artistic Works, Washington DC, 1987, p. 168-204.
17 J. van der Weerd, *Microspectroscopic analysis of traditional oil paint*. PhD Thesis, University of Amsterdam, 2002 (http//www.amolf.nl/publications/theses/), p. 93-95.
18 J. van der Weerd, H. Brammer, J.J. Boon, R.M.A. Heeren, *Fourier transform infrared micro scopic imaging of an embedded paint cross-section*, Applied Spectroscopy, 56, 2002, p. 275-283.
19 Van Heel ACS, *Inleiding in de optica,* Martinus Nijhoff, 's Gravenhage, 1958
20 B. Harbecke, *Application of Fourier's allied integrals to the Kramers Kronig transformation of reflectance data*, Applied Physics A, 40, 1986, p. 151-158.
21 J.I. Goldstein *et al., scanning electron microscopy and X-ray microanalysis*, 3rd ed. Kluwer Academic/Plenum Publishers, New York, 2003, p. 446-449.
22 J.I. Goldstein *et al.*, s*canning electron microscopy and X-ray microanalysis*, 3rd ed. Kluwer Academic/Plenum Publishers, New York, 2003, p. 40.
23 J.I. Goldstein *et al.*, s*canning electron microscopy and X-ray microanalysis*, 3rd ed. Kluwer Academic/Plenum Publishers, New York, 2003, chapter 6.
24 J.C. Vickerman, *ToF-SIMS - an overview,* In: ToF-SIMS: Surface Analysis by Mass Spectrometry, J.C. Vickerman, D. Briggs (Eds.), IM Publication and SurfaceSpectra Limited, Manchester, 2001, Chapter 1.
25 A. van Loon, K. Keune and J.J. Boon, *Improving the surface quality of paint cross-sections for imaging analytical studies with specular reflection FTIR and Static-SIMS,* submitted to Art2005: 8th International Conference on Non-destructive Testing and Microanalysis for the

Diagnostics and Conservation of the Cultural and Environmental Heritage.
26 S. Giger, *Reducing scattered light in photomicroscopy of opaque cross-sections*, Studies in Conservation, 7, 1967, p. 43-48.
27 D. Saunders and J. Kirby, *Light-induced colour changes in red and yellow lake pigments*, National Gallery Technical Bulletin, 15, 1994, p. 79- 97.
28 M. H. van Eikema Hommes, *Changing pictures-discolouration in 15th to 17th century oil paintings*, Archetype Publications, London, 2005
29 A. van Loon and J.J. Boon, *Characterization of the deterioration of bone black in the 17th century Oranjezaal paintings using electron-microscopic and micro-spectroscopic imaging techniques*, Spectrochimica Acta Part B: Atomic Spectroscopy, 59, 2004, p. 1601-1609.
30 H. Kühn and M. Curran, *Chrome yellow* In: Artists' Pigments, vol. 1, R.L. Feller (Ed.), National Gallery of Art, Washington, 1986, p. 190.
31 B. Leone, A. Burnstock, C. Jones, P. Hallebeek, J. Boon, K. Keune, *The deterioration of cadmium sulphide yellow artists' pigments*, In: Conference Proceedings 14th Triennial Meeting of the ICOM Committee for Conservation in the Hague, September 12-16, 2005.
32 A. Wallert, *Methods and materials of still-life painting in the seventeenth century* In: Still lifes: Techniques and Style, an examination of paintings from the Rijksmuseum, A. Wallert (Ed.), Zwolle/Amsterdam, Waanders/Rijksmuseum, 1999, p. 7-24.
33 V. Daniels and B. Leach, *The occurrence and alteration of realgar on ancient Egyptian papyri*, Studies in Conservation, 49, 2004, p. 73-84.
34 J.J. Boon, K. Keune, J. van der Weerd, M. Geldof and J.R.J. van Asperen de Boer, *Imaging microscopic, secondary ion mass spectrometric and electron microscopic studies on discoloured and partially discolored smalt in cross-sections of 16th century paintings*, Chimia, 55, 2001, p. 952-960.
35 J.J. Boon *et al.*, *Molecular aspects of mobile and stationary phases in aging tempera and oil paint films*, In: Early Italian Paintings: Techniques and Analysis, T. Bakkenist, R. Hoppenbrouwers and H. Dubois (Eds.), Stichting Restauratie Atelier Limburg (SRAL), Maastricht, 1996, p. 35-56.
36 J.S. Mills and R. White, In *The Organic Chemistry of Museum Objects*, Butterworth-Heinemann Ltd, 1994, p. 143.
37 B. Mühlethaler and J. Thissen, *Smalt*, In: Artists' Pigments, vol. 2, A. Roy (Ed.), National Gallery of Art, Washington, 1993, p. 116-120.
38 P. Noble, J. J. Boon and J. Wadum, *Dissolution, aggregation and protrusion. lead soap formation in 17th century grounds and paint layers*, Art Matters, 1, 2003, p. 46-61.
39 C.A. Klein, *The manufacture of white lead,* The paint and varnish society, 1913, p. 11-15.
40 P. N. Hasluck, *Painters' oils, colours and varnishes*, Cassell and Company Ltd. London, 1913, p. 47-48.
41. A. Ure, *A dictionary of arts, manufactures, and mines*, New York, D Appleton and Company, vol. II, 1853, p. 945-946.
42 N. J. Eastaugh, *Lead tin yellow: its history, manufacture, colour and structure,* PhD thesis, University of London, Courtauld Institute of Arts, 1988.

Chapter 2

Imaging secondary ion mass spectrometry of a paint cross-section taken from an early Netherlandish painting by Rogier van der Weyden

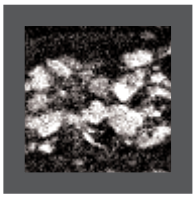

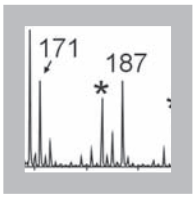

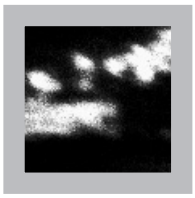

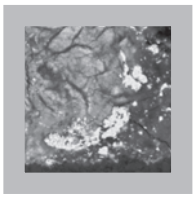

Static secondary ion mass spectrometry (SIMS) is introduced as an analytical technique for the examination of paint cross-sections to obtain simultaneous information about the nature and distribution of pigments, and the binding medium from a single sample. A sample taken from the virgin's blue robe in the panel painting 'The Descent from the Cross' (Museo del Prado, Madrid) of the Early Netherlandish painter Rogier van der Weyden (1399/1400-1464) was selected for investigation. Data were compared with reference compounds and reference lead white-containing linseed oil paint and egg tempera paint. The static SIMS technique gave position sensitive mass spectra that were used to image the elemental distribution of pigments and the molecular signature of components of the oleaginous binding medium. SIMS ion images of sodium and aluminium superimposed with the blue pigment ultramarine, and those of copper, lead, and calcium with the position of the mineral pigments of azurite, lead white and chalk, respectively. Preserved monocarboxylic acids of palmitic and stearic acid present as fatty acids and fatty acid lead soaps pointed to the use of linseed oil as binding medium. Images from the oleaginous binding medium fatty acids show a correlation with the three main paint layers. The observed palmitic/stearic acid ratios for the two ultramarine layers and azurite layers are 1.3, 1.4 and 1.8 respectively. Almost no fatty acids were detected in other layers visible by light microscopy. The fatty acid lead soaps point towards a mature ionomeric oil paint system that developed over centuries. SIMS evidence for egg tempera, still used in the fifteenth century, is not detected in the paint cross-section. SIMS images correlate well with SEM/EDX, FTIR and light microscopic images and the SIMS spectral data additionally support the identification of pigment particles, lead soaps and other binding media components.

2.1 Introduction

2.1.1 Static SIMS in the examination of paint cross-sections

Secondary ion mass spectrometry (SIMS) has been well explored in the analytical surface analysis of materials such as polymers and semiconductors.[1] In this chapter static SIMS is applied as a new technique for the examination at paint cross-sections.[2] Paintings are complex chemical systems and SIMS can provide information about the nature of the paint. The layer structure of paintings can be observed by the preparation of a paint cross-section.[3] Analytical techniques such as SEM-EDX, imaging FTIR, Raman spectroscopy and visible light microscopy are usually applied to identify pigments and organic binding media. The advantage of static SIMS applied to paint cross-sections would be that the distribution of pigment and binding media and their interaction in a paint sample can be studied in detail at the same time. The mass spectral data obtained using SIMS may inform identification of the materials in a cross-section. By selecting a mass of interest, this information can be plotted as an image illustrating the spatial distribution of binding media constituents and elements specific for pigments. Depending on the image size the lateral resolution obtained with SIMS using a liquid metal ion gun is about 1 μm. An important advantage of static SIMS probing the upper atomic layers of the surface is that no structural damage is visible. As paint cross-sections are single exemplars and available in limited supply, the advantages mentioned above make SIMS a particularly useful technique for the study of paint cross-sections.

2.1.2 A paint cross-section of Rogier van der Weyden's 'The Descent from the Cross' (Prado, Madrid)

Rogier van der Weyden and his colleagues Jan van Eyck and Robert Campin, are seen as the most prominent painters of the period of Early Netherlandish painting in the 15th century. They formulated their own oil paints to depict religious scenes in detailed environments on oak panels.[4] Most of their paintings are presently in excellent condition. A cross-section made from a fragment of paint from the virgin's blue robe from the panel painting *The Descent from the Cross* (Museo del Prado, Madrid) by the Early Netherlandish painter Rogier van der Weyden (1399/1400-1464) was available for investigation. There are very few samples from this painting because of its pristine condition. This sample provided an unusual opportunity to address questions on 15th C painting materials and methods with imaging SIMS.[5,6] Because egg tempera paint with its binding medium components of protein and lipids was still used in the 15th century, questions remain as to what extent oil and egg tempera mixtures were used. The paint cross-section in the present study contained several blue layers, including pigments ultramarine and

azurite identified by light microscopy.[7] Two other samples taken from this painting were analysed and the binding medium was identified as linseed oil, on the basis of the ratio between palmitic and stearic acid.[7] Many researchers have investigated the composition and chemical drying properties of oil.[8, 9, 10, 11, 12, 13] The fresh oil consisting of polyunsaturated triacylglycerols passes through various stages of chemical drying and ageing to develop into a mature oil paint that consists of polyanionic ionomeric networks of metal carboxylate bonds.[9, 14, 15] Using imaging SIMS, it is now possible to identify and determine the distribution of the oil- or egg-derived fatty acids and metal soaps.

In this chapter, we present our analytical approach that combines application of light microscopy, imaging-FTIR, scanning electron microscopy combined with energy dispersive X-ray (SEM/EDX) and SIMS to a single 15th century paint cross-section elucidating the build-up of the paint, the nature and the distribution of pigments and binding media in separate layers. The focus of the chapter is on the contribution by static SIMS. Spectra of well-defined reference materials are presented for comparison to support the results found with SIMS.

2.2 Experimental

2.2.1 Instruments

The static SIMS experiments were performed on a Physical Electronics (Eden Prairie, MN) TRIFT-II time-of-flight SIMS (TOF-SIMS).[16] The surface of the sample was scanned with a 25 keV primary ion beam from an $^{115}In^+$ liquid metal ion gun. The pulsed beam was non-bunched with a pulse width of 20 ns, a current of 60 pA and the spot size of ~ 120 nm. The primary beam was rastered over a 250 x 250 μm sample area, divided into 256 x 256 pixels. The measurements in both positive and negative mode were made, each with a total primary ion dose of 7.2 x 10^{10} ions/cm^2, well within the static SIMS regime.[2] The surface of the sample was charge compensated with electrons pulsed in between the primary ion beam pulses. To prevent large variations in the extraction field over the large insulation surface area of the paint cross-section a non-magnetic stainless steel plate with slits (1 mm) was placed in top of the sample. The paint cross-section (150 x 50 x 3 mm) was rinsed in hexane to reduce contamination of poly (dimethyl siloxanes).

A 15KeV $^{115}In^+$ primary ion beam was used for the reference samples, with primary ion pulses that were compressed (bunched) to ~1 ns to obtain a better mass resolution. These experiments were performed with 600 pA beam current with a total primary ion dose of 1.0 x 10^{12} ions/cm^2. All these measurements were charge compensated with electrons pulsed in between the primary ion beam pulses.

The dark field reflected light microscopic images were obtained on a Leica DMRX microscope (Leica, Wetzlar, Germany). Normal light was provided by a 100 W Halogen projection lamp. Images were recorded with a Nikon digital still camera DXM1200 (Nikon Instech Co., Ltd., Japan).

The Bio-Rad Stingray (Bio-Rad, Cambridge, MA), combining the Bio-Rad FTS-6000 spectrometer equipped with a Bio-Rad UMA 500 infrared microscope with a 64 x 64 mercury-cadmium telluride (MCT) focal plane array camera was used to record the FTIR-images.[17] Analysis of the embedded cross-section was carried out in reflection mode recorded with a 16 cm^{-1} spatial resolution, a step scan frequency of 1 Hz, and an UDR of 4. The reflection measurements were corrected by the Kramers-Krönig transformation.[18]

Scanning electron microscopy studies in combination with energy dispersive X-ray analysis (SEM-EDX) were performed on a XL30 SFEG high-vacuum electron microscope (FEI, Eindhoven, The Netherlands) with EDX system (spot analysis and elemental mapping facilities) from EDAX (Tilburg, The Netherlands). Backscattered electron images of the cross-sections were taken at 20 kV acceleration voltage at a 5 mm eucentric working distance and a spot size of 3 that corresponds to a beam diameter of 2.2 nm with current density of ~ 130 pA. EDX analysis was performed at a spot size setting of 4 (beam diameter 2.5 nm and current density 550 pA) to obtain a higher count rate and at an acceleration voltage of 22 kV. EDX Mapping parameters were: 512 x 400 matrix, 1028 frames, 70 µs dwell time and 35 µs amplitude time. Samples were carbon-coated to improve surface conduction in a CC7650 Polaron Carbon Coater with carbon fibre (Quorum Technologies, East Sussex, UK).

2.2.2 Samples

The paint sample (A166/1b) obtained by Van Asperen de Boer from the virgin's blue robe from the panel painting *The Descent from the Cross* was embedded in Technovit® 2000LC (Heraeus Kulzer, Germany) and dry polished with Micro-mesh® polishing cloths (final step, 12 000 mesh) (Scientific Instruments Services Inc., Fridley, MN). The following references were used: The lead white-containing linseed oil paint (ZD) was prepared by Carlyle in 1999 in the course of the Dutch national MOLART project (Molecular Aspects of Ageing of Painted Art) in our institute using freshly pressed linseed oil (linseeds provided by MACOS bv., Swifterbant, The Netherlands) mixed with Dutch stack process lead white (loodwit Schoonhoven de Kat, in stock at MOLART).[19] The paint was applied to Melinex sheets and kept under ambient conditions. A 3-year-old paint sample taken from these sheets in 2002 was analysed by SIMS and other techniques.

The reference binding media of the lead white-containing egg tempera paint was prepared according to the method of van den Brink *et al.*;[20] the lead white was obtained from Aldrich (Sigma-Aldrich Chemie GmbH). The egg tempera paint was applied to

Melinex films and light aged for 64 days using Philips TLD94 58-W fluorescent daylight tubes in the Tate Gallery ageing box.[21] The paint was kept in the dark and oxygen free afterwards. A tiny paint sample taken from the Melinex sheets was attached to a glass substrate and analysed.

Stearic acid (Sigma-Aldrich Chemie GmbH) was pressed into a tablet using a high power KBr pellet press. Tripalmitin (Sigma-Aldrich Chemie GmbH) was dissolved in a mixture of ethanol (Biosolve) and dichloromethane (Fluka) (3 : 7) and dropped onto a silicon substrate. After evaporation of the solvents the tripalmitin was measured with SIMS.

2.3 Results and discussion

2.3.1 Analysis paint cross-section by light microscopy, imaging-FTIR and SEM/EDX

Light microscopy and imaging-FTIR give a first approximation of the composition of the paint cross-section A166/1b. Seven layers in the paint cross-section can be distinguished in the light microscopic image of A166/1b (Fig. 2.1). Below the varnish layer (7-12 µm; layer 7) situated at the top of the cross-section, three paint layers can be discerned. The upper paint layer is a clear blue layer with dark blue ultramarine particles in a white matrix (36-54 µm; layer 6). The second paint layer consists of a grayish-blue layer with dark blue ultramarine and some unknown red particles in a white matrix (54-60 µm; layer 5). The third and lowest paint layer, a light blue underpaint, contains greenish-blue azurite and small red particles in a white matrix (36-42 µm; layer 4). A thin cream–light brown intermediate layer with unidentified black and brown particles is present below the three paint layers (6 µm; layer 3). Then a very thin brownish-black layer, most likely representing an underdrawing is visible (1-2 µm; layer 2). Finally, a thick white coloured layer (168-186 µm) is observed, representing the chalk ground (layer 1).

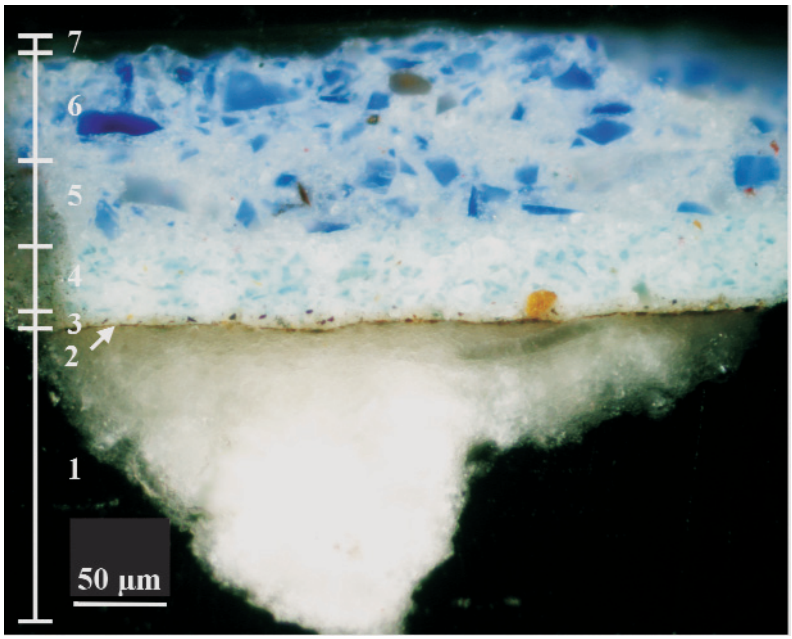

Fig. 2.1 Light microscopic image of paint cross-section van der Weyden (A166/1b); seven layers in this paint cross-section can be distinguished and are numbered from top to bottom (layers 1-7) (see coloured version at the end of this thesis).

There is sufficient resolution to discriminate the main paint layers (1, 4, 5 and 6) by reflection imaging-FTIR (Fig. 2.2). The image at 1706 cm^{-1} (carbonyl vibration) in figure 2.2a represents the embedding medium and outlines the paint cross-section. Images around 1400 cm^{-1}, see figure 2.2b and c, correspond to carbonate stretching vibrations, which are present in the chalk ground layer (layer 1), in the light blue azurite layer (layer 4) and in lower intensities in the darker blue ultramarine layers (layer 5 and 6). Depending on the position in the image, the maximum of the intense carbonate peak has a slight shift from 1419 to 1386 cm^{-1}. By imaging the peak at the different maximums it is possible to discern in the ground layer a higher contribution at the maximum at 1419 cm^{-1} (Fig. 2.2b) representative for the carbonate present in chalk ($CaCO_3$). At a maximum of 1386 cm^{-1} (Fig. 2.2c) a high intensity homogenously distributed carbonate is detected in layer 4, which is assigned to the carbonate group in azurite ($2CuCO_3 \cdot Cu(OH)_2$) and lead white ($2Pb(CO_3) \cdot Pb(OH)_2$). Layer 5 and 6 show a lower carbonate intensity distribution at 1386 cm^{-1} except on the position of the ultramarine particles where no intensity is visible. These carbonate-containing areas correspond to the lead white matrix. The different maximums of the carbonate peak (chalk versus lead white and azurite) can be explained as a difference in the binding of specific counter ions in the carbonate structure of the pigment particles. In the two upper paint layers "hot" spots of silicon-oxygen vibrations

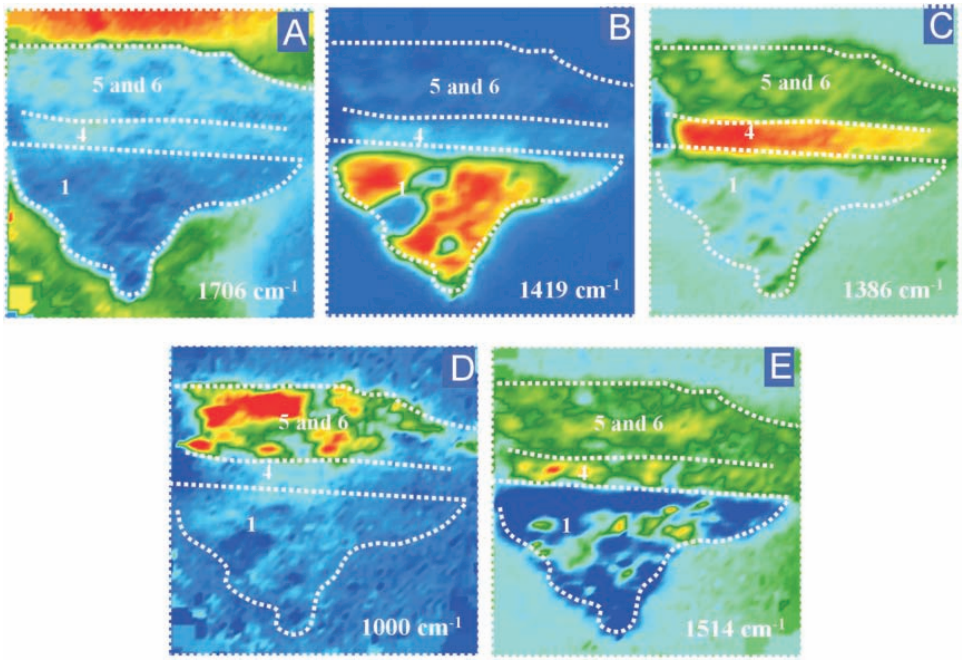

Fig. 2.2 Reflection FTIR-images; false colour images. Red represents a high absorption; FTIR-image (a) at 1706 cm^{-1} represents the embedding medium, (b) at 1419 cm^{-1} and (c) at 1382 cm^{-1} show the presence of carbonates. The FTIR-image (d) at 1000 cm^{-1} images the silicon-oxygen vibration and (e) at 1514 cm^{-1} the asymmetric vibration of lead carboxylate. The layers (1, 4, 5 and 6), which can be discerned, are indicated in the images (see coloured version at the end of this thesis).

at 1000 cm^{-1} are visible, which outline the silicate containing ultramarine particles (Fig. 2.2d). The three paint layers (layer 4-6) show an almost homogeneous distribution of the asymmetric vibration of metal carboxylates, at 1514 cm^{-1} (Fig. 2.2e), which is characteristic for a mature aged oil medium.[22]

The layer buildup and elemental composition was further examined by backscattered electron (BSE) imaging and elemental mapping using X-ray microanalysis (EDX). Figure 2.3 depicts a thumbnail picture of light microscopic image, the BSE-image and elemental maps of Na, Pb, Cu and Ca. The measured area for EDX analysis is outlined in the light microscopic image and the scanned area for the SIMS measurement is illustrated in the BSE-image (Fig. 2.3a and b). The layers observed by light microscopy (layers 1, 3-7) and their pigment particles can clearly be distinguished in the BSE-image due to variations in emission intensity of the electrons back-scattering from the different elements. The elemental maps presented in Figure 2.3 are illustrative for the main elements present in the various layers. The distribution of the sodium plotted in Figure 2.3c correlates exactly with the blue ultramarine particles present in the layers 5 and 6. Figure 2.3d illustrates the lead distribution in the layers 3-6. The lead is equally distributed over the four layers and correlates with the lead white matrix. No lead is detected at the position of the

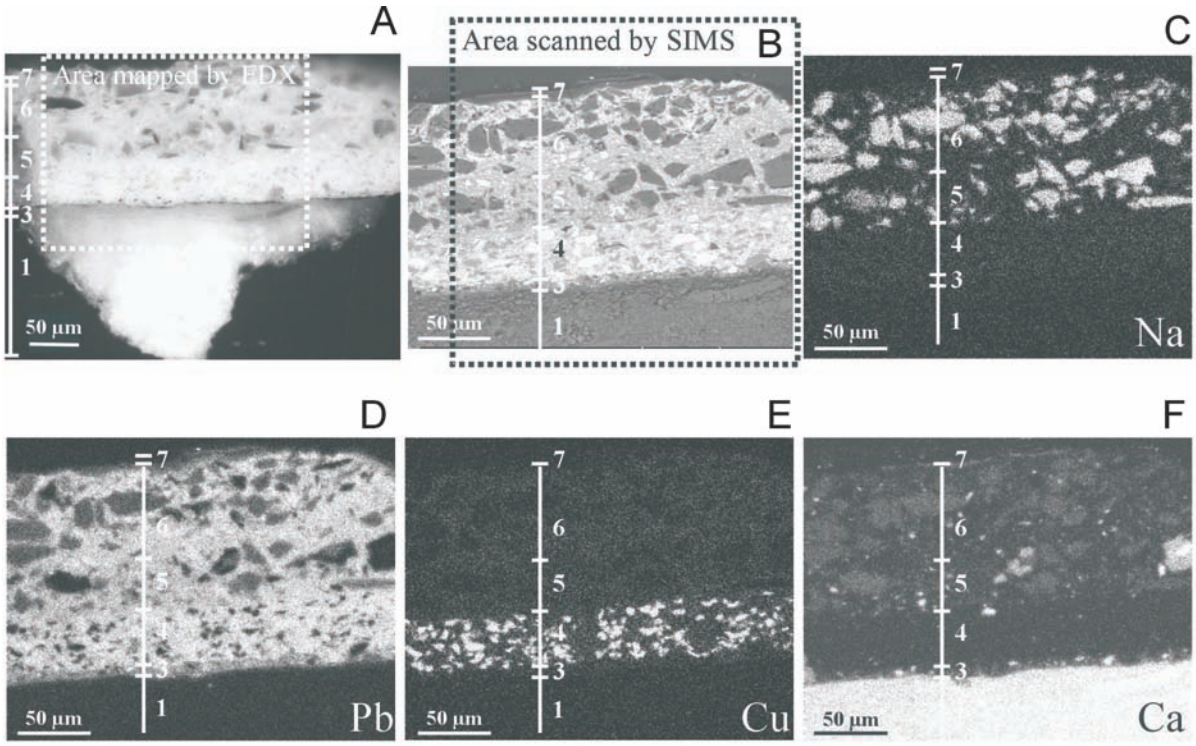

Fig. 2.3 (A) Light microscopic image of paint cross-section van der Weyden (A166/1b) with a square indicating the measured area for the backscattereded image and X-ray maps; (B) backscattered electron (BSE) image of paint cross-section van der Weyden (A166/1b) with a square outlining the scanned SIMS area; (C-F) X-ray maps of sodium (C), lead (D), copper (E) and calcium (F).

coloured pigment particles. EDX analysis demonstrates small "hot" spots of copper in layer 4, which match with the small light blue azurite particles in this layer (Fig. 2.3e). The X-ray map of calcium shows an intense homogenous calcium distribution in layer 1, whereas in layer 5 and 6 low calcium intensities are observed at the position of the ultramarine particles (Fig. 2.3f). A more detailed discussion of the significance of the elemental distribution maps in the cross section will be presented below in the section on SIMS images.

2.3.2 Spectral SIMS information of paint cross-section and reference materials

Figure 2.4a shows a set of relevant partial positive ion SIMS spectra of the paint cross-section and Figure 2.5a-d partial positive ion SIMS spectra of the reference samples of the lead white-containing linseed oil paint, tripalmitin, stearic acid and lead white-containing egg tempera paint. The data were obtained under conditions of a gliding scale of mass resolutions ($m/\Delta m$ from 600 to 1500 over the range of m/z 12 to 2000 amu). The spectra are presented as nominal mass plots. Higher resolution spectral data in the mass ranges corresponding to aluminium, copper, calcium and iron were selected manually for imaging in order to minimize spectral overlap with peaks from organic fragment ions. Data on elemental composition in the positive SIMS spectrum of the paint cross-section, which are characteristic for the pigments observed in the light microscopic image, are sodium (m/z 22.99), aluminium (m/z 26.98), copper (m/z 62.93), lead (m/z 207.98), calcium (m/z 39.96) and iron (m/z 55.94) (Fig. 2.4a). In the lead-containing samples clusters of lead (m/z 208 and 416), lead oxides (m/z 225, 432, 656, 880, 1104, 1328) and lead hydroxides (m/z 449, 673, 897, 1121, 1345) ($PbOH^+$, $Pb^+_xO_{x-1}$, $Pb_xO_xH^+$; x = 1-6) were detected (Fig. 2.4a and Fig. 2.5a,d). Characteristic peaks representative of the binding media in the paint cross-section in positive SIMS were lead soaps of palmitic (m/z 461-463) and stearic acid (m/z 489-491) (Fig. 2.4a). The distribution of the elements in the paint cross-section will be discussed in the section *SIMS images of the spatial distribution of paint characteristics*.

Positive ion peaks characteristic of oil paint are also observed in the lead white oil reference paint sample (Fig. 2.5a). Additional fatty acid lead soaps detected in this oil paint sample are the azelaic acid mono lead soap (m/z 393-395) and an acylium ion representing water loss from this molecule (m/z 375-377). Other characteristic peaks of oil paint in this sample are monoacylglycerols of palmitic and stearic acid (m/z 313 and 341), diacylglycerols (m/z 551, 579 and 607), protonated palmitic and stearic acid (m/z 257 and 285) and their acylium ions (m/z 239 and 267) (Fig. 2.5a). Characteristic positive ion peaks for the reference samples of tripalmitin (Fig. 2.5b), stearic acid (Fig. 2.5c) and the egg tempera reference paint (Fig. 2.5d) are respectively, the monoacylglycol cation (m/z

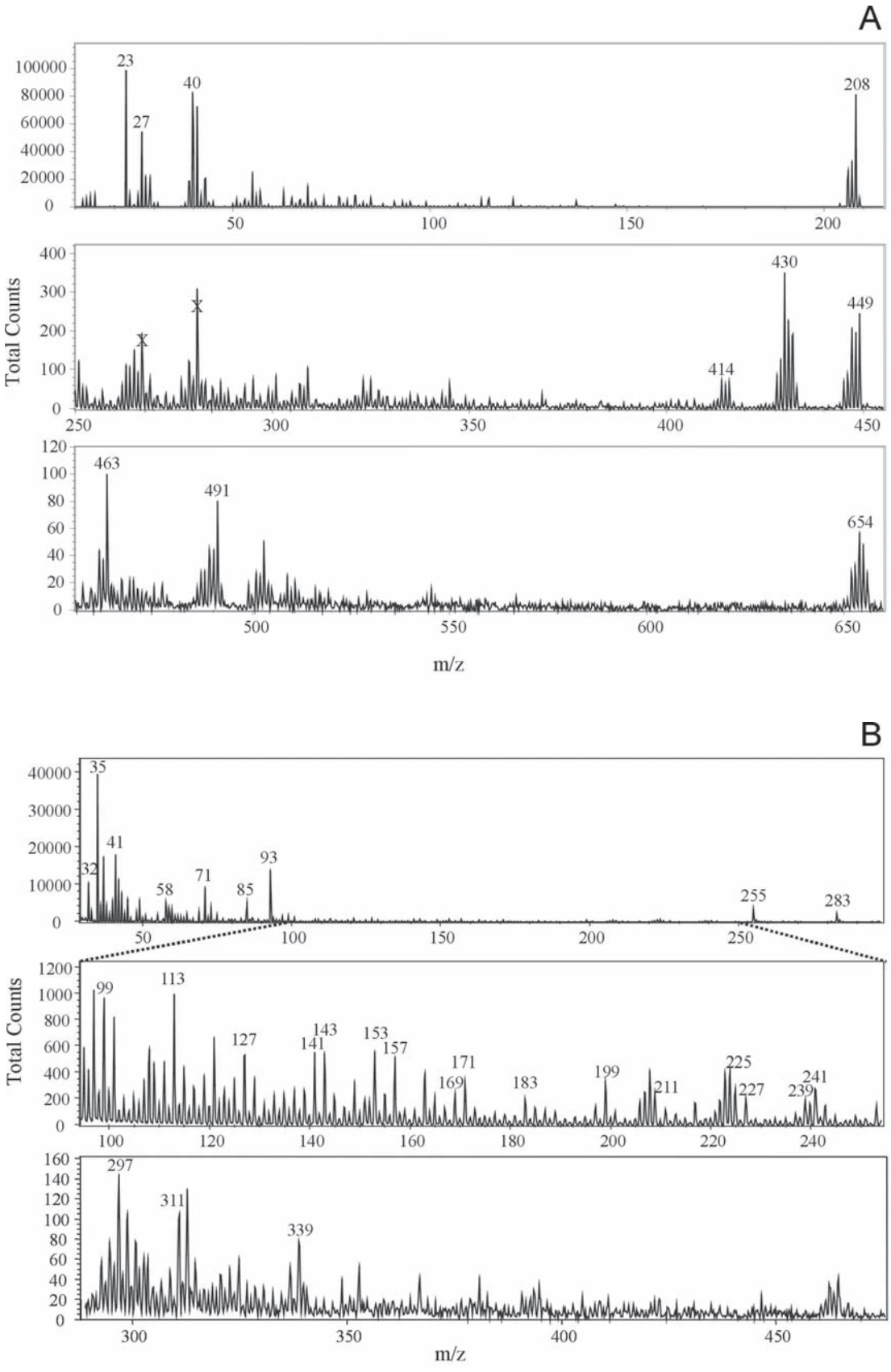

Fig. 2.4 Set of relevant SIMS spectra of paint cross-section van der Weyden (A) positive ion mode (X = poly (dimethyl siloxane) contamination); (B) negative ion mode.

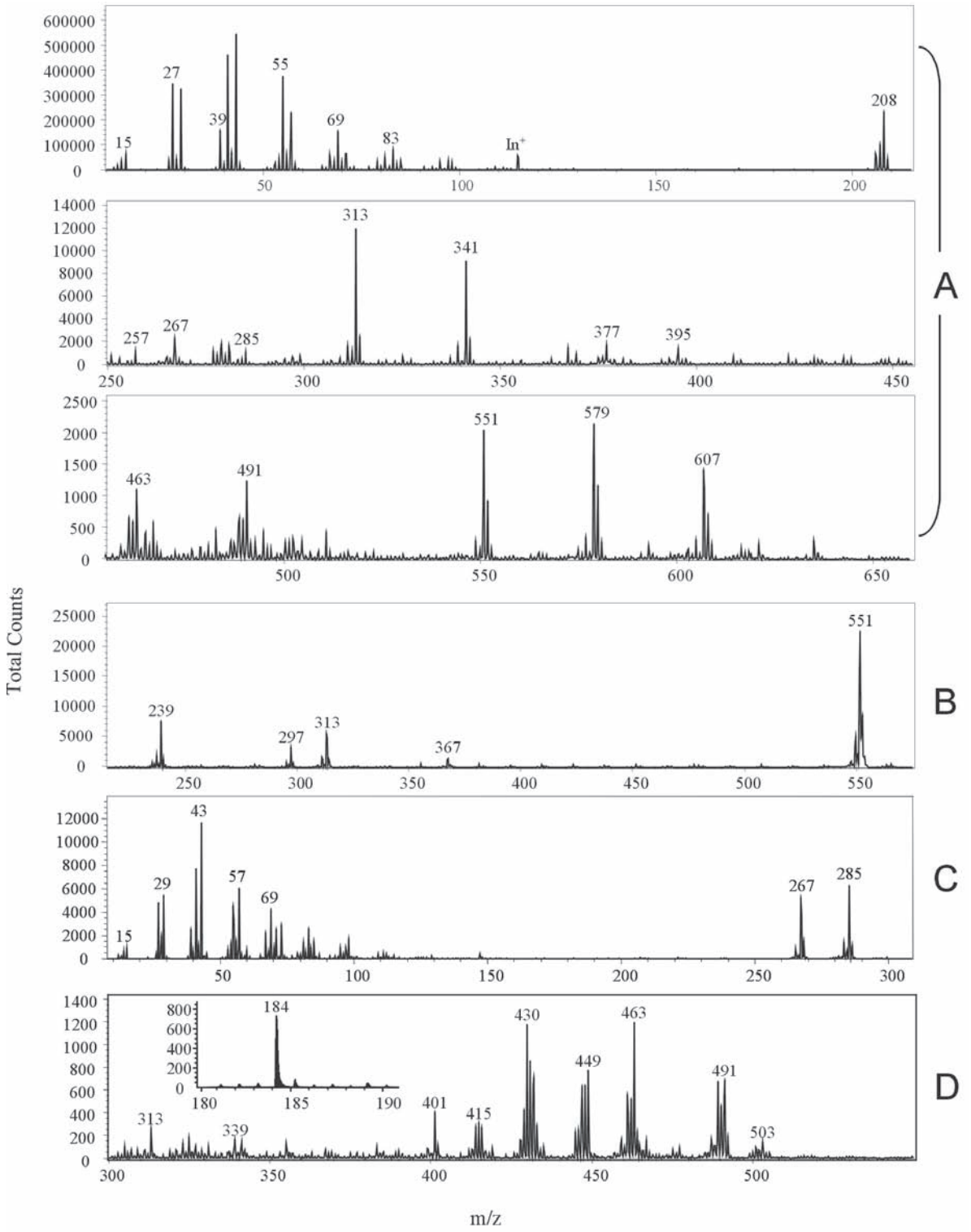

Fig. 2.5 SIMS spectra in positive mode of reference materials: (a) lead white-containing oil paint; (b) tripalmitin; (c) stearic acid; (d) lead white-containing egg tempera paint.

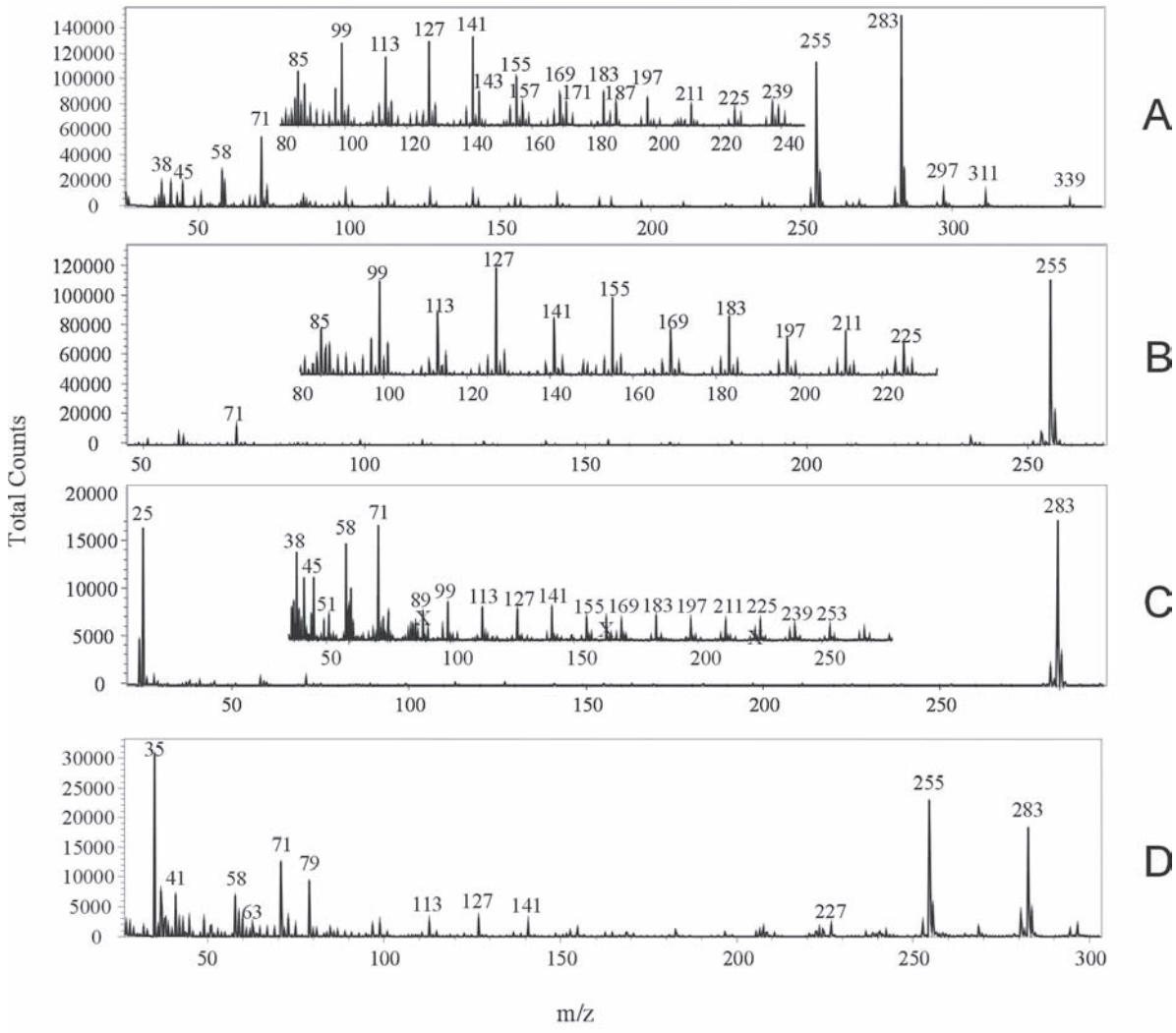

Fig. 2.6 SIMS spectra in negative ion mode of reference materials; (a) lead white-containing oil paint; (b) tripalmitin; (c) stearic acid; (d) lead white-containing egg tempera paint (X = poly (dimethyl siloxane) contamination).

313) and the acylium ion of palmitic acid (*m/z* 239) for tripalmitin, the protonated stearic acid (*m/z* 285) and the acylium ion of stearic acid (*m/z* 267) for stearic acid and protonated palmitic and stearic acid, phosphocholine (*m/z* 184) and protonated ketocholesterol (*m/z* 401)[27, 28] for the egg tempera paint.

Figure 2.4b illustrates relevant parts of the negative ion SIMS spectrum of the paint cross-section and Figure 2.6a-d illustrates partial negative ion spectra of the reference samples where in all the cases deprotonated fatty acids are the main detectable constituents. In the negative SIMS spectrum of the paint cross-section (Fig. 2.4b) ions indicative of elements and fragments such as chlorine (*m/z* 34.97), sulphur (*m/z* 31.97), carbonate (*m/z* 59.98) and clusters of lead oxides (*m/z* 224, 240) and lead hydroxides (*m/z* 463, 687, 911, 1135, 1359) (PbO^-, $PbO{\cdot}O^-$, $(PbO)_x{\cdot}OH^-$; x = 1-6) are observed. The paint cross-section shows a series of deprotonated fatty acids $[M\text{-}H]^-$ (*m/z* 283, 255, 241, 227,

199, 185, 171, 157, 143) in different relative proportions. The negative SIMS spectrum of the oil paint (Fig. 2.6a) shows deprotonated palmitic and stearic acid (*m/z* 255 and 283), deprotonated azelaic acid (*m/z* 187), deprotonated octanoic, nonanoic and decanoic acid (*m/z* 143, 157 and 171) and fragment ions of fatty acids (*m/z* 239, 225, 211, 197, 183, 169, 155, 141, 127, 113, 99, 85, 71). The SIMS spectrum of tripalmitin (Fig 2.6b) shows, in addition to the molecular ion peak, deprotonated palmitic acid (*m/z* 255) and the ion pattern of fragments of the fatty acid (*m/z* 239, 225, 211, 197, 183, 169, 155, 141, 127, 113, 99, 85, 71), whereas in the stearic acid SIMS spectrum (Fig. 2.6c), the molecular ion peak of stearic acid dominates (*m/z* 283). In the negative SIMS spectrum of egg tempera paint (Fig. 2.6d), palmitic and stearic acid (*m/z* 255 and 283) and deprotonated myristic acid (*m/z* 227) (present in a higher concentration compared to the vegetable oils) are observed.

2.3.3 Binding media components visible by SIMS in the paint cross-section

In the negative SIMS spectrum of the van der Weyden paint cross-section (Fig. 2.4b), shorter-chain fatty acids with 8, 9 and 10 carbon ($^{-}OOC(CH_2)_6CH_3$, $^{-}OOC(CH_2)_7CH_3$ and $^{-}OOC(CH_2)_8CH_3$) (*m/z* 143, 157 and 171) are detected in addition to the deprotonated palmitic and stearic acids. Observed ions of fatty acids with a chain length of 11, 12, 14 and 15 carbons (*m/z* 185, 199, 227 and 241) have a lower intensity, as compared to the peaks ascribed to fatty acids with an 8, 9 and 10 hydrocarbon chain length. These short-chain fatty acids are not a result of fragmentation of palmitic or stearic acids, which is confirmed by the absence of these fatty acids ions in reference spectra of pure stearic acid or tripalmitin (Fig. 2.6b, c). Note that the cross-section and the reference SIMS spectra were taken under different experimental conditions (beam energy and current); however, the fragmentation pattern and relative intensities for the reference materials under the two experimental conditions were comparable.[23] The short-chain fatty acids with 8, 9 and 10 carbons are normally not a constituent of the fresh oil, but are formed during the oxidation and chemical drying. They are degradation products of hydroperoxide intermediates of the unsaturated fatty acids that have been thoroughly identified with conventional mass spectrometry techniques in other samples.[9] The same three fatty acids were present in the spectrum of a naturally aged lead white-containing oil paint (Fig. 2.6a). This significantly aged oil paint sample has passed the stage of curing, and oxidative degradation products have formed.

Aliphatic chain fragment ions of fatty acids with a mass increment of 14 amu are observed in the negative reference spectra (*m/z* 239, 225, 211, 197, 183, 169, 155, 141, 127, 113, 99, 85, 71) (Fig. 2.6a). These ions are derived from the precursor ion, deprotoned fatty acid ($R\text{-}COO^{-}$), and are formed by a thermally driven charge-remote reaction.[24] In this fragmentation process H_2 is split off and the remaining negatively charged

fragments are of the type $C_2H_3(CH_2)_xCOO^-$. The cleavage occurs on every position of the chain and the fragmentation starts at *m/z* 253 for the palmitic acid precursor ion and at *m/z* 281 for stearic acid. In both cases the lowest *m/z* fragment, *m/z* 71, corresponds to $C_2H_3COO^-$ (Fig.2.6a). A pattern of ion peaks similar to that of the $C_2H_3(CH_2)_xCOO^-$ type (same *m/z* values) is observed in the spectrum from the cross-section of the van der Weyden sample (Fig. 2.4b). These ion fragments are less specific, but provide supporting evidence for an oil-containing binding medium. Another indication of the original presence of oil paint in the paint cross-section is that the fragments *m/z* 311 and 339 are detected in the negative spectrum (Fig. 2.4b). These negative ions, assigned to monoacylglycerols of palmitic and stearic acids, are present in the negative spectra of the lead white -containing oil paint sample and the van der Weyden paint cross-section (Fig. 2.6a and 2.4b).

The reference spectra show that the free or ester-bound nature of palmitic and stearic acid can be determined with SIMS. The positive spectrum of the triacylglycerol (tripalmitin), which consists of ester-bound fatty acids, shows no protonated fatty acids but only acylium ions (*m/z* 239) (Fig. 2.5b). The positive spectrum of the free fatty acid (stearic acid) shows the ion of the protonated molecular ion and the acylium ion (*m/z* 267) in the same relative intensity (Fig. 2.5c). The intensity of the protonated fatty acids and their acylium ions in the positive SIMS mass spectrum can be used to provide an indication of the relative amount of ester-bound and free fatty acid in the oil paint. Remarkably, these ions are not present in the positive spectrum of the paint cross-section, which implies that there are neither free nor ester-bound fatty acids present (Fig. 2.4a). Palmitic and stearic acid are only detectable in the paint cross-section in the negative ion mode as $(M-H)^-$ (*m/z* 255 and *m/z* 283) (Fig. 2.4b). This observation is not unexpected, however, and matches the composition of a mature ionomeric oil paint system, where a low content of free and ester-bound fatty acids and higher abundance of fatty acid metal soaps are expected. Indeed, lead soaps of palmitic and stearic acid are the only observed components characteristic of the oil-containing binding medium observed in the positive spectrum of the van der Weyden paint cross-section. These fatty acid lead soaps are always observed in lead-containing mature oil paints.[23] The inference that the paint cross-section consist of an ionomeric oil paint system with a low content of free and ester-bound fatty acids is supported by the results from FTIR, showing the presence of metal carboxylates and SIMS reference data on stearic acid lead soap. In the positive SIMS spectrum of stearic acid lead soap,only the stearic acid lead soap (*m/z* 489-491) is detected, and the ions of protonated stearic acid and its acylium ion are absent. Ions of deprotonated stearic acid and ions with the fragmentation pattern $C_2H_3(CH_2)_xCOO^-$ are detected the negative mass spectrum (spectra not shown).

The vegetable origin of drying oils - linseed, walnut or poppy seed oil - is distin-

guished in the technical art history studies of paintings on the basis of the relative amounts of palmitic and stearic acid in paint samples using GC/MS of the methyl esters after wet chemical workup.[25] A palmitate/stearate (P/S) ratio < 2 suggests linseed oil, a ratio of > 5 points to poppy seed oil and the intermediate ratio can be assigned to walnut, poppy seed oil or mixtures.[25] The negative SIMS ions from palmitic (*m/z* 255) and stearic acid (*m/z* 283) in our data on the van der Weyden paint cross-section were used to calculate the palmitic/stearic acid ratio directly. The overall average P/S ratio of 1.7 corresponds to the use of linseed oil as binding medium. The P/S ratio of the naturally aged lead white reference oil paint made with linseed oil was 0.9 (this ratio changed to 1.4 after accelerated ageing). The P/S ratio was also calculated for each of the paint layers. The upper ultramarine layers show ratios of 1.3 (layer 6) and 1.4 (layer 5). The azurite layer (layer 6) shows a P/S ratio of 1.8. This is the first time that such ratios can be derived in a spatially resolved manner.

Proteinaceous components either as tempera or as a dispersed phase in oil have been shown by staining techniques to exist in other Early Netherlandish painting.[26] This possibility was explored by analysis of egg tempera paint as reference to extract possible SIMS mass spectral features. Egg tempera paint is a water-based paint made with egg yolk and egg whites and thus contains proteins, triacylglycerols, phospholipids and cholesterol.[15] Oil- and egg-based media both have triacylglycerols as common ingredient and this makes egg-oil mixtures more difficult to characterise using traditional methods. Egg lipids are relatively saturated (< 15% poly-unsaturated fatty acid moieties) and have a higher relative abundance of myristic acid. In the negative ion spectrum of the lead white-containing egg tempera paint reference (Fig. 2.6d), the most abundant peaks are derived from the triacylglycerols (*m/z* 255 and *m/z* 283 from palmitic and stearic acid). Myristic acid (*m/z* 227) is present in a relatively high abundance, but the smaller fatty acids with an 8, 9 and 10 carbon chain length are not observed. An aspecific ion pattern corresponding of fragments of fatty acids of the type $C_2H_3(CH_2)_xCOO^-$ is an indication of aliphatic lipid-derived moieties in the sample.

Ions indicative of phosphate-containing compounds in the egg tempera paint spectrum are the *m/z* 63 and 79 of PO_2^- and PO_3 in the negative SIMS spectrum, and *m/z* 184, a prominent ion in the positive SIMS spectrum, assigned to the phosphocholine moiety of the phosphatidylcholine in the phospholipid fraction of egg (Fig. 2.5d and 2.6d).[21, 27] Cholesterol is a main compound in egg yolk and thus in tempera paint, but the compound is not preserved and turns into various oxidation products over time.[21] *m/z* 401, a prominent peak in the positive SIMS spectrum in Figure 2.5d, is from protonated ketocholesterol, an oxidation product of cholesterol. No ions indicative for proteins could be detected under our SIMS conditions. Ions indicative of cholesterol or phosphate containing compounds were not detected in the SIMS data of the paint cross-section (Fig. 2.4a and

2.4b).[28] In the absence of these characteristic egg tempera compounds, we conclude that SIMS cannot detect evidence for the use of egg or egg/oil emulsions. However, it is not impossible that SIMS mass peaks characteristic for very old egg tempera are present but remain unrecognised. Further studies are underway to shed more light on this matter.

2.3.4 SIMS images of the spatial distribution of paint characteristics

Six layers can be distinguished in the total positive (TIC+) and negative ion count (TIC-) SIMS image (Fig. 2.7). The layers 1 and 3-7 are clearly visible in the SIMS image, whereas the 1-2 μm layer 2 is presumably not observed due to low ion yields. A contour based on the structure visible in the light microscopic image is plotted over the SIMS images (Fig. 2.7). Elements such as sodium, aluminium, copper, lead, calcium and iron show a characteristic spatial distribution corresponding to specific pigment particles (Fig. 2.7). The negative ions of deprotonated palmitic acid (*m/z* 255) and deprotonated stearic acid (*m/z* 283) and sum of the positive ions palmitic acid and stearic acid lead soaps (*m/z* 461-463 and 489-491) are indicative of the distribution of the oil binding medium in the paint layers (Fig. 2.8).

Sodium and aluminium that have a similar distribution in the paint cross-section show large "hot" spots in layer 5 and 6. The shapes of the "hot" spots correspond with the form and position of the blue ultramarine particles in the light microscope image (Fig. 2.1 and Fig. 2.7). The blue pigment ultramarine has the following general chemical formula $(Na,Ca)_8(AlSiO_4)_6(SO_4,S,Cl)_2$ (*i.e.* the formula representing lazurite a synonym for ultramarine, which is the purified blue mineral extracted from lapis lazuli).

Unfortunately, silicon, another main element in ultramarine, shows an aspecific homogeneous distribution over the whole sample (not shown), due to contamination at the surface of silicones adsorbed from the laboratory environment despite the hexane wash. Sodium gave the best signal for the differentiation of pigment particles with sizes between 1 and 2 μm. The particles in the sodium map have sharp edges and sodium is the characteristic marker for ultramarine. The sodium distribution visualised with SIMS matches the sodium distribution visualised with X-ray analysis (Fig. 2.3c), although the sodium containing particles in the SIMS image are sharper outlined compared to those in the X-ray map. The sodium image visualises the two separate ultramarine layers (layer 2 and 3) very well. Between the two layers, an area lower in sodium yield is present. By overlaying the light microscopic images, we can see that a white matrix is mainly present in this area (not shown). The ultramarine particles are also easily recognizable in the aluminium map, although at a lower intensity, as compared with the sodium map. The intensity of calcium was too low for a good outline of the ultramarine particles (Fig. 2.7); however, the intense calcium spot in the third layer (assigned with an *), which corresponds with the greyish

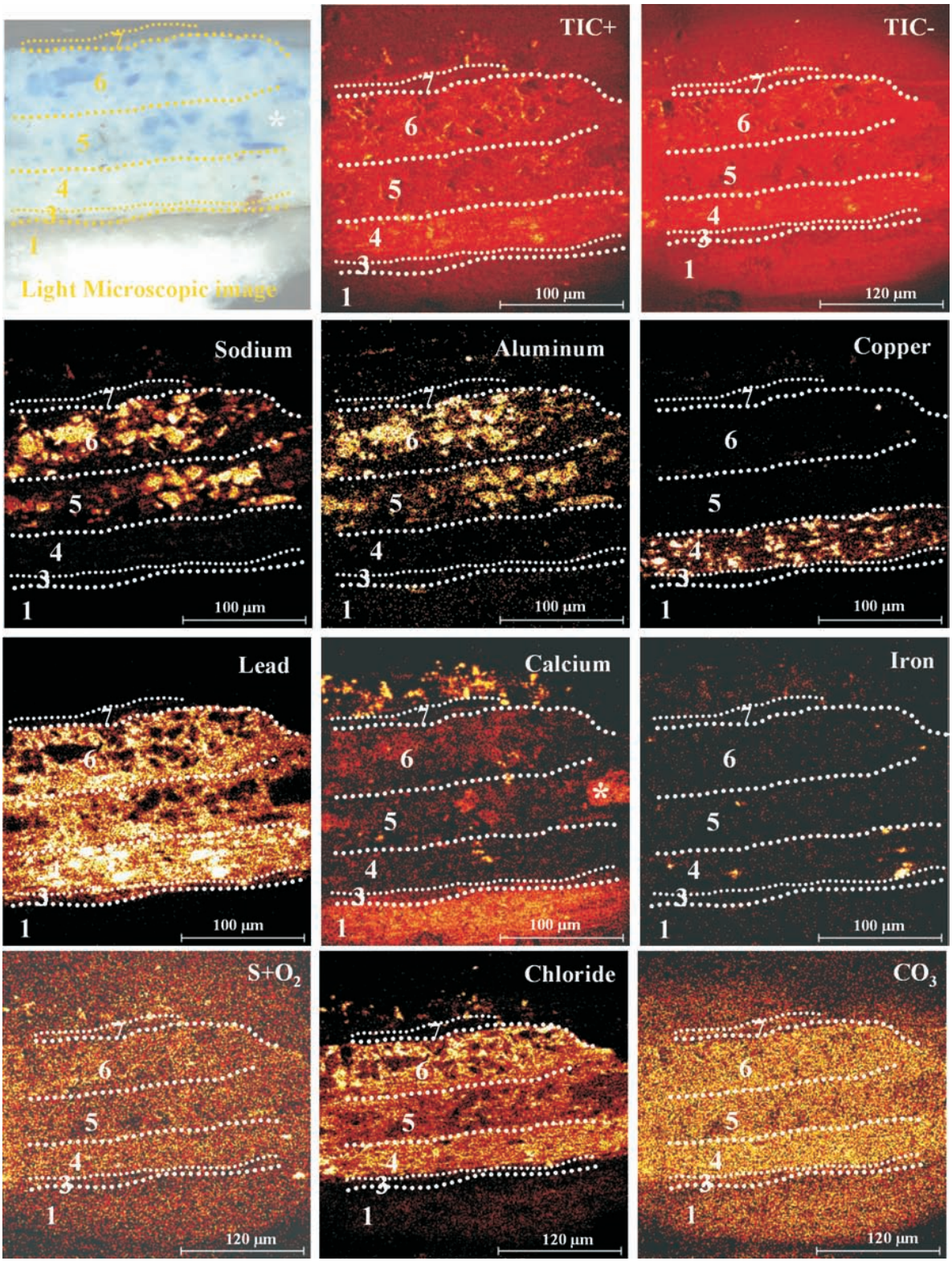

Fig. 2.7 SIMS images showing the spatial distribution of the total ion counts (TIC+ and TIC-), sodium, aluminium, copper, lead, calcium, iron, sulphur, chloride and carbonate detected in the SIMS spectra of the paint cross-section van der Weyden in positive (250 x 250 µm²) and negative mode (300 x 300 µm²). The layers (1, 3-7) detectable with SIMS are indicated in the images. Yellow represents high intensity and black low yields (see coloured version at the end of this thesis).

blue particle in the light microscopic image (also assigned with an *, in Fig. 2.7) originates from a mineral associated with lazurite. Traces of minerals present in ultramarine are calcite ($CaCO_3$), pyroxene ($X_{1-p}Y_{1+p}Z_2O_6$ where X = Ca, Na; Y = Mg, Fe, Mn, Li, Ni, Al, Cr, Ti; Z = Si, Al), pyrite (FeS_2) and other silicates.[30] The impure composition of ultramarine in layer 5 might also be the cause of the greyish appearance of that layer, which contains a high abundance of colourless material, and fewer and smaller blue particles.[31] The sulphur in the ultramarine mineral (S^-, *m/z* 31.97) has a low intensity in the mass spectrum, and moreover the sulphur peak overlaps with O_2^- (*m/z* 31.99) (Fig. 2.7). Therefore, the sulphur image does not give recognisable positional information on the ultramarine particles. This is also true for chlorine (Cl^-) in the ultramarine mineral (Fig. 2.7). On the other hand, chlorine is homogeneously and intensely distributed between the ultramarine particles. It is present mainly in the three top layers and follows the lead map. At present, little is known about chlorine in paints although it is regularly found to be associated with lead white-containing paints.[32]

Copper is only located in layer 4 as finely divided small "hot" spots. The position of the copper corresponds with the location of the small light greenish blue azurite particles ($2CuCO_3 \cdot Cu(OH)_2$) in the visual light image (Fig. 2.1 and Fig 2.7). The size and distribution of copper "hot" spots in the SIMS image corresponds accurately with the X-ray map of copper (Fig 2.3e). An ion corresponding to CO_3^-, *m/z* 59.9 is equally distributed over the whole paint cross-section, which suggests that is originates from a common chemical functional group in the paint layers (Fig. 2.7). Indeed, the FTIR image in Fig. 2.2c shows a high intensity carbonate vibration of azurite in this layer.

Lead shows a more-or-less homogeneous distribution in layer 3-6 (Fig. 2.7). The lead map of layer 5 and 6 reveals large gaps at the positions of ultramarine particles and small gaps at the positions of the azurite in layer 4. Additionally, layer 4 also contains small "hot" spots of lead, which correspond to the white particles in this layer. Mapping of the lead cluster ions follows the distribution of the lead map. The lead corresponds with the white areas (and small white grains) around the blue pigment grains observed in the visual light image (Fig. 2.1 and Fig 2.7). This points to the presence of lead white ($2Pb(CO_3) \cdot Pb(OH)_2$). The FTIR images confirm the presence of a carbonate moiety in layer 4-6 (Fig. 2.2c). The lead X-ray map has similar distribution and sharpness compared to the SIMS image of lead (Fig. 2.3d). In both images (X-ray map and SIMS image) the intensity of lead in layer 3 is low compared to the layers on top of it. Only layer 4 shows a difference between the X-ray map and SIMS image. The SIMS image shows lead "hot" spots corresponding to lead white particles whereas the X-ray map reveals a more uniform intensity distribution. Another difference visible in layer 4 is the sharper outlining of the azurite particles in the X-ray map where lead is absent. This phenomenon is less obvious in the SIMS image.

Calcium is mainly present in layer 1, the ground layer, but the calcium map also shows some "hot" spots towards the top of the image (Fig. 2.7). These "hot" spots lie outside the paint cross-section and their origin is not clear. The calcium-rich areas in layer 5 and 6, which partially overlap with the sodium and aluminium distribution correspond to the ultramarine particles that have been discussed above. The calcium in the ground layer points to a chalk ground ($CaCO_3$). The carbonate moiety is observed with SIMS (ion at *m/z* 59.9) and FTIR-imaging proves the presence of carbonate at a maximum of 1419 cm^{-1} (Fig. 2.2b). The correlation between the distribution of the calcium in the X-ray map and the SIMS image is compatible. Images from both techniques show a high intensity in layer 1 (Fig. 2.3f and 2.7). The calcium X-rays portray the ultramarine particles present in layer 5 and 6 better than SIMS.

The iron map shows a few "hot" spots, mainly positioned in layer 4 (Fig. 2.7). The position of these spots overlap with the few orange-red particles seen in the light microscopic image. This suggests the presence of an iron oxide (a peak indicative of FeO, *m/z* 71.92, is present in the positive ion spectrum).

The ions of deprotonated palmitic acid ($(^-OOC(CH_2)_{14}CH_3)$, *m/z* 255), deprotonated stearic acid ($(^-OOC(CH_2)_{16}CH_3)$, *m/z* 283) and palmitic acid lead soap ($Pb^{2+}[^-OOC(CH_2)_{14}CH_3]$, *m/z* 460-463)) are present in layers 4-6 (Fig. 2.8). These ions are not detected in the ground (layer 1) or in intermediate layers (layer 3). Since the binding medium is present as a coating on the pigment particles, their constituent fatty acids are not so sharply outlined in the images as the crystalline mineral particles. The contrast in these images is also poor due to the relatively low intensity of these ions under our static SIMS conditions. The distribution of palmitic and stearic acid overlay with the lead distribution and show a higher intensity in the lead "hot" spots in layer 4 and lower intensities in the areas of the blue ultramarine pigment particles in layers 5 and 6. A similar distribu-

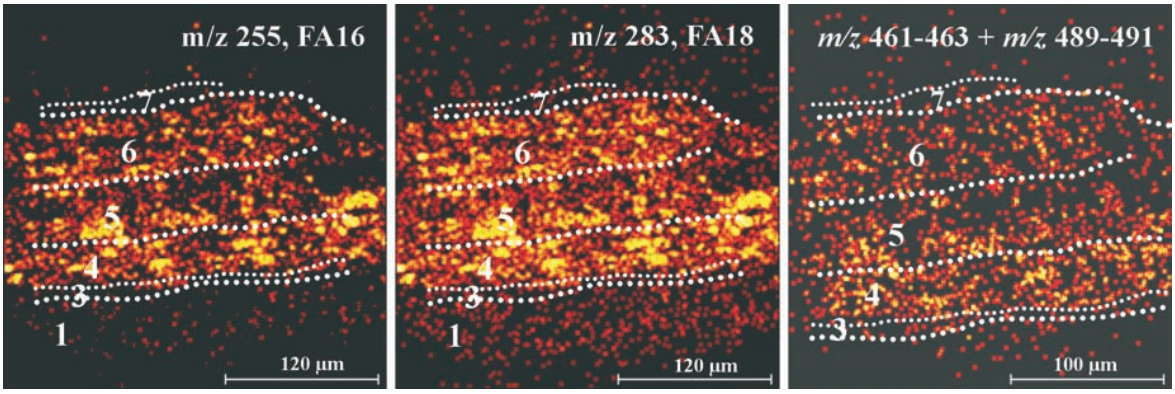

Fig. 2.8 SIMS images showing the spatial distribution of deprotonated palmitic acid (m/z 255) and stearic acid (m/z 283) and a sum image of palmitic and stearic acid lead soap (m/z 461-463, 489-491) (see coloured version at the end of this thesis).

tion pattern can be seen for the palmitic and stearic acid lead soaps, although a precise correlation cannot be observed visually due to low intensity of the ions. The strong correlation of the fatty acids and lead is often observed in our studies of paint cross-sections.[23] We suggest that fatty acids derived from oleaginous aged binding medium are highly concentrated at the surface of lead white grains and have reacted there to form fatty acid lead soaps. On the other hand, it cannot be ruled out at present that the secondary ion yield of organic constituents is boosted by an interaction of the indium primary ions with the lead in the lead white mineral matrix nearby. This quantitative aspect requires further fundamental study and higher-resolution SIMS imaging studies.

The presence of a fatty acid lead soap in the three paint layers (4, 5 and 6) is supported by the imaging-FTIR data, which show the presence of the asymmetric vibration peak of metal carboxylates. SIMS and FTIR data therefore point to a mature oil containing binding medium. The absence of fatty acids in layer 1 and 3 could point to different (proteinaceous) media in these layers, but a possible suppression of secondary ion production of fatty acids below the detection limit cannot be ruled out at present. Under our SIMS analysis conditions, it was not possible to obtain information from proteins. It is therefore not possible to preclude the use of an emulsion paint of oil and proteinaceous components for binding of the ultramarine paint layers.

2.4 Conclusions

Static SIMS is a useful additional analytical tool for the identification and localisation of the materials present in precious paint samples. Characteristic ions and elements representative of the pigments and binding medium can be mapped onto an image of the layered cross-section. The resolution obtained matches that of high magnification light microscopy or better. Pigments and constituents of the binding medium can be localised in the paint cross-section, and the position and characteristic shapes of the pigments detected with SIMS correlate accurately with the pigments visible in the light microscopic image. The elemental SIMS images correlate accurately with the elemental X-ray maps. The analyses result in similar distributions and comparable intensities of the elements present in the paint cross-section. In contrast to SIMS, EDX provides no information on the organic constituents.

Binding medium components, such as fatty acids, fatty acid soaps, and ions from aliphatic chains of fatty acid moieties, yield image data that can be used to identify the type of oil and its distribution in the paint. The three oil-containing paint layers in this paint showed slightly varying palmitic/stearic acid ratio ranging from 1.3 to 1.8 indicative of linseed oil. The presence of fatty acid lead soaps of palmitic and stearic acid in the three

upper paint layers point to a mature oil paint, which is confirmed by the imaging FTIR data.

The static SIMS results match the results obtained with the light microscope, imaging-FTIR, and SEM/EDX. The additional value of SIMS is the detailed chemical information obtained on the oil binding medium present in the paint cross-section. SIMS data result not only in specific molecular characterisation of the paint, but also detects the position of the molecules in the multilayered paint system on the microscale.

2.5 Acknowledgements

Prof. J. R. J. van Asperen de Boer is thanked for providing the paint cross-section A166/1b. Dr. Leslie Carlyle and Dr. Oscar van den Brink provided the samples of lead white-containing linseed oil paint and lead white-containing egg tempera paint.

2.6 References

1 J.C. Vickerman, *et al.* In: ToF-SIMS: Surface Analysis by Mass Spectrometry, J.C. Vickerman, D. Briggs (Eds.), IM Publication and Surface Spectra Limited: West Sussex and Manchester, 2001, chapter 18-28.

2 A. Benninghoven, *The history of static SIMS: a personal perspective*, In: ToF-SIMS: Surface Analysis by Mass Spectrometry, J.C. Vickerman, D. Briggs (Eds.). IM Publication and SurfaceSpectra Limited: West Sussex and Manchester, 2001, chapter 1.

3 J. Plesters, *Cross-sections and chemical analysis of paint samples,* Studies in Conservation, 2, 1965, p. 110-157.

4 National Gallery Technical Bulletin, 18, 1997, p. 68-86.

5 J. Dunkerton, S. Foister, D. Gordon, N. Penny, In: Giotto to Dürer; Early Renaissance Painting in The National Gallery, National Gallery Publications Limited, London, 1991, Chapter 5.

6 National Gallery Technical Bulletin, 18, 1997, p. 6-67.

7 J.R.J. van Asperen de Boer, In: Robert Campin, New Directions in Scholarship, S. Foister, S. Nash (Eds.), Brepols, Turnhout, 1996, p. 21-26.

8 H. Wexler, *Polymerization of drying oils*, Chemical Reviews, 64, 1964, p. 591-611.

9 J.D.J. van den Berg, *Analytical chemical studies on traditional linseed oil paints*, PhD Thesis, University of Amsterdam, 2002 (http//www.amolf.nl/publications/theses/).

10 E.N. Frankel, *Analytical methods used in the study of autoxidation processes*, In: Autoxidation in food and biological systems, M.G. Simic, M. Karel (Eds.), Plenum Press: New York, 1980, p. 141-170.

11 E.N. Frankel, In: *Oily press lipid library,* The Oily Press Ltd., Dundee, 10, 1998, p. 55-77.

12 A.E. Rheineck, R.O. Austin, *Drying oils - modifications and use*, In: Treatise on coatings, R.R. Myers, J.S. Long (Eds.), Marcel Dekker, New York, 1, 1968, p. 181-248.

13 Z.W., Wicks Jr., F.N. Jones, S.P. Pappas, *Drying oils*, In: Organic coatings: science and technology, John Wiley & Sons, Inc., New York, 1, 1992, p. 133-143.

14 J.D.J. van den Berg, *Chemical changes in curing and aging oil paints*, 12th Triennial Meeting ICOM-CC, J. Bridgland (Ed.), Lyon 29 August- 3 September, 1999.

15 J.J. Boon *et al.*, *Molecular aspects of mobile and stationary phases in aging tempera and oil paint films*, In: Early Italian Paintings: Techniques and Analysis, T. Bakkenist, R. Hoppenbrouwers and H. Dubois (Eds.), Stichting Restauratie Atelier Limburg (SRAL), Maastricht, 1996, p. 35-56.

16 B. Schueler, *Microscope imaging by time-of-flight secondary ion mass spectrometry*, Microscopy Microanalysis Microstructures, 3, 1992, p. 119-139.

17 E.N. Lewis, *et al.*, *Fourier-transform spectroscopic imaging using an infrared focal-plane array detector*, Analytical Chemistry, 67, 1995, p. 3377-3381.

18 B. Harbecke, *Application of Fourier's allied integrals to the Kramers-Kronig transformation of reflectance data*, Applied Physics A, 40, 1986, p. 151-158.

19 L. Carlyle, *Historical reconstructions of artists' oil paint: an investigation of oil processing methods and the use of medium-modifiers*, Molart Fellowship Report, Ottawa, Canadian Conservation Institute, 2000.

20 O.F. van den Brink, G.B. Eijkel, J.J. Boon, *Dosimeter of paintings; determination of the degree of chemical change in museum-exposed test paintings by mass spectrometry*, Thermochimca Acta, 365, 2000, p. 1-23.

21 O.F. van den Brink, *Molecular changes in egg tempera paint dosimeters as tools to monitor the museum environment*, PhD Thesis, University of Amsterdam, Amsterdam, NL, 2001, (http//www.amolf.nl/publications/theses/).

22 J. van der Weerd, *et al.*, *Chemical changes in old master paintings: dissolution, metal soap forma tion and remineralization processes in lead pigmented paint layers of 17th century paintings,* Zeitschrift für Kunsttechnologie und Konservierung, 16, 2002, p. 35-51.

23 Unpublished Observations

24 C. Cheng, M.L. Gross, *Applications and mechanisms of charge-remote fragmentation*, Mass Spectrometry Reviews, 19, 2000, p. 398-420.

25 M.R. Schilling and H.P. Khaijan, *Gas chromatographic determination of fatty acid and glycol content of lipids I. The effect of pigments and aging on the composition of oil paints*. In: Preprints of the 11th triennial meeting of the ICOM Committee for Conservation. Edinburgh, 1, 1996, p. 242-247.

26 P.W.F. Brinkman, L. Kockaert, L. Maes, E.M.M. Thielen, J. Wouters, *Het Lam Godsretable van Van Eyck. Een heronderzoek naar de materialen en schildermethoden, 2de hoofdkleuren. blauw,*

groen, geel en rood, Bulletin (Institut royal du patrimoine artistique), 22, 1988, p. 26-50.

27 R.C. Murphy, K.A. Harrison, *Fast-atom bombardment mass-spectrometry of phospholipids*, Mass Spectrometry Reviews, 13, 1994, p. 57-75.

28 J.C. Ingram, W.F. Bauer, R.M. Lehman, S.P. O'Connell and A.D. Shaw, *Detection of fatty acids from intact microorganisms by molecular beam static secondary ion mass spectrometry*, Journal of Microbiological Methods, 53, 2003, p. 295-307.

29 J. Plesters, *Ultramarine blue, natural and artificial*, In: Artists' Pigments of their History and Characteristics, A. Roy (Ed.), National Gallery of Art, Washington, vol. 2, 1993, p. 37-42.

30 C. Klein, In: Mineral Science, 22nd ed., John Wiley & Sons, Inc., New York, 2002, p. 556-557.

31 J. Plesters, *Ultramarine blue, natural and artificial*, In: Artists' Pigments of their History and Characteristics, A. Roy (Ed.), National Gallery of Art, Washington, vol. 2, 1993, p. 39.

32 MOLART, unpublished observations

Chapter 3

SIMS studies on oil binding media in paint cross-sections

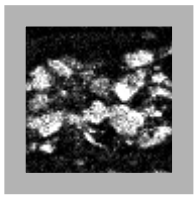

Secondary ion mass spectrometry (SIMS), a relatively novel technique in painting research, was applied to identify and localise of oil binding medium constituents in paint cross-sections. This chapter is divided into three sections: 1) the interpretation of the SIMS spectra, 2) the localisation of organic constituents of oil paint, and 3) the enhancement of the organic ion yields.

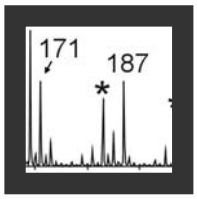

In the first section, three mass spectrometric techniques, SIMS, direct temperature resolved mass spectrometry (DTMS) and gas chromatography/mass spectrometry (GC/MS), are applied for the analysis a natural and accelerated aged linseed oil paint reconstruction. The comparative study facilitated the significance of the ions produced by SIMS and demonstrates the advantages and limitations of oil medium identification with SIMS.

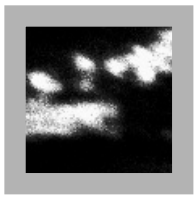

In the second section, the ratio between palmitic and stearic acid (P/S ratio) indicative for the type of oil used in the paints, is determined directly from the paint cross-section by analysis of the negative ions of palmitic and stearic acids. The P/S ratios are determined in test samples and in various layers present in paint cross-sections from 15th- to 19th-century paintings. The positive ion SIMS mass spectrum gives information on the speciation of the fatty acids in free, ester-bound or metal carboxylate form, which is indicative of the drying stage of the oil.

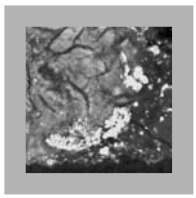

In the third section, the surface of a cross-section is coated with an ultra-thin gold layer, which improves the yields of secondary ions from the fatty acids and diacids. A comparative study of a native and gold-coated surface from an aged linseed oil paint reconstruction demonstrates the enhancement of the yields of organic ions produced by SIMS in a paint cross-section relevant for painting studies.

3.1 Secondary ion mass spectrometry characterisation of traditional oil paint: comparative studies with DTMS and GC/MS

3.1.1 Introduction

Binding medium analysis, on a paint scraping of 10-100 μg, is traditionally carried out with well established mass spectrometric techniques, such as GC/MS and DTMS.[1-5] The disadvantage of analysing a scraping is the loss of the information concerning the spatial distribution of the organic constituents in the multi-layered paint systems. Secondary ion mass spectrometry (SIMS) offers the opportunity to overcome this problem as it is a highly sensitive surface analytical mass spectrometry technique. With this technique the oil binding medium can be identified and localised in a multi-layered paint system by analysing paint cross-sections.[6, 7] SIMS is a relatively new technique in painting research and it is therefore important to compare its analytical information with that from other mass spectrometric techniques such as GC/MS and DTMS. Exact attribution of the mass peaks in the SIMS spectra is complex as no separation method is coupled to this mass spectrometric technique.

In this chapter we focus on the oleaginous-containing binding media. Oil is a historically important binding medium and much work has been reported on the composition and drying properties.[5, 8-12] The main components of oil are triacyglycerols, which react during drying and aging of the paint film. The polyunsaturated moieties in the triacylglycerols of the fresh oil form radicals, which react with oxygen to form a cross-linked network. As the three dimensional network ages hydrolysis of the ester bonds occurs leading to free fatty acids groups, diacids and acid-rich network oligomers. These acid groups are immobilised and stabilised by coordination to metals (such as lead), originating from pigment or drier, to form metal carboxylate bonds. The obtained mature aged oil paint therefore consists of polyanionic ionomer networks.[13]

GC/MS or DTMS studies on oil paint result in detailed identification of un- and saturated, oxidised and unsaturated, mono- and di-carboxylic acids in free form, ester or metal bound as well as, various oxidation products and metal present.[5] Some information of the inorganic components of the paint film can also be obtained by DTMS. A systematic SIMS study on the characterisation of mature oil paint systems is not found in the literature. The few oil studies described reported focus mainly on the characterisation of the fatty acid constituents of oils.[14-16] Fatty acids are have been extensively studied with SIMS in self-assembled monolayers, such as Langmuir-

Blodgett films.[17-21] Furthermore, analyses on lipids *e.g.* phospholipids in biological samples provide relevant information on the ionisation processes of fatty acids.[22, 23] Fatty acids under SIMS conditions form quasi-molecular ions $[M+H]^+$ in the positive ion mode and $[M-H]^-$ in the negative ion mode. The main fragmentation of di- and monocarboxylic acids in the positive ion mode is lost of water $[M + H - H_2O]^+$ and loss of formic acid $[M + H - HCOOH]^+$ in case of a dicarboxylic acid.[20, 24, 25] Recently, Spool (2004) has postulates proposed a model or the ionisation and fragmentation pathways of carboxylic acids and corresponding esters.[25]

In this chapter, we compare the analytical data obtained from well defined paint samples, by three distinct mass spectrometric techniques: SIMS, py-TMAH-GC/MS and DTMS. The selected samples are naturally and artificially aged traditional lead white oil paint reconstructions. The naturally aged oil paint sample is a relative young paint whereas the artificially aged sample approaches a mature oil paint. These two aging stage will be characterised with SIMS, which will be evaluated in a qualitative manner by comparing with pyrolysis-tetramethylammonium hydroxide methylation gas chromatography/mass spectrometry (py-TMAH-GC/MS)and DTMS equivalent spectral data. SIMS spectra of reference materials are used to assist the detailed characterisation of the different oil constituents analysed.

3.1.2 Methods and materials

3.1.2.1 Analytical techniques

3.1.2.1.1 SIMS

The static SIMS experiments were performed on a Physical Electronics (Eden Prairie, MN) TRIFT-II time-of-flight SIMS (TOF-SIMS). The surface of the sample was scanned with a 15 keV primary ion beam from an $^{115}In^+$ liquid metal ion gun. The pulsed beam was compressed (bunched) to ~1 ns to obtain a better mass resolution, a current of 60 pA and the spot size of ~ 120 nm. The primary beam was rastered over a 150 x 150 µm sample area, divided into 256 x 256 pixels. The measurements in both positive and negative mode were made, each with a total primary ion dose of 1.0 x 10^{12} ions/cm^2, well within the static SIMS regime. The surface of the sample was charge compensated with electrons pulsed in between the primary ion beam pulses. To prevent large variations in the extraction field over the large insulation surface area of the sample a non-magnetic stainless steel plate with slits (1 mm) was placed in top of the sample.

Tiny paint samples of the paint film ZD and ZDC taken from the Melinex

sheets (see section 3.1.2.2 for further details on these samples) were attached to a glass substrate and analysed. Stearic acid (Sigma-Aldrich Chemie GmbH) was pressed into a tablet using a high power KBr pellet press. Tristearin (Sigma-Aldrich Chemie GmbH) was dissolved in a mixture of ethanol (Biosolve) and dichloromethane (Fluka) (3 : 7) and dropped onto a silicon substrate. After evaporation of the solvents the tristearin was measured with SIMS. A well homogenised mixture of chalk (Merck) with 1% lead stearate (kindly supplied by M. Verhoeve, University Leiden, The Netherlands) was pressed into a tablet using a KBr pellet press.

3.1.2.1.2 DTMS

Although the sensitivity of the DTMS method allows analysis of smaller samples, approximately 50-100 µg was scraped off the Melinex support and homogenised into ethanol (~ 100 µl), in order to ensure statistically more representative sampling. Aliquots of 2.5 µl of the sample suspension were deposited on a 0.1 mm diameter, platinum/rhodium (90 : 10) filament (Drijfhout, The Netherlands) of the DTMS probe. DTMS analyses were performed on a JEOL JMS-SX/SX 102A four-sector instrument of B/E-B/E geometry. In the ion source of this instrument, the wire was resistively heated by ramping the current at a rate of 0.5 A/min. Using this ramp the temperature was linearly increased from ambient to approximately 800 °C in two minutes. Desorbed and pyrolysed material was ionised by 16 eV electron ionisation. The mass spectrometer was scanned over a *m/z* range of 20-1000 using a 1 s cycle time.

DTMS analysis of the reference materials was performed under the same conditions, using µM ethanol solutions. Similarly to previously described, aliquots of 1-2 µL were applied on the platinum/rhodium (90 : 10) filament.

3.1.2.1.3 On-line TMAH (tetramethylammonium hydroxide) methylation Py-TMAH-GC/MS

The samples were analysed by Curie point Py-TMAH-GC/MS equipped with a reagent-venting module. A small sample (50-200 µg) was placed in a GC vial and 50 µL of TMAH (2.5% w/v in H_2O) was added. The vial was capped and placed in the ultrasonic bath for 5 minutes until a fine suspension was formed. About 2-5 µL of the paint film suspension was applied to the rotating 610 °C Curie point wire and the sample dried in vacuo. The ferromagnetic wire was inserted in a glass liner and placed in the pyrolysis unit (temperature of the base of the pyrolysis unit 185 °C). Curie-point pyrolysis was performed with a FOM 5-LX pyrolysis unit. The ferromagnetic wire was inductively heated for 9 s in a 1 MHz RF field to its Curie-point temperature (610 °C). Methylated compounds were flushed into the pre-column/column set-up

mounted in a Carlo-Erba gas chromatograph (series 8565 HRGC MEGA 2) coupled directly to the source of a JEOL SX 102A/102, a double sector instrument via an inhouse build interface, kept at 300 °C. Pre-column: Chrompack VF-1ms, length 3 m, id 0.32 mm, film thickness 0.10 μm. Analytical column: Chrompack VF-5 ms, length 30 m, internal diameter 0.32 mm, film thickness 0.50 μm.

TMAH is a basic reagent, known to attack the bonded phase of the column. In order to eliminate most of the unreacted TMAH, a venting module was installed between the pre-column and the analytical column. This module is open for 10 seconds during pyrolysis to remove the very volatile reagent while concentrating the sample on the retaining pre-column. The slightly less polar bonded phase of the retaining pre-column was chosen due to its higher resistance to reagent attack. Helium was used as carrier gas at a flow rate of approximately 2 ml/min. The initial oven temperature was 50 °C, maintained for 2 minutes then increased to 320 °C at a rate of 8 °C/min. Ions were generated by 70 eV electron impact ionisation. The mass spectrometer was scanned from *m/z* 40-800 with a cycle time of 1s. A JEOL MS-MP9020D data system was used for data acquisition. The 70 eV electron spectra of the eluted compounds were used for structural identification. normally insufficient in lake/pigment identification.

3.1.2.2 Samples

The lead white-containing linseed oil paint reconstruction (ZD) was prepared by Carlyle in 1999 in the course of the MOLART project at FOM-AMOLF using freshly pressed linseed oil (linseeds provided by MACOS bv., Swifterbant, The Netherlands) mixed with Dutch stack process lead white (loodwit Schoonhoven de Kat, in stock at MOLART). The paint was applied on polyester film (Melinex) and kept under ambient conditions. A three-year-old sample was taken from these paint films in 2002 and analysed with SIMS. Part of the ZD paint film was artificially aged for 30 days at 50 °C and 80% RH marked as ZDC.

3.1.3 Results

3.1.3.1 SIMS of linseed oil-containing paint reconstructions

3.1.3.1.1 SIMS of reference compounds - positive ions

The spectra of reference materials relevant for the oil paint composition, such as triacylglycerols (a source of ester-bound fatty acids), free and metal-bound mono- and dicarboxylic fatty acids are the basis for the interpretation of the SIMS spectra of samples ZD and ZDC. The characteristic peaks in positive and negative ion mode will be attributed; small hydrocarbon fragments (below *m/z* 100) are not specific enough and will not be discussed here.

The positive SIMS spectrum of tristearin, a triacylglycerol of stearic acid, shows main fragments at *m/z* 607 (diacylglycerols of palmitic stearic acids), *m/z* 341 (monoacylglycerols of palmitic stearic acid) and *m/z* 267 (acylium ion of palmitic stearic acid) (Fig. 3.1.1a). Uncharacterised fragments of triacylglycerol are observed at *m/z* 325 and 395. The quasi-molecular ion of tristearin detected at *m/z* 891 is minor (not shown). The main peaks in the SIMS spectrum of the free monocarboxylic fatty acid, stearic acid, are the protonated molecular ion (*m/z* 285) and its corresponding acylium ion (*m/z* 267) in similar intensities (Fig. 3.1.1b). The positive ion spectrum of a metal-bound monocarboxylic fatty acid, stearic acid lead soap, shows ions at *m/z* 489-491. The peaks corresponding to the protonated stearic acid and its acylium ion are not detected (Fig. 3.1.1c). Other ions detected in the analysis of lead soaps are of lead (*m/z* 206-208, 412-416), lead oxides (*m/z* 428-432; $Pb^{+}_{2}O$) and lead hydroxides (*m/z* 223-225, 445-449; $PbOH^{+}$, $Pb_2O_2H^{+}$). The peak at *m/z* 323 is calcium stearic acid soap; the calcium is derived from the chalk matrix, particular to this reference sample. The spectrum of free nonanodioic acid (azelaic acid), shows a peak at *m/z* 171, the acylium ion, which is which is dominant over the peak more intense than the quasi-molecular ion at *m/z* 189, the protonated molecular ion (not shown). The positive ion spectrum of a metal-bound dicarboxylic fatty acid, lead azelate, shows ions at *m/z* 393-395, and ions attributed to the lead-bound acylium ion at *m/z* 375-377 in equal intensities (not shown). Neither the protonated azelaic acid (*m/z* 189) nor its acylium ion (*m/z* 171) is detected. Dominant peaks in the spectrum are lead (*m/z* 206-208, 412-416), lead oxides (*m/z* 428-432; $Pb^{+}_{2}O$) and lead hydroxides (*m/z* 223-225, 445-449; $PbOH^{+}$, $Pb_2O_2H^{+}$).

3.1.3.1.2 SIMS description of sample ZD - positive ions

The positive ion SIMS spectra of the top surface side of the lead white-containing linseed oil paint film sample ZD shows characteristic fragment peaks of

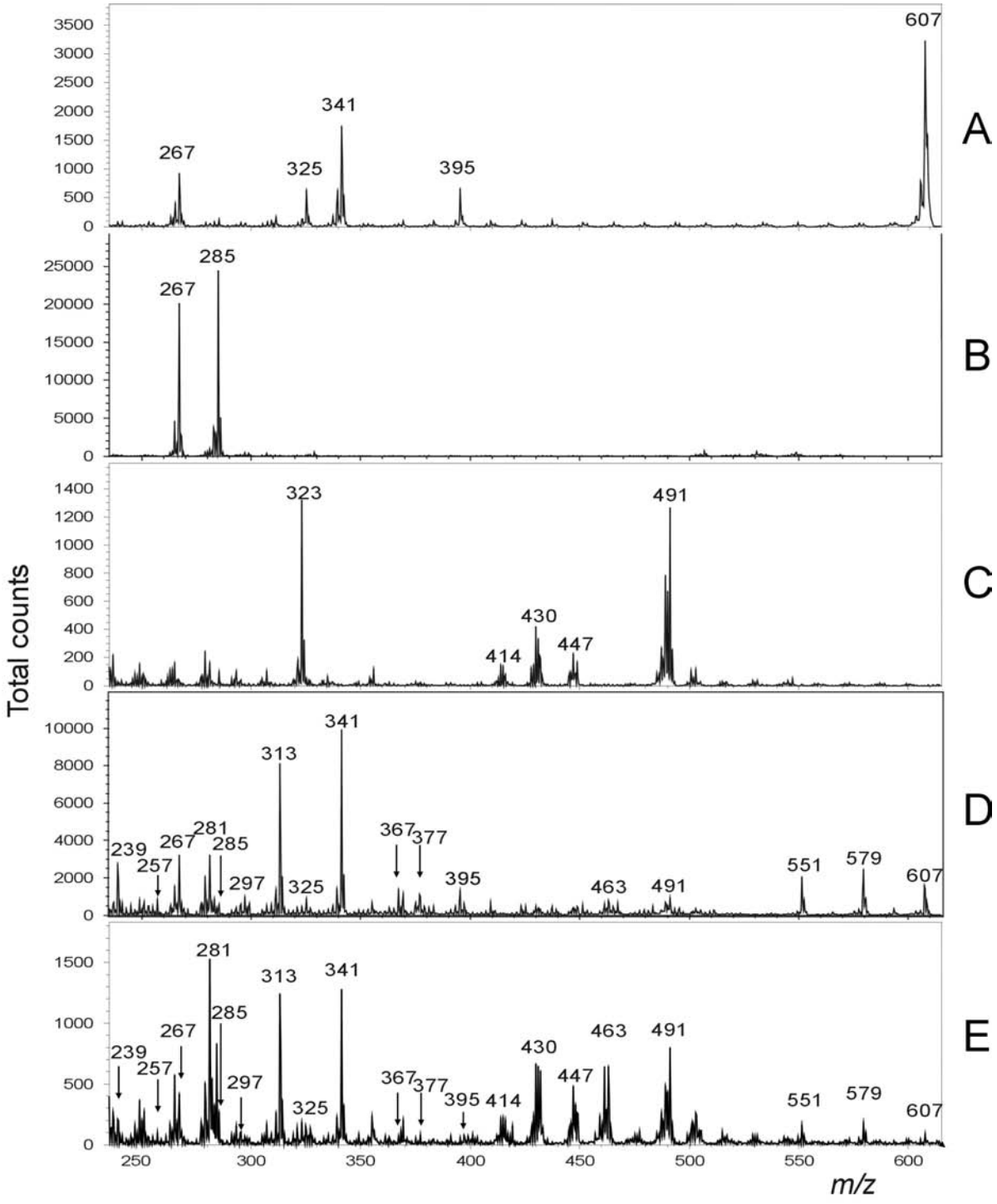

Fig 3.1.1 The SIMS spectra (mass range m/z 235 - 615) in positive mode of tristearin (A), stearic acid (B), stearic acid lead soap (C), lead white-containing oil paint sample ZD natural aged (top side of the film) (D) and lead white-containing oil paint sample ZDC artificially aged (top side of the film) (E).

triacylglycerols at *m/z* 551, 579 and 607 (diacylglycerols of palmitic and stearic acids), *m/z* 313 and 341 (monoacylglycerols of palmitic and stearic acid), *m/z* 297, 325, 367 and 395 (unidentified) and *m/z* 239 and 267 (acylium ions of palmitic and stearic acid) (Fig. 3.1.1d). The secondary ion yields of the free fatty acids, palmitic and stearic acid (*m/z* 257 and *m/z* 285), are low. In the lower mass range a peak at *m/z* 171 is detected which is representative for the acylium ion of azelaic acid (not shown). Lead soaps of palmitic and stearic acid, characteristic for a mature oil paint, are present at *m/z* 461-463 and *m/z* 489-491 in very low intensities (Fig. 3.1.1d). Furthermore, the fatty acid lead soap of the acylium ion of azelaic acid is detected at *m/z* 375-377 (Fig. 3.1.1d).

As SIMS is a sensitive surface technique it is possible to detect differences in composition between the top and bottom sides of the paint film. The positive SIMS spectrum of the bottom side of the ZD sample is identical to the spectrum of the top side. Peaks detected at *m/z* 265, 281, 295, 339, 369, 413, 443, 517 derived from silicon contamination (poly (dimethyl siloxane)) on the surface of the sample.

3.1.3.1.3 SIMS description of sample ZDC - positive ions

Positive ion SIMS analyses show that the composition of the naturally and artificially aged oil paint film, sample ZD and ZDC respectively, is different. In the positive spectrum of sample ZDC, peaks characteristic of fragments of triacylglycerols are mainly detected at *m/z* 313 and 341, corresponding to the monoacylglycerol fragments (Fig. 3.1.1e). The diacyglycerol fragment ion peaks at *m/z* 551, 579 and 607, and the acylium peaks at *m/z* 239 and 267, are present in much lower yields compared to the spectrum of ZD (Fig 3.1.1d). The secondary ion yields of free palmitic and stearic acid (*m/z* 257 and *m/z* 285) are also detected in low yields. The acylium ion of azelaic acid at *m/z* 171 is not detected (not shown). The most intense peaks in spectrum of ZDC are the lead isotope peaks (*m/z* 206-208). Lead clusters (*m/z* 223-225, 414-416, 428-432, 445-449) and palmitic and stearic acid lead soaps (*m/z* 461-463 and 491-493, respectively) are dominant features in the spectrum, although there is no relative increase of the ion yields in comparison to the sample ZD (Fig. 3.1.1e). The peaks characteristic of the lead soap of azelaic acid is are absent.

The SIMS spectrum of the bottom surface of the paint film of sample ZDC is different to that of the top. The mass spectrum of the bottom side shows a relatively higher yield of the diacylglycerols compared to the monoacylglycerols, indicating a lower degree of hydrolysis than the top surface of the paint film. The metal soaps of palmitic and stearic acid have relative lower ion yields in the bottom of the film, and the peaks representative for lead soap of the acylium ion of azelaic acid are clearly detected (not shown). This suggests inhomogeneity during drying and humidity aging

of the film, as the Melinex is an impermeable support. Light, oxygen and humidity can only be introduced into the paint film via the top side.

3.1.3.1.4 SIMS of reference compounds - negative ions

The negative SIMS spectrum of tristearin shows a main peak at *m/z* 283 representative attributed to deprotonated stearic acid (Fig. 3.1.2a). Aliphatic chain fragment ions of fatty acids with a mass increment of 14 amu (*m/z* 71, 85, 99, 113, 127, 141, 155, 169, 183, 197, 211, 225, 239 and 253) are detected in lower yields. These negatively charged fragments are of the type $C_2H_3(CH_2)_xCOO^-$.[7] The negative SIMS spectrum of free and metal-bound stearic acid contain a significant peak of deprotonated stearic acid at *m/z* 283 (not shown). In both spectra, aliphatic chain fragment ions of stearic acids are detected in lower yields (not shown). From these results it can be concluded that in the negative SIMS mode free, ester- or metal-bound fatty acids all give origin to deprotonated fatty acid peaks. However, the deprotonated ion yields for the free fatty acid is higher than those for the ester- (in the ratio 1:2) and metal-bound fatty acids (in the ratio 1 : 1.5).[26]

The intensity of the protonated fatty acids, their acylium ions and the ions of the metal carboxylate fatty acid salt in the positive ion mode provides an indication of the relative amount of free, ester- and metal-bound fatty acid in an oil paint.[26] The SIMS spectra of free and lead-bound azelaic acid reveal a deprotonated molecular ion peak at *m/z* 187 as main peak. Aliphatic chain fragment ions of fatty acids are observed at *m/z* 71, 85, 99, 113, 127, 141 and 169 (not shown).

3.1.3.1.5 SIMS description of sample ZD - negative ions

The negative SIMS spectrum of the top side of the paint film of sample ZD shows two dominant negative ions peaks at *m/z* 255 and 283 from deprotonated palmitic and stearic acid, respectively (Fig. 3.1.2.b). The reference materials indicated that these ions are not informative about the origin of the fatty acid moiety (free, ester- or metal-bound). The detected aliphatic chain fragment ions of fatty acids (*m/z* 71, 85, 99, 113, 127, 141, 155, 169, 183, 197, 211, 225, 239 and 253) are marked with an asterisk in Fig 3.1.2b. The peaks detected at *m/z* 143, 157, 171 are attributed to deprotonated short chain monocarboxylic fatty acids, octanoic, nonanoic and decanoic acid and the peak at *m/z* 187 for the dicarboxylic acid, azelaic acid (Fig. 3.1.2b). These short chain fatty acids and dicarboxylic acids are known oxidation and degradation products of aged oil paint.[5] Other negative ions observed, characteristic of oil paint, are *m/z* 311 and 339 corresponding corresponding to monoacylglycerol esters of palmitic and stearic acids.

The negative SIMS spectrum of the bottom side of the ZD sample is identical

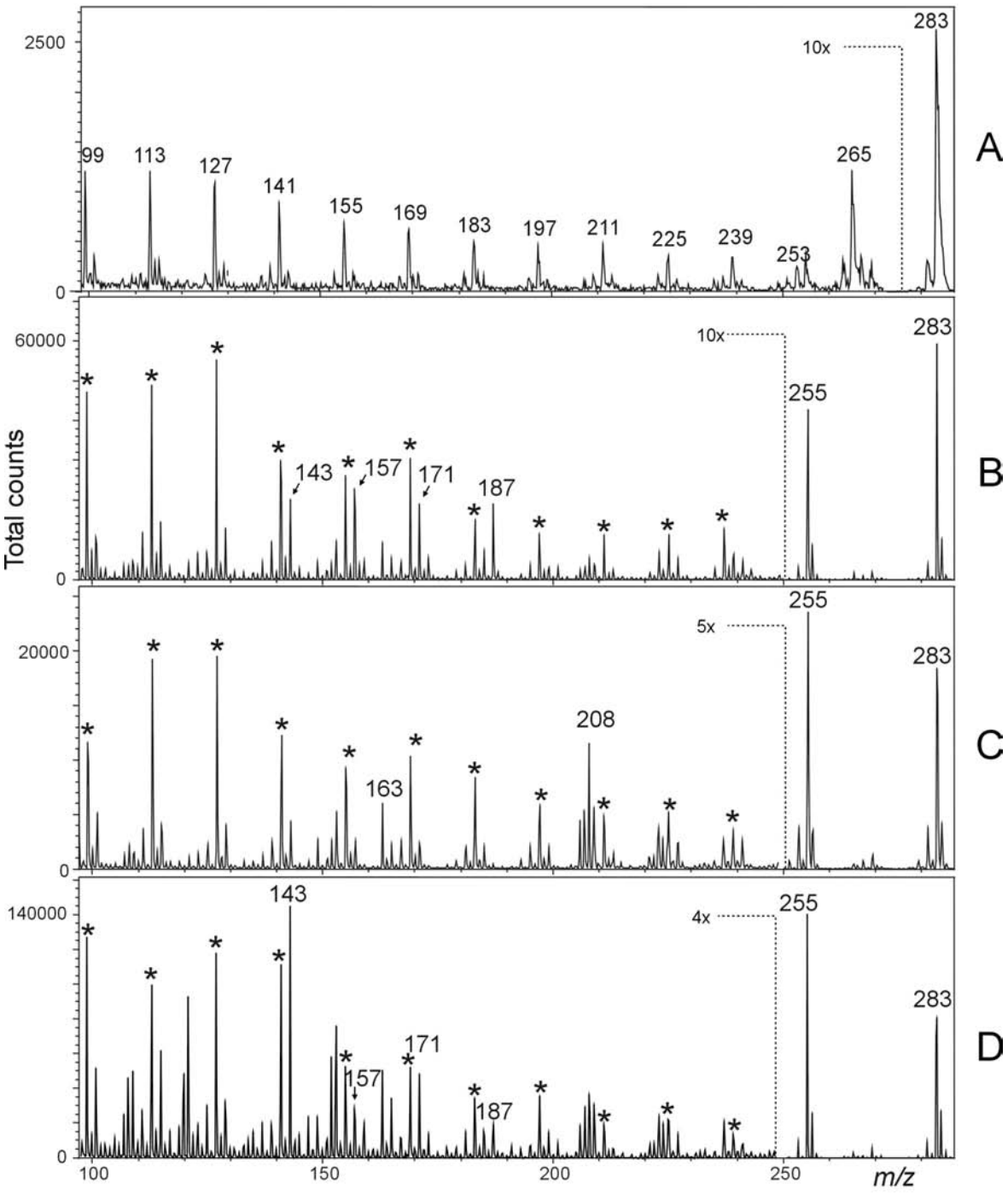

Fig 3.1.2 The SIMS spectra (mass range m/z 98 - 289) in negative mode of tristearin (A), lead white-containing oil paint sample ZD natural aged (top side of the film) (B) and lead white-containing oil paint sample ZDC artificially age: top side (C) and bottom side of the film (D). The asterisks in B-C are indicative for the aliphatic chain fragment ions of fatty acids. The counts of mass peaks before the dotted line indicates that the counts of the mass peaks before the line have to be multiplied by 4, 5 or 10 times (value indicated in the figure).

to the spectrum of the top side (not shown).

3.1.3.1.6 SIMS description of sample ZDC - negative ions

The deprotonated palmitic and stearic acid at *m/z* 255 and 283, respectively, are dominant in the spectrum of the top side of the paint film of sample ZDC (Fig. 3.1.2c), similarly to what was observed for the sample ZD. The characteristic fragments of compounds for the first stage of drying are either present in low yields (in the case of the short chain fatty acids *m/z* 143, 157 and 171) or not detected (diacids *m/z* 187) in the top surface of the artificially aged sample ZDC (Fig. 3.1.2c). As observed in the positive ion mode, the composition of the top side and bottom side of the paint film ZDC is different. In the spectrum of the bottom (Fig. 3.1.2d) the small chain fatty acids, as well as the diacids are present.

Summarising, on the top side of ZDC paint film, which is exposed to light, oxygen and moisture, the more volatile degradation and oxidation products are not detected. However, these products are still abundant in the environmentally shielded bottom side (Fig. 3.1.2d).

3.1.3.2 DTMS of linseed oil-containing paint reconstructions

3.1.3.2.1 DTMS of reference compounds

Detailed interpretation of the different components found in oil paint can be found elsewhere[5] however it is relevant to describe here the most significant features in the DTMS spectra of linseed oil-containing paint reconstructions, by comparison to the analysis of reference materials.

During the DTMS analytical process, the non-bonded or free components of the oil (resulting from the hydrolysis process and prior to being metal coordinated) are volatile and desorb early from the paint particles coated on the pyrolysis wire at lower temperature. These free fatty acids ionise readily and the main peak detected is the molecular ion. As an example the case of stearic acid is described here where the base peak is *m/z* 284. Minor peaks include the chain fragments *m/z* 241, 185, 129, 73 and a γ-H rearrangement ion at *m/z* 60. Free diacids also desorb at low temperatures the early scans and the main electron ionisation generated peak is $[M - 2H_2O]^{\bullet+}$ (*e.g.* in the case of azelaic acid *m/z* 152). Other peaks include *m/z* 84, 98, 111 and 124. The main peak of the metal-coordinated monocarboxylic fatty acids is the acylium ion, however, the molecular ions can also be detected. For example in the case of lead stearate *m/z* 267 and 489-491 are the main peaks. Metal-coordinated diacids show a different behaviour. The example of lead azelate is studied here: lead ion isotopes (*m/z* 206-208) are the main peaks. Other important peaks detected are *m/z* 348-350 resulting from decarboxylation, as well as the molecular ions at *m/z* 392-394. Minor

fragment peaks include fatty acid chain fragments such as *m/z* 73, 87, 101 and a γ-H rearrangement ion at *m/z* 60.

With respect to the ester-bound fraction, the analysis of pure triacylgly-cerols shows that the main ions resulting from their desorption/ionisation of these contain either one or two fatty acid moieties. It is expected that in the case of paint samples where some of the original fatty acid moieties of the triacylglycerols have reacted and are incorporated into an oil network, the main peaks would be the acylium ions and to a lesser extent the mono- and diacylglycerol ions. In practice, elimination reactions releasing fatty acids with $M^{\bullet+}$ are more prominent than formation of acylium ions.

The inorganic components of the network or pigment particles can also be detected in some cases. Not all metals will go through the reduction, pyrolysis and ionisation steps required for their detection. For this reason not all inorganic elements are detectable by DTMS. In the cases studied here lead is the only metal present and is detected in the higher scan number with its isotope pattern (*m/z* 206, 207, 208).

There is another important fraction in the paint system for which it is difficult to find adequate reference materials and therefore the interpretation of the different peaks detected is complex. This is the highly cross-linked network fraction of the paint sample. Due to the pyrolysis of this fraction it is detected as an unresolved peak pattern with mainly aromatic components (*e.g. m/z* 105, 91).

On the basis of this information Table 3.1.1 was assembled and will be used for interpretation of changes in the chemistry of the lead white-containing oil paint reconstructions studied.

*3.1.3.2.2 DTMS description of sample ZD***.**

The TIC of the DTMS analysis of ZD lead white sample (Fig. 3.1.3) shows that there are four separate events in the analysis.

Event A (Fig. 3.1.3a), Scans 1 - 54. The spectrum is dominated by the molecular ion of palmitic and stearic acids. The monocarboxylic acid molecular ion corresponds to the desorption of the free form (*m/z* 256 and 284 for palmitic and stearic acids respectively). The desorption profile of palmitic acid (*m/z* 256 in Fig. 3.1.4) however suggests that the monocarboxylic fatty acids are not present in the free form, but also in a bound form. Although *m/z* 256 is not present in the spectrum of pure tripalmitin or lead palmitate, this ion can be formed by an elimination reaction of the bound fatty acid when in a complex organic matrix. The acylium ions of palmitic and stearic moieties (*m/z* 239, 267 respectively), the corresponding monoacylglycerols (*m/z* 313, 341) and diacylglycerols (*m/z* 550, 578, 606) suggest that the hydrolysis of the ester bonds is not yet complete in the ZD sample. This is in agreement with the SIMS data.

Event B (Fig. 3.1.3b), Scan 55 - 67. A small amount of lead can be detected in this event suggesting the presence of organic lead (lead carboxylates for example). Fatty acid fragments present include *m/z* 60, 73, 129, 171, 185. These fragments (*e.g. m/z* 129 in Fig. 3.1.4) are detected in different events suggesting that the fatty acids are present in different forms. In addition, the acylium ions of the saturated monocarboxylic fatty acids (*e.g. m/z* 239 in Fig. 3.1.4) desorb in two distinct maxima (scan 49, event A and scan 62 event B) corresponding to the ester- and metal-bound fractions

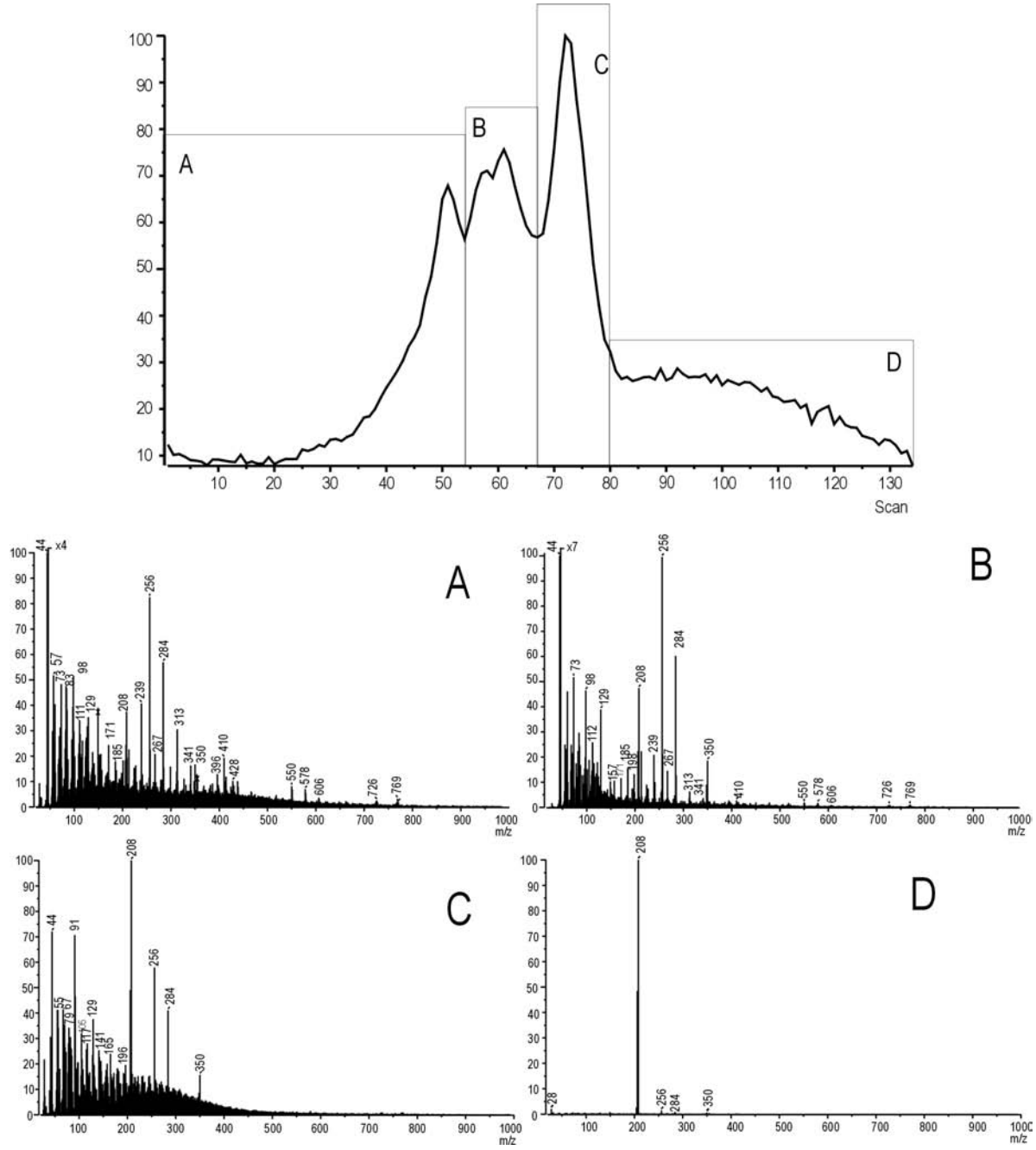

Fig 3.1.3 TIC and partial mass spectra of the ZD sample. (A) Scans 1 - 54, (B) scans 55-67, (C) scans 68-80, (D) Scans 81-130.

respectively. Evidence of the presence of metal soaps of azelaic acid is given from ions at *m/z* 348, 349, 350. The comparison of the desorption profiles of *m/z* 350 and *m/z* 152 suggest that the azelaic acid is present in different forms: ester and metal bound (Fig. 3.1.4). The desorption maximum of *m/z* 152 at scan 48 in event A points to its presence in ester-bound form.

Event C (Fig. 3.1.3c) – Scans 68 - 80. The third event can be described as the pyrolysis of the polymeric oil network. As can be observed in this spectrum, a fraction of the monocarboxylic fatty acids and lead azelate are released in combination with the pyrolysis of the network. Fig. 3.1.4 present a maximum of *m/z* 91 in this event, which is characteristic of the pyrolysis of the network.

Event D (Fig. 3.1.3d) – Scans 81 - 130. Inorganic lead

3.1.3.2.3 DTMS description of ZDC sample.

In general the composition of the ZDC sample is qualitatively similar to that of ZD. This is indicative by the similarity of the TIC. However the relative amounts of the different components have changed, which elucidates the chemical processes involved in the accelerated aging under high humidity and temperature.

There is a decrease in the relative intensity of the peaks corresponding to the glycerol bound moieties (*m/z* 550, 578, 606, 341. 313, 267 and 239). This suggests that during the high humidity and temperature aging, hydrolysis of the glycerol ester bonds was induced. The analysis of the thermogram of *m/z* 239 (acylium ion originating from the different species of palmitic acid) shows that the intensity of the first event (max around scan 49, desorption of ester-bound compounds) decreases from ZD to ZDC (data only shown for ZD).

Although the molecular ions of lead palmitate and stearate are present in the spectra of the corresponding reference materials, these peaks cannot be detected in significant intensities in the spectra of ZD or ZDC samples. However, the presence of the acylium ion at higher scan numbers (maximum at scan number 62) together with the presence of a lead peak (scan number too low for inorganic lead) suggests the presence of lead carboxylates of the monocarboxylic saturated fatty acids both in the ZD and ZDC samples but in slightly higher amounts in the latter sample.

The lead azelate peaks are detected in the second event clearly indicating their presence.

At scan number 70 the event characteristic of the network is detected. This event is characterised by an intense unresolved spectrum, the interpretation of which is not straightforward.

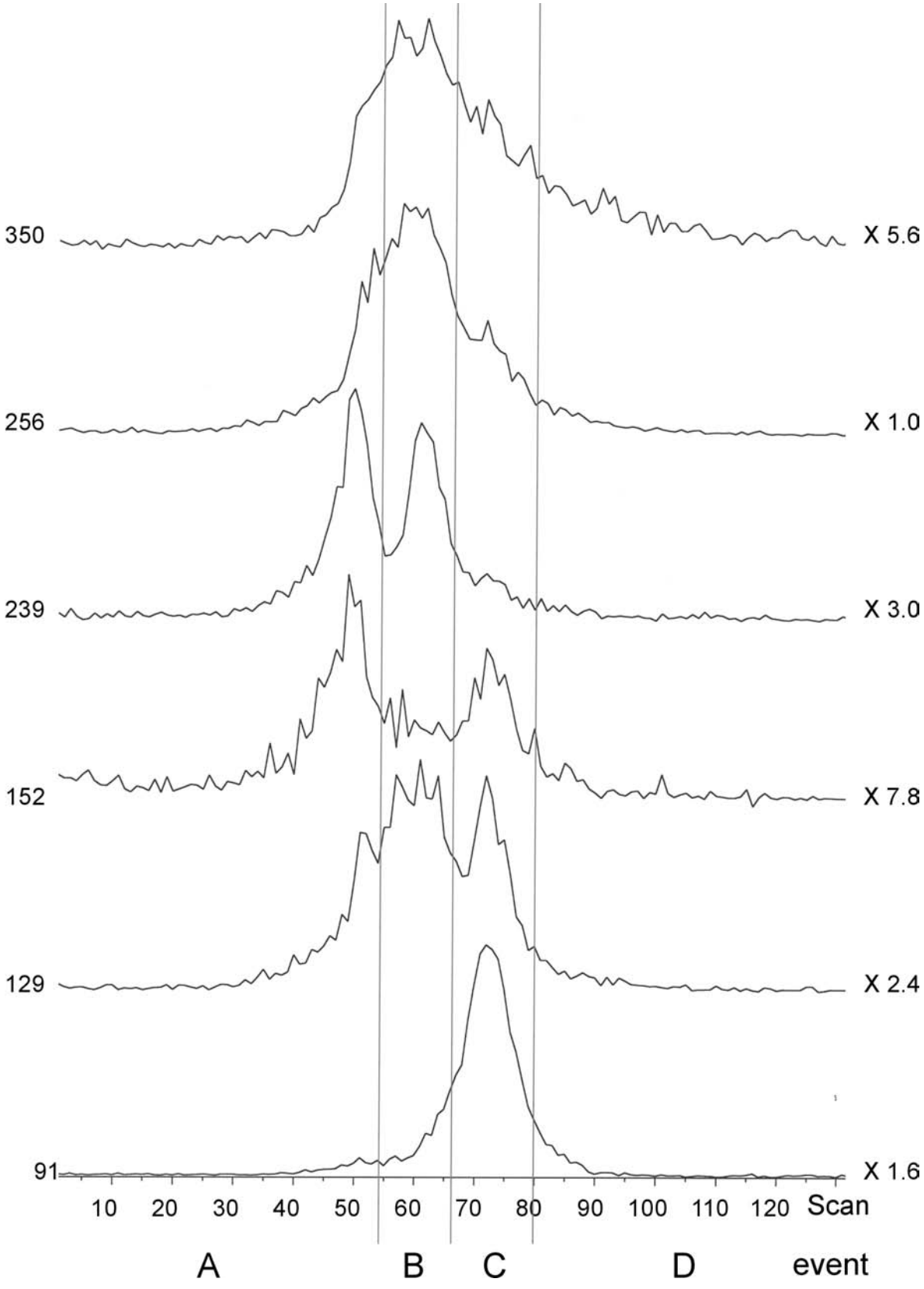

Fig 3.1.4 Mass thermograms (MTs) of m/z 91, 129, 152, 239, 256 and 350 derived from the DTMS data of the ZD sample. The MTs are normalised for the maximum intensity of m/z 256. The horizontal lines illustrate the the four different events indicated in Fig. 3.1.3.

3.1.3.3 Py-TMAH-GC/MS of linseed oil-containing paint reconstructions

This technique has a number of advantages including the minimal chemical workup and the simultaneous derivatisation of acids, esters, metal soaps as well as ethers, amines, amides, and alcohols.[27] Due to the sample derivatisation method Py-TMAH-GC/MS is not a strictly quantitative method.

There is a very significant advantage, which is the separation of the different components in the GC run which makes their identification by means of their EI mass spectrum unequivocal. However, since all acids, esters and metal-bound components are derivatised simultaneously, it is not possible to distinguish the differences in speciation. For example tripalmitin, palmitic acid and lead palmitate will all be detected as methyl palmitate.

3.1.3.3.1 Py-TMAH-GC/MS description of samples ZD and ZDC.

The chromatogram in figure 3.1.5 for *m/z* 74 (McLafferty rearrangement fragment, characteristic for methyl esters of fatty acids) for the ZD sample is shown. The main components of the binding media of the ZD sample, as detected by the current methodology, include the methyl esters of the long chain saturated fatty acids (nr. 14, 16, 17, 18, 20, 22, 23), dimethyl esters of diacids (nr. 4, 6, 8, 10) and of methoxy substituted diacids (15), traces of methyl esters of short chain saturated fatty acids (nr. 1, 2, 3, 5, 9) as well as some unsaturated (nr. 19) and/or oxidised C18 fatty acids (nr. 21). This is in agreement with what had been previously observed in oil paint films.[5] Other components include ω-methoxy substituted short chain saturated fatty acids (nr. 7). Very small traces of oleic acid are also detected.

In figure 3.1.5 the chromatogram for *m/z* 74 for the ZDC sample is shown. The main components of the binding media of the ZDC sample, are the same as those detected in the ZD sample. However the relative quantities present are different. In fact a higher percentage of diacids (nr. 8, 10, 13), short chain fatty acids in particular C9 (nr. 3) is detected in the aged sample. This indicates that this sample is in a more advanced state of oxidation.

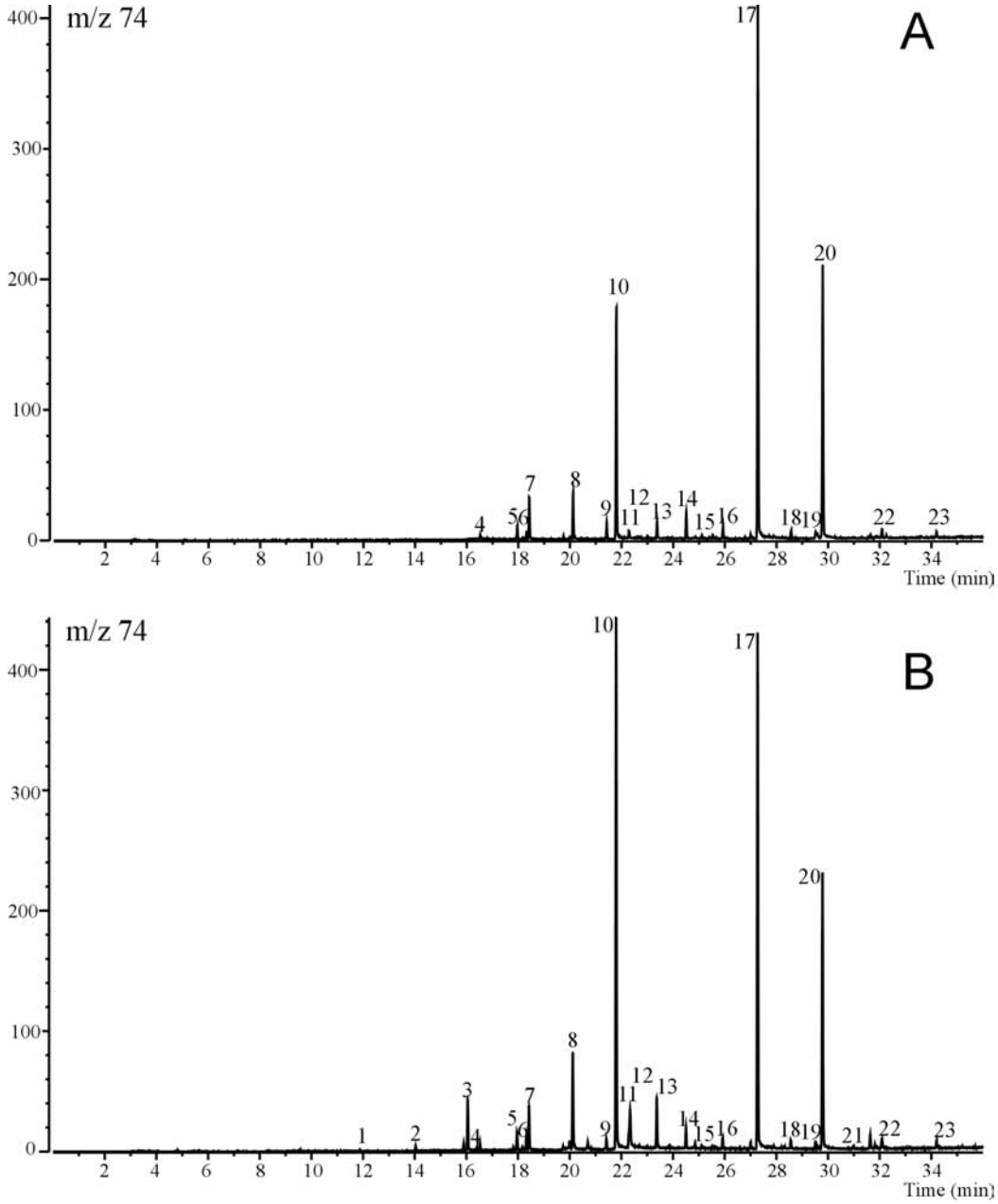

Fig 3.1.5 Py-TMAH-GC/MS analysis of (a) ZD and (b) ZDC paint sample. Single ion chromatogram for m/z 74.

The main components detected are: (1) heptanoic acid methyl ester (2) octanoic acid methyl ester (3) nonanoic acid methyl ester (4) hexanedioic acid dimethyl ester (5) decanoic acid methyl ester (6) heptadioic acid dimethyl ester (7) 8-methoxyoctanoic acid methyl ester (8) octanedioic acid dimethyl ester (9) dodecanoic acid methyl ester (10) nonanedioic acid dimethyl ester/ azelaic acid dimethyl ester (11) α-methyl azelaic acid dimethyl ester (12) α-methoxysuberic acid dimethyl ester (13) decanedioic acid dimethyl ester (14) tetradecanoic acid methyl ester (15) α-methoxydecanedioic acid dimethyl ester (16) pentadecanoic acid methyl ester (17) hexadecanoic acid methyl ester/ palmitic acid methyl ester (18) heptadecanoic acid methyl ester (19) octadecenoic acid methyl ester/ oleic acid methyl ester (20) octadecanoic acid methyl ester/ stearic acid methyl ester (21) 9(or 10)-methoxyoctadeca-11 (or 8)-enoic acid methyl ester (22) eicosanoic acid methyl ester (23) docosanoic acid methyl ester.

Detectable Compounds relevant for oil paint		SIMS		DTMS	py-GC/MS
Group	*Examples*	*secondary + ions*	*secondary - ions*	electron impact *+ ions*	*TMAH derivatising reagent + ions*
Metal	Lead, lead compounds	206-208, 223-225, 412-416, 428-432, 445-449	(206-208, 223-225)	206-208 *(scan 80- 130)*	No information
Triacylglycerol	Tripalmitin	239, 313, 367, 525	255, 71, 85, 99, 113, 127, 141, 155, 169, 183, 197, 211, 225, and 239	239, 313, 550,…	
Free monocarboxylic fatty acid	Free palmitic acid	239, 257	255, 71, 85, 99, 113, 127, 141, 155, 169, 183, 197, 211, 225, and 239	60, 73, 129, 185, 256 *(scan 1-54)*	270, 227, 143, 129, 87, 74, 55, 43 (methyl palmitate) (rt 27.3 min)
Ester-bound monocarboxylic fatty acid	Ester-bound palmitic acid	239	255, 71, 85, 99, 113, 127, 141, 155, 169, 183, 197, 211, 225, and 239	60, 73,129, 171, 185, 239 *(scan 1-67)*	
Fatty acid metal carboxylate	Lead palmitic acid soap	206-208, 223-225, 412-416, 428-432, 445-449, 461-463	71, 85, 99, 113, 127, 141, 155, 169, 183, 197, 211, 225, 239, 255	60, 73,129, 171, 185, 239, 461-463 *(scan 55-67)*	
Free dicarboxylic fatty acid	Azelaic acid (C9)	171, 189	71, 85, 99, 113, 127, 141, 169, 187	84, 98, 111, 124, 152 *(scan 1-54)*	185, 152, 143, 111, 83, 74, 55 (dimethyl azelate) (rt 21.8)
Fatty acid metal dicarboxylate	Lead azelaic acid soap	206-208, 223-225, 375-377, 393-395, 412-416, 428-432, 445-449	99, 113, 127, 141, 169, 187	(60, 73, 87, 101) 84, 98, 124, 138, 152 *(scan 1-67)* 348-350 *(scan 57)*	

Table 3.1.1 Detectable compounds relevant oil paint by SIMS, DTMS and py-TMAH-GC/MS.

3.1.4 Discussion

SIMS

The positive and negative SIMS spectra provide information on different fatty acids (free, ester or metal bound), diacids, monoacylglycerol, diacylglycerol, metal and metal clusters. The combined spectral data of the positive and negative ion mode describe the composition of the lead white-containing linseed oil paint ZD. The yields of free and metal-bound fatty acids are relatively low in sample ZD, whereas the mono- and diacylglycerols of fatty acids are relatively abundant. We conclude that most of the fatty acids present are still ester bound. This implies that the hydrolysis of the paint film is not complete. In this stage, SIMS detects degradation and oxidation products. After exposure to high humidity and temperature the relative amount of ester-bound fatty acids (and free fatty acids) diminishes, as the peaks representative for the acylium ions of fatty acids and the diacylglycerol of fatty acids decrease. The degradation and oxidation products are not detected anymore in the sample possibly due to evaporation. This is indicative for a higher degree of hydrolysis of the paint film. The advantage of SIMS is that it analyses only the upper atomic layers, thus allowing the detection of different aging stages inside sample ZDC.

DTMS

Careful study of the DTMS spectra of the ZD sample shows that part of the fatty acids present are still bound to the glycerol units. However the presence of metal soaps (in particular diacid metal soaps) is clearly detected, suggesting that the metal coordination of carboxylic acid moieties occurred early in the drying/maturing stages of this paint film. Further evidence of a presence of a polymeric paint film is given by the pyrolysis of the network fraction. DTMS is also able to distinguish the different forms in which some inorganic elements are present, in this case organic lead and the intense signal of intact lead white pigments. By comparison ZDC shows features indicative of a higher level of hydrolysis due to the high relative humidity and temperature conditions to which this sample was exposed.

Py-TMAH-GC/MS

The py-TMAH-GC/MS run shows very clearly the individual detectable components of the paint films including different short chain di- and monocarboxylic acids in a semi-quantitative way. The results show that the degree of oxidation of the aged sample (ZDC) is higher that the unaged one. They also show that the azelaic acid species (this technique does not distinguish between free, ester- or metal-bound) is a dominant constituent of the aged oil paint.

General discussion

An overview of the characterisation of samples ZD and ZDC with SIMS, DTMS and GC/MS is given in Table 3.1.2. The characterisation of the samples ZD and ZDC with the three different techniques indicates a chemical change caused by the accelerated aging conditions.

SIMS results show that there is an increase in the degree of hydrolysis upon aging, based on the relative amounts of ester-bound fatty acids. This observation is clearly supported by the DTMS results, which also show decreased yields of ester-bound fatty acids. Py-TMAH-GC/MS does not provide any information concerning the origin of the fatty acid moieties (*i.e.* does not distinguish between free, ester- and metal-bound fatty acids) and is therefore not informative on the degree of hydrolysis of the paint film.

Characterization by:	**Sample ZD**	**Sample ZDC**
SIMS	*Top and bottom of film:* Hydrolysis not complete, small amount of short chain fatty acids and diacid C9.	*Top of film*: approaching mature oil paint, *Bottom of film:* Hydrolysis not complete, small amount of short chain fatty acids and diacid C9.
DTMS	Hydrolysis not complete, amount of diacids and diacid metal soaps	Qualitative similar to ZD Higher degree of hydrolysis
Py-TMAH-GC/MS	Semi quantitative identification of the short and long chain fatty acids and diacids. C9 diacid is the main component identified.	Higher degree of oxidation that the unaged sample

Table 3.1.2 Description of the samples ZD and ZDC by SIMS, DTMS and py-TMAH-GC/MS.

SIMS detects three small chain fatty acids (C8, C9 and C10) formed as result of the aging of the oil paint, in both sides of the paint film of sample ZD. Py-TMAH-GC/MS data support the presence of these short chain fatty acids, detected in very small amounts. No characteristic peaks for these compounds are prominent in the DTMS spectra. After accelerated aging, SIMS does not detect the small chain fatty acids in significant amounts on the top side of the paint film ZDC, whereas these compounds are still detectable on the bottom side. This observation is in apparent disagreement with the py-TMAH-GC/MS results, which detects a high content of the

small chain fatty acids in the sample ZDC. This different observation can be explained by the fact that SIMS is a surface technique whereas py-TMAH-GC/MS probes the bulk. During aging the small chain fatty acids are formed, which is shown by py-TMAH-GC/MS. But in a mature paint system these compounds will have evaporated eventually. This process is first observed on the surface of the paint film exposed to the high humidity conditions, whereas the environmentally shielded bottom side still contains the small chain fatty acids. SIMS is the only technique that can show this subtle chemical change.

SIMS, as well as DTMS, provide limited information on the free, ester- and metal-bound dicarboxylic fatty acid. Py-TMAH-GC/MS shows that the azelaic acid is the main component in the oil paint system, particularly after accelerating aging. This is not deduced from the spectra of SIMS and DTMS (although in the DTMS spectra the lead bound azelaic acid is clearly detected, but it is not dominant). It can be concluded that the ionisation conditions of SIMS are not favourable for the analysis of dicarboxylic fatty acids. DTMS is the only technique that provides information concerning the polymeric oil network.

The characteristic constituents of the oil paint detectable with SIMS, DTMS and py-TMAH-GC/MS are summarised in Table 3.1.1. For illustration purposes the palmitic and azelaic acid-containing oil constituents are included in this table.

3.1.5 Conclusions

SIMS provides combined organic and inorganic information about the oil paint composition, while preserving the speciation information of the fatty acids. Uniquely it gives spatial resolved information for the upper atomic layers. The SIMS analysis shows characteristic oil paint constituents peaks, which are supported by DTMS and/or py-TMAH-GC/MS. However, the dicarboxylic fatty acids are not detected with SIMS in high yields, whereas py-TMAH-GC/MS proves these to be major components of the oil paint film. SIMS provides non-specific information about the polymeric oil network, the presence of which is demonstrated by DTMS. Taking this into consideration, it can be concluded that SIMS is a valid technique for the characterisation of the oil binding medium in paint samples.

3.1.6 Acknowledgements

Dr. Ester Ferreira is thanked for the DTMS and Py-TMAH-GC/MS analyses and data interpretation and J. van de Horst is for his technical assistance in the DTMS and py-TMAH-GC/MS measurements.

3.1.7 References

1 J.S. Mills and R. White, *Analyses of paint media*, National Gallery Technical Bulletin, 4, 1980, p. 65-68.
2 J.S. Mills, *The gas chromatography examination of paint media. Part I. fatty acid composi tion and identification of dried oil films*, Studies in Conservation, 11, 1966, p. 92-108.
3 J.D.J. van den Berg, K.J. van den Berg and J.J. Boon, *Determination of the degree of hydrol-ysis of oil paint samples using a two-step derivatisation method and on-column GC/MS*, Progress in Organic Coatings, 41, 2001, p. 143-155.
4 J.J. Boon, *Analytical pyrolysis mass-spectrometry - new vistas opened by temperature-resolved in-source py-MS*, International Journal of Mass Spectrometry and Ion Processes, 118, 1992, p. 755-787.
5 J.D.J. van den Berg, *Analytical chemical studies on traditional linseed oil paints*, PhD Thesis, University of Amsterdam, 2002 (http//www.amolf.nl/publications/theses/).
6 J. Plesters, *Cross-sections and chemical analysis of paint samples*, Studies in Conservation, 2, 1965, p. 110-157.
7 K. Keune and J.J. Boon, *Imaging secondary ion mass spectrometry of a paint cross-section taken from an early Netherlandish painting by Rogier van der Weyden*, Analytical Chemistry, 76, 2004, p. 1374-1385.
8 H. Wexler, *Polymerization of drying oils*, Chemical Reviews, 64, 1964, p. 591-611.
9 E.N. Frankel, *Analytical methods used in the study of autoxidation processes*, In: Autoxidation in food and biological systems, M.G. Simic, M. Karel (Eds.), Plenum Press: New York, 1980, p. 141-170.
10 E.N. Frankel, In: *Oily press lipid library*, The Oily Press Ltd.: Dundee, 10, 1998, p. 55-77.
11 A.E. Rheineck, R.O. Austin, *Drying oils - modifications and use*, In: Treatise on coatings, R.R. Myers, J.S. Long (Eds.), Marcel Dekker: New York, 1, 1968, p. 181-248.
12 Z.W., Wicks Jr., F.N. Jones, S.P. Pappas, *Drying oils*, In: Organic coatings: science and technology, John Wiley & Sons, Inc., New York, 1, 1992, p. 133-143.
13 J.J. Boon *et al.*, *Molecular aspects of mobile and stationary phases in aging tempera and oil paint films*, In: Early Italian Paintings: Techniques and Analysis, T. Bakkenist, R. Hoppenbrouwers and H. Dubois (Eds.), Stichting Restauratie Atelier Limburg (SRAL), Maastricht, 1996, p. 35-56.
14 U. Bexell, M. Olsson, P.-E. Sundell, M. Johansson, P. Carlsson and M. Hellsing, *A ToF-SIMS study of linseed oil bonded to mercapto silane treated aluminum*, Applied Surface Science, 231-232, 2004, p. 362-365.
15 R.D. Boyd, *et al.*, *Surface characterization of glass and poly(methylmethacrylate) soiled with a mixture of fat, oil and starch*, Journal of Adhesion Science and Technology, 14, 2000, p. 1195-1207.
16 W.J. Muizebelt and M.W.F. Nielsen, *Oxidative crosslinking of unsaturated fatty acids studied*

with mass spectrometry, Journal of Mass Spectrometry, 31, 1996, p. 545-554.
17 J.-X. Li, J.A. Gardella Jr. and P.J. McKeown, *A quantitative time-of-flight secondary ion mass spectrometry study of ion formation mechanisms using acid-base alternating Langmuir-Blodgett film*, Applied Surface Science, 90, 1995, p. 205-215.
18 L. Laxhuber, H. Möhwald and M. Hashmi, *Secondary ion mass spectroscopic study of the selective ion binding to fatty acid monolayers*, Colloids and Surfaces, 10, 1984, p. 225-231.
19 J.H. Wandass, R.L. Schmitt and J.A. Gardella Jr., *Secondary ion formation from Langmuir-Blodgett films: studies of positive molecular ions*, Applied Surface Science, 40, 1989, p. 85-96.
20 J.H. Wandass and J.A. Gardella Jr., *Secondary ion mass spectrometry of monomolecular layers of fatty acids prepared by Langmuir-Blodgett techniques*, Journal of the American Chemical Society, 107, 1985, p. 6192-6195.
21 A. Chilkoti, *Biomolecules on surfaces*, In: ToF-SIMS: Surface Analysis by Mass Spectrometry, J.C. Vickerman, D. Briggs (Eds.), IM Publication and SurfaceSpectra Limited, Manchester, 2001, p. 633, 643.
22 J.C. Ingram, W.F. Bauer, R.M. Lehman, S.P. O'Connell and A.D. Shaw, *Detection of fatty acids from intact microorganisms by molecular beam static secondary ion mass spectrometry*, Journal of Microbiological Methods, 53, 2003, p. 295-307.
23 S. Karlsson, B. Holmbom, P. Spetz, A. Mustranta and J. Buchert, *Reactivity of Trametes laccases with fatty and resin acids, Applied Microbiology and Biotechnology*, 55, 2001, p. 317-320.
24 K. Varmuza, *et al.*, *Organic substances in cometary grains: comparison of secondary ion mass spectral data and californium-252 plasma desorption data from reference compounds*, International Journal of Mass Spectrometry, 189, 1999, p. 79-92.
25 A.M. Spool, *Interpretation of static secondary ion spectra*, Surface and Interface Analysis, 36, 2004, p. 264-274.
26 see Chapter 3.2
27 J.M. Challinor, *Special issue preface - thermally assisted hydrolysis and methylation (THM) reactions*, Journal of analytical and applied pyrolysis, 61, 2001, p. 3-34.

3.2 Characterisation and localisation of the oil binding medium in paint cross-sections using imaging secondary ion mass spectrometry

3.2.1 Introduction

Saturated monocarboxylic fatty acids - palmitic and stearic acid - are markers of oleaginous binding media in paintings since their carbon chains remain unaffected by the drying and aging of the oil. Furthermore, the ratio of palmitic (C16) and stearic (C18) acid is, to a certain extent, characteristic of the drying oils commonly used by painters. A mature oil paint can be described as an ionomeric network of metal carboxylates of mono- and dicarboxylic acids.[1] The fatty acids in the mature oil network are speciated as ester- and metal-bound or free acids. Several analytical techniques are necessary to determine the identity and the speciation of the fatty acids and diacids in a paint sample.[1, 2, 3] If a pure drying oil has been used the binding medium identification is possible on the basis of the ratio of the monocarboxylic fatty acids *i.e.* the relative amounts of palmitic and stearic acid expressed in the P/S ratio. This ratio is usually determined by gas chromatography-mass spectrometry (GC/MS) of paint scrapings[4] or alternatively by direct temperature resolved mass spectrometry (DTMS). The technique of imaging secondary ion mass spectrometry (SIMS) applied to embedded paint cross-sections has not only the potential to identify mono- and dicarboxylic fatty acids but can also determine their spatial distribution over the individual paint layers. SIMS is a highly sensitive surface analytical technique that uses a high-energy primary ion beam to generate secondary ions. SIMS detects organic as well as inorganic compounds and as it probes the upper atomic layers it is regarded as non-destructive. The distribution of pigment and binding media components in paint can be studied simultaneously with SIMS.[5] By selecting a mass of interest an image can be plotted illustrating the spatial distribution with a resolution of about 1 μm.

In this chapter we report the identification and localisation of monocarboxylic fatty acids in embedded paint cross-sections and experimental model systems by SIMS. SIMS is applied to paint cross-sections with lead white-containing paint layers from 15th- to 19th-century paintings to characterise and localise the monocarboxylic fatty acids, and to determine the type of binding medium using the P/S ratios in individual layers in the paint cross-sections. SIMS studies on the various oil paint model systems elucidate the speciation of the fatty acids in free, ester-bound and metal carboxylate form, the significance of the fatty acids ratios (P/S) and their unusual spatial distribution in young paint films.

3.2.2 Experimental and analytical approach

3.2.2.1 Instrument

The static SIMS experiments were performed on a Physical Electronics (Eden Prairie, MN) TRIFT-II time-of-flight SIMS (TOF-SIMS). The surface of the sample was scanned with a 15 KeV primary ion beam from an $^{115}In^{+}$ liquid metal ion gun. The pulsed beam was non-bunched with a pulse width of 20 ns, a current of 600 pA and the spot size approximately 120 nm. The primary beam was rastered over the sample area, divided into 256 x 256 pixels. The surface of the sample was charge compensated with electrons pulsed in between the primary ion beam pulses. To prevent large variations in the extraction field over the large insulation surface area of the paint cross-section a non-magnetic stainless steel plate with slits (1 mm) was placed in top of the sample.

3.2.2.2 Samples

The oil paint reconstructions are listed in Table 3.2.1. A well-homogenised mixture of chalk (Merck) with 1% palmitic, stearic and arachidic acid (added in molar ratio 1 : 1 : 1) (Sigma-Aldrich Chemie GmbH) was pressed into a tablet using a KBr pellet press.

Sample	**Composition and Treatment**
Chalk Tablet	chalk tablet with containing a mixture of 1 % palmitic, stearic and arachidic acid (1:1:1)
ZD	Lead white in freshly pressed linseed oil, *naturally aged for 3 years*
ZDC	Lead white in freshly pressed linseed oil, *30 days of artificially ageing at 50 °C and 80 % RH after 3 years naturally ageing*
LMP	multi-layered system of linseed oil, mastic and poppy seed oil, *the layers are applied within 12 hours 4 month naturally aged*
P	lead white in poppy seed oil, *4 month naturally aged*
L	lead white in linseed seed oil, 4 *month naturally aged*

Table 3.2.1 List of the different lead white-containing oil paint reconstructions.

The lead white linseed oil paint reconstruction (ZD) was prepared by Carlyle in 1999 in the course of the MOLART project at FOM-AMOLF using freshly pressed linseed oil (linseeds provided by MACOS bv., Swifterbant, The Netherlands) mixed with Dutch stack process lead white (loodwit Schoonhoven de Kat, in stock at MOLART). The paint was applied on polyester film (Melinex) and kept under ambient conditions. A three-year-old sample taken from these paint films in 2002 and was analysed with SIMS. Part of the ZD paint film was artificially aged for 30 days at 50 °C and 80% RH marked as ZDC.

Reconstructions of lead white paint with either poppy oil or linseed oil were prepared by Carlyle in 2004. Linseed oil expressed from organically grown flax seeds in 1999 (Molart stock) was used for the lower paint layer, which was applied to polyester film (Melinex). Freshly extracted oil from poppy seeds (Kremer-Pigmente stock 2003) used to prepare the paint used for the top layer. The lead white was prepared with the traditional stack method (Seynaeve 2003). An intermediate layer of mastic varnish (2 : 1 mastic to turpentine) had been allowed to dry 24 hours on the bottom paint prior to the application of the top layer.

Table 3.2.2 gives an overview of the SIMS analysed section, the preparation of the oil paint reconstructions. The surface of the paint film is analysed by placing a 2 x 2 mm sample of the paint film of the reconstructions on double-sided tape. The reconstructions listed in Table 3.2.2 as polished were embedded in Technovit® 2000LC (Heraeus Kulzer, Germany) and polished with micro-mesh cloths (Scientific Instruments Services Inc., Minnesota) up to 1 micron. The reconstructions in Table 3.2.2 tested as *microtomed* were also embedded in Technovit but cut with a hand microtome (R. Jung, Heidelberg, Germany) in thin sections. Sample ZDC + ZD is a paint cross-section prepared by embedding the two samples ZD and ZDC.

Sample	***Analysis of paint surface***	***Analysis of paint cross-section***
ZD	top and bottom	polished
ZDC	top and bottom	polished
ZDC+ZD	-	microtomed
LMP	-	microtomed
P	-	2x with and without embedded medium, both microtomed
L	-	microtomed

Table 3.2.2 Overview of the oil paint reconstructions and their preparation analysed with SIMS.

Sample P is microtomed with and without embedding medium. For practical reasons sample P without embedding medium is mounted between two Teflon sheets during microtoming.
The paint cross-sections discussed in the paper are listed in Table 3.2.3.

Artist	**Painting**	**Century**	**Paint cross-section number**	**Provided by**
Rogier van der Weyden	*The Descent from the Cross*	15th	A166/1b	Prof. van Asperen de Boer
Jan van Eyck	*Three Maria at the Tomb*	15th	A161/12	Prof. van Asperen de Boer
Pieter van Aertsen	*Seven Sorrows of Mary*	16th	A102/11	Prof. van Asperen de Boer
Christiaen van Couwenbergh	*Herald (south-west)*	17th	HSTB 43.3	L. Speleers, Oranjezaal Huis ten Bosch, The Hague
Rembrandt van Rijn	*The Anatomy Lesson of Dr. Nicoleas Tulp*	17th	MH146/B39 MH146/B37	P. Noble, Mauritshuis, The Hague
Johannes Vermeer	*Diana and her companions*	17th	MH406/16	P. Noble, Mauritshuis, The Hague
Frederic Edwin Church	Primed unused canvas	19th		J. Zucker, Olana, Hudson, New York

Table 3.2.3 List of the paint cross-sections from the 15th to 19th century.

3.2.3 Results and discussion

3.2.3.1 Analysis of fatty acids by SIMS in the negative ion mode

SIMS produces and detects fatty acids in the negative or positive ion mode as deprotonated $(M-H)^-$ or protonated $(M+H)^+$ molecular ions respectively. Negative ions of the monocarboxylic fatty acids are especially dominant and are a marker for an oleaginous binding medium in paintings. To compare the ionisation ratios of different monocarboxylic fatty acids, a chalk tablet-containing palmitic (FA16), stearic (FA18) and arachidic (FA20) acid in a molar ratio of 1 : 1 : 1 was prepared. Deprotonated negative ions of these free fatty acids are shown in the partial SIMS spectrum in Fig.

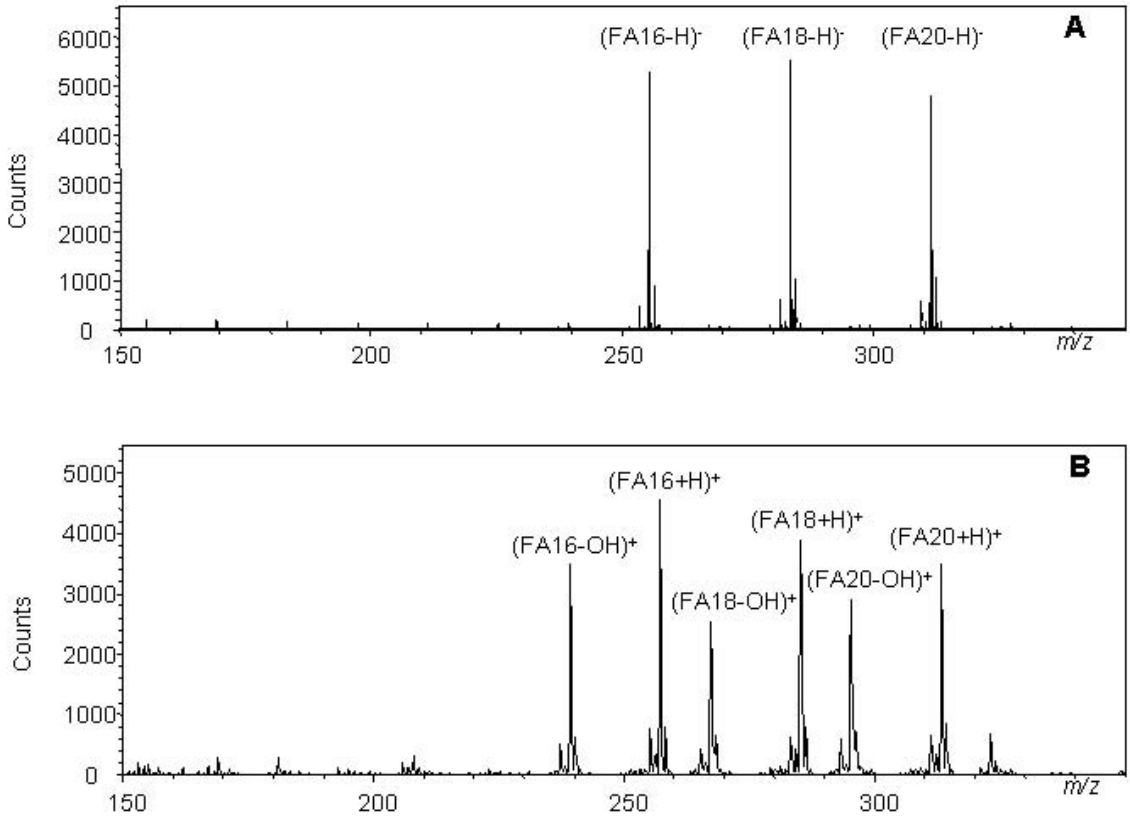

Figure 3.2.1 Negative ion mass spectrum (A) of C16, C18 and C20 in a chalk tablet (mass range m/z 150-350). Deprotonated molecular ion peaks of palmitic, stearic acid and arachidic acid are detected at m/z 255, m/z 283 and m/z 311, respectively. Positive ion mass spectrum (B) of C16, C18 and C20 in a chalk tablet (mass range m/z 150-350). Protonated molecular ion peak of palmitic, stearic acid and arachidic acid are detected at m/z 257, m/z 285 and m/z 313, respectively. Corresponding acylium ions are detected for palmitic, stearic acid and arachidic acid at m/z 239, m/z 267 and m/z 295, respectively.

3.2.1a. The ratio derived from spectra of ten 100 x 100 µm areas is 1.0 : 1.1 : 1.1 (± 0.3) also, which proves that the ionisation efficiency of the negative ions of monocarboxylic fatty acids relevant for oil binding medium characterisation is comparable and corresponds to the relative concentration of these acids in an inorganic matrix. There may however be complications when the fatty acids are present in ester-bound form or as metal soaps. In GC/MS, the P/S ratio is based on the peak areas of the methylated fatty acids derived from free, ester- and metal-bound fatty acids collectively. In DTMS the sum of the yields of free, ester- and metal-bound fatty acids detected as *m/z* 256 and 284 during desorption and pyrolysis of the oil paint sample determines the P/S ratio. In SIMS the negative fatty acid ions also originate from ester- and metal-bound fatty acids, the ionisation of the free fatty acid is twice as efficient as that of the ester-bound fatty acid and 1.5 as efficient as that of the metal-bound fatty acids. Assuming that palmitic and stearic acid have the same reactivity and therefore are

present in the same relative amounts as free, ester- or metal-bound forms, the different ionisation efficiencies will not influence the overall P/S ratio. SIMS only obtains information on the upper atomic layers of the sample surface and the data may not be representative of the bulk composition. This was tested in a comparative study of a lead white-containing oil paint reconstruction (sample ZD) by GC/MS, DTMS and SIMS (see chapter 3.1). The P/S ratio determined by negative ion SIMS is 1.5 ± 0.1 whereas the values obtained by GC/MS and DTMS result in a P/S ratio of 1.9.

3.2.3.2 Variation of the P/S ratio in oil paint reconstructions

SIMS studies on the lead white-containing oil paint reconstructions ZD and ZDC (Table 3.2.1) show a difference in the P/S ratio of the surface of the paint layer and the bulk of the paint film in cross-section. The P/S ratio of the surface of the paint film ZD is 1.0 ± 0.1 and the P/S ratio of the bulk of the film, determined in two different cross-sections is 1.5 ± 0.1. After artificially aging (sample ZDC) the surface P/S ratio is 1.3 ± 0.2 whereas the P/S ratio in bulk is 1.8 ± 0.4.

As ZD and ZDC are derived from the same paint film it is remarkable that different P/S ratios are observed. We had assumed that the palmitic and stearic acid would be homogeneously distributed over the paint layer. The different P/S ratios between sample ZD and ZDC and the variation between the surface and bulk of the paint layer show otherwise. The P/S variation within the paint sample explains the different P/S value between GC/MS, DTMS and SIMS, discussed in the section *Analysis of fatty acids by SIMS in the negative ion mode*. GC/MS and DTMS result in an average P/S value of the whole paint sample, whereas SIMS gives specific localised information.

3.2.3.3 P/S ratio of paint layers from traditional paintings

The oil paint model systems illustrate the potential variation of the P/S ratio within one sample. The P/S ratio determined from cross-sections of reconstructions made with linseed and poppy seed oil lead white paint is 2.0 and 3.6 respectively. These differences are large enough to give an indication of the type of oil. A P/S ratio > 5 is indicative of a poppy seed oil while a P/S < 2 indicates linseed oil in the binding medium. Intermediate ratios can be assigned to walnut, poppy seed oil or mixtures.[2] Therefore, the P/S ratio determined with SIMS can be used as an indication for the type of oil used in different layers in paintings.

The investigated paint cross-section taken from a 15th century panel painting by van der Weyden shows P/S ratios varying from 1.3, 1.4 and 1.8, indicative of the presence of linseed oil in the ultramarine and azurite paint layers.[5] Comparison to SIMS data from a cross-section with a similar layer build up from his contemporary

van Eyck shows that fatty acids are absent in the ultramarine glazing top layer. Literature indeed suggests that this ultramarine glaze is made with an aqueous medium.[6] A paint cross-section from white layer partially covered by the hair of the Herald in *Herald* (south-west) by Christaen van Couwenbergh (1651) (Oranjezaal Huis ten Bosch, The Hague) shows a P/S ratio of 3.5. This value is too high to be linseed oil and is indicative for walnut or poppy oil. In a paint cross-section taken from the 17th-century painting by van Rijn (MH 146), the P/S ratio in the lead white-containing ground deduced from the SIMS spectra is indicative of linseed oil, 1.9, whereas P/S ratio of the lead white-containing layer on top, a flesh tone, is relative higher, 2.2 and might be indicative of walnut oil or a mixture of oils. In a second paint cross-section from the same painting and the same ground gives a P/S ratio of 2.0 and is compatible with the first one. The P/S ratio of 3.7 in a lead-tin yellow paint in Vermeer's *Diana and her Companions* might be poppy seed oil, walnut or a mixture of oils. A comparable indication is obtained for smalt layer in a painting by Van Aertsen A102/11, which has a P/S. The paint cross-section taken from the lead white/chalk ground belonging to the 19th century painter F.E. Church has a P/S of 1.5 indicative for linseed oil. The P/S ratio of 1.5 determined GC/MS supports this result.

3.2.3.4 Analysis of fatty acids by SIMS in the positive ion mode

The positive SIMS ions indicative of fatty acids give information about their speciation as a free, ester-bound or metal carboxylate. This information is not obtained in the negative ion mode. SIMS studies on reference compounds in a calcium carbonate tablet show that a free fatty acid yields a protonated molecular ion and its acylium ion $(M\text{-}OH)^+$ (Fig. 3.2.1b) in a ratio 1.2 : 1. An ester-bound fatty acid leads to an acylium ion, while the protonated fatty acid ion is absent. In the positive mass spectrum of a metal-bound fatty acid the molecular ion of metal carboxylate fatty acid salt is observed together with a very small peak for the protonated fatty acid, while the acylium ion is absent. The intensity of the protonated fatty acids and their acylium ions in the positive SIMS mass spectrum and the ions of the metal fatty acid carboxylate can be used to provide an indication of the relative amount of free, ester- and metal-bound fatty acid in an oil paint.

As the positive ions are indicative for the coordination characteristics of fatty acids, it is possible to detect a difference in composition between the surface and the bulk of a paint film in cross-section. Measurements on the surface and in the bulk of the paint film with relatively fresh poppy seed oil (P) show that free fatty acids, protonated palmitic and stearic acid, are only located on the surface. The bulk as well as the surface of the paint film contains ester- and metal-bound fatty acids. SIMS measurements on sample ZD show the opposite, free fatty acids are more abundant in the

bulk of the film.

3.2.3.5 Drying characteristics of reconstructions and critical issues on their preparation

A difference in composition between reconstructed paint films is not only seen for a fresh (P) and naturally aged (ZD) paint, discussed above, but also observed for a naturally aged (ZD) and artificially aged (ZDC) paint film. The SIMS information obtained from the positive and negative ion mode gives a detailed picture of the composition of the paint film. Positive ion SIMS analysis shows that the surface layer at the top of the mature oil paint film ZDC contains, in contrast to ZD, predominantly metal soaps. The free and ester-bound fatty acids are present in higher abundance in sample ZD. Characteristic fragments for the first stage of drying *i.e.* small chain fatty acids, diacids (degradation products) are detected in the negative ion mode in sample ZD. We conclude that sample ZDC is approaching a mature oil paint composition based on the fragments detected in the positive mode, whereas sample ZD is a younger paint.

SIMS data on top and bottom side of paint film ZDC shows metal soaps to be more predominant near the top side of the paint film whereas degradation products and various acylglycerolesters predominate on the bottom side. This suggests a heterogeneous drying process across the paint film as well as different rates of humidity-induced aging due to an impermeable Melinex support. The preparation of a multi-layered system also requires special attention. Oil triacylglycerols migrate between the layers in a multi-layer oil paint system when the lower layers are not completely cured. SIMS analysis of a cross-section of the multi-layered paint reconstructions with linseed oil, a separating mastic layer and poppy seed oil (LMP) show the same P/S ratio of 3.5 for the linseed as well as for the poppy seed oil layer. The P/S ratio determined from cross-sections of single layer oil paint gives 2.0 for linseed oil (sample L) and 3.6 for poppy seed oil (sample P). As the layers in sample LMD were applied within 12 hours, the individual layers were not cured properly and migration of oil constituents has taken place. The mastic layer in between the linseed and poppy seed oil layer does not act as a barrier. This observation is also relevant for the interpretation of data from paints in wet-in-wet technique used by painters in the 19th century.

3.2.4 Conclusions

SIMS is able to detect and localise monocarboxylic fatty acids in paint cross-sections. Chalk tablet studies prove that the two main fatty acids in oil paint - palmitic and stearic acid (examined in free acid form) - have a similar ion response under SIMS conditions. Therefore, extrapolating to ester- and metal-bound species, it is accurate to use the peak area ratio of the two fatty acids (P/S) as an indication. The P/S ratio of reconstruction ZD determined with SIMS is close to the values determined with GC/MS and DTMS. However, SIMS studies on the oil paint reconstructions reveal an inhomogeneous distribution of the palmitic and stearic acid in the paint film. The P/S ratio varies between the surface and the bulk of the paint layer as well as within the paint layer. This difference cannot be shown by GC/MS and DTMS as these techniques measure the whole sample resulting in an average P/S ratio. The variance of the P/S ratio within one layer is not sufficiently high to hinder the use of this parameter in oil identification. SIMS allows the detection of differences in P/S ratio in the different paint layers of paint cross-sections from 15th- to 19th-century paintings.

The fatty acids analysed with SIMS can be attributed to the speciation of the fatty acid, *i.e.* free, ester-bound or metal carboxylate bound. The localisation of these characteristic fragments leads to new insights in the drying process of oil paint reconstructions. In a fresh oil paint (P) the free fatty acids are present on the surface of the paint compared to a paint film, which is naturally aged for three years (ZD). The artificially aged (ZDC) approached compared to the natural aged (ZD) a mature oil paint, due to the presence of metal soaps and absence of degradation products. SIMS analysis on the top side and bottom side of ZDC showed that the accelerated aging of the paint film is inhomogeneous. The top side reaches the mature oil paint state in contrast to the bottom side, due to the impermeable support. SIMS studies on a paint cross-section of the multi-layered reconstruction, prepared wet-in-wet, elucidate a migration of oil constituents between the layers. SIMS proved to be a suitable technique to identify and localise oil constituents in painted works of art.

3.2.5 Acknowledgements

We are grateful to Leslie Carlyle, (ICN, The Netherlands) for preparing and providing all lead white-containing oil paint reconstructions. We would like to thank Prof. J.R.J. van Asperen de Boer, L. Speleers, P. Noble and J. Zucker for providing the

paint cross-sections. Some of the results were obtained while on an exchange at the GCI (USA). The authors are grateful to M. Schilling and J. Keeney for assistance with GC/MS work.

3.2.6 References

1 J.D.J. van den Berg, *Analytical chemical studies on traditional linseed oil paints*. Ph.D. Dissertation, University of Amsterdam, Netherlands, 2001.

2 M.R. Schilling and H.P. Khaijan, *Gas chromatographic determination of fatty acid and glycol content of lipids I. The effect of pigments and aging on the composition of oil paints*. In: Preprints of the 11th triennial meeting of the ICOM Committee for Conservation. Edinburgh, 1, 1996, p. 242-247.

3 M.P. Colombini, F. Modugno, M. Giacomelli and S. Francesconi, *Characterisation of proteinaceous binders and drying oils in wall painting samples by gas chromatography-mass spectrometry*, Journal of Chromatography A, 846, 1999, p.113-124.

4 J.S. Mills and R. White, In: The organic chemistry of museum objects. Butterworth-Heinemann Ltd, 1994, p 143.

5 K. Keune and J.J: Boon, *Imaging secondary ion mass spectrometry of a paint cross-section taken from an early Netherlandish painting by Rogier van der Weyden*, Analytical Chemistry, 76, 2004, p. 1374-1385.

6 E.M. Gifford, In: *Le Dessin sous-jacent dans la peinture*, Colloque X*,* 5-9 September 1993, H. Verougstraete, R. Van Schoute (Eds.), Louvain-la-neuve, 1995.

3.3 Enhancement of the static-SIMS secondary ion yields of lipid moieties by ultrathin gold coating of aged oil paint surfaces

3.3.1 Introduction

Paint layers on traditional paintings are complex mixtures of organic binding material and inorganic components present as pigment or chemical drier. Combined information on nature and spatial distribution of organic and inorganic compounds in the paint layers can be obtained with static SIMS. SIMS data are usually acquired from a paint cross-section: a paint chip embedded in a synthetic resin. We have recently reported on the paint cross-section taken from the fifteenth century panel painting *The Descent of the Cross* by Rogier van der Weyden as a representative example from broader range of paint cross-sections investigated with static SIMS.[1] It was possible to determine the fatty acid signature of the three upper paint layers of this sample in imaging mode, revealing linseed oil paints with slightly different compositions. The elemental image maps correlated well with the pigments observed in the light microscopic and Fourier transform infrared (FTIR) images. Static SIMS is also suitable for characterisation of paint cross-sections from modern paintings.[2] In general however, the relative secondary ion yields from the mineral phases is much better than the ion yields for to the organic fragments of the binding medium-aged paint systems. For a better characterisation and localisation of the binding medium within the paint layers it was, therefore, desirable to develop methodology to improve the organic ion yields.

In this chapter we explore the enhancement of the secondary ion yields from fatty acids derived from aged oil paint systems after application of a thin coating of gold. Metal substrates generally improve the sputter yields of the organic molecules by complexation to the substrate atom.[3] Benninghoven *et al.* have found that the yields of the quasimolecular ion emission enhanced significantly when a solution is deposited on a metal surface (droplet preparation resulting in monolayers).[4] A silver substrate is the best cationising agent to improve the secondary ion yields followed by Au, Pd, Cu, Ni, Pt and Cr.[3, 5] This method is not practical for the system of paint cross-sections that we are interested in, because only thin monolayer films can be studied in this manner. Alternatively, Linton *et al.* have covered polymer sample surfaces with a thick layer (1500 Å) of silver ions to induce cationised organic secondary ions.[6] Recently, Delcorte *et al.* used a gold coating to improve the organic yields from bulk samples of oligomers, high-molecular-weight polymers and polymers additives.[7] The benefit of using gold to enhance the organic yields is that gold is a noble metal and it

is an electron donor and good cationisation agent. The exact mechanism of promotion of the organic yields by gold is currently not clear from the literature. It is clear that the thickness of the gold coating determines the secondary ion yield. The optimum gold thickness for polystyrene bulk samples is 20 Ångstrom.[7] The thin gold coating is not continuous but resembles gold "islands" on the surface.
To test whether gold coating of paint cross-sections would be a good method to improve the secondary organic yield of oil paint components, a well-defined paint model system of a lead white-containing oil paint reconstructed according traditional recipes and naturally aged for four years was chosen for investigation. Lead white is one of the most important pigments used in old master paintings and the mineral matter acts as template and chemical drier for cross-linking of the polyunsaturated triacylglycerols in drying oil. Static SIMS in positive and negative ion mode was performed on gold coated and gold free areas. To avoid bias with respect to inhomogeniety of the sample surface, a second test system was developed that consisted of the surface of a chalk tablet with 1% of stearic acid that was partially covered during gold deposition. This chapter demonstrates that the secondary ions yield of the relevant organic molecules is indeed enhanced by the surface covering with a thin gold coating layer.

3.3.2 Experimental

The static SIMS experiments were performed on a Physical Electronics (Eden Prairie, MN) TRIFT-II time-of-flight SIMS (TOF-SIMS).[8] The surface of the sample was scanned with a 15 KeV primary ion beam from an $^{115}In^{+}$ liquid metal ion gun. The pulsed beam was compressed (bunched) to ~1 ns to obtain a better mass resolution, a current was 600 pA and the spot size ~120 nm. The primary beam was rastered over a 150 x 150 µm sample area, divided into 256 x 256 pixels. Measurements in both positive and negative mode were performed, each with a total primary ion dose of 1.0×10^{12} ions cm^{-2}, well within the static SIMS regime.[9] The surface of the gold free sample was charge compensated with electrons pulsed in-between the primary ion beam pulses. After acquiring the SIMS data on this sample, the sample was gold-coated and again measured with SIMS under similar conditions using a different area to avoid surface damage effects.

The lead white linseed oil paint (ZD) was prepared by Carlyle in 1999 in the course of the MOLART project at FOM-AMOLF using freshly pressed linseed oil (linseeds provided by MACOS bv., Swifterbant, The Netherlands) mixed with Dutch stack process lead white (loodwit Schoonhoven de Kat, in stock at MOLART).

The paint was applied to Melinex sheets and kept under ambient conditions. A three-year-old paint sample taken from these sheets in 2002 was analysed by SIMS.

A well homogenised mixture of chalk (Merck) with 1% stearic acid (Sigma-Aldrich Chemie GmbH) was pressed into a tablet using a KBr pellet press. The tablet was partially covered with aluminum foil during the exposure to gold vapor. The gold layer of 2 nm was deposited by thermal evaporation *in vacuo* (3 x 10^{-5} Pa) at a deposition rate of 0.5 Å s^{-1}.

3.3.3 Results

3.3.3.1 Secondary ion mass spectrometry of a partially gold coated stearic acid-containing tablet

Fig. 3.3.1a presents SIMS negative ion image of the deprotonated stearic acid (*m/z* 283). The left side of the image was covered during gold deposition whereas the right part of the image is gold coated. The arrow in the image indicates the direction in which a line scan is taken. The yields of the negative ions of gold (*m/z* 197; grey line) and stearic acid (*m/z* 283; black line) of the line scan are plotted in the graph in Fig. 3.3.1b. An increase of the organic signal (*m/z* 283) by a factor of 4.7 is observed in the gold-coated area. The negative ion of stearic acid in the gold-free area (-Au) has an intensity of about 4 counts per pixel whereas in Au-coated area (+Au) the intensity increases to about 19 counts per pixel. The gold ion has 0 counts per pixel in the non-coated area and 12 counts per pixel in the gold-coated area. These positive results merited a further exploration of a real oil paint surface.

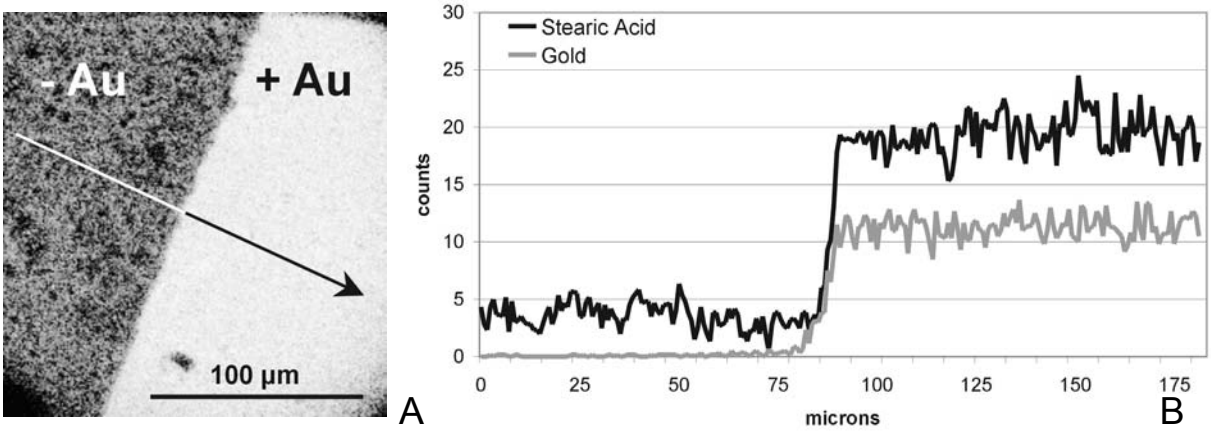

Figure 3.3.1 SIMS image showing the spatial distribution of stearic acid (m/z 283) in a chalk tablet-containing 1% stearic acid (A). The tablet is partially (right side) coated with 20Å gold. The arrow indicated the direction of the line scan. The yields negative ions of gold (m/z 197; gray line) and stearic acid (m/z 283; black line) of the linescan are plotted in the graph (B).

3.3.3.2 Secondary ion mass spectrometry of native lead white-containing linseed oil paint

The aged model system investigated has not reached full maturity yet. A mature oil paint consists of polyanionic ionomeric network coordinated by lead or another metal coordinating the carboxylic groups.[10, 11] The system investigated is a relative young oil paint with organic constituents representative of fresh oil paint. However, most of the organic ions characteristic for a mature oil paint can be detected as well.[12]

The SIMS mass spectrum of positive ions detected from lead white-containing linseed oil paint (sample ZD) contains peaks characteristic for the linseed oil as well for the lead white pigment. The most important positive ion peaks are assigned in Table 3.3.1. Lead (*m/z* 208), lead oxides (*m/z* 225, 432, 656) and lead hydroxides (*m/z* 449, 673, 897) ($PbO{\cdot}H^+$, $Pb^+_xO_{x\text{-}1}$, Pb_xO_xH; x = 1-4) are derived from the lead white pigment. Pb^+, Pb^+_2O and $Pb_2O_2H^+$ are observed in the positive mass spectrum in Fig. 3.3.2. High-mass peaks characteristic for triacylglycerols, the main constituents of the original oil paint, are also found in the positive SIMS spectrum. Smaller hydrocarbon fragments (below *m/z* 100) are too common and are detected in many other sample surfaces than oil paints. These fragments will not be discussed here. Fig. 3.3.2 presents several higher mass peaks molecular characteristic of oil: protonated palmitic and stearic acid (*m/z* 257 and 285) and their acylium ions (*m/z* 239 and 267), monoacylglycerol esters of palmitic and stearic acid (*m/z* 313 and 341) and the diacylglycerol esters with these acids (*m/z* 551, 579 and 607). Azelaic acid is an oxidation product of unsaturated C18 fatty acids produced in aged oil paint systems.[11] A fragment present in very low yield is the acylium ion of azelaic acid (*m/z* 171) is visible in Fig. 3.3.2. Markers for aged lead-containing oil paint are fatty acid lead soaps formed during chemical drying and aging of the oil. The two dominant fatty acid lead soaps are the lead soaps of palmitic and stearic acid detected in the positive mass spectrum at *m/z* 461-463 and *m/z* 489-491 respectively (Fig. 3.3.2). Fatty acid lead soaps of azelaic acid (*m/z* 393-395) and of the acylium ion from azelaic acid (*m/z* 375-377) are detected in lower yield.

The most important ion peaks in the negative SIMS spectrum of sample ZD are presented in Table 3.3.2. Ions indicative for lead white pigments such as clusters of lead and lead hydroxides are not observed in the negative ion spectrum (Fig. 3.3.3). The two main negative ions detected are the deprotonated palmitic and stearic acids (*m/z* 255 and 283 respectively), both fatty acids representative as the main fatty acid moieties in oil paint. Negative ions detected in lower yields are deprotonated azelaic acid (*m/z* 187), deprotonated octanoic, nonanoic and decanoic acid (*m/z* 143, 157

m/z	**(Fragment) Ion**	**Assignment**
171	$[HOOCRCO]^+$	Acylium ion of azelaic acid
206-208	Pb^+	Lead
239	$[RCO]^+$	Acylium ion of palmitic acid
225, 432, 656	$Pb_xO_{x-1}^+$; x = 1-4	Lead Oxides
257	$[RCOOH_2]^+$	Protonated palmitic acid
267	$[RCO]^+$	Acylium ion of stearic acid
285	$[RCOOH_2]^+$	Protonated stearic acid
313	$[RCO + 74]^+$	Monoacylglycerolester of palmitic acid
341	$[RCO + 74]^+$	Monoacylglycerolester of stearic acid
375-377	$[Pb + OCRCOO]^+$	acylium ion of lead soap from azelaic acid
393-395	$[Pb + HOOCRCOO]^+$	Lead soap of azelaic acid
449, 673, 897	$Pb_xO_xH^+$; x = 1-4	Lead Hydroxides
461-463	$[Pb + RCOO]^+$	Lead soap of palmitic acid
489-491	$[Pb + RCOO]^+$	Lead soap of stearic acid
551, 579, 607	$[M-RCOO]^+$	Diacylglycerolester of palmitic/palmitic, palmitic/stearic and stearic/stearic acid

Table 3.3.1 Characteristic positive secondary fragment ions of lead white-containing oil paint (ZD) analysed with SIMS.

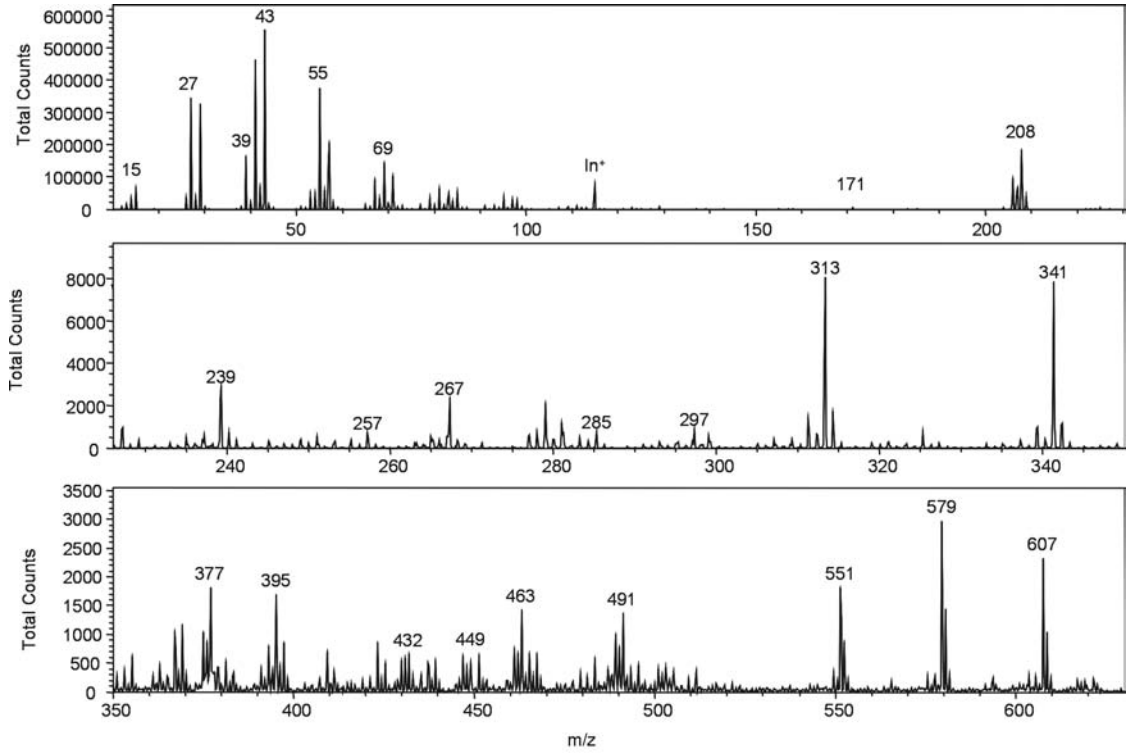

Figure 3.3.2 The SIMS spectra in positive mode of the lead white-containing oil paint (sample ZD).

m/z	**(Fragment) ion**	**Assignment**
71, 85, 99, 113, 127, 141, 155, 169,183, 197, 211, 225 and 239	$[C_2H_3(CH_2)_xCOO]^-$	Aliphatic chain fragment ions of fatty acids (x = 1-15)
187	$[HOOC(CH_2)_7COO]^-$	Deprotonated azelaic acid
143	$[RCOO]^-$	Deprotonated octanoic acid
157	$[RCOO]^-$	Deprotonated nonanoic acid
171	$[RCOO]^-$	Deprotonated decanoic acid
255	$[RCOO]^-$	Deprotonated palmitic acid
283	$[RCOO]^-$	Deprotonated stearic acid
269	unknown	Derived from tripalmitin
297	unknown	Derived from tristearin
311	$[RCO + 72]^-$	Monoacylglycerolester of palmitic acid
339	$[RCO + 72]^-$	Monoacylglycerolester of stearic acid

Table 3.3.2 Characteristic negative secondary fragment ions of lead white-containing oil paint (ZD) analysed with SIMS.

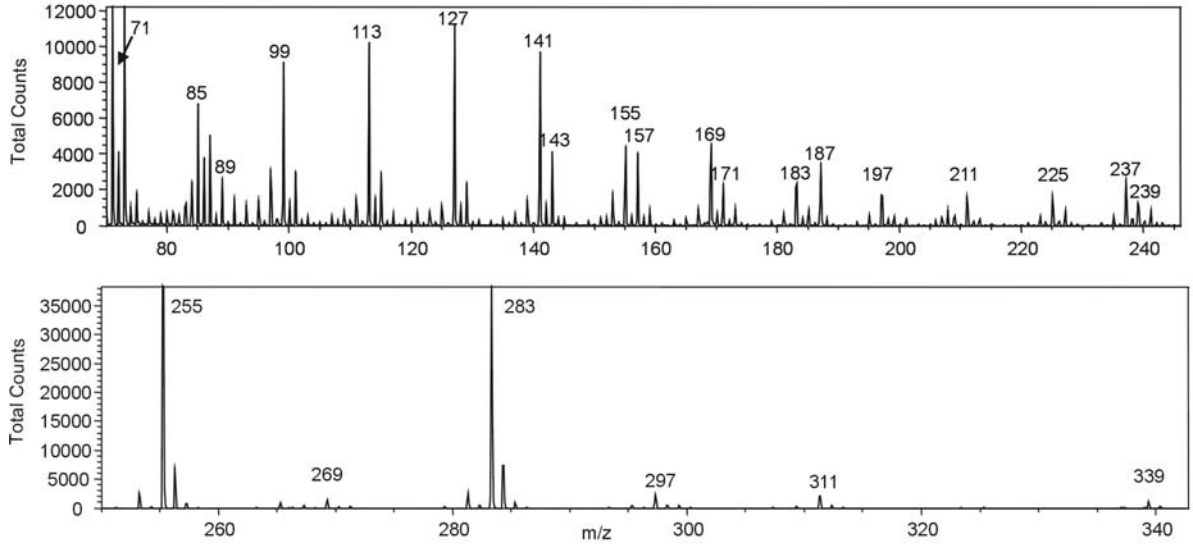

Figure 3.3.3 The SIMS spectra in negative mode of the lead white-containing oil paint (sample ZD).

and 171) and aliphatic chain fragment ions of fatty acids with a mass increments of 14 amu (*m/z* 239, 225, 211, 197, 183, 169, 155, 141, 127, 113, 99, 85 and 71). Azelaic acid as well as octanoic, nonanoic and decanoic acid are oxidation and degradation products of aged oil paint.[11] Other negative ions, characteristic for oil paint, observed are *m/z* 311 and 339 corresponding to monoacylglycerol esters of palmitic and stearic acids. The observed negative ions at *m/z* 269 and 297 in the mass spectrum remain unidentified. These fragments are also detected in the negative mass spectrum of standard triacylglycerols (tripalmitin and tristearin respectively) (not shown), and are always found in negative spectra of oil paint.

3.3.3.3 Secondary ion mass spectrometry of gold-coated lead white-containing linseed oil paint

The positive ion mass spectrum of lead white-containing linseed oil paint (sample ZD + Au) coated with a 20Å thick gold layer displays the oil-derived mass peaks as detected in the positive mass spectrum of the non-coated ZD sample (Table 3.3.1 and Fig. 3.3.4). It is remarkable that only the lead ions are observed and clusters of lead, lead oxides or lead hydroxides are absent, perhaps due to a milder primary ion regime. Additional peaks showing up in this positive mass spectrum are gold (*m/z* 197) and clusters with odd numbers of gold atoms ($Au_{3,5,7,9}$; *m/z* 591, 985, 1379, 1773 respectively). Peaks representing clusters with an even number of gold atoms have a very low intensity and are visible in Fig. 3.3.4 at *m/z* 1576 (Au_8) and *m/z* 1970 (Au_{10}). Other types of clusters observed are gold clusters with one lead atom attached (*m/z* 403-405, 600-602, 797-799, 994-996, 1191-1193, 1388-1390, 1585-1587, 1782-1784 and 1979-1981). New peaks detected in the mass spectrum of the ZD + Au sample compared to the ZD sample were found at *m/z* 225, 239, 251, 253 and 255. We suspect that these ions correspond to gold cations of small fragments of hydrocarbons (Au + 28 amu, Au + 42 amu, Au + 54 amu, Au + 56 amu and Au + 58 amu respectively) (Fig. 3.3.4). Prominent peaks from silicones are detected at *m/z* 28, 73, 147, 207, 221, 265, 267, 279, 281, 323-329, 339, 341 and 355 pointing to contamination of the surface of the sample with silicones adsorbed from the laboratory environment.

No fragments from the lead white pigments such as clusters of lead and lead hydroxides are detected in negative mass spectrum of ZD + Au, just as in the non-coated sample (Fig. 3.3.5). Ions observed in the negative mass spectrum of ZD + Au are comparable with ions detected in the mass spectrum of sample ZD (Table 3.3.2 and Fig. 3.3.5). Additional peaks due to the gold coating are ascribed to gold (*m/z* 197) and clusters of gold (*m/z* 394, Au_2; 591, Au_3; 788, Au_4; 985, Au_5; 1182, Au_6;

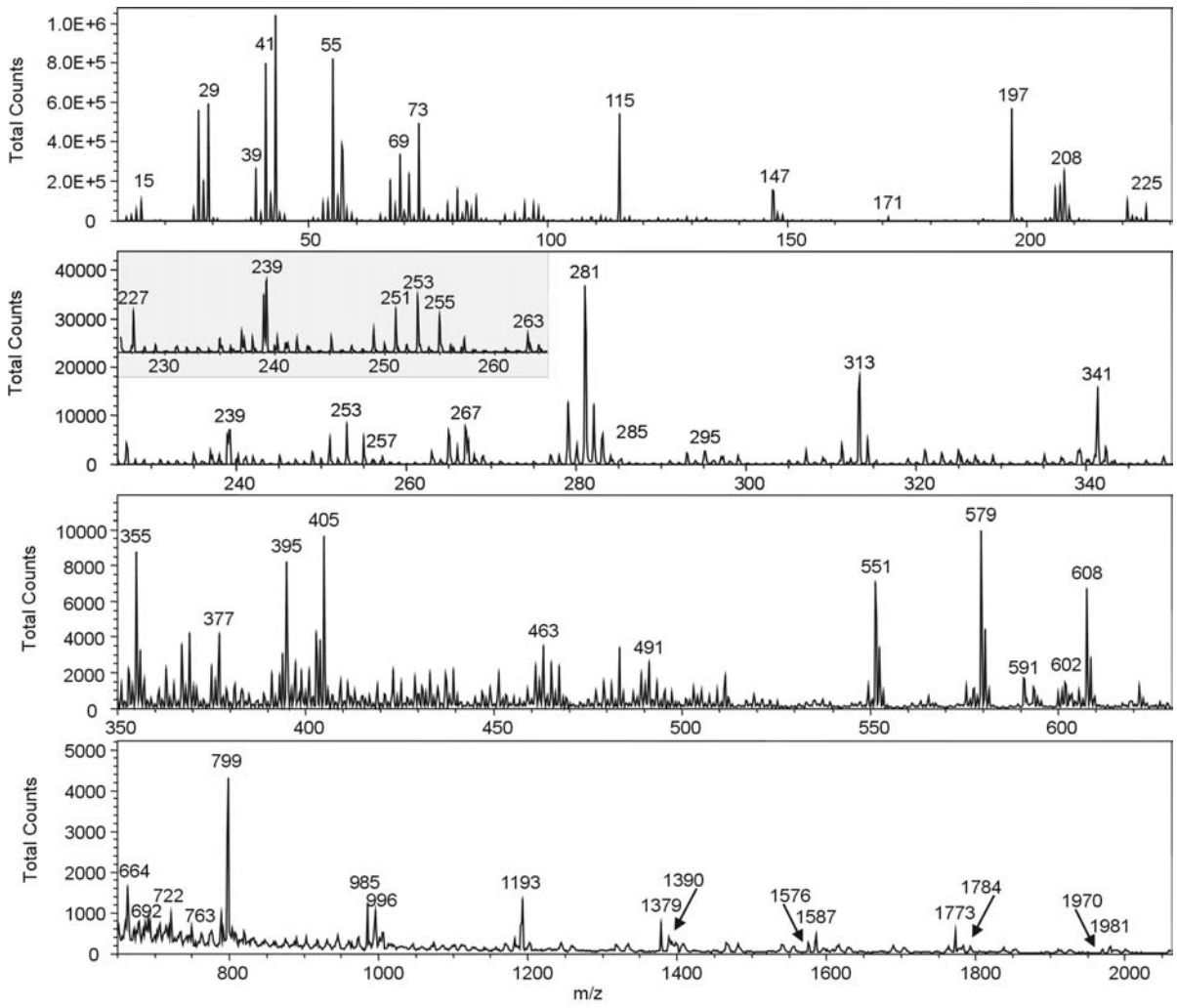

Figure 3.3.4 The SIMS spectra in positive mode of the lead white-containing oil paint with a 20Å gold coating (sample ZD + Au).

1379, Au_7; 1576, Au_8; 1773, Au_9; 1970, Au_{10}; 2167, Au_{11} and 2364 Au_{12}). In general, the peaks related to gold clusters with even numbers of atoms have a lower intensity than clusters with odd gold atoms. A second series of peaks at 1 amu higher than the clusters with even numbers of gold atoms (Au_2, Au_4, Au_6, Au_8 and Au_{10}) (*m/z* 395, 789, 1183, 1577 and 1971) is detected with the same intensity: the peaks for Au_x and Au_{x+1} (x = 2, 4, 6, 8 and 10) overlap in Fig. 3.3.5 due to the large mass range plotted. Several new peaks due to the gold coating show up in the negative mass spectrum. Two prominent peaks detected are assigned to gold-anionised neutral palmitic and stearic acid ($C_{16}H_{32}O_2Au^-$ at *m/z* 453 and $C_{18}H_{36}O_2Au^-$ at *m/z* 481) (Fig. 3.3.5). Deprotoned and thus negatively charged fatty acids coordinated to a gold cluster are found at *m/z* 649 and *m/z* 677: Au_2 + 255 ($C_{16}H_{31}O_2Au_2^-$) and Au_2 + 283 ($C_{16}H_{35}O_2Au_2^-$), respectively (mass range not shown). Other peaks present in nega-

tive spectrum, which presently remain unidentified, are detected at *m/z* 408, 411, 419, 420 and 435. We suggest that these peaks represent Au_2 clusters with a small unidentified fragments attached (Au_2 + 14 at *m/z* 408; Au_2 + 17 at *m/z* 411; Au_2 + 25 at *m/z* 419; Au_2 + 26 at *m/z* 420 and Au_2 + 41 at *m/z* 435), however no pattern in these types of organic fragments is evident.

Silicones, present as contaminant on the surface of in gold-coated sample, are visible in Fig. 3.3.5 at *m/z* 163, 223, 237, 297 and 313. These fragments overlap with oil paint characteristics.

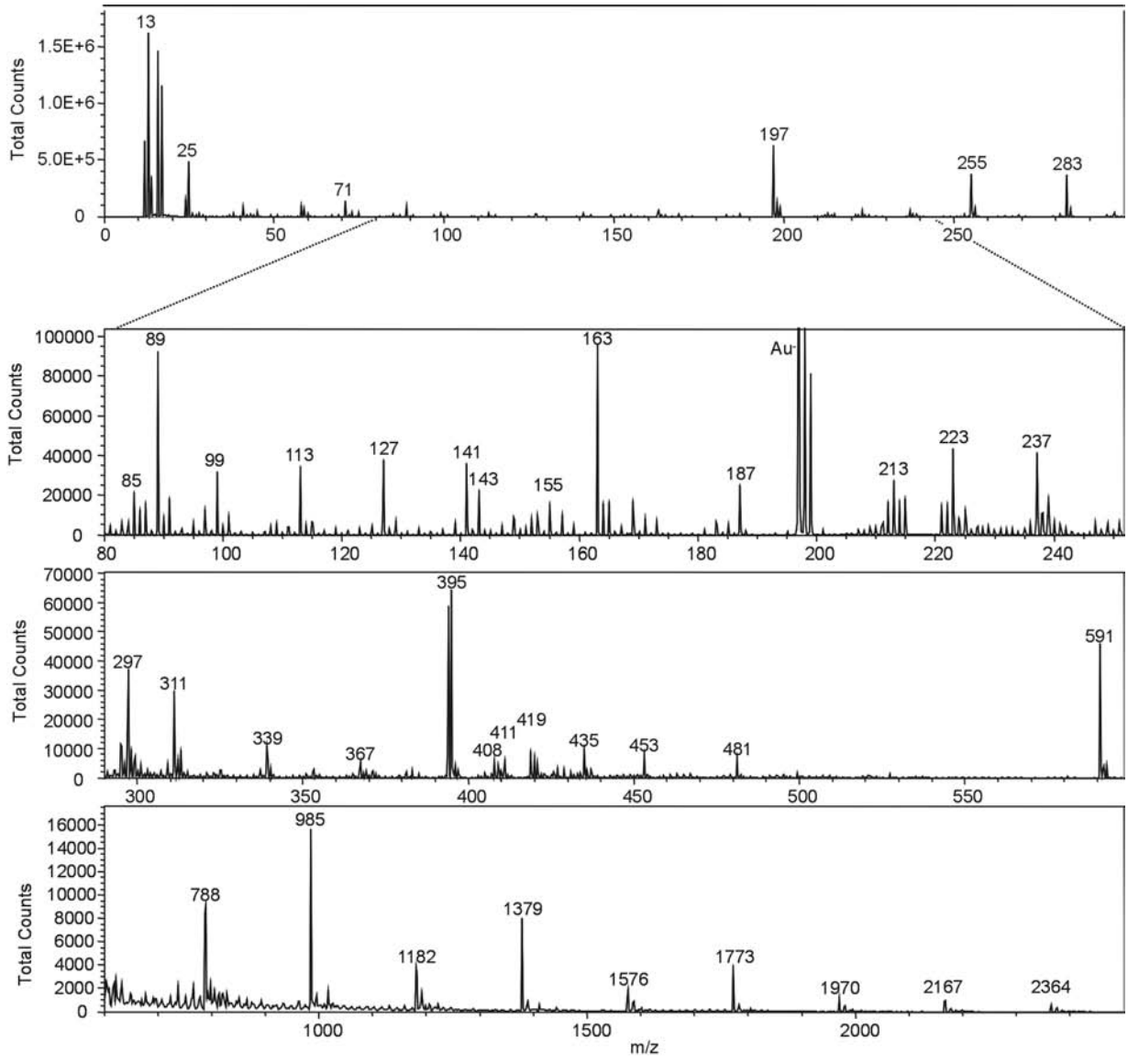

Figure 3.3.5 The SIMS spectra in negative mode of the lead white-containing oil paint with a 20Å gold coating (sample ZD + Au).

3.3.3.4 Ion yield improvement

The graph in Fig. 3.3.6 illustrates the enhancement of the ion yields of the ZD + Au sample. The peak areas of positive ions characteristic for the oil medium (Table 3.3.1) and the lead white pigment (*m/z* 208) in samples ZD and ZD + Au are plotted (Fig. 3.3.6). On the left axis the organic yields of samples ZD (circles) and ZD + Au (squares) are plotted on a logarithmic scale. On the right axis the factor of improvement of the secondary ion yields due to gold-coating is plotted (triangle). This factor is calculated by dividing the gold-coated sample ion yield by the ion yield of the corresponding non-coated sample. All positive ions plotted from the gold-coated sample result in higher yields compared to the non-coated sample. These ions do not increase with a constant factor. In general, the yields of the positive ions fatty components and fatty acid metal soaps increase by a factor of 2 - 3. The positive ions from diacylglycerol esters (*m/z* 551, 579 and 607) increase by a factor of 3.5 - 4. The gold coating does not enhance significantly the yields of metals: the lead counts are improved with a factor of 1.5. Whereas ions from lead clusters and lead hydroxides are suppressed and not detected in the positive mass spectrum of sample ZD + Au.

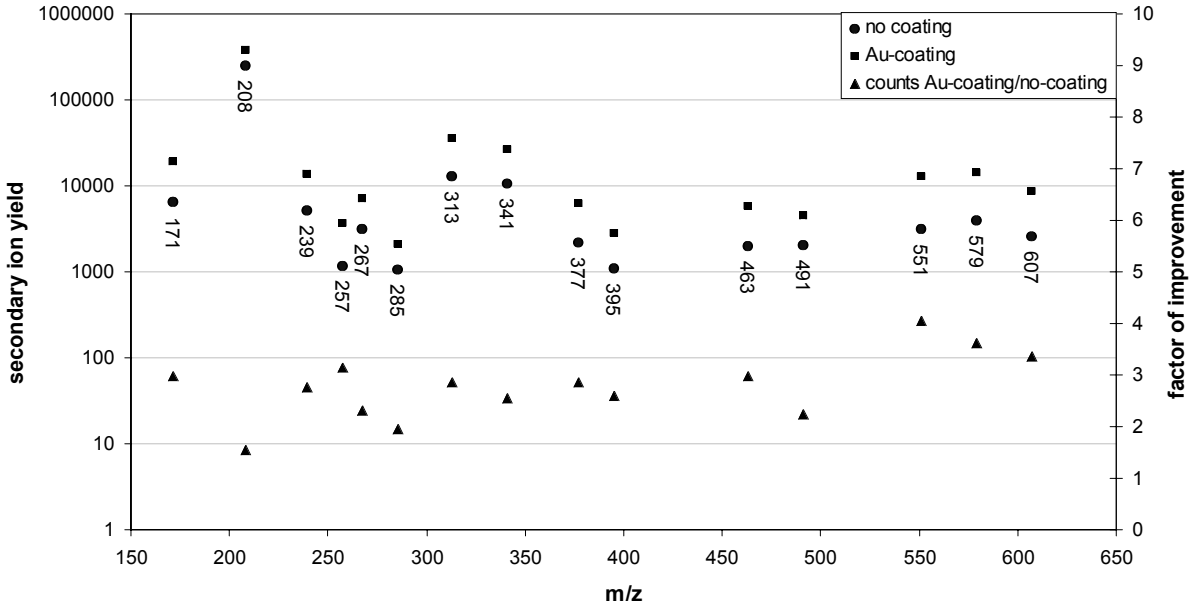

Figure 3.3.6 The left axis represents the yields of positive secondary ions from gold-coated (circle) and non-coated (square) ZD sample. The yields represent the peak areas of the plotted secondary positive ions. On the right axis the factor of improvement of the organic yields due to a gold coating is determined (triangle). This factor is calculated by dividing the gold-coated ion yields by the corresponding non-coated ion yields.

The enhancement of the secondary organic ion yields in the negative ion mode due to gold-coating increases with constant factor. The organic negative ions plotted in Fig. 3.3.7 represent ions derived the oil paint system (Table 3.3.2 and Fig. 3.3.7). The yields of the negative ions are enhanced by approximately a factor of 3, with the exception of two ions at *m/z* 143 and 187 (Fig. 3.3.7). The yields of octanoic acid (*m/z* 143) -an oxidation product of oil- increases by a factor of 5, whereas the yields of azelaic acid (*m/z* 187) increases by a factor of 6.5.

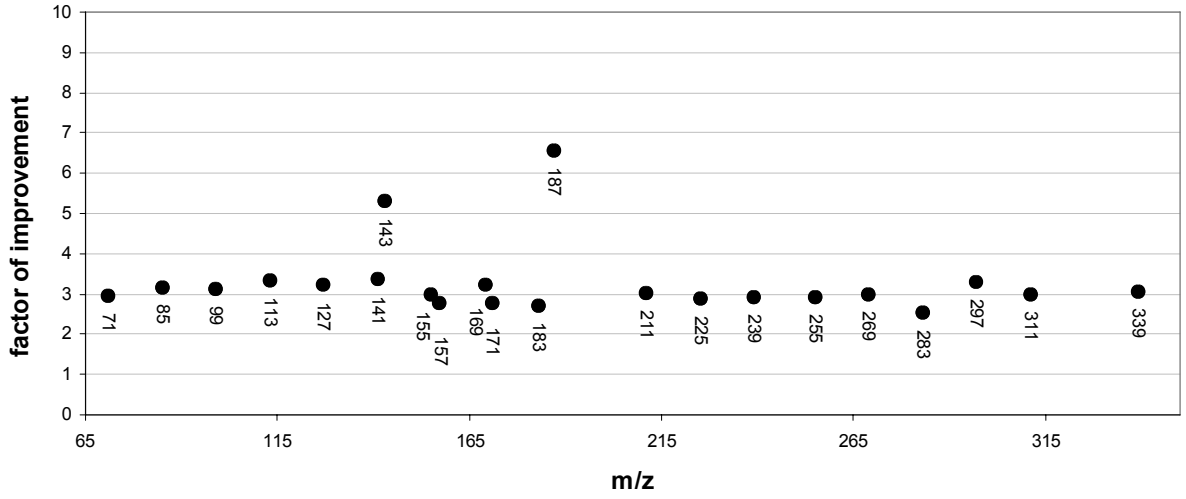

Figure 3.3.7 The factor of improvement of the negative organic ion yields is estimated. This factor is calculated by dividing the gold-coated ion yields by the corresponding non-coated ion yields.

3.3.4 Discussion

Gold coating improves the yields of the organic ions characteristic for aged oil paint. Our test results indicate that the methodology of gold coating is suitable for improvement of the organic information that can be obtained from paint cross-section of traditional paintings.

Our tablet study proves that the organic yields are only enhanced due to the presence of a gold layer. The two areas (coated and non-coated) within the sample were exposed to the same gold coating and SIMS analytical conditions. The line scan (Fig. 3.3.1b) demonstrates that the organic yields increase dramatically where gold is present. These data also reassured us that the surfaces of the oil paint sample ZD were sufficiently comparable to measure an effect due to gold coating, thus avoiding bias due to our decision to analyse fresh (*i.e.* untouched by the primary beam) before and after gold coating.

3.3.4.1 Factor of improvement of the organic ion yields

The absolute number increase in organic yield due to a gold coating for the negative ion of stearic acid is not the same for the chalk tablet and sample ZD. The factor of improvement is 4.7 for the tablet and 3 for sample ZD. This difference may due to differences in surface composition of the sample. Stearic acid in the oil paint is present in a complex mixture of other organic substances and more reactive mineral matter compared to the organic-free and inert chalk.

The factors of improvement between the yields of the negative and positive ions in sample ZD are different. The negative ion mode shows an increase of a factor 3, with the exception of two fragments, whereas in the positive mode this factor varies in the range 2 - 4. Deprotonation of the acid group facilitates ionisation for all the negative ion species observed and therefore the secondary ion yields show similar results. One of the two outliers in the negative mode is a deprotonated diacid (*m/z* 187) that is quite unstable, especially compared to a mono-acid. A gold coating seems to be stabilised the deprotonated diacid ion resulting in much higher yield. The high factor of improvement of the second outlier, a mono-acid (*m/z* 143), is supposed to caused by overlap of an unknown peak introduced after gold coating. The type of group, facilitating the charge for the positive ions species, varies between protonated acid groups, metal carboxylates, acylium ions and protonated fragments of triacyl-glycerol. No trend is obvious in ion yields between these different groups of positive ions.

3.3.4.2 Effect of gold coating on organic and inorganic molecules

Gold coating leads to primarily to an enhancement of the ionisation and less to a reduction in fragmentation of the molecules. This deduced from the graph of the yield improvement factor of the negative ions (Fig. 3.3.7), where the yields of aliphatic chain fragment ions of the fatty acids are increased with the same factor as the fatty acid ions. If the fragmentation is reduced due to the gold coating, factor of improvement for the deprotonated fatty acid should be higher than the factor of aliphatic chain fragments of the fatty acids.

Gold coating improves the organic ion yields, but suppresses the yields of the metal ions. In the positive mode the yield of the lead ion is improved but not as strongly as the improvement of organic ion. A qualitative difference is that gold coating eliminates the formation of clusters of lead, lead oxides or lead hydroxides, which are believed to be formed in the selvedge. This might be an indication that the primary energy deposited on the surface is reduced due to the stopping power of the gold coating, which results in a lower consumption of the lead white.

3.3.4.3 Gold-organic complex ions

Different gold-organic complex ions are detected in the positive as well as the negative SIMS spectra. In the positive mode, cations with small organic masses of 28, 42, 54, 56 and 58 amu are observed. The accurate mass of these ions indicates the presence of a gold ion attached to a neutral $C_xH_{2x\ (x\ =\ 2\text{-}4)}$ fragment ($C_xH_{2x\text{-}2}$ in the case of 54 amu and C_xH_{2x+2} in the case of 58 amu). In the negative ion mode, different types of gold anions are observed. Two prominent ions detected are neutral palmitic and stearic acid, each attached to one gold ion. According to the literature, these types of ions are only found in the positive mode.[14] However, the system described in our paper differs because in our case the gold is on top of the sample and not underneath a thin layer of stearic acid as is the case in Ref. 14. Positively charged gold ions with neutral fatty acids are not observed in our data. From our experiments we would suggest that negatively charged gold ions have a higher affinity to neutral fatty acid species compared to positively charged gold ions. Other anions detected in the negative mass spectrum are of the type Au_2 + organic anion. Two peaks present in the mass spectrum are assigned to a gold cluster with a deprotonated fatty acid, *i.e.* palmitic and stearic acid. This observation - the existence of a gold cluster with an organic anion - supports the idea that the peaks observed at lower mass belong to gold clusters with a small organic fragment. The accurate masses of the small organic fragments attach to the gold cluster correspond to the negative ions CH^-_2, OH^-, C_2H^-, $C_2H^-_2$ and $C_3H_5^-$ (14, 17, 25, 26 and 41 amu, respectively). Why only these negative fragments attach to the gold cluster is not yet clear.

3.3.5 Conclusions

An ultrathin gold coating enhances the secondary positive and negative ion yields of lipid moieties of aged oil paint. The negative organic ion yield is enhanced with a factor of 3, whereas the positive organic ion yield increases by a factor of 2 - 4. The negative charge is localised on the deprotonated acid groups of oil species observed, which result in a similar improvement of the secondary ion yield. The improvement of the positive secondary ion yields fluctuates because the charge is located on different chemical functional groups. Gold coating improves the ionisation process of the organic molecular ions and does not effect the fragmentation of fatty acids. The dissociation of the mineral matter, lead white, is reduced due to the gold coating.

The methodology of gold coating is a very promising tool to improve the organic yields from SIMS of paint cross-sections from paintings, thus leading to a more accurate mass spectral identification and an improved localisation of the spatial distribution of the organic constituents representative for the binding medium present in a traditional painting.

3.3.6 Acknowledgements

Dr. Leslie Carlyle is thanked for providing the samples of lead white linseed oil paint. We are grateful to Hans Zeijlemakers who performed the accurate gold coating of our samples.

3.3.7 References

1 K. Keune and J.J. Boon, *Imaging secondary ion mass spectrometry of a paint cross-section taken from an early Netherlandish painting by Rogier van der Weyden*, Analytical Chemistry, 76, 2004, p. 1374-1385.

2 J.J. Boon, K. Keune, T. Learner, *Identification of pigments and media from a paint cross-section by direct mass spectrometry and high-resolution imaging mass spectrometric and microspectroscopic techniques*, In: R. Vontobel (Ed.), Preprint of the 13th Triennial Meeting of ICOMCC in Rio de Janeiro, Volume I, James and James, London, 2002, p. 223-230.

3 A. Benninghoven, F.G. Rüdenauer, H.W. Werner, In: *Secondary Ion Mass Spectrometry*, John Wiley & Sons: New York, USA, 1987.

4 A. Benninghoven, *The history of static SIMS: a personal perspective*, In: ToF-SIMS: Surface Analysis by Mass Spectrometry, J.C. Vickerman, D. Briggs (Eds.). IM Publication and SurfaceSpectra Limited: West Sussex and Manchester, 2001, p. 57.

5 B. Hagenhoff, *Optimisation methods: cationisation*, In: ToF-SIMS: Surface Analysis by Mass Spectrometry, Vickerman JC, Briggs D (Eds.). IM Publication and SurfaceSpectra Limited: West Sussex and Manchester, 2001, p. 286-287.

6 R.W. Linton, *et al.*, *Time-of-flight ion mass spectrometric analysis of polymer surfaces and additivies,* Surface and Interface Analysis, 20, 1993, p. 991.

7 A. Delcorte, N. Médard, P. Bertrand, O*rganic secondary ion mass spectrometry: sensitivity enhancement by gold depostition*, Analytical Chemistry, 74, 2002, p. 4955-4968.

8 B. Schueler, *Microscope imaging by time-of-flight secondary ion mass spectrometry*, Microscopy Microanalysis Microstructures, 3, 1992, p. 119-139.

9 J.C. Vickerman, *ToF-SIMS - an overview*, In ToF-SIMS: Surface Analysis by Mass Spectrometry, J.C. Vickerman, D. Briggs (Eds.). IM Publication and SurfaceSpectra Limited: West Sussex and Manchester, 2001, p. 1-40.

10 L. Carlyle, *Historical reconstructions of artists' oil paint: an investigation of oil processing methods and the use of medium-modifiers*, Molart Fellowship Report, Ottawa, Canadian Conservation Institute, 2000.

11. J.D.J. van den Berg, *Analytical chemical studies on traditional linseed oil paints*, PhD Thesis,

University of Amsterdam, 2002 (http//www.amolf.nl/publications/theses/).

12 J.D.J. van den Berg, *Chemical changes in curing and aging oil paints*, 12th Triennial Meeting ICOM-CC, J. Bridgland (Ed.), Lyon 29 August- 3 September, 1999.

13 Unpublished observations.

Chapter 4

Analytical imaging studies clarifying the process of the darkening of vermilion in paintings

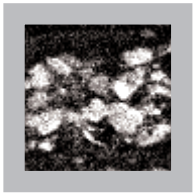

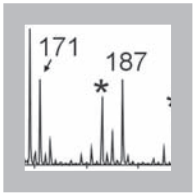

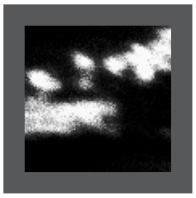

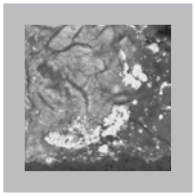

Imaging-secondary ion mass spectrometry (SIMS) is applied for the first time to paint cross-sections with degraded vermilion (red mercury sulphide) paint to cast new light on the well-known problem of its light induced darkening. The static SIMS data are combined with light microscopic, electron microscopic studies and energy dispersive X-ray analysis (SEM/EDX) to identify and localise the various reaction products. The spatial distribution of atomic and molecular species in paint cross-sections of the native vermilion and the reaction products leads to the formulation of a new hypothesis on the reaction mechanism of the photo-degradation of vermilion where two black and white coloured reaction products are formed sequentially. Under the influence of light some of the vermilion (HgS) is converted into Hg(0) and S(0). In this process the chlorine ions, present in the native vermilion, act as a catalyst. We propose that the Hg(0) is deposited on the surface of the remaining HgS as elementary mercury nanoparticles, which turns the vermilion black. Chloride, derived from an external source, is accumulating in the black phase. The metallic mercury and the remaining HgS react away with the excess of chloride. Two intermediate products and a white end product, mercuric chloride ($HgCl_2$), are formed.

4.1 Introduction

Blackening of vermilion (HgS, trigonal), a light induced degradation phenomenon of HgS, is observed on the raw mineral cinnabar as well as on vermilion paint in works of art. The colour change may strongly disfigure the painted image.[1] The highlights in a detail of *Triumphal Procession with Sacrificial Bull* by P. de Grebber (1650) (Oranjezaal, Huis Ten Bosch Palace, The Hague, The Netherlands) should have been vivid red, but are transformed into greyish strokes (Fig. 4.1).This irreversible surface degradation process takes place irrespective of the origin of the vermilion and the type of binding medium.[1] It does not matter whether vermilion has been processed wet or dry, or is derived from a natural source as cinnabar[1]. Until recently, the black product on vermilion was thought to be meta-cinnabar (HgS, cubic).[2, 3, 4, 5] However, Dreyer suggested already in 1938 that the blackening resulted from a superficial layer of colloidal mercury in solid solution on the cinnabar and that the blacking process was accelerated by impurities.[6] McCormack and others have shown recently that halogen impurities in and around vermilion particles play a dominant role in the darkening process.[4, 7, 8] Small concentrations of chlorine in cinnabar (average between 0.05 - 1 wt%) can already cause blackening, where as cinnabar with a chlorine concentration less than 0.01 wt% remains unaffected by sunlight.[7] Not only chlorine, but also other halogens (mainly iodine), trigger the blackening of vermilion.[4, 5, 7] Recently, Spring *et al.* observed two degradation products in blackened vermilion[9], a black and white one, which were assumed to be formed simultaneously. It was inferred that vermilion is first transformed into the photo-

Fig. 4.1 Detail of 'Triumphal Procession with Sacrificial Bull' by P. de Grebber (1650) (Oranjezaal, Huis Ten Bosch Palace, The Hague, The Netherlands) showing grayish strokes on top of the red dress. These highlights consist of blackened vermilion. Photo: L. Speleers, Stichting Restauratie Atelier Limburg (SRAL), Maastricht, The Netherlands (see coloured version at the end of this thesis).

sensitive mineral corderoite ($Hg_3S_2Cl_2$) after exposure to humidity and chloride ions. This corderoite subsequently degrades into the black meta-cinnabar, the white calomel $(HgCl)_2$ and elemental sulphur by a light induced reaction. The chloride was postulated to originate from external sources.

In general, the degraded vermilion layers in paint cross-sections are extremely thin (less than a few microns) and most analytical techniques do not have sufficient spatial resolution and sensitivity to study the changes within the paint layer.[4, 9] The availability of a paint cross-section taken from a (17th century ?) overpaint on the painting *Portrait of a Young Woman* by Peter Paul Rubens (1620s) (Mauritshuis, The Hague; sample number MH251/26) with an extraordinary thick layer of partially degraded, blackened vermilion particles made it possible to investigate the degradation process in more detail (Fig. 4.2a and 4.3a). In this paper a second paint cross-section from an original layer in *Minerva and Hercules opening the doors for Victory* by Christiaan van Couwenberg (1651), (Oranjezaal Huis ten Bosch Palace, The Hague; sample number HSTB 34/2), derived from a different collection than the first sample, is examined as well.

Portrait of a Young Woman by Peter Paul Rubens (1620s) displayed in Royal Picture Gallery Mauritshuis, The Hague (inv. no. 251) (see coloured version at the end of this thesis).

An important advantage of investigating the blackening process of vermilion in paint cross-sections is the clear visualisation of a gradient in the deterioration from the light exposed top to the light shielded bottom. In addition, the pigment particles are embedded in an organic binding medium layer, so the components possibly released during the blackening of vermilion are embedded and fixed in position so they can be investigated by microscopy.

The analytical data obtained from light microscopy (LM), scanning electron microscopy combined with energy dispersive X-ray analysis (SEM/EDX) and secondary ion mass spectrometry (SIMS) presented here lead to new insight in the mechanism of the blackening of vermilion. In contrast to work presented earlier,[9] we observe that a black reaction product is formed first, which is spatially separated and thus followed by a white compound. We prove that meta-cinnabar cannot be formed and with the exclusive results from secondary ion mass spectrometry, we could identify another white reaction product that was never before described in paintings.

4.2 Experimental

4.2.1 Samples

The paint sample MH251/26 was embedded in polyester resin Polypol using the Easysection™ system. Sample HSTB 34/2 was embedded in Technovit® 2000LC (Heraeus Kulzer, Germany). Both paint cross-sections were dry polished with Micromesh® polishing cloths (final step 12 000 mesh) (Scientific Instruments Services Inc., Minnesota). The following reference materials were used: mercury sulphide (HgS) (Merck), mercuric chloride ($HgCl_2$) (Merck) and mercurous chloride ($(HgCl)_2$) (Fluka).

4.2.2 Instruments

The static SIMS experiments were performed on a Physical Electronics (Eden Prairie, MN) TRIFT-II time-of-flight SIMS (TOF-SIMS). The surface of the sample was scanned with a 15 KeV primary ion beam from an $^{115}In^+$ liquid metal ion gun. The pulsed beam was non-bunched with a pulse width of 20 ns, a current of 600 pA and a spot size approximately 120 nm. The primary beam was rastered over a 50 x 50 µm sample area, divided into 256 x 256 pixels. The surface of the sample was charge compensated with electrons pulsed in between the primary ion beam pulses. To prevent large variations in the extraction field over the large insulation surface area of the paint cross-section a non-magnetic stainless steel plate with slits (1 mm) was placed on top of the sample. The paint cross-section (150 x 50 x 3 mm) was rinsed in hexane to eliminate contamination of airborne silicones.

A 15 KeV $^{115}In^{+}$ primary ion beam was used for the reference samples, with primary ion pulses that were compressed (bunched) to ~1 ns to obtain a better mass resolution. These experiments were performed with 600 pA beam current. All these measurements were charge compensated with electrons pulsed in between the primary ion beam pulses. The oil immersion reflected light microscopic images were obtained on a Leica DMRX microscope (Leica, Wetzlar, Germany). White light was provided by a 100 W halogen lamp, and an Osram HBO 50 W lamp and Leica filter D (excitation 360-425 nm, emission > 460 nm) were used for fluorescence microscopy. The surface of the paint cross-section was covered with immersion oil (cat. nr. 11 513 787, Leica, Germany) Images were recorded with a Nikon digital still camera DXM1200 (Nikon Instech Co., Ltd., Japan).

Scanning Electron Microscopy studies in combination with Energy Dispersive X-ray analysis (SEM-EDX) were performed on a XL30 SFEG high vacuum electron microscope (FEI, Eindhoven, The Netherlands) with EDX system (spot analysis and elemental mapping facilities) from EDAX (Tilburg, The Netherlands). Backscattered electron images of the cross-sections were taken at 20 kV accelerating voltage at a 5 mm eucentric working distance and a spot size of 3, which corresponds to a beam diameter of 2.2 nm with current density of approximately 130 pA. EDX analysis was performed at a spot size setting of 4 (beam diameter 2.5 nm and current density 550 pA) to obtain a higher count rate and at an acceleration voltage of 20 kV. EDX Mapping parameters were: 256 x 200 matrix, 1028 frames, 100 µs dwell time and 50 µs amplitude time. Samples were carbon coated to improve surface conduction in a CC7650 Polaron Carbon Coater with carbon fibre (Quorum Technologies, East Sussex, UK).

4.3 Results

4.3.1 Light microscopy

Light microscopic images of a highly magnified area of discoloured vermilion in the paint cross-section MH251/26 are shown in Fig. 4.2a, 4.3a and 4.4a (normal light) and 4.2b and 4.3b (UV light). The area of the panel painting of the sample MH251/26 is overpainted and the paint build up consist now of at least six layers. The original paint layers consist of a chalk ground, a lead white- and charcoal-containing imprimatura and finally several layers of vermilion and red lake. A bone black layer blocks out this original red paint. On top a thin organic intermediate layer is applied with as final layer the now degraded vermilion with red lake (paint cross-section not shown). The total thickness of the vermilion layer is 25 mm of which 15 mm is discoloured, containing both the black and white degradation products. The vermilion particles are coarse grained

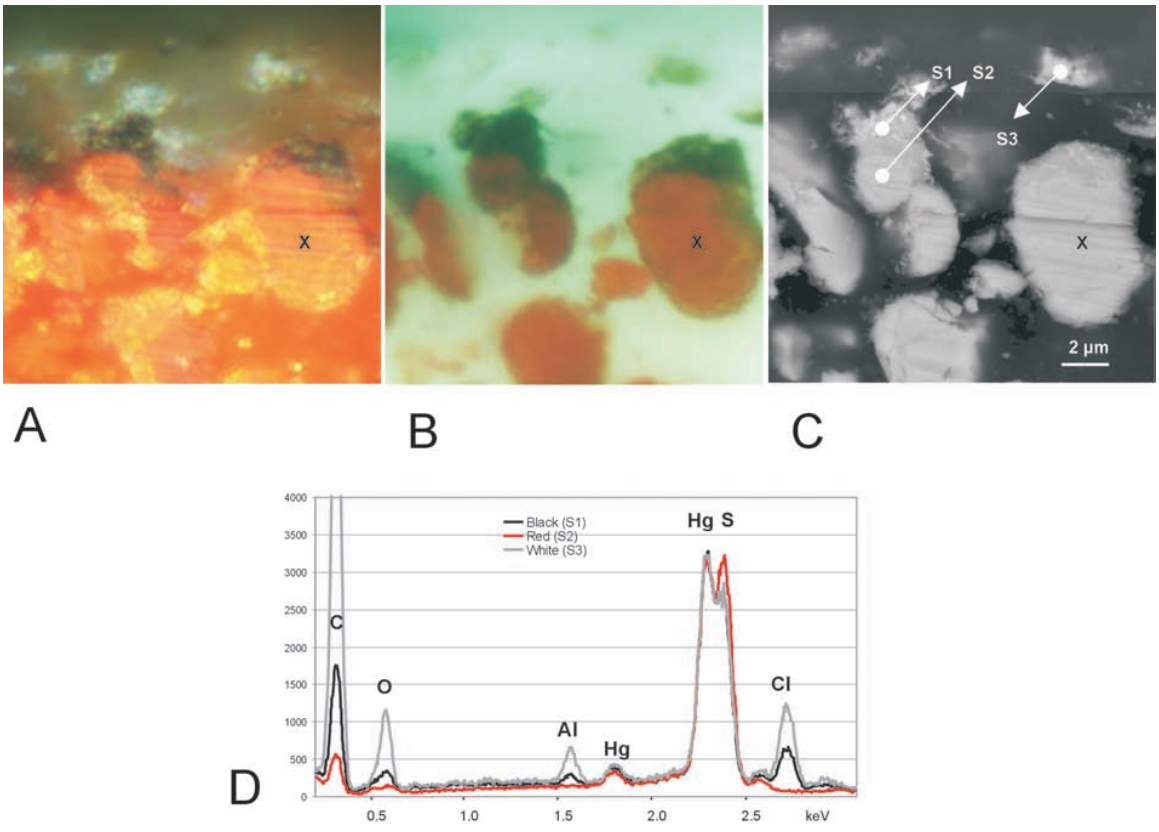

Fig. 4.2 Light microscopic image under white light (A) and UV illumination (B) illustrating the partial photodegradation of a vermilion particle. The backscattered electron image (BSE) (C) shows the structural difference between the red and the black area. The horizontal lines are due to polishing, the text refers to the particle marked X. EDX spectra of spot analyses (D) in black (S1), red (S2) and white (S3) area demonstrate the different elementary compositions of the native material and the reaction products (see coloured version at the end of this thesis).

and the individual particles are partially degraded in some instances. These latter particles consist of a black upper part and a red lower part (in UV light the colours remain black and red). The white product is positioned on top and around the black product and is transparent under UV illumination.

A magnified area of the darkened vermilion in paint cross-section HSTB 34/2 is shown in Fig. 4.5a and b (normal and UV light). There are three layers in the area of the panel painting where the sample was removed: a grayish lead white ground, a reddish-brown iron oxide paint layer and on top a red paint layer with a mixture of vermilion and red lake (paint cross-section not shown). The degraded top layer with black and white products is very thin (4 mm), while the total thickness of the vermilion and red lake layer is 50 mm. The intact layer consists mainly of finely dispersed vermilion particles with a few larger ones. The red lake in the vermilion layer is recognisable by the pinkish fluoresce in the UV image (Fig. 4.5b).

4.3.2 SEM/EDX

The backscattered electron image (BSE-image) illustrates the presence of a structural change in the partially degraded vermilion particle of MH251/26 (Fig. 4.2c). The structure of the red vermilion particle differs from the structure of the black product. The red part of particle X (indicated in Fig. 4.2c) is flat and homogeneous. The horizontal lines in the particles are polishing marks. The black part of the particle X is irregular and broken up. Spots with a higher BSE intensity and a size smaller than 100 nm are visible in the degraded black phase (Fig. 4.2c and supplementary Fig. 4.1). The white areas display the same BSE intensity as the black and the red areas.

The two elements in vermilion - mercury and sulphur - are detected with EDX spot analysis in the red (S2), black (S1) and white (S3) particles (Fig. 4.2d). EDX spot analyses of the red (S2), black (S1) and the white (S3) phases demonstrate that there is relatively less sulphur in the degraded particles (Fig. 4.2d), considering the sulphur/mercury ratio. This sulphur/mercury ratio is only indicative because the X-ray intensity peaks of the mercury *M*-shell and the sulphur *K*-shell are partially overlapping. EDX spot analysis from the black area (S1) and white area (S3) show relatively high chlorine counts; the chlorine concentration in the white particle is much higher than in the black particle (taking the mercury peak as reference). The EDX spectrum of the white area reveals that the intensities of carbon, oxygen and aluminium are high compared to the black and red area. However, these elements are representative for the organic binding medium and are only detected due to the fact that the interaction volume of the beam is larger than the volume of the particle. The sulphur to mercury ratio in the binding medium of both the degraded and intact part is higher than the red particles (spectrum not shown), which indicates that sulphur besides being a constituent of HgS, is also present in another

form in the binding medium.
Elemental X-ray maps of the affected vermilion layer in MH251/26 visualise the distribution of mercury, sulphur and chlorine (Fig. 4.3). The dotted line in the elemental images indicates the compositional transition between red (R) and black (B) particles (Fig. 4.3). The elemental X-ray map of mercury illustrates that mercury is only present inside the pigment particles and has not diffused into the binding medium. Sulphur is present in high relative intensity in the mercury-containing particles of the intact layer (R), whereas lower sulphur X-ray counts are observed in and around the degraded particles (B). The chlorine is only detected in high counts in the degraded vermilion particles.

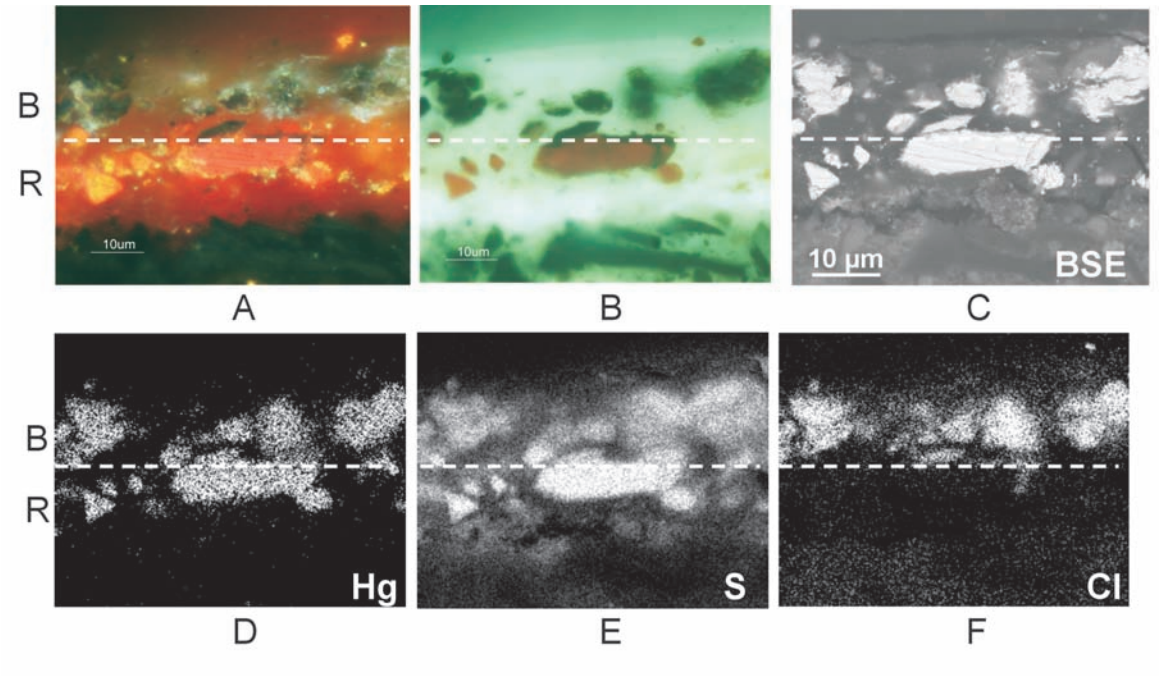

Fig. 4.3 The light microscopic images under white light (A) and UV light (B) illumination and back-scattered electron image (BSE)(C) of the partially degraded vermilion paint in paint cross-section MH251/26 corresponding with the area analysed by EDX imaging. X-ray maps of intact (R) and blackened (B) vermilion in the layer reveals the spatial distribution of mercury (Hg L)(D), sulphur (S K)(E) and chlorine (Cl K)(F) (see coloured version at the end of this thesis).

4.3.3 SIMS

SIMS spectra were acquired in the negative ion mode. Chloride and sulphide dominate in the SIMS spectra of MH251/26 and HSTB 34/2. The spatial distribution of the sulphide and chloride ions in sample MH251/26 is plotted in Fig. 4.4b and 4.4c, respectively. Fig. 4.4a represents the light microscopic image of the scanned SIMS area. Three horizontal lines in the images in Fig. 4.4 outline the blackened layer (B) and the red vermilion layer (R). The intact red vermilion particles contain sulphide and chloride (see layer R in Fig. 4.4b and c). The chloride is present in higher amounts in the degraded

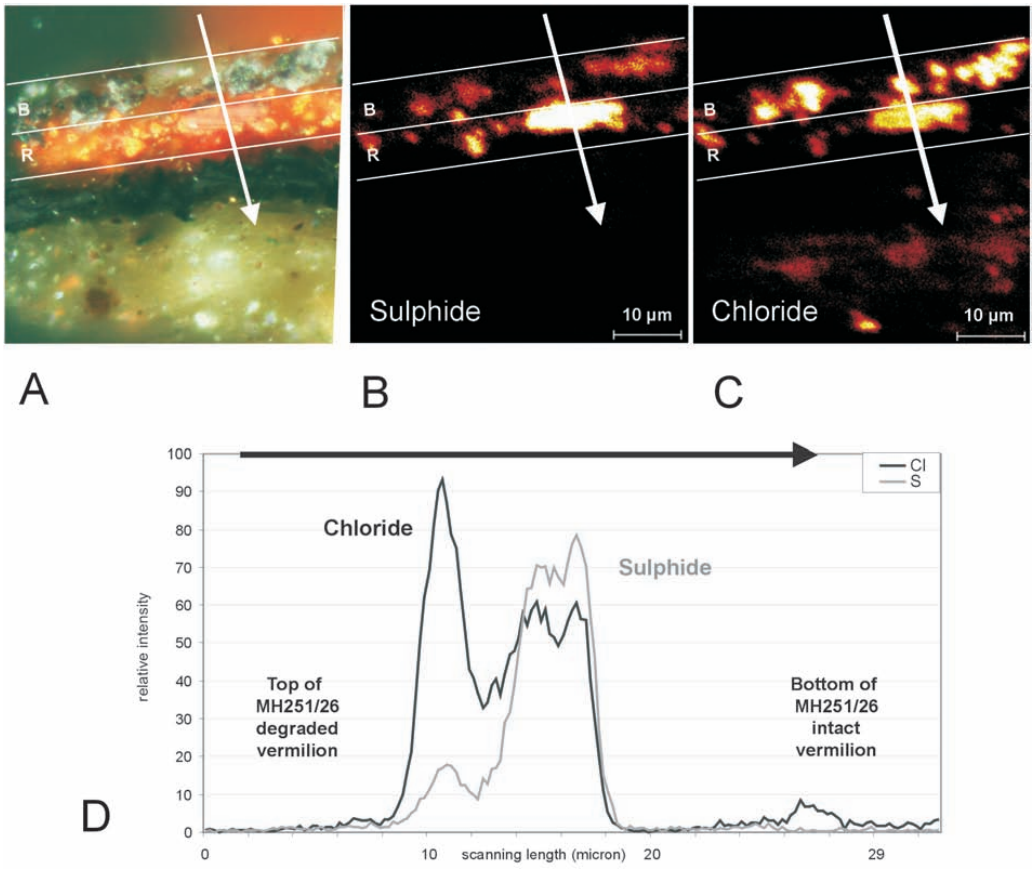

Fig. 4.4 The arrow in the light microscopic image (A), which is representing the scanned SIMS area of the partially degraded vermilion paint in MH251/26, indicates the direction of the line scan. SIMS images of the sulphide (B) and chloride (C) represent the distribution of these ions over the partially degraded vermilion paint layer. The line scan (D), illustrates the distribution of chlorine and sulphur from top to bottom in the paint cross-section (see coloured version at the end of this thesis).

layer (B) and corresponds to the black and white particles. Line scans drawn from the top to the bottom of the layer (see white arrows in Fig. 4a, b and c) visualise the distribution of the secondary ion yields. The secondary ion yields of both chloride and sulphide ions are depicted in Fig. 4.4d. The line scan, with a resolution of 1 mm, first crosses a degraded vermilion particle (3 mm) and then scans an intact vermilion particle (5 mm). The chloride ion yield is higher for degraded vermilion compared to the intact vermilion. The sulphide ion yield is relatively diminished in the degraded particles compared to the intact vermilion. The same phenomenon is observed in paint cross-section HSTB 34/2 (Fig. 4.5c). The line scan crosses the degraded vermilion layer (4 mm) and two intact vermilion particles (6 mm) (Fig. 4.5a, b and c). The chloride and sulphide ion distribution are displayed in Fig. 4.5d and e.

Similar negatively charged mercury-halogen cluster ion patterns were detected in the paint cross-sections MH251/26 and HSTB34/2. The corresponding molecules were deduced on the basis of their molecular weight distribution and isotopic pattern. The

SIMS spectra of HSTB 34/2 show the cluster ions from $[Hg_nS_nCl]^-$ (n = 1-6), $[Hg_nS_{n-1}Cl_3]^-$ (n = 1-4) and $[Hg_nS_{n+1}Cl_2]^-$ (n = 1-3). The spectra of sample MH251/26 show the same types of cluster ions, but only for n = 1-2 (full spectra not shown, a partial negative ion spectrum of HSTB 34/2 with n = 3 is discussed in the next paragraph). The ions are interpreted as chloride adduct ions from $(HgS)_n$ [$(HgS)_n \cdot Cl^-$ (n = 1-6)], $(HgS)_n(HgCl_2)$ [$(HgS)_n(HgCl_2) \cdot Cl^-$ (n = 0-3)] and $(HgS)_n(SCl)$ [$(HgS)_n(SCl) \cdot Cl^-$ (n = 1-3)], respectively. Other types of cluster ions detected with lower ion yields in the paint sample are $(HgCl)_2 \cdot Cl^-$ and $Hg_nS_yCl^-$ ($y = n + 1$, $n + 2$ or $n + 3$). $(HgS)_n \cdot Cl^-$, $(HgS)_n(SCl) \cdot Cl^-$ and $Hg_nS_yCl^-$ are detected in the intact and degraded vermilion particles of HSTB 34/2,

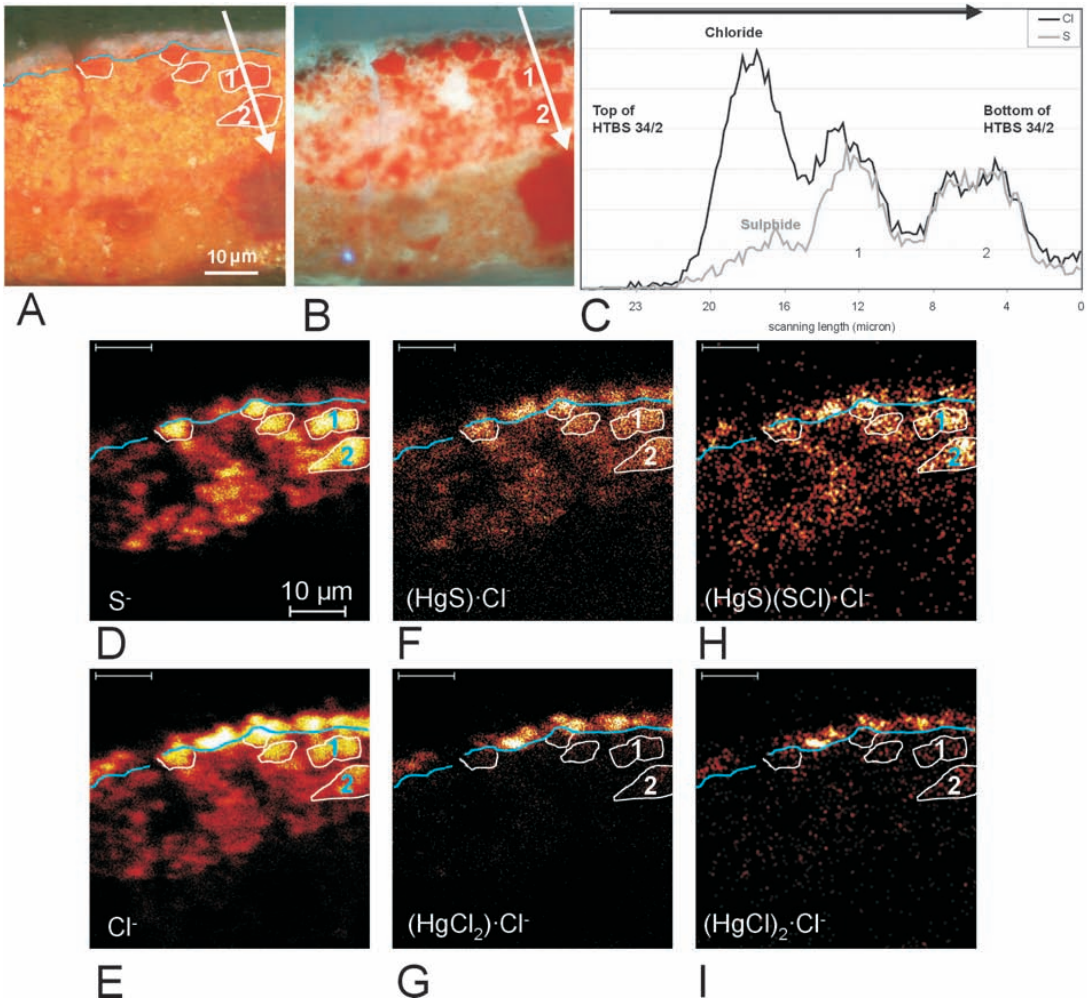

Fig. 4.5 Distribution of sulphur and chloride and the molecular distribution in a partially degraded vermilion paint; the arrow in the light microscopic image (A) and UV-light image (B), which is representing the scanned SIMS area, indicates the direction of the line scan (C). The negative SIMS image of mercury-halogen cluster ions elucidates the position of S^- (D), Cl^- (E), $(HgS)Cl^-$ (F), $(HgCl_2)Cl^-$ (G), $(HgS)(SCl)Cl^-$ (H), $(HgCl)_2Cl^-$ (I) in the partially degraded vermilion paint. The numbers 1-4 in the SIMS images refer to vermilion particles in the corresponding light microscopic images (see coloured version at the end of this thesis).

whereas $(HgS)_n(HgCl_2)\cdot Cl^-$ and $(HgCl)_2\cdot Cl^-$ are only detected in the degraded layer. The SIMS images in Fig. 4.5f-i illustrate this distribution of $(HgS)\cdot Cl^-$, $(HgCl_2)\cdot Cl^-$, $(HgS)(SCl)\cdot Cl^-$ and $(HgCl)_2\cdot Cl^-$ in HSTB 34/2. A contour drawn on the basis of the light microscopic image and the total negative ion image, outlines five red vermilion particles and the boundary in blue between the intact and degraded paint.

Fig. 4.6a-f represent partial negative ion mass spectra of the reference materials HgS, $(HgCl)_2$ and $HgCl_2$ and their mixtures HgS + $(HgCl)_2$ and HgS + $HgCl_2$. The reference materials, $HgCl_2$ and $(HgCl)_2$, are two separate white mercury chloride complexes that are suspected to be present in the degraded vermilion layer of paint cross-section HSTB 34/2. Part of the negative ion mass spectrum of the degraded vermilion paint in paint cross-section HSTB 34/2 is depicted in Fig. 4.6g. The spectrum is acquired after selecting the region of interest (ROI) in the total area analysed (50 μm^2). The SIMS spectrum of the intact vermilion is represented by Fig. 4.6h. Fig. 4.6i represents the calculated isotopic distributions of the ion clusters $(Hg_3S_3)Cl^-$, $(Hg_3S_2Cl_2)Cl^-$, $(Hg_3S_5)Cl^-$, $(Hg_3S_6)Cl^-$. These ions were chosen for calculation because they match the mass window of the relevant cluster ion peak patterns from mercury-halogen cluster ions with 3 mercury atoms in the regions of interest.

The SIMS spectra of the reference materials and their mixtures support the identification of the new products present in the degraded vermilion paint layer of HSTB 34/2. Vertical dotted lines pasted over the mass spectra in Fig. 4.6 divide these into four mass windows corresponding to the four columns in the Table 4.1. Table 4.1 gives an overview of the interpreted mercury-halogen cluster ion patterns in four mass windows deduced from the spectra of the various reference materials and the paint cross-section present (Fig. 4.6 and Table 4.1). In the mass window from 720-750 amu, $(HgS)_3Cl^-$ (*m/z* 726-743) is detected in the mass spectrum of intact and degraded vermilion in HSTB 34/2 (Fig. 4.6g and h). The reference spectra of both mixtures (HgS + $HgCl_2$ and HgS + $(HgCl)_2$) show the same cluster ions (Fig. 4.6e, f), while the spectrum of pure HgS shows a $(HgS)_3S^-$ cluster ion without a chloride ion attached (Fig. 4.6a). In the mass window from 750-790 amu, peaks at 760-781 amu assigned to $(Hg_3S_2Cl_2)Cl^-$ are dominant in the mass spectrum of the degraded vermilion (Fig. 4.6g). The ion cluster $(Hg_3S_2Cl_2)Cl^-$ is only found in the spectrum of the mixture of HgS + $HgCl_2$ (Fig. 4.6f). A relative small amount of $(Hg_3S_4)Cl^-$ and $(Hg_3SCl_3)Cl^-$ in this mass range is detected in the degraded vermilion (these cluster ions partially overlap with the cluster ions of $(Hg_3S_2Cl_2)Cl^-$). In the intact vermilion relatively minor contributions from $(Hg_3S_2Cl_2)Cl^-$ and $(Hg_3S_4)Cl^-$ are detected (Fig. 4.6h). The mass window from 790-820 amu shows $(Hg_3S_5)Cl^-$ and $(Hg_3S_4Cl)Cl^-$ in the mass spectrum of the intact vermilion of HSTB 34/2. The latter cluster ion is found in low yields in the spectrum of the mixture [HgS + $HgCl_2$]. In the

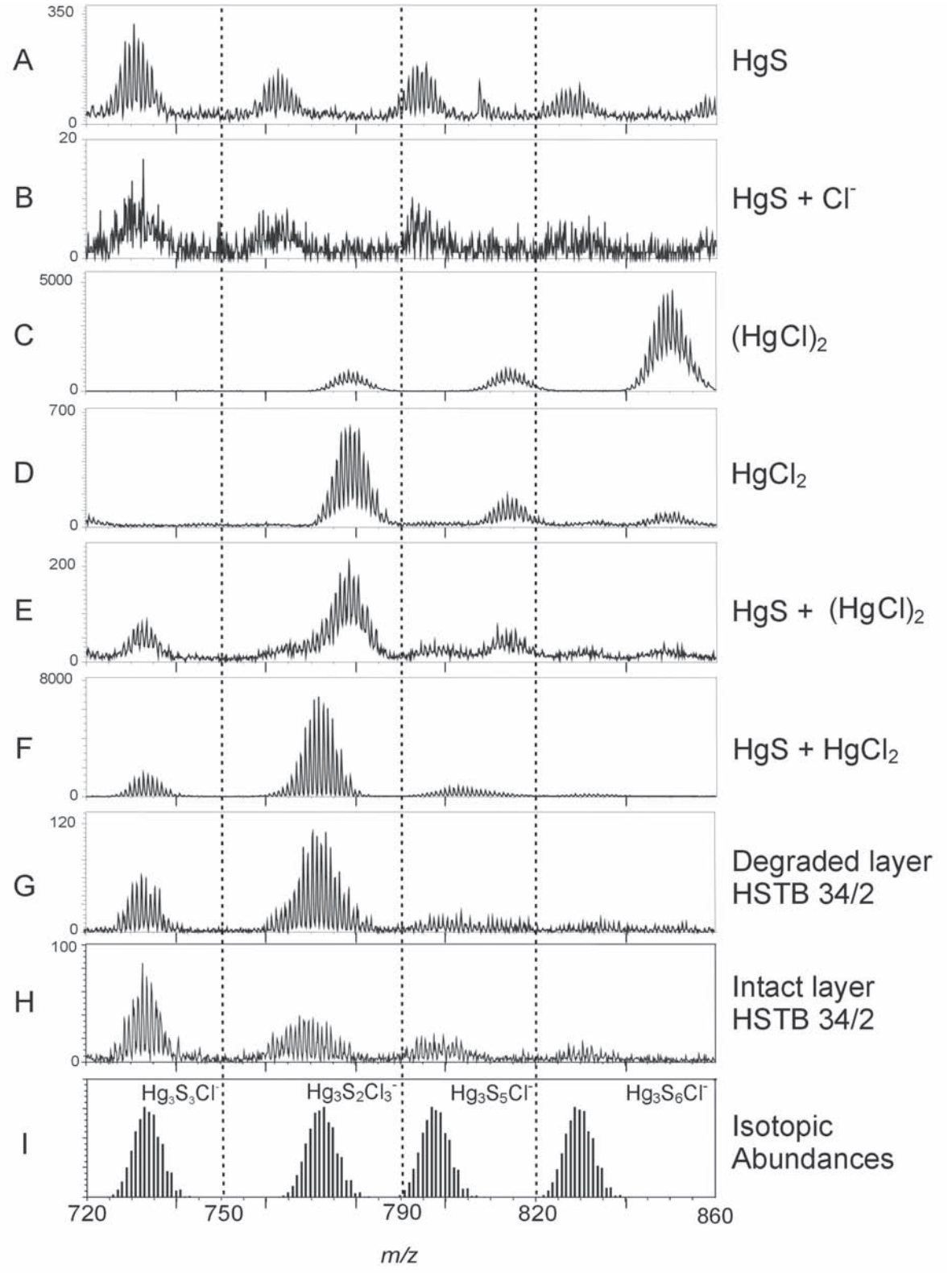

Fig. 4.6 Part of the negative ion mass spectrum in the mass window from 720-860 amu of pure HgS (A), HgS + Cl- ions (B), pure $(HgCl)_2$ (C), pure $HgCl_2$ (D); a mixture of HgS + $(HgCl)_2$ (E); mixture of HgS + $HgCl_2$ (F) and paint cross-section HSTB 34/2 (G). The vertical dotted lines divide the spectra into four mass ranges which correspond with the columns in Table 4.1.

Sample	mass range 720-750 amu	mass range 750-790 amu	mass range 790-820 amu	mass range 820-860 amu
HgS	$(HgS)_3S^-$	$Hg_3S_5^-$	$Hg_3S_6^-$	$Hg_3S_7^-$
HgS + Cl^-	…	…	$Hg_3S_6^-$	-
$HgCl_2$	-	$(Hg_3Cl_4)Cl^-$	$(Hg_3Cl_5)Cl^-$	$(Hg_3Cl_6)Cl^-$
Hg_2Cl_2	$-^-$	$(Hg_3Cl_4)Cl^-$	$(Hg_3Cl_5)Cl^-$	$(Hg_3Cl_6)Cl^-$
HgS + $HgCl_2$	$(HgS)_3Cl^-$	$(Hg_3S_2Cl_2)Cl^-$	$(Hg_3S_2Cl_3)Cl^-$ $(Hg_3S_3Cl_2)Cl^-$ $(Hg_3S_4Cl)Cl^-$	$Hg_3S_6Cl^-$
HgS + Hg_2Cl_2	$(HgS)_3Cl^-$	$(Hg_3Cl_4)Cl^-$	$(Hg_3Cl_5)Cl^-$	$(Hg_3Cl_6)Cl^-$
Degraded layer HSTB 34/2	$(HgS)_3Cl^-$	$(Hg_3S_2Cl_2)Cl^-$ $Hg_3S_4Cl^-$ $Hg_3SCl_3Cl^-$	-	-
Intact layer HSTB 34/2	$(HgS)_3Cl^-$	$(Hg_3S_2Cl_2)Cl^-$ $Hg_3S_4Cl^-$	$Hg_3S_5Cl^-$	$Hg_3S_6Cl^-$

Table 4.1 Overview of the various mercury-halogen cluster ions detected in the negative ion mass spectra in the mass window from of 720-860 amu that originate from spectra of the reference materials, their mixtures and the paint cross-section HSTB 34/2. The four mass ranges correspond to the mass windows indicated in Fig. 4.6.

mass window from 820-860 amu the cluster $(Hg_3S_6)Cl^-$ is detected in low yields in spectra of the paint cross-section as well as in the mixture HgS + $HgCl_2$ (Fig. 4.6f and h and Table 4.1*)*.

Fig. 4.6b represents the SIMS spectrum of the reference material HgS with an excess of chloride ions added as KCl. We conclude that the mercury-halogen cluster ions detected in the paint cross-section are not formed by gas-phase ion chemistry just above the surface after SIMS of HgS and KCl, because $(HgS)_n(HgCl_2)\cdot Cl^-$ and $(HgCl)_2\cdot Cl^-$ are not observed in this spectrum. The exact identification of the composition of the mercury-halogen cluster ions in Fig. 4.6b is difficult as the yields and thus the resolution is low.

4.4 Discussion

The two paint cross-sections investigated that originate from paintings made by two different painters and that were kept under different conditions give similar analytical information on the colour changes in vermilion. The analytical imaging studies on the darkened vermilion oil paint layer in sample MH251/26 demonstrate the degradation phenomena in detail. As light is a requirement for the degradation process, it is concluded that the light must have penetrated the whole affected layer as all particles in sample MH251/26 are homogenously transformed. On the basis of the transition of the red into the black materials observed in the partially degraded particles and the position of the white materials around the black materials, we propose that the black coloured material is formed first. In a later stage the white product is formed from the black reaction product.

Both the SIMS and EDX techniques show relatively high amounts of chloride and relatively low amounts of sulphide in the degraded particles. The relative amount of mercury in the intact and degraded particles is considered to be constant, since the backscattered electron intensity in the BSE image is the same for all phases. The EDX images lead us to conclude that sulphur leaches from the particles in the degraded layer into the environment. However, EDX spot analyses detect sulphur in the organic binding medium of both the degraded and the intact part. The organic binding medium also has been shown to contain aluminium. Sulphur and aluminium are known constituents of the inorganic substrate of red lakes.[10] It is therefore possible that red lake possible has been mixed into the paint although no distinct pigment particles are visible.

The mercury-halogen cluster anions detected in the whole vermilion layer with SIMS are charged by attachment of Cl^- ions. Neutral molecules are known to be anionised by chloride to form a negatively charged complex.[11, 12] The ions $(HgS)_nCl^-$ and $(HgS)_n(SCl)Cl^-$ are found in the intact vermilion paint layer and are representative for intact HgS. $(HgS)_nS^-$, detected in the pure HgS, is not present in the SIMS spectra of the mixtures and may be suppressed by the presence of chloride. Ions from $(HgS)_n(HgCl_2)\cdot Cl^-$ (n = 0-6) are detected and mainly present in the degraded vermilion layer. These types of ions are also formed from the mixture of HgS + $HgCl_2$ but not from the mixture HgS + $(HgCl)_2$. We conclude on the basis of the presence of these types of ions found in the degraded vermilion layer that it is indicative for mercuric chloride ($HgCl_2$). In addition, the ions from $(HgS)_n(HgCl_2)\cdot Cl^-$ detected in SIMS data of a mixture of HgS + $HgCl_2$ indicates that HgS is still present in the degraded vermilion layer, because these ions are absent in the spectra of pure $HgCl_2$. The ions $(HgCl)_2\cdot Cl^-$ are not only representative for $(HgCl)_2$ (calomel), because these ions are also detected in the spectrum of HgS + $HgCl_2$

(part of the spectrum not shown). It is concluded that the presence of calomel in the paint sample cannot be proven with SIMS, because this ion $(HgCl)_2 \cdot Cl^-$ is not characteristic for $(HgCl)_2$ (calomel) and $(Hg_3Cl_4) \cdot Cl^-$ is only detected in the HgS + $(HgCl)_2$ reference mixture and not in the paint sample.

On the basis of our results and literature data, we propose that the transformation of vermilion from red into black materials is a conversion from HgS into Hg(0) and S(0) by a photochemical reaction catalysed by chloride (Step 1 in Fig. 4.7). The conversion of Hg(0) from photo-reduced Hg(II) has been reported both in solid phase[13] and aqueous media.[14, 15, 16, 17, 18, 19] This supports the idea of the light induced conversion of Hg(II)S into Hg(0). After the photo-reduction reaction, the metallic mercury is deposited on the intact HgS surface resulting in a black reaction product. The remaining HgS in the degraded vermilion is identified with SIMS. The metallic mercury is present as nanoparticles, which is supported by the "hot" spots smaller than 100 nm visualised in the BSE-image (Fig. 4.2c and supplementary Fig. 4.1). The Hg(0) precipitation on the vermilion surface has never been proven directly, but has been suggested by other authors.[6, 16, 20] Elementary sulphur is also detected as a product of photo-degraded HgS.[19] The sulphur leaves the paint particles possibly in the form of volatile sulphur oxide, as sulphur has been shown to oxidise to sulphate ions via polythionic acids.[21] Since the sulphur is lost from the particle, it is inferred that a conversion of vermilion to meta-cinnabar is unlikely. The small relative concentration of sulphur still present in the particles is ascribed to intact residual intact vermilion. XRD measurements performed on reconstructions and other paint samples elsewhere by other authors support this conclusion.[1, 2, 4, 7, 9] It is shown that

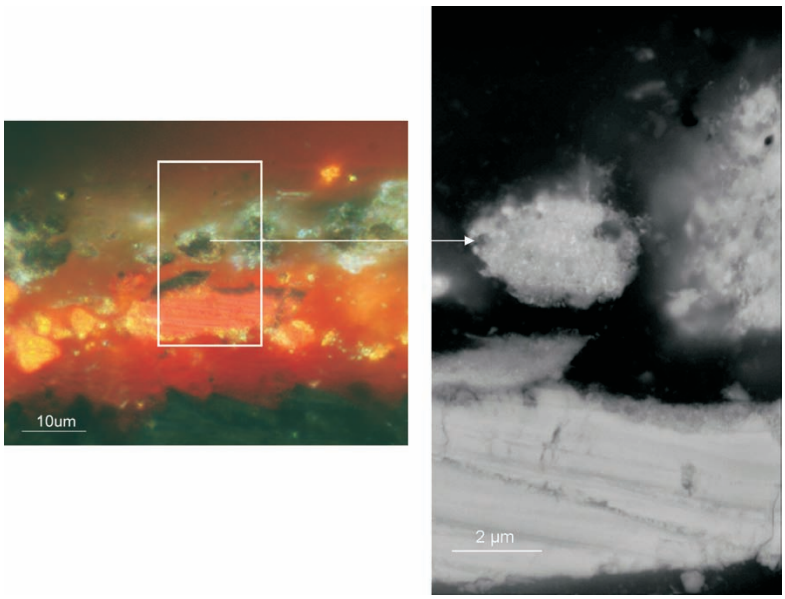

Supplementary Fig. 4.1 The BSE-image visualises a black particle containing hotspots of smaller than 100 nm. These hotspots are nanoparticles of metallic mercury (see coloured version at the end of this thesis).

vermilion is still present in the XRD spectra of the blackened vermilion as is deduced from the decreased intensity of the XRD patterns of vermilion. No black meta-cinnabar was shown in the XRD spectra.

Chlorine plays a dominant role in the light induced blackening phenomenon, as already is suggested in the literature.[7, 9] The much more sensitive surface technique of SIMS demonstrates, in contrast to the EDX results, that chloride is present inside the vermilion particles of both MH 251/26 and HSTB 34/2. The concentration of chloride in the red particles must be below the detection limit of EDX. As small quantities of chloride make vermilion photosensitive[7], the small amounts of chloride detected in the intact vermilion trigger the blackening process. Due to the fact that only small quantities of chloride are necessary to form blackened cinnabar and that other compounds besides chloride ions, such as iodide, enhance the blackening as well, it is concluded that chloride initially acts as a catalyst and is not part of the primary reaction products. The exact minimum concentration of chloride necessary to trigger the process is not known. McCormack states that cinnabar is light stable below 0.01wt% (± 0.01 wt%) chloride, as determined with a wavelength-dispersive microprobe analyser, cinnabar is light stable and that it blackens at a concentration of 0.05 wt% and higher[7].

The exact mechanism of the photo-degradation of vermilion catalysed by chloride is still an open question. We suggest that under the influence of light an electron-hole pair is generated and a photoeletrochemical process takes place, which enables an electron transfer from chlorine anion to mercury and from sulphide back to chloride (i.e. chloride has a catalytic function). Assuming that chlorine anions are oxidised by the positive holes of the valence band of HgS, the valence band edge of HgS must be more positive than the redox potential of Cl^-/Cl_2.[16, 22] The exact position of the valence band edge of HgS is not clear, but the value of this position is expected to be close to the redox potential of Cl^-/Cl_2.[22]

The relatively high quantity of chloride in the degraded part is hard to explain from an original vermilion source alone. We also have to conclude that the chloride is not introduced via the binding medium, as EDX did not detect chloride in the binding medium of the intact area. In order to explain the relatively high yields of chloride ions in the degraded vermilion particles it is necessary to invoke additional source of chlorides. Chloride is possibly transported by diffusion from paint layers positioned lower or introduced from an external source.

After the first transformation, the black product is thought to trap chloride to transform subsequently into a white reaction product. Although the elemental composition (Hg, S, and Cl) of the black and the white phase is the same, the EDX spot analysis shows a higher relative intensity of chlorine and a fairly lower relative intensity of sulphur in the white product (S3) compared to the black product (S1) (Fig. 4.2a and d). SIMS iden-

tifies the mercury chlorine complex $HgCl_2$ in the degraded vermilion layer. Mercuric chloride ($HgCl_2$) has never been identified in paintings before. Calomel $(HgCl)_2$ cannot be identified positively with SIMS, however, Spring *et al.* had identified calomel as the white product in paintings-containing degraded vermilion using Raman microscopy.[9]

The two components in the black product, metallic mercury and residual vermilion, react with chloride supplied by sources external to the vermilion. The residual vermilion reacts with this external chloride to the light sensitive mineral corderoite, which degrades under the influence of light into calomel, metallic mercury and sulphur. Corderoite ($Hg_3S_2Cl_2$) can easily be formed in a mixture of HgS and NaCl solution kept at room temperature after a long period[7, 9] and will after light exposure degrade into a dark grey product containing $(HgCl)_2$.[9] The formation of corderoite could not have taken place in the first degradation steps, because of the high amount of chloride required that is suggested to accumulate after the blackening. The $(HgCl)_2$ formed photo-degrades under normal light into $HgCl_2$ and Hg(0).[23] The metallic mercury, derived from the photo-reduction in the first step, the corderoite and the $(HgCl)_2$, react with chloride to form mercuric chloride $HgCl_2$. In vitro $HgCl_2$ can be formed from metallic mercury via the reaction with chlorine gas or by via the formation of mercury(II)sulphate.[24] The white end product is found around the black product, which means that external sources, light and a higher concentration of chloride are necessary to create the white product.

Fig. 4.7 illustrates the scheme of the proposed mechanisms of the degradation process of the red vermilion into the black and subsequently the white reaction product. The scheme describes the degradation phenomena qualitatively to clarify the process. The products observed in the paint cross-sections are mixed phases and consequently cannot be classified in a single category in the scheme. For example, the black product in sample MH251/26 has a relatively higher concentration of chloride compared to the intact red vermilion. Based on its colour this black product would be classified in the black box after step 1 in the diagram, but a relative increase in chloride is taking place. This accumulation in the black product is indicated in step 2, but a conversion into a white product is not observed with light microscopy. Therefore, the black product would be classified in the box after step 2, which is indicated in the scheme as grey. Furthermore, not all the degraded vermilion is converted into $HgCl_2$ in sample HSTB 34/2, some of the former reaction products are still expected to be present.

The obtained knowledge implies that the quality of the vermilion used in paintings is of significant importance for the changes of preservation of the red colour. Small chloride or other halogen impurities in the vermilion makes the red pigment photosensitive. Chloride present in the medium or derived from other external sources can drive subsequent reactions. Works of art such as easel and mural paintings can be expected to be exposed to light and chlorides.

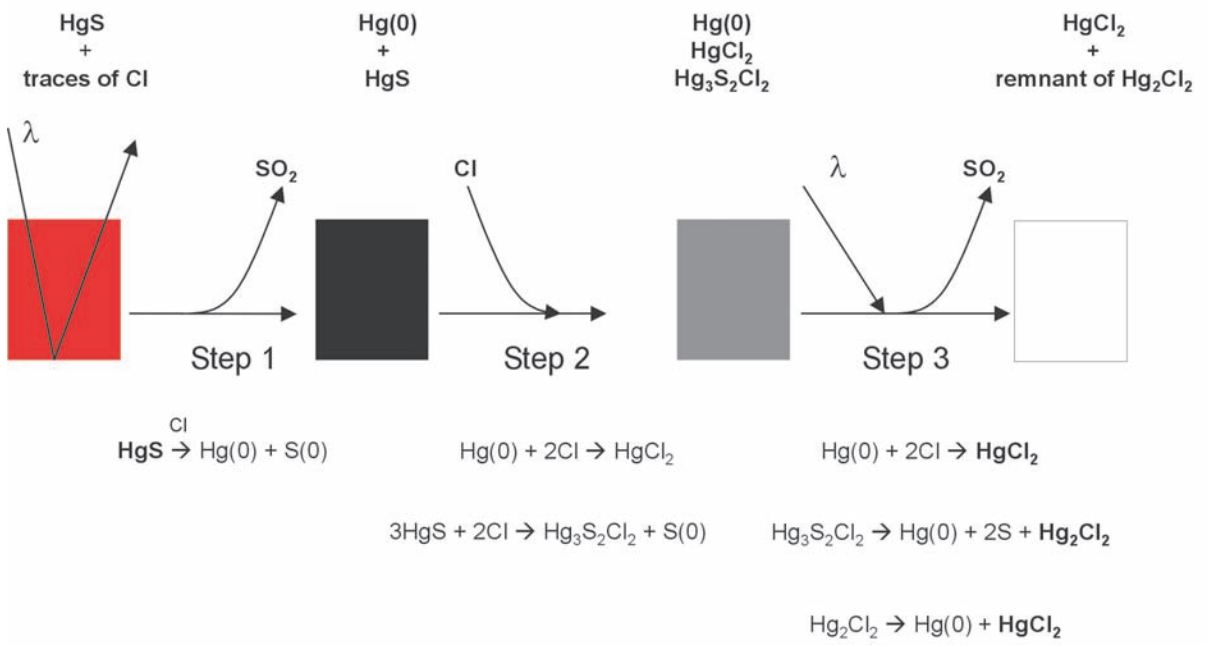

Fig. 4.7 Scheme of the proposed mechanisms of the degradation process of the red vermilion into a black and finally a white product (see coloured version at the end of this thesis).

4.5 Conclusions

Analytical studies on paint cross-sections containing darkened vermilion reveal the light induced degradation phenomena in detail. Light microscopic images reveal two coloured reaction products, a white product positioned above and around a black product. SEM/EDX data give information about the elemental distribution and the structural changes between the three coloured phases. SIMS detects, in contrast to EDX, traces of chloride in the native vermilion The additional benefit of imaging SIMS applied for the first time to investigate this phenomenon in paint cross-sections is that the molecular information from SIMS is able to identify the white reaction product as mercuric chloride. We propose a new hypothesis, which describes a three-step process where black and white reaction products are formed from each other. Chloride acts as catalyst in the first step of the photo-induced chemical degradation of vermilion. In the formed black reaction product, an excess of chloride is accumulated. The black phase will react further with the excess of chloride to form the white product, mercuric chloride. The combination of both techniques, SEM/EDX and SIMS, is essential to elucidate the familiar phenomenon of 'blackening of vermilion' in detail.

4.6 Acknowledgements

We are grateful to Linnaea Saunders, Kress Fellow 2003 - 2004, Mauritshuis, The Hague, The Netherlands who provided us the paint cross-section MH251/26. We would also like to thank Lidwien Speleers, AMOLF, Amsterdam, The Netherlands for providing the paint cross-section HSTB 34/2.

4.7 References

1 R. Grout, A. Burnstock, *A study of the blackening of vermilion*, Zeitschrift für Kunsttechnologie und Konservierung 2000, Hft 1, p. 15-22.

2 R.L. Feller, *Studies on the darkening of vermilion by light*, National Gallery of Art, Report and Studies in the History of Art 1967, Washington, DC, 1967.

3 R.J. Gettens, R.L. Feller, W.T. Chase, *Madder and alizarin*, In: Artists' pigments, vol. 2, A. Roy (Ed.), Oxford University Press, New York, 1993, p. 167-168.

4 V. Daniels, *The blackening of vermilion by light*, In: Recent Advances in the Conservation and Analysis of Artifacts, J. Black (Ed.), Summer School press, London, 1987, p. 280-282.

5 R.S. Davidson, C.J. Willsher, *The light-induced blackening of red mercury(II)sulphide,* Journal of the Chemical Society Dalton Transactions, 3, 1981, p. 833-835.

6 R.M. Dreyer, *Darkening of cinnabar in sunlight*, American Mineralogist, 23, 1938, p. 457-460.

7 J.K. McCormack, *The darkening of cinnabar in sunlight,* Mineralium Deposita, 35, 2000, p. 796-798.

8 R.S. Davidson, C.J. Willsher, C.L. Morrison, *Influence of some solvents and solutes on illuminated red mercury(II)sulphide electrodes*, Journal of the Chemical Society Faraday Transactions 1, 78, 1982, p. 1011-1019.

9. M. Spring, R. Grout, *The blackening of vermilion: an analytical study of the process in paintings,* National Gallery Technical Bulletin, 23, 2002, p. 50-61.

10 H. Schweppe, J. Winter, *Vermilion and cinnabar*, In: Artists' pigments*,* vol. 3, E. West FitzHugh (Ed.), Oxford University Press, New York, 1997, chapter 4.

11 G.S. Groenewold, *et al., Characterization of copper chloride cluster ions formed in secondary ion mass spectrometry*, International Journal of Mass Spectrometry, 178, 1998, p. 19-29.

12 A. Delcorte, *Fundamental aspects of organic SIMS,* In: ToF-SIMS: Surface Analysis by Mass Spectrometry, J.C. Vickerman, D. Briggs (Eds.), IM Publication and Surface Spectra Limited, 2001, p. 183.

13 M.S. Gustin, H. Biester, C.S. Kim, *Investigation of the light-enhanced emission of mercury from naturally enriched substrates*, Atmospheric Environment, 36, 2002, p. 3241-3254.

14 Y.H. Hsieh, S. Tokunaga, C.P. Huang, *Some chemical reactions at the HgS(s)-water interface as affected by photoirradiation,* Colloids and Surfaces, 53, 1991, p. 257-274.

15 M. Ravichandran, *Interactions between mercury and dissolved organic matter- a review*, Chemosphere, 55, 2004, p. 319-331.

16 B. Pal, S. Ikeda, B. Ohtani, *Photoinduced chemical reactions on natural single crystals and synthesized crystallites of mercury (II) sulfide in aqueous solution containing naturally occur ring amino acids*, Inorganic Chemistry, 42, 2003, p. 1518-1524.

17 M.I. Litter, *Heterogeneous photocatalysis transition metal ions in photocatalytic systems*, Applied Catalysis B-Environmental, 23, 1999, p. 89-114.

18 D. Strömberg, A. Strömberg, U. Wahlgren, *Relativistic quantum calculations on some mercury sulfide molecules*, Water Air and Soil Pollution, 56, 1991, p. 681-695.
19 S. Okouchi, S. Sasaki, *Photochemical behaviour of mercury ore in water*, Environment International, 9, 1983, p. 103-106.
20 M.S. Gaustin, R.A. Maxy, P. Rasmussen, *Mechanisms influencing the volatile loss of mercury from soil*, In: Symposium volme of Air Pollutance, Cary, NC, September 1998.
21 K. Naito, S. Takei, T. Okabe, T., *The chemical behavior of low valence sulfur compounds. II. Thin-layer chromatographic separation and photometric determination of low valence sulfur compounds*, Bulletin of the Chemical Society of Japan, 43, 1970, p. 1360-1364.
22 Personal communication with professor B. Ohtani (Catalysis Research Center, Hokkaido University, Japan), 2004.
23 C. Chambers, A.K. Holliday, In: Modern Inorganic Chemistry, Butterworth & Co, London, 1975, p. 437.
24 A.F. Holleman, E. Wilberg, In: Inorganic Chemistry, Academic Press, San Diego, 2001, p. 1310.

Chapter 5

Metal soap aggregates in oil paintings from the 15th - 20th century

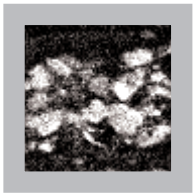

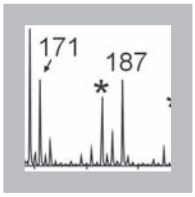

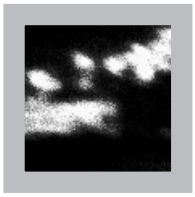

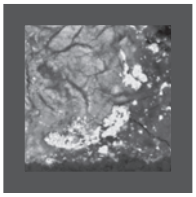

Metal soap aggregates can be found in lead or zinc-containing oil paint layers in paintings from the 15th - 20th century. Ten paint cross-sections affected by metal soaps formation were selected from a questionnaire and investigated with analytical imaging techniques. The imaging studies elucidate that reactive lead- and zinc-containing pigments or driers react with the fatty acids to form lead or zinc soaps. In most cases the pigment particles react away leading to saponified regions, which can grow further, swell and finally protrude through the paint surface. In some cases metal soaps appear to have formed at an early stage of the drying of the paint and under these conditions, the reactive mineral matter appears not to be affected. A mature oil paint system can become saponified when an excess of free monocarboxylic fatty acids, derived from external sources, e.g. other layers or from internal sources, e.g. de-esterfication of the oil, is introduced in the anionic network. The fatty acids cannot be directly incorporated in the network and react with a reactive metal source. Inside the aggregates lead or zinc carbonate is often observed, which can precipitate from the metal soap with atmospheric CO_2. Another newly formed mineral regularly observed inside lead soap aggregates is minium.

5.1 Introduction

Defects associated with metals soaps are so far only observed in oil paintings with lead or zinc-containing paint layers irrespective of the type of support. The affected painted works of art originate from the 15th to the 20th century and come from wide number of geographical locations. The phenomena of increased transparency of paint, metal soap aggregation and protrusion in paint layers, increased brittleness of paint layers and efflorescence can be ascribed to the existence of metal soap structures or excess metal soaps in paintings. A questionnaire designed by Noble and Boon in 2002 that asked conservators and restorers to report on protrusions and related phenomena associated with metal soap formation, provided some idea of the extent of metal soap related defects. The questionnaire and answers received are reproduced in Appendix I. Examples presented in this chapter were selected using the results from the questionnaire.

This chapter focuses specifically on the painting as information source on the aggregation of metal soaps in oil paint layers. Their existence was first observed and characterised in 1997 during the research associated with the restoration (1996 - 1998) of a painting by Rembrandt van Rijn - *The Anatomy Lesson of Dr. Nicolaes Tulp,* MH inv. no. 146 - in the collection of the Mauritshuis in The Hague. Several articles have already been published on the large lead soap aggregates present in the lead-containing ground of this painting[1, 2] as well as in other 17th-century paintings.[3, 4, 5] However their process of formation is still not fully understood.[1] Analytical imaging approaches of embedded paint cross-sections that enable spatially resolved studies of metal soaps, their aggregates and the surrounding paint have been especially fruitful for the study of their properties. Imaging specular reflection Fourier Transform Infrared (FTIR) microscopic studies were found to be a vital analytical method for the identification of metal soap in paint cross-sections.[6, 7] Imaging secondary ion mass spectrometry (SIMS) was able to localise and map lead, monocarboxylic fatty acids (monoacids) and lead soaps inside metal soap aggregates.[8, 9, 10] Scanning electron microscopy (SEM) images revealed the absence of pigment particles in the aggregates and visualised lamellar "Liesegang" bands of nanocrystals, a sign of remineralisation processes in the larger lead soap aggregates. In the light microscope lead soap aggregates look transparent to whitish opaque while they strongly fluoresce under UV illumination. In some aggregates small orange particles are observed, which have been identified as minium by VIS imaging.[7, 10] The chemical significance of these minium particles has been proposed to be marking rather basic conditions that must have or are existing in the paint.[8, 10]

Lead soap aggregates are often observed in red lead and lead-tin yellow-

containing paints.[4, 11 ,12, 13] The constituent monocarboxylic fatty acids have been identified by FTIR and GCMS studies in samples from these lead soap aggregates.[4, 11] Lead carbonates and basic lead carbonates were detected in the lamellar structures in these lead soap aggregates.[4, 7] Zinc soap formation and aggregation was demonstrated in the 19th-century painting *Falling Leaves; les Alyscamps* by Vincent van Gogh.[14] Part of these zinc soap aggregates are remineralised as what is proposed to be zinc oxide,[14] but new research presented in this chapter proves that another mineral phase has precipitated. Paintings conservator Osmond attracted our attention to several paintings at the Queensland Art Gallery that were affected by zinc soap formation, which were studied further at AMOLF. SEM-EDX imaging studies reveal numerous small zinc soap aggregates dispersed in their paint layers.[15] Examples will be presented in this chapter.

'The Anatomy Lesson of Dr. Nicolaes Tulp' by Rembrandt van Rijn (canvas, lined) displayed in Royal Picture Gallery Mauritshuis, The Hague, The Netherlands (inv. no. 146) (see coloured version at the end of this thesis).

Two descriptive schemes have been proposed describing the development of lead soap aggregates in lead white-containing underpaint[9, 10] and in lead-tin yellow paints.[13] The scheme for the lead white paint is based on imaging analyses of paint cross-sections from *The Anatomy Lesson of Dr. Nicolaes Tulp*. We proposed a scheme in which the lead white particles react with the fatty acids derived from the de-esterifying cross-linked oil (Scheme A). The lead white grains partially or totally react away and the resulting lead soap is dispersed in the paint layer. As the lead soaps aggregate and grow in volume, they can break up the overlying paint layer and protrude through

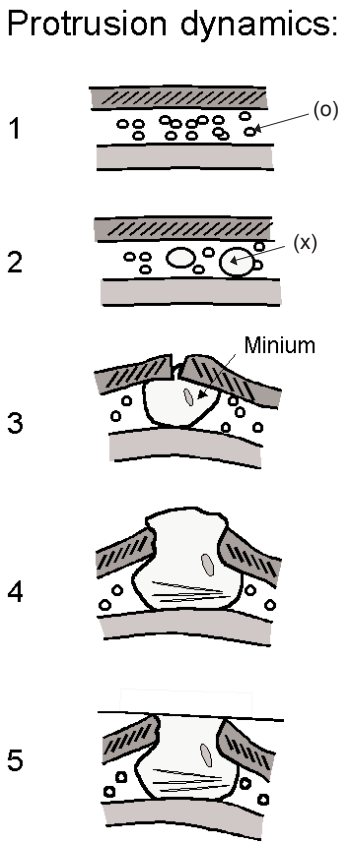

Scheme A Schematic diagrams of protrusion formation in ground/intermediate paint layers.

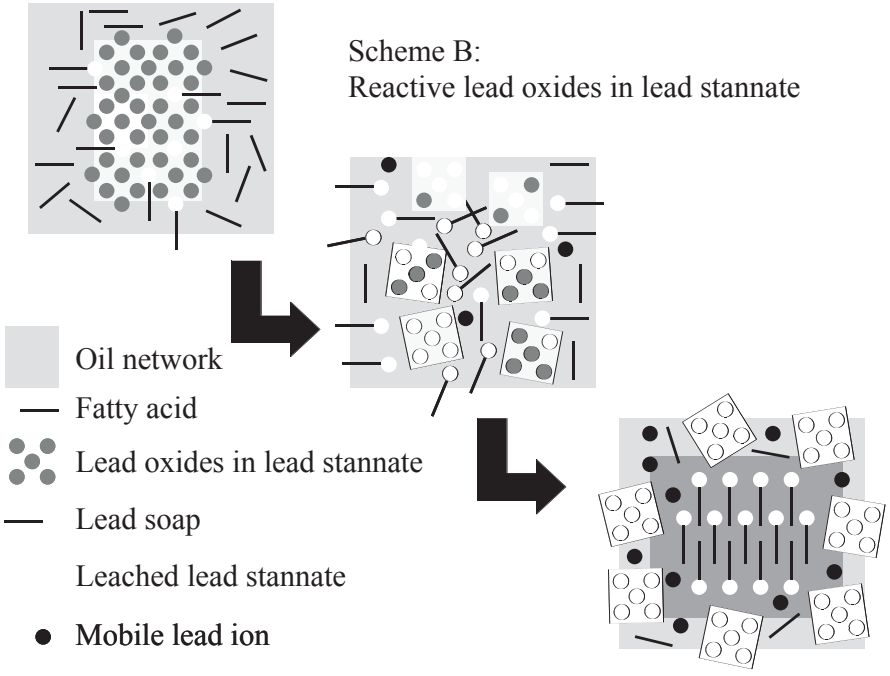

Schema B Proposed scheme of lead soap aggregate formation by reaction of a hypothetical mixed phase lead-tin yellow pigment with fatty acids from an aging oil paint.

the surface of the painting. During and after aggregation and swelling, remineralisation takes place inside the aggregate.[8, 9, 10] In lead-tin yellow paints the hypothesis is put forward that the lead-tin yellow originally not only consisted of lead stannates but contained other lead-containing mineral phases that reacted quantitatively with fatty acids released by ageing from the oil binding medium (Scheme B).[13] Consequently residues of the lead-tin yellow pigment are presently assembled around the lead soap aggregates. The process of metal soap aggregation in paintings is not fully understood,

Title Painting	**Artist**	**Period**	**Location Painting**	**Sample Number**	**Sample Origin**	**Sample Provided by**
The Anatomy lesson of Dr. Nicolaes Tulp	Rembrandt van Rijn	1632	Royal Picture Gallery Mauritshuis, The Hague, The Netherlands	MH146/B38	The lip of figure 4, Adriaen Slabbraen	Petria Noble
The Anatomy lesson of Dr. Nicolaes Tulp	Rembrandt van Rijn	1632	Royal Picture Gallery Mauritshuis, The Hague, The Netherlands	MH146/B39	The cheek in the face of figure 5, Jacob de Wit	Petria Noble
The Anatomy lesson of Dr. Nicolaes Tulp	Rembrandt van Rijn	1632	Royal Picture Gallery Mauritshuis, The Hague, The Netherlands	MH146/B37	The face (shadow near hairline) of figure 4, Adriaen Slabbraen	Petria Noble
Herald (south-west)	Christiaen van Couwenbergh	1651	Oranjezaal of the Royal Palace Huis ten Bosch, The Hague, The Netherlands	HSTB 43/3	A white layer partially covered by the hair	Lidwien Speleers
Preprimed Canvas	Frederic E. Church estate	1826-1900	Olana archive, Hudson, New York	PCC01	Residual piece of commercially bought preprimed canvas	Joyce Zucker
Sherborne Triptych	Anonymous	15th Century	Sherborne Abbey Almshouse, Dorset, UK	CIA 1577 RS06	The green drapery of the robe	Aviva Burnstock
The Bad Chief	Master of Flémalle (Robert Campin)	15th Century	Städelsches Kunstinstitut, Frankfurt, Germany	A342/18	The yellow paint of the baldachin	Prof. van Asperen de Boer
Impasse des deux frères and Moulin de Poivre	Vincent van Gogh	1887	Van Gogh Museum, Amsterdam, The Netherlands	F347-1	The sand path depicted at the right edge	Ella Hendriks
Woolshed, New South Wales	R. G. Rivers	1890	Queensland Art Gallery, Australia	RWS5	The iron roofing of the shearing shed	Gillian Osmond
Sydney Harbour, overlooking Taylor's Bay	W. Lister Lister	1912	Queensland Art Gallery, Australia	LLSH1 and LLSH2	-	Gillian Osmond

Table 5.1 List of the paintings and sample numbers presented in the chapter.

but aspects have been discussed in several papers.[4, 16, 17] Studies on model systems describe aggregation of ionic molecules in polymeric systems.[18, 19, 20] A phase separation is the most likely mechanism while electrostatic interaction between ion pairs is proposed to be the driving force for agglomeration.[21] This model is proposed for example for metal salt aggregates formed in polymeric systems.[22] How these models could explain some of the phenomena observed in the paint cross-sections presented in this chapter would require extensive studies with historically accurate model systems.

In this chapter, studies on various paint cross-sections are presented that were selected from the questionnaire mentioned earlier (Appendix I). The ten case studies selected from the large collection of analysed samples are illustrative for various phenomena of metal soap aggregation in paint layers. Seven case studies are presented on lead soap aggregates in paintings from the 15th, 17th and 19th centuries. Five case studies show lead soap aggregation in lead white-containing grounds, and two present lead soap aggregates in lead-tin yellow paint layers. A further three case studies present zinc soap aggregates in paintings from the 19th and 20th centuries. The paintings and sample numbers are listed in Table 5.1. Data on lead soap aggregates formed in red lead (minium) paints are not presented. The selected paint cross-sections are analysed with the analytical imaging techniques of specular reflection imaging FTIR, SEM/EDX and SIMS.

5.2 Experimental

The dark field reflected light microscopic images were obtained on a Leica DMRX microscope (Leica, Wetzlar, Germany). White light was provided by a 100 W halogen lamp, and an Osram HBO 50 W lamp and Leica filter D (excitation 360-425 nm, emission > 460 nm) were used for fluorescence microscopy. Images were recorded with a Nikon digital still camera DXM1200 (Nikon Instech Co., Ltd., Japan).The Bio-Rad Stingray (Bio-Rad, Cambridge, MA), combining the Bio-Rad FTS-6000 spectrometer equipped with a Bio-Rad UMA 500 infrared microscope with a 64 x 64 mercury-cadmium telluride (MCT) focal plane array camera was used to record the FTIR images. Analysis of the embedded cross-section was carried out in reflection mode recorded with a 16 cm^{-1} spatial resolution, a step scan frequency of 1 Hz, and an UDR of 4. The reflection measurements were corrected by the Kramers-Krönig transformation. Scanning electron microscopy studies in combination with energy dispersive X-ray analysis (SEM-EDX) were performed on a XL30 SFEG high-vacuum electron microscope (FEI, Eindhoven, The Netherlands) with EDX system (spot

analysis and elemental mapping facilities) from EDAX (Tilburg, The Netherlands). Samples were carbon-coated to improve surface conduction in a CC7650 Polaron Carbon Coater with carbon fibre (Quorum Technologies, East Sussex, UK).

The static SIMS experiments were performed on a Physical Electronics (Eden Prairie, MN) TRIFT-II time-of-flight SIMS (TOF-SIMS). The surface of the sample was scanned with a 15 keV primary ion beam from an $^{115}In^{+}$ liquid metal ion gun. The pulsed beam was non-bunched with a pulse width of 20 ns, a current of 600 pA and the spot size of ~ 120 nm. The surface of the sample was charge compensated with electrons pulsed in between the primary ion beam pulses. To prevent large variations in the extraction field over the large insulation surface area of the paint cross-section a non-magnetic stainless steel plate with slits (1 mm) was placed in top of the sample. The paint cross-sections were rinsed with hexane to reduce contamination of polydimethyl siloxanes. The paint samples were embedded in polyester resin Polypol or in Technovit® 2000LC (Heraeus Kulzer, Germany). All paint cross-sections were dry polished with Micro-mesh® polishing cloths (final step 12 000 mesh) (Scientific Instruments Services Inc., Minnesota).

5.3 Results and discussion

5.3.1 'The Anatomy Lesson of Dr. Nicolaes Tulp' by Rembrandt van Rijn (1632)

The greyish lead white-containing ground of *The Anatomy Lesson of Dr. Nicolaes Tulp* by Rembrandt van Rijn (canvas, lined) displayed in Royal Picture Gallery Mauritshuis, The Hague (inv. no. 146), is affected by extensive lead soap aggregate formation, which leads to crater-like holes and protrusions with diameters of approximately 100 μm on the surface of the painting. Three paint cross-sections representing the early stages of lead soap formation are depicted in figure 1a (sample MH146/B38), 2a (sample MH146/B39) and 3a (MH146/B37). The samples originate from the red lip of Adriaen Slabbraen, from the flesh paint cheek in the face of Jacob de Wit and from the flesh paint face of Adriaen Slabbraen (shadow near the hairline) respectively. These three paint cross-sections show a layer build up of paint on a so-called double ground, which consists of a red brown earth-pigmented layer below a greyish lead white-containing ground that also contains a little yellow ochre and lamp black particles. This is a traditional grey-on-red double ground on canvas used in the 17th-century Netherlands.[23] More advanced stages of lead soap formation leading to large aggregating protrusions in this painting have been presented before.[1, 2, 6, 7, 9, 10]

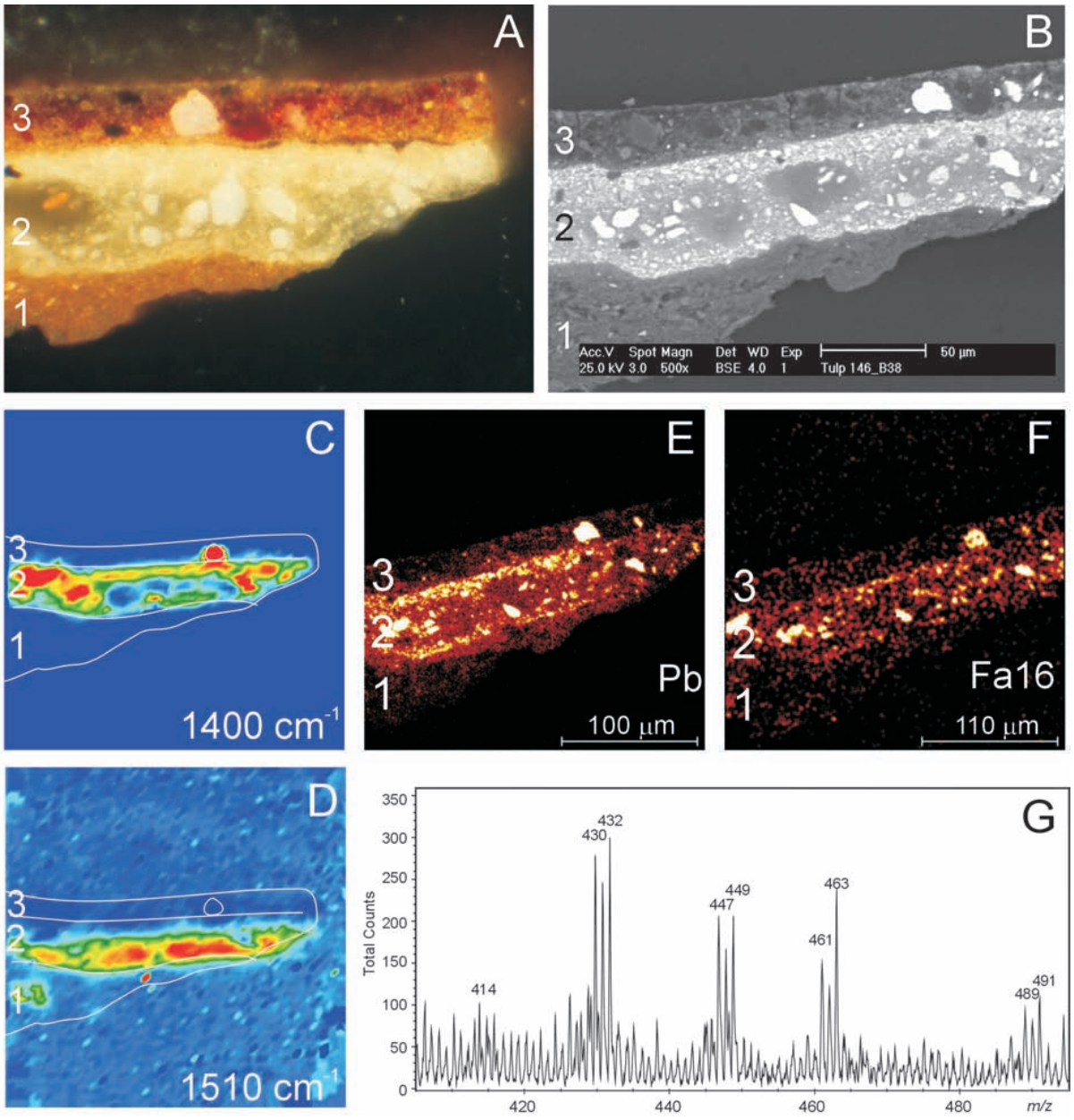

Fig. 5.1 Analytical imaging studies of paint cross-section MH146/B38 taken from 'The Anatomy Lesson of Dr. Nicolaes Tulp' by Rembrandt van Rijn (1632). White light microscopic image (A) and backscattered electron image (BSE-image) (B) reveal the layer buildup and granulometry. FTIR images represent carbonate carbonyl groups at 1400 cm^{-1} (C) and lead carboxylates at 1510 cm^{-1} (D) (red represents high and blue low intensity). An outline illustrates the three layers and the circle in layer 3 is indicative for the large lead white particle in this layer. SIMS-images represent lead (+; m/z 206-208) (E) and deprotonated palmitic acid (-; m/z 255) (F). A part of the positive SIMS spectrum presents Pb_2O at m/z 426-432, Pb_2O_2H at m/z 443-449, $PbOOC(CH_2)_{14}CH_3$ at m/z 461-463 and $PbOOC(CH_2)_{16}CH_3$ at m/z 489-491 (G) (see coloured version at the end of this thesis).

5.3.1.1 Paint cross-section MH146/B38 - Results

The greyish ground layer (2) is more transparent in the middle while the bottom and especially the top of this layer are opaque white (Fig. 5.1a). Large lead white particles are visible in the middle of the layer 2 while on the left side a small transparent mass is present that contains an orange minium ($Pb_2(PbO_4)$) particle. Data have been published earlier.[8] The top red paint layer (layer 3 in Fig. 5.1a) corresponding to the lip in sample MH146/B38, which contains earth pigments, organic red, carbon black and a few lead white particles, was applied on top of the above described double ground. The backscattered electron image (backscatter image) reveals large lead white particles in greyish regions in middle of layer 2, while mainly in the top but also in the bottom of this layer many small pigment particles are present (Fig. 5.1b). This difference in composition observed within this layer was investigated by specular reflection FTIR-imaging. FTIR images of the C-O stretch vibration of carbonates (1400 cm^{-1}) and the asymmetric COO^- stretch vibration of metal carboxylate (1510 cm^{-1}) are shown in Fig. 5.1c and d. The carbonate peak overlaps and predominates over the symmetric COO^- stretch vibration of metal carboxylate (expected at about 1400 cm^{-1}). An outline is plotted over the images to indicate the position of the different layers, the red coloured areas are indicative for high and the blue areas for low intensities. The carbonates (representative for intact lead white) are present in the top of layer 2 and in "hot" spots that correlate with the large intact particles of this layer. Lead soap is dominant in the middle towards the bottom of the layer, which corresponds with the poor electron reflecting areas observed in the backscatter image (Fig. 5.1b). Fig. 5.1e and f depict SIMS images of the paint cross-section representative of lead (Pb: *m/z* 206-208) and the negative ion of deprotonated palmitic acid (*m/z* 255). Lead is dominant in layer 2; the "hot" spots of lead in this layer match the intact lead white grains and orange minium particle (minium was identified by VIS-imaging according to van der Weerd *et al.*).[7] Apart from the "hot" spots, the lead is equally and finely distributed over layer 2. The fatty acids of palmitic and stearic acid (the stearic acid ion map is similar to the palmitic acid ion image) are also prominent in layer 2. The fatty acids have a relative higher yield near the lead white particles, which could be caused by assistance of lead in the secondary ion formation. Peaks representing lead soaps are seen in the SIMS spectra but their intensity is too low to obtain a good picture for a spatial distribution map. Fig. 5.1g presents part of the positive ion spectrum in the range of 405-495 amu. The following cluster peaks are interpreted on the basis of the mass and isotopic pattern: Pb_2O at *m/z* 426-432, Pb_2O_2H at *m/z* 443-449, $PbOOC(CH_2)_{14}CH_3$ at *m/z* 461-463 and $PbOOC(CH_2)_{16}CH_3$ at *m/z* 489-491.

5.3.1.2 Paint cross-section MH146/B38 - Discussion

A description of the present composition of the paint sample is given by the combination of the different analytical imaging data. The presence of lead soaps in layer 2 is determined by FTIR and SIMS. The absence of the finer lead white particles in this layer as visualised by the backscatter image leads to the proposal that the smaller lead white particles have reacted away to form lead soaps. This would imply that the ground in layer 2 was originally relatively medium rich delivering enough fatty acids by de-esterification of its cross-linked oil network. A possible further source of reactive fatty acids is the lower red ground layer (1), which in that case would be a medium-rich layer as well albeit with a poor trapping potential for fatty acids because of its low lead content. The residual large lead white particles and the presence of lead white in the top part of layer 2 suggest that there were insufficient reactive fatty acids to completely dissolve all the mineral matter. A burning remaining question is the absolute concentration of the reactive fatty acids. SIMS, the technique used to visualise the fatty acids, is unable to confirm a fatty acid rich layer 1 as the mineral matrix negatively influences the ionisation yield of the fatty acids. On the other hand when the fatty acids would have migrated and reacted with lead white in layer 2, the present relative concentration of the fatty acids in layer 1 would be much lower. The effects of the reactivity between fatty acids and lead white on the distribution of materials in the paint layers are further investigated in the next two case studies. The presence of the minium crystal inside the soap mass is worth some discussion. Minium is often observed in lead soap aggregates.[4, 7] Minium is mostly seen in the rim of lead soap aggregates, although in this cross-section (B38) minium is appears to be situated in the centre of the aggregate (although this may be an artefact of the cross-sectioning process and the aggregate observed might actually be the rim of a large aggregate). It has been suggested that minium inside or around lead soap aggregates is original mineral matter present as drier.[4] Historical recipes indeed mention minium boiled with the oil to improve the chemical drying.[24] Although this possibility can not be excluded, it appears unlikely that such large particles would still be remaining in view of the reactivity of fatty acids and minium. Minium is not observed in the lead white-contaiting paint matrix of the grey ground. More paintings from the 1630s made by Rembrandt also have minium free lead white-containing grounds.[25] We conclude therefore that minium was not originally present, but it is formed as part of the lead soap formation process (see further in the section of *general discussion*).

5.3.1.3 Paint cross-section MH146/B39 - Results

The second paint cross-section from *The Anatomy Lesson of Dr. Nicolaes Tulp* is a multi-layered system with two different types of lead white-containing paint layers

on top of each other. This sample was chosen because it could give some insight into the question whether metal soap formation is limited to a single layer and whether the nature of the lead white paint itself plays a role in the formation of metal soaps. Sample MH146/B39 contains a flesh-toned paint layer (3) composed mainly of finely grained lead white, a few small vermilion particles (few larger particles in the top of the layer) and some carbon black and yellow particles (Fig 5.2a). The backscatter image visualises a different granulometry in the two lead white-containing layers 2 and 3 (Fig. 5.2b). Two silicon particles with a low backscattering intensity are present in layer 2. Layer 2 is loosely packed and the size distribution of the lead white grains in this layer is broad. Overall, layer 2 is darker grey compared to layer 3, which means that it has a lower backscattered electron (BSE) intensity indicative for a lower relative amount or density of a heavy metal, in this case lead. Layer 3 is considered to be a single layer, but the backscatter image reveals less electron backscattering in the lower part of the layer and higher backscattering in the upper part.

The same partition in layer 3 is seen in the specular reflection FTIR images of carbonates (1395 cm^{-1}) and metal carboxylate (1514 cm^{-1}) (Fig. 5.2c and d). The carbonates representative for intact lead white are located in the upper part of layer 3 and in "hot" spots corresponding to the position of the large lead white particles in layer 2. The metal carboxylates are predominant in the lower part of layer 3 and in several areas in layer 2. FTIR spectra from the upper and lower part of layer 3 also illustrate a difference in composition (Fig. 5.2e).

Figures 5.2f-h depict backscatter images at higher magnification of the metal soap rich areas detected with imaging FTIR. The metal soap rich areas contain lead white particles with greyish pigment-reduced halos (Fig. 5.2f and g). Arrow 1 in figure 2f indicates a lead white particle surrounded by a greyish lead soap region with several tiny lead white particles. Arrow 2 points towards a large lead white particle, which is partially reacted away and is surrounded by a greyish halo indicating lead soaps. Fig. 5.2g visualises a lead soap-rich area: the relative amount of pigment particles is strongly reduced and these areas are less electron backscattering. In Fig. 5.2g the boundary between layer 2 and 3 is hardly visible, while in Fig. 5.2f the boundary is more obvious. Fig. 5.2h illustrates the difference in particle composition between the upper and lower part of layer 3. The lead white particles are densely packed in the top in contrast to the bottom part of the layer. SIMS images representative for lead (+; *m/z* 208) and deprotonated palmitic acid (-; *m/z* 255) are depicted in Fig. 5.2i and j. The lead is detected in layer 2 and 3, the "hot" spots correspond with the intact lead white particles. The iron, here representative for earth pigments, is located in the red brown ground layer. Fatty acids are detected in layer 2 and 3. The palmitic acid distribution corresponds with the lead distribution. Note that the ionisation of fatty acids is enhanced near lead and lead

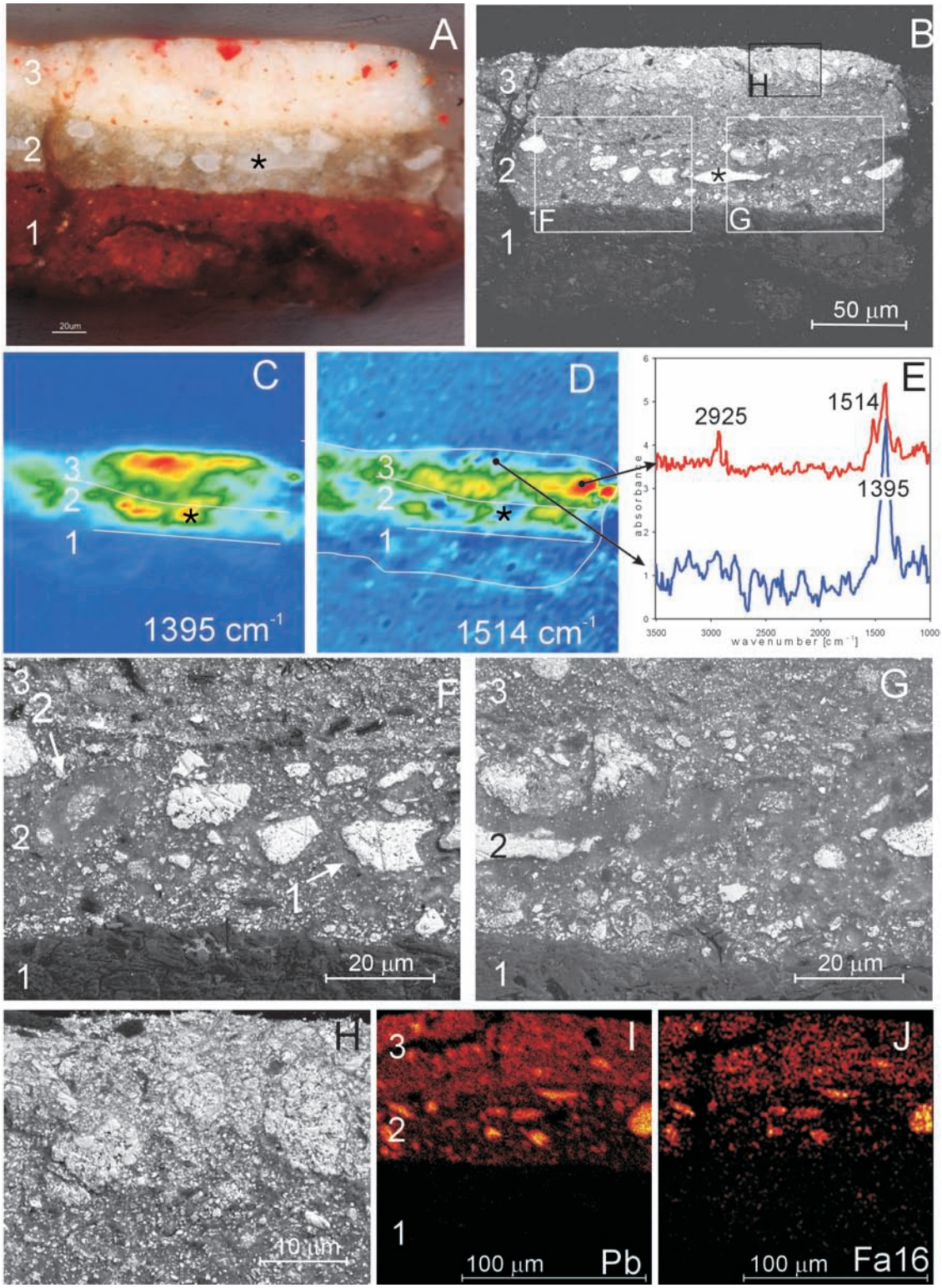

Fig. 5.2 Light microscopic image (A) and corresponding BSE-image (B) elucidates paint cross-section MH146/B39. FTIR images of carbonates at 1395 cm^{-1} (C) and lead carboxylates at 1514 cm^{-1} (D) reveal a partially saponified layer 3. Two FTIR spectra (E) derive each from a pixel in the FTIR image, indicated with an arrow. The asteriks indicates a large lead white particle in layer 2. BSE-images represent detailed areas of layer 2 (F, G) and layer 3 (H) (detail of layer 3 is indicated with a square in fig. 5.2b). SIMS image of lead (+; m/z 208) and deprotonated palmitic acids (-; m/z 255) are depicted in Fig. 5.2I and J, respectively (see coloured version at the end of this thesis).

white. The ratio between the palmitic and stearic acid ions (P/S ratio) in layer 2 is 1.9 and 2.2 in layer 3 suggesting linseed oils.[26] The ion yields of lead soaps were too low to image accurately.

5.3.1.4 Paint cross-section MH146/B39 - Discussion

The lead soap regions shown by FTIR in layer 2 correspond with pigment-free greyish halos around lead white particles and the transparent greyish region in the backscatter image. This suggests a reaction of fatty acids with lead white particles to lead soaps. As most of the mineral matter is absent in the saponified region of layer 2 - see for example Fig. 5.2g - and a few tiny remaining particles are seen in the 'halos' it is believed that primarily smaller lead white particles have been converted to lead soaps. The FTIR data and the backscatter image elucidate that two-thirds of layer 3 - the bottom part - is affected by lead soap formation also. The question arises whether layer 3 is really a single layer, especially because the few large vermilion particles are observed in the top of this layer. However, the light microscopic image shown reveals only the right side of the paint cross-section, while in the middle and left side of this sample the vermilion is rather homogenously distributed. Furthermore, a partially saponified lead white top layer is also observed in paint cross-section MH146/B37, which originates from a different location in the painting (discussed in the next section). As the phenomenon is observed in two different samples, we conclude that layer 3 is indeed a single layer, which is partially saponified. Layer 3 has a relatively high pigment/binder ratio which makes the layer most likely medium poorer compared to layer 2. The electron transparency in the backscatter image points out that only the lower part of layer 3 is affected by lead soap formation and that the mineral fraction is reduced. Reactive fatty acids are thought to have been introduced into layer 3 from hte underlyng layer as free fatty acid and not as lead soaps. The reasoning is that existing lead soaps would not attack the lead white crystals while free fatty acids can react readily. The reactive fatty acids are thought to derive from paint layers positioned lower. An argument for this proposal is the poorly defined boundary between layer 2 and 3 (see backscatter image). It cannot be excluded that layer 3 has expanded due to the lead soap formation in this layer. Both types of lead white paints (layer 2 and 3) are thus postulated to react with fatty acids to form metal soaps.

5.3.1.5 Paint cross-section MH146/B37 - Results

The third paint cross-section (MH146/B37) from *The Anatomy Lesson of Dr. Nicolaes Tulp* has a similar multi-layered structure as paint cross-section MH146/B39 (Fig. 5.3a). The top layer (3) is a flesh-toned paint layer with lead white as well as a few red vermilion and carbon black particles. In layer 2 (grey ground) a transparent

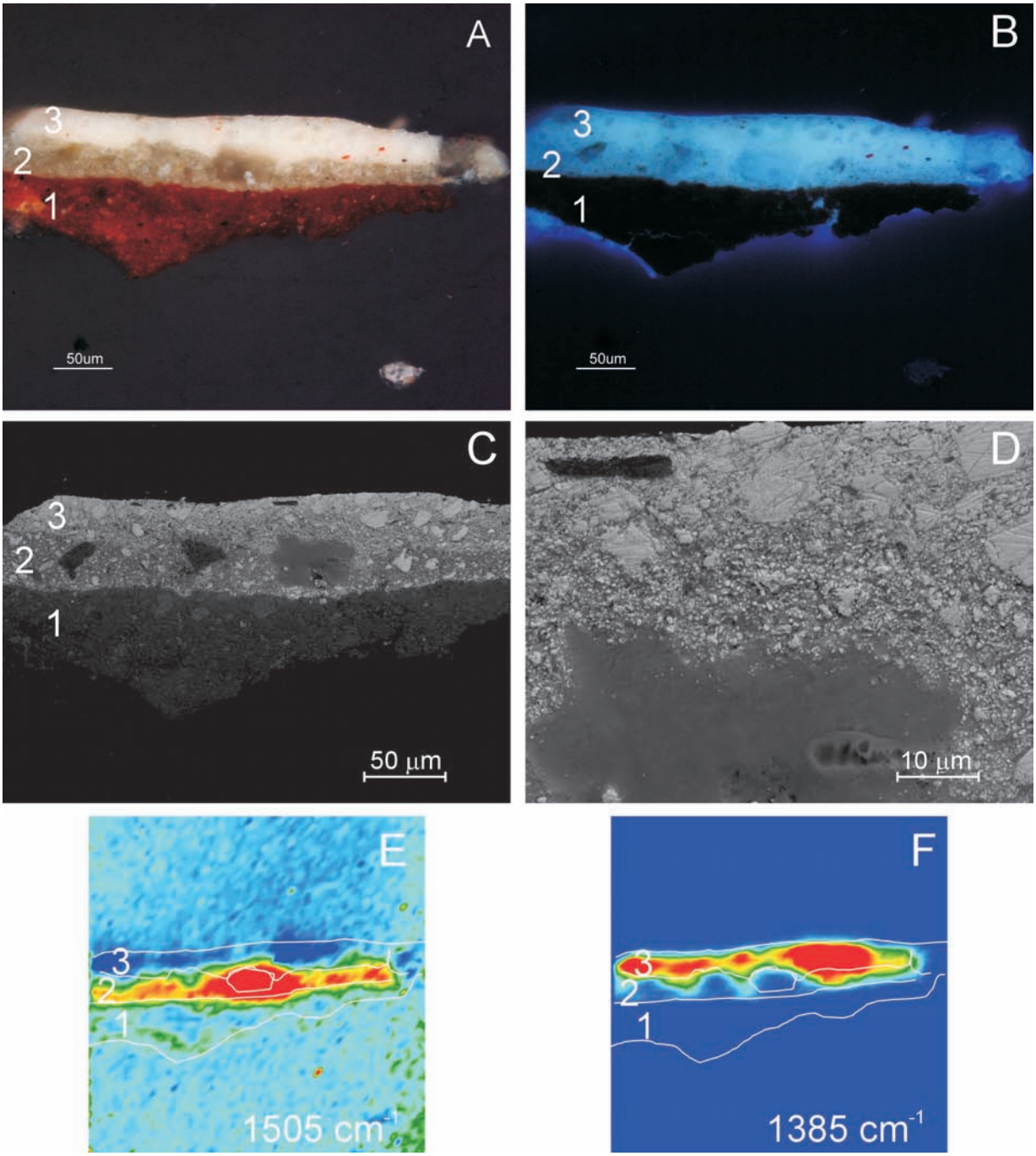

Fig. 5.3 Paint cross-section MH146/B37 contains a lead soap aggregate in the layer 2 and in layer 3, which is visible in the white light (A) and UV microscopic image (B). BSE-image (C) reveals different granulometry in the two lead white-containing layers 2 and 3. BSE-image (D) of a magnified area elucidates the top side of the aggregate positioned in layer 3. Fig. 5.3E and F represent the FTIR images of lead carboxylate at 1505 cm^{-1} (E) and carbonates at 1385 cm^{-1} (F). The loop in the outline indicates the position of the aggregate (see coloured version at the end of this thesis).

aggregate is visible. The square aggregate, which is positioned in layer 2 and 3, strongly fluoresces under UV illumination (Fig. 5.3b). The upper part of layer 3 does not fluoresce. The backscatter image of layer 2 and 3 shows a comparable granulometric composition as the layers 2 and 3 in sample MH146/B39 (compare Fig. 5.2b and 3c). Similar to sample MH146/B39, the lower part of layer 3 shows a lower BSE intensity than the upper part of that layer (Fig. 5.3c). A detail of the top of the square aggregate and part of layer 3 is depicted in Fig. 5.3d. Tiny lead white particles are visible around the square aggregate. The number of particles and their size decreases towards the rim of the aggregate. No distinct edge is observed between the paint and the aggregate. An outline indicating the position of the layers and aggregate is plotted over the FTIR images representative for metal soaps (1505 cm^{-1}) and carbonates (1385 cm^{-1}) (Fig. 5.3e-f). The metal soaps are homogenously present in layer 2, but also predominate in the lower part of layer 3 especially around the aggregate. This distribution of metal soaps in layer 3 corresponds with the lower BSE intensity in this layer.

5.3.1.6 Paint cross-section MH146/B37 - Discussion

The metal soap formation is not restricted to the grey ground (layer 2). The lower part of layer 3 is also affected by lead soap formation. The distribution of the lead soaps corresponds with the fluorescence of layer 2 and 3. The non-fluorescent the upper part of layer 3 is unaffected. Note that the paint of layer 3 is not pushed up around the lead soap aggregate. It can be deduced from the backscatter image that a conversion of lead white particles in layer 2 as well as in layer 3 is taking place. The reaction of fatty acids with lead white crystals in the bottom part of layer 3 is comparable to the chemical reactivity observed in sample MH146/B39.

5.3.2 'Herald' (south-west) by Christiaen van Couwenbergh (1651)

The *Herald* (south-west) painted by Christiaen van Couwenbergh (1651, canvas) is part of the paintings ensemble in the Oranjezaal of the Royal Palace Huis ten Bosch (The Hague, The Netherlands). This ensemble of 40 paintings was restored between 1998-2001. It is an excellent collection for in-depth studies, because the paintings remained in the same place in a relatively stable environment, their conservation history is known and they experienced minimal interventions by conservators.[27] The paint sample HSTB 43/3 originates from a white area partially covered by the hair of the herald. No paint defects were observed on the surface of the area sampled. The cross-section was initially taken to reveal the layer build-up. Because of the presence of a large lead soap mass with many minium crystals inside in a lower layer, it was chosen for further investigation.

5.3.2.1 Paint cross-section HSTB 43/3 - Results

The paint sample in the cross-section consists of four layers (Fig. 5.4a and b). The cream-coloured ground layer containing lead white and umber is applied in two layers marked 1 and 2. The large lead white particles in layer 2 have a fluorescent halo and a fluorescent area is visible in the middle of the layer. Layer 2 contains a large heterogeneous aggregate (diameter about 100 µm) with many horizontally oriented orange minium particles of about 3-4 µm wide inside the transparent and partially white opaque mass (Fig. 5.4a). The centre of the aggregate does not fluoresce in contrast to the left, right and top side near the rim (Fig. 5.4b). Layer 3 is a pure lead white-containing layer, which strongly fluoresces under UV illumination. A very thin non-fluorescent layer with boneblack, umber and red ochre particles are visible as the top layer 4.

'Herald with trophy, medallion and cartouche containing pictures of the triumph of Frederik Hendrik at Breda (1637) and at Gennep (1641)' painted by Christiaen van Couwenbergh (1651, canvas) is part of the paintings ensemble in the Oranjezaal of the Royal Palace Huis ten Bosch, The Hague, The Netherlands (inv. no. SC/1307) (see coloured version at the end of this thesis).

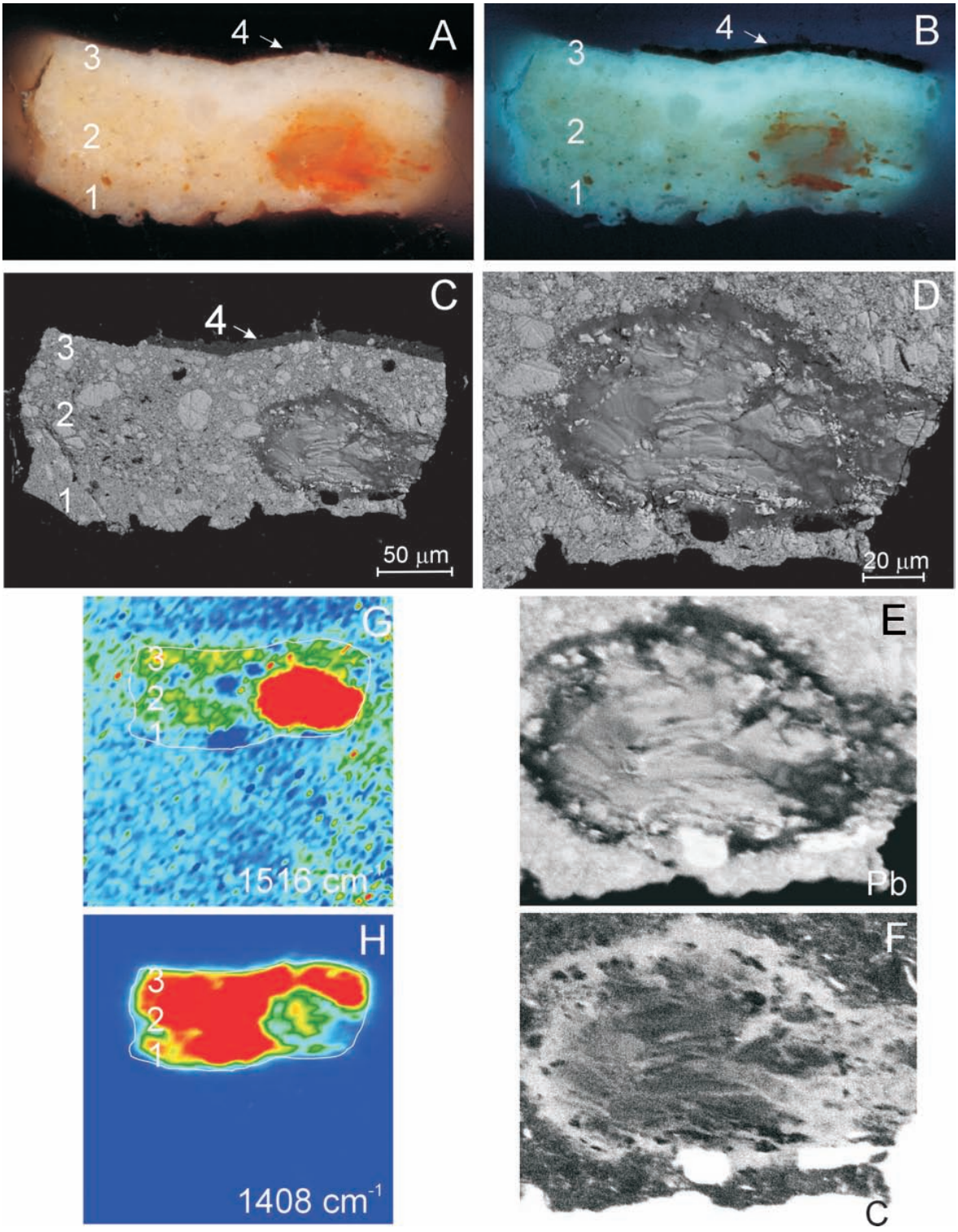

Fig. 5.4A-H Paint cross-section HSTB43/3 originating from 'Herald' (south-west) by Christiaen van Couwenbergh (1651) is depictured in the light microscopic images, white light (A) and UV (B), and in the corresponding BSE-image (C). BSE-image (D) and X-ray maps of lead (PbM) (E) and carbon (CK) (F) reveal the large lead soap aggregate. Lead carboxylates are detected and imaged with FTIR at 1516 cm^{-1} (G) and carbonates at 1408 cm^{-1} (H) (see coloured version at the end of this thesis).

The backscatter image reveals a densely packed paint with a broad size distribution of lead white particles (Fig. 5.4c). The boundaries between layer 1, 2 and 3 are hardly visible. Layer 1 has a higher BSE intensity compared to layer 2 and 3 (if we ignore the tiny dark spots corresponding to the brown particles in layer 2). The aggregate has a heterogeneous structure with fine particulate lamellar bands in the centre (Fig. 5.4d) and multiple coarser grained crystals. The rim shows a lower BSE intensity compared to the centre. The bright highly electron reflecting particles inside the aggregate correspond to the orange minium particles seen in the light microscopic image. Note that some of the crystals observed in the light microscopic image are positioned deeper in the lead soap mass. EDX maps of carbon and lead show high carbon and low lead intensities in the rim of the aggregate (Fig. 5.4e, f). The "hot" spots of lead in the rim, which are carbon free, are representative of the orange minium particles. The intensities in the carbon and lead maps are reversed in the lamellar structures in the centre of the aggregate. The distribution of oxygen (map not shown) resembles the lead distribution.

Imaging FTIR at 1516 cm^{-1} reveals metal soaps with a high relative intensity inside the aggregate and with much lower intensities in layer 2 and 3 (Fig. 5.4g). The areas, where no metal soaps are detected, correspond to the large lead white particles. The FTIR peaks representative of metal soaps are absent in layer 1 (Fig. 5.4h). The carbonates at 1408 cm^{-1} are very abundant in all the layers and have a higher intensity in the centre of the aggregate. The difference between lead carbonate ($PbCO_3$) and basic lead carbonate ($2PbCO_3 \bullet Pb(OH)_2$) can not be deduced from the FTIR spectrum because the relevant spectral features are outside the range of our detector.

The SIMS images in Fig. 5.4i-l show the distribution of lead (+ ; *m/z* 208), chloride (- ; *m/z* 35), deprotonated palmitic acid (- ; *m/z* 255) and sodium (+ ; *m/z* 23) . The lead is homogenously distributed in the aggregate and in layer 1 and 2. Chloride and deprotonated palmitic acid predominate in the aggregate. The chlorine is more abundant in the centre of the aggregate, whereas the palmitic acid ion yields are higher near the rim on the left side. The secondary ion yields of palmitic acid are lower in layer 1, 2 and 3. Sodium is detected in layer 1, 2 and 3, but is absent in the aggregate. The lead soaps of palmitic and stearic acids are not abundant in the positive ion spectrum and their intensities are too low to image. Fig. 5.4m that presents part of the positive ion spectrum (range *m/z* 405-495) calculated for the aggregate shows the lead cluster ions of Pb_2 (*m/z* 410-416), Pb_2O (*m/z* 426-432) and Pb_2O_2H (*m/z* 443-449). The palmitic acid lead soap ions expected at *m/z* 461-463 overlap with isotope peak from Pb_2ClO (*m/z* 461-469). Two maxima in nominal ion peak of *m/z* 463 occur at 463.2 D and 462.9 D that are representative for $PbOOC(CH_2)_{14}CH_3$ and PbOCl, respectively. The stearic acid lead soap ions overlap with an ion pattern of an unidentified compound.

Various lead-chloride clusters were detected in the negative as well as in the positive SIMS spectrum. The significance of these peaks will not be discussed further but they suggest the presence of a chlorinated lead mineral phase in the lead soap aggregate.

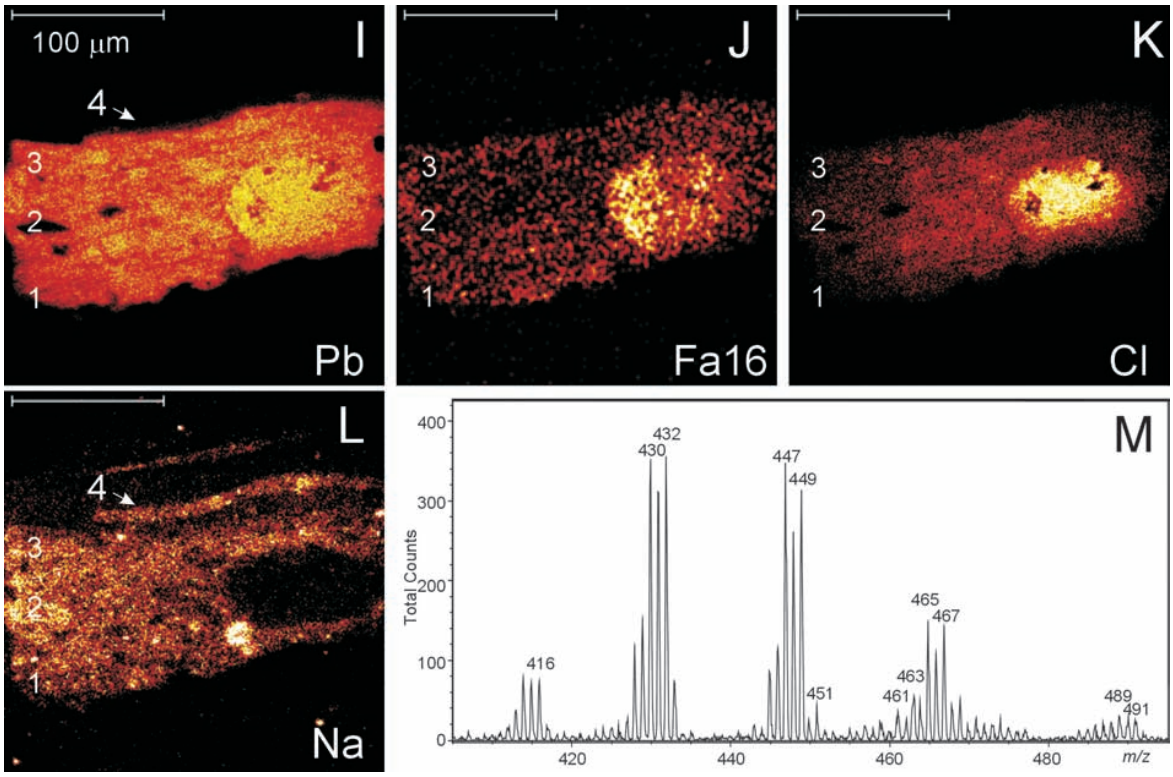

Fig. 5.4I-M SIMS images show the distribution of lead (+; m/z 208)(I), deprotonated palmitic acids (-; m/z 255)(J), chloride (-; m/z 35)(K) and sodium (+; m/z 23)(L). A partial positive SIMS spectrum presents Pb_2 at m/z 410-416, Pb_2O at m/z 426-432, Pb_2O_2H at m/z 443-449, Pb_2ClO (m/z 461-469), which overlaps with $PbOOC(CH_2)14CH_3$ at m/z 461-463 (M) (see coloured version at the end of this thesis).

5.3.2.2 Paint cross-section HSTB 43/3 - Discussion

Lead soaps are present in a dispersed form in layer 2 and 3. The lead source of the soaps found in the aggregate is believed to be originating from lead white particles because we have found no other source of lead in this sample. The presence of sodium in the paint matrix and its absence in the aggregate is considered evidence for the growth of the aggregate inside the paint rather than a pre-existence in the paint matrix. In the centre of the aggregate lead carbonates have precipitated, because FTIR detected carbonates in the centre. The rim of the aggregate is lead soap rich as it is more organic rich compared to the centre (see EDX map and the deprotonated palmitic acid ion image). The existence of lead chloride mineral phases in the aggregate cannot be excluded. In earlier work fiedlerite ($Pb_3Cl_4(OH)_2$) has been identified with X-ray diffraction analysis in a large remineralised aggregate of *The Anatomy Lesson of Dr. Nicolaes Tulp*.[2]

The relative number, size and position of orange minium particles made us conclude that the minium was not originally present in the paint. In the hypothetical case that minium would have been the starting material for lead soap formation, it is expected that it would have reacted away.[28] Minium is observed in none of the numerous cross-sections made during an extensive study of 30 paintings with lead white-containing oil grounds in the Oranjezaal. The minium particles are positioned in the aggregate between the lamellar structure and the lead soap rich rim. This indicates that they are created during the formation of the lamellar structure or at least during the growth of the aggregate.

5.3.3 Preprimed Canvas used by Frederic E. Church (1826-1900)

Spotty translucency (ground staining) and efflorescence are degradation phenomena that strongly affect the appearance of the paintings by Frederic E. Church and other painters from the Hudson River School. A residual piece of commercial preprimed canvas used by F.E. Church shows efflorescence and aggregates protruding through the paint surface. The canvas is part of the F.E. Church estate in Olana (near Hudson, New York). A sample was kindly provided by J. Zucker (New York State Bureau of Historic Sites at Peebles Island).

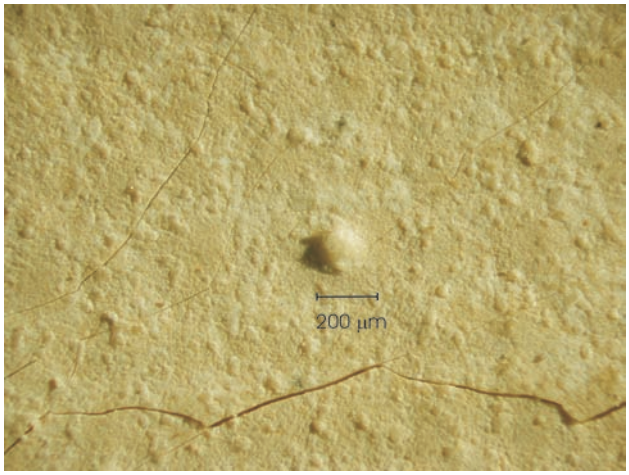

Detail of a residual piece of commercial preprimed canvas used by F.E. Church in the middle a large aggregate protruding through the paint surface. The canvas is part of the F.E. Church estate in Olana (near Hudson, New York) (see coloured version at the end of this thesis) (photo: Dr. E. Ferreira).

5.3.3.1 Paint cross-section PCC01 - Results

Fig. 5.5a illustrates a paint cross-section originating from the preprimed canvas revealing the layer structure of the ground and a large aggregate in the middle of the sample. The very thin dark layer on top of the cross-section is a layer of dust. The backscatter image reveals a calcium carbonate layer (1), a mixture of calcium carbonate

and lead white (2) and a pure, densely packed lead white-containing top layer (3) (Fig. 5.5b). The open holes in the aggregate are artefacts due to electron beam exposure. The aggregate is a heterogenous greyish mass with a dark grey core and a lighter grey rim without particles inside. The dark grey tone in the centre is indicative for a lower lead density, which contrasts with the rim of the aggregate. The pigment particles around the aggregate and in the rest of the paint sample appear to be intact; no transparent grey dissolution halos are observed around the pigment grains as is observed in Rembrandts *The Anatomy Lesson of Dr. Nicolaes Tulp*. EDX maps of carbon, oxygen, lead and calcium are presented in Fig. 5.5c-f. The carbon map elucidates high carbon X-ray yields around the paint cross-section that correspond with the embedding medium, and inside the aggregate (particularly in the core of the aggregate). Oxygen is dominant in

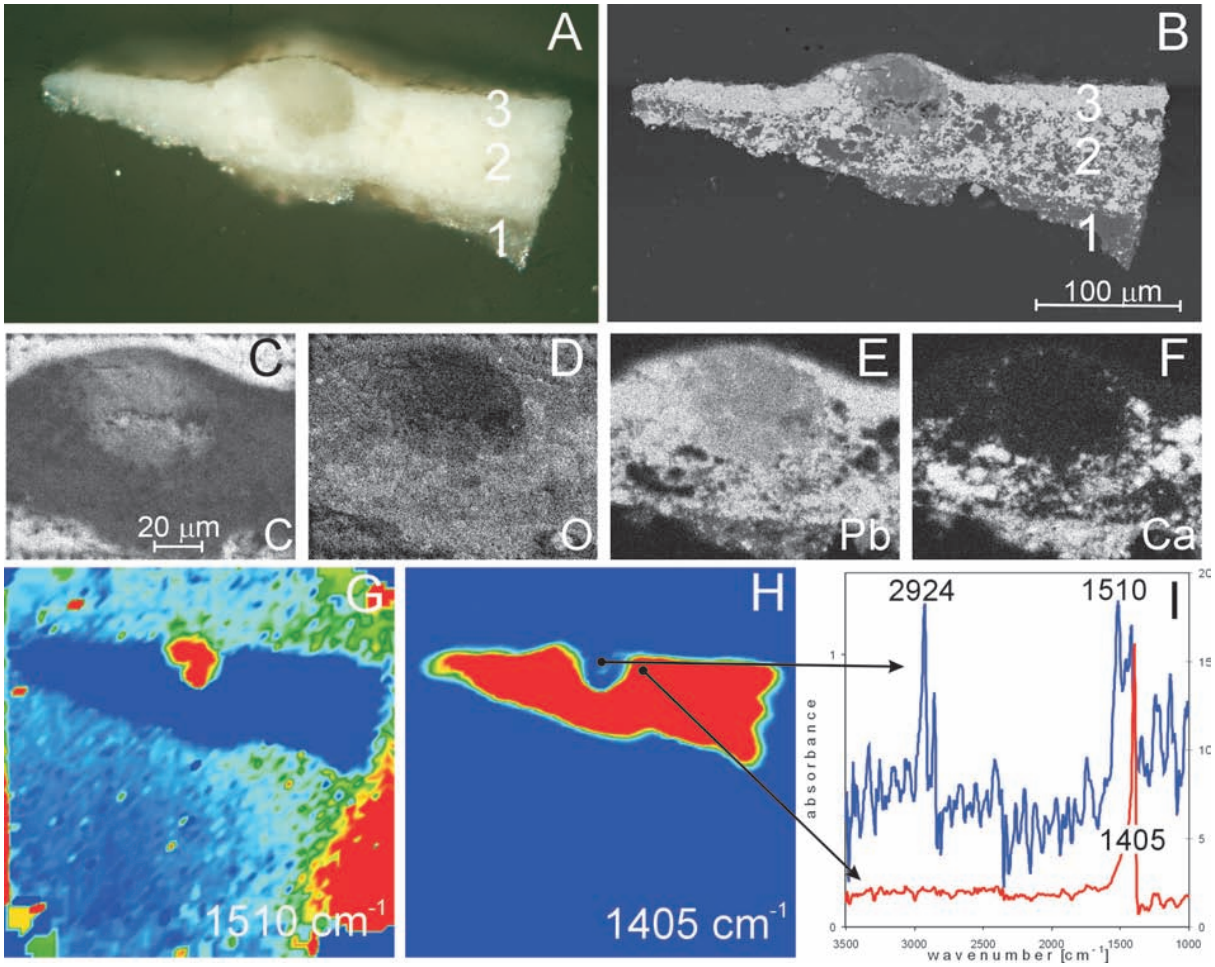

Fig. 5.5A-I A large lead soap aggregate is visible in the white light microscopic image (A) of a paint cross-section originating from the preprimed canvas used by Frederic E. Church (1826-1900). The BSE-image and X-ray maps of carbon (CK) (C), Oxygen (OK) (D), lead (PbM) (E) and calcium (CaK) (F) expose the particle and elemental distribution. FTIR images show lead carboxylates (G) in the aggregate and carbonates (H) in the rest of the paint sample. Two FTIR spectra derived from a single point in the aggregate and in the paint matrix (I) (see coloured version at the end of this thesis).

the intact mineral phases and with somewhat higher X-ray yields from the calcium carbonate particles. The lead is homogenously present in the aggregate and corresponds with the brightest particles of the paint matrix in the backscatter image. Calcium matches with the grey particles in layer 1 and 2, but is absent in the aggregate and layer 3.

Specular reflection imaging FTIR supports these observations. FTIR images visualise carbonates (1405 cm^{-1}) that are located in all the three layers, but are absent in the aggregate; the metal carboxylates (1510 cm^{-1}) are only detected in the aggregate (Fig. 5.5g and h). The FTIR spectrum of a pixel in the aggregate illustrates two sharp peaks of C-H stretch vibrations at 2924 and 2856 cm^{-1} of the aliphatic chains and the asymmetric and symmetric COO^- stretches of lead carboxylate at 1510 and 1415 cm^{-1} (Fig. 5.5i). A spectrum derived from a pixel directly next to the aggregate reveals only the intense peak of the C-O stretch vibration of carbonates at 1405 cm^{-1} (Fig. 5.5i).

The cross-section was also subjected to imaging SIMS, but prior to this analysis the cross-section was gold coated (2 nm) to improve the organic ion yields.[29] Figures 5.5j-o depict the positive secondary ion images of lead (*m/z* 206-208), calcium (*m/z* 40) and lead stearic acid salt (*m/z* 489-491) and the negative secondary ion images corresponding to deprotonated stearic acid (*m/z* 283), deprotonated azelaic acid (*m/z* 187) and $C_2H_3(CH_2)_5COO^-$ fragment ion of fatty acids (*m/z* 141). An overlay derived from the backscatter image is plotted over the SIMS images (Fig. 5.5p). Unfortunately, a few artefacts were introduced in the sample during/after gold coating: a circular feature in the centre of the paint sample (also observed in the corresponding backscatter image (Fig. 5.5p), an area on the right covering some of layer 3 and furthermore a scratch leading from middle top to right centre damaging the paint surface next to the aggregate. Lead is homogenously distributed in layer 3 with higher yields in the core of the aggregate (ignore the artefacts). Lead is not homogeneously divided in layer 2, where the areas with higher ion intensities correspond roughly to the brighter areas of the lead white in the backscatter image. Calcium is only detected in layer 2 and in low yields in layer 1. The relatively low ion yields of lead and calcium in layer 1 and 2 can be explained by the suppression of ions from inorganic elements due to the gold coating.[29] Note that without gold coating the calcium and lead would have been much more defined and sharper. There is a relatively high concentration of stearic acid in the core of the aggregate, corresponding to the dark grey area of the aggregate in the backscatter image. The distribution of stearic acid in layer 3 also correlates with the higher yield of lead in this layer (palmitic acid has a similar distribution but is not shown here). The ion yields of stearic acid lead soap (*m/z* 489-491) are high in the core of the aggregate and low in the rim. The lead soap ion intensity is lower in layer 2 and 3, where the intensity is lower but corresponds roughly with the distribution of stearic acid (the ions

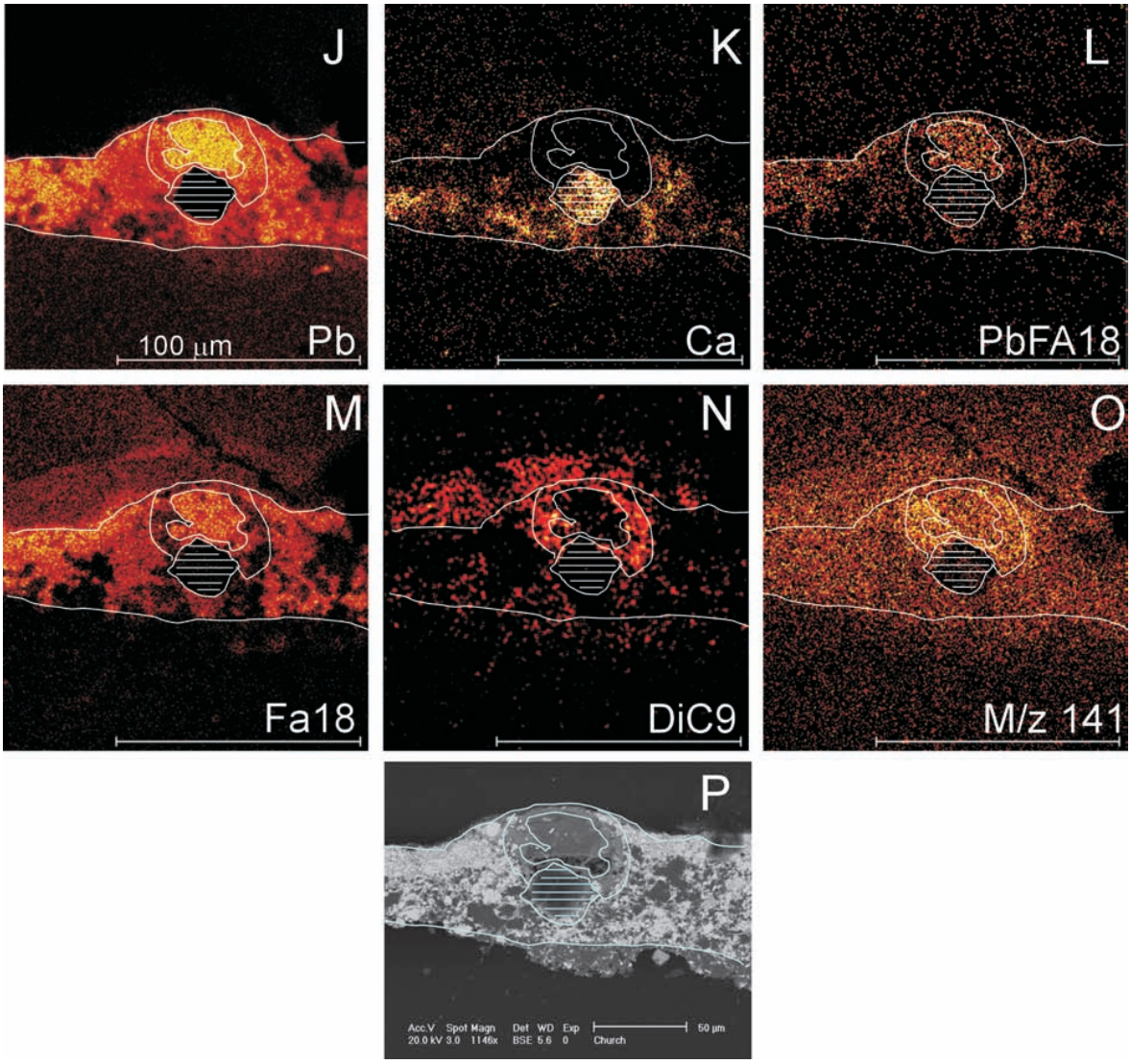

Fig 5.5J-P SIMS images of the gold-coated paint cross-section (2 nm) depicture lead (+; m/z 206-208) (J), calcium (+; m/z 40) (K) and lead stearic acid salt (+; m/z 489-491) (L), deprotonated stearic acid (-; m/z 283) (M), deprotonated azelaic acid (-; m/z 187) (N) and the $C_2H_3(CH_2)_5COO^-$ fragment ion of fatty acids (-; m/z 141) (O). An overlay derived from the corresponding BSE-image (P) is plotted over the SIMS images. The circular feature in the centre of the paint sample (indicated with the dashed area), an area on the right covering some of layer 3 and a scratch leading from middle top to middle right centre are sample preparation artefacts (see coloured version at the end of this thesis).

of palmitic acid lead soap have similar distribution and are not shown here). The azelaic acid ion is detected in the rim of the aggregate and corresponds with the lighter grey region of the aggregate visualised in the backscatter image. The fragment ion intensities of fatty acid alkyl chains, derived from palmitic and stearic acid as well as azelaic acid, are highest in the core and rim of the aggregate. Lower ion intensities are found equally distributed around the aggregate. The distribution of the fragment $C_2H_3(CH_2)_5COO^-$ at *m/z* 141 is only shown in Fig. 5.5o, but related fragments,

$C_2H_3(CH_2)_nCOO^-$ with n = 0-12, are however detected with a similar distribution (images not shown). This points to high relative concentrations of these binding medium components. Secondary ions of azelaic acid as well as the stearic acid are detected outside the paint sample, especially above the sample. Although the gold coating enhances the "chemical" noise, the counts detected above the sample are assignable to fatty acids. Since the gold coating is thermally deposited on the paint sample, it is likely that the fatty acids have evaporated and were deposited above the sample. Taking this into account, the fatty acids detected in the paint sample are metal or ester bound and cannot be easily released by evaporation.

5.3.3.2 Paint cross-section PCC01 - Discussion

All the imaging techniques, FTIR, SEM and SIMS reveal a relative high concentration of lead and lead soaps in the aggregates. Based on the FTIR and SEM data, it seems that lead soaps are very concentrated in the aggregate. SIMS results confirm that lead soaps are present in the aggregate, but also in the top layer and occasionally in layer 3. The concentration of lead soaps in layer 2 and 3 are below the detection limit of specular reflection FTIR. We are not quite sure whether the distribution detected by SIMS is a representative quantitative picture of the fatty acid distribution. We point however to the interesting difference in distribution of monocarboxylic fatty acids in the core and dicarboxylic acids those are only detected in the rim of the aggregate. This distribution suggests a phase separation possibly due to crystallisation into pure phases.

In comparison to other cases presented, we see no indications for dissolution of the mineral matter in this paint cross-section. It is known that lead acetate, another source of reactive lead, has been added as drier, especially in the upper layers, to speed up the drying of this commercially prepared canvas.[30] Traces of this type of drier are no more detectable in the analytical imaging data. Free fatty acids, but perhaps also esterified fatty acids, are thought to react preferentially in an early stage of the drying process with the lead from the more reactive lead acetate. Free fatty acids are also thought to be delivered from the layers positioned lower in later stages of the ageing of the ground. The formed lead soaps aggregate in the top layer or appear on the surface of the canvas, as efflorescence.[16, 17] Direct temperature resolved mass spectrometry (DTMS) and FTIR studies on isolated aggregates and efflorescence show the presence of free and lead bound palmitic and stearic acids and low amount of free azelaic acid.[16, 17] The preprimed canvas is clearly a source of fatty substances and mobile lead soap. If these compounds penetrated the overlying paints in Church's paintings, they could explain the changes in transparency observed. This hypothesis needs further testing by study of the affected paint layers in his paintings.

5.3.4 The Sherborne Triptych - unknown northern painter 15th Century

The triptych (oak panel) is displayed in Sherborne Abbey Almshouse (Dorset, UK) and is presently owned by the National Trust. Extensive studies have been performed on the technical history of the triptych when it was restored in the Conservation & Technology of the Courtauld Institute of Art, London. Cross-sections from the triptych were investigated at AMOLF as part of the master thesis on the occurrence of lead soaps in 15th- to 20th- century paintings by Emily Gore.[31] Paint cross-section CIA 1577 RS06 originates from the green drapery of the robe of third figure portrayed in the right panel.

The triptych (oak panel) by unknown nothern painter is displayed in Sherborne Abbey Almshouse (Dorset, UK) and owned by the National Trust (see coloured version at the end of this thesis).

5.3.4.1 Paint cross-section CIA 1577 RS06 – Results

The green robe is build up in four layers (Fig. 5.6a). The glue-chalk ground (1) is followed by an imprimatura layer (2), which is not visible in this paint cross-section. Paint layer 3 is a lead-tin yellow type I paint (lead stannate, Pb_2SnO_4) with a large transparent area on the left and a smaller yellow coloured area on the right. The top layer is a copper green glaze (4). In the lead-tin yellow layer lead soap formed. Lead-tin yellow pigment itself is transparent for infrared in the measured range (3500-1000 cm^{-1}). Fig. 5.6b depicts the FTIR image of the lead carboxylate (1531 cm^{-1}). A contour based on the boundary of the embedding medium (image not shown) is plotted over the FTIR image. Metal soaps are present in the large aggregate on the left. When the image of the metal soaps is overscaled, metal soaps can also be characterised in relatively low proportion to the rest of the lead-tin yellow layer, but they are not detected in the intact yellow particle on the right (Fig. 5.6c). A peak at 1582 cm^{-1} characteristic for the copper carboxylate is observed in the spectrum of the green glaze in the top layer (Fig. 5.6d).

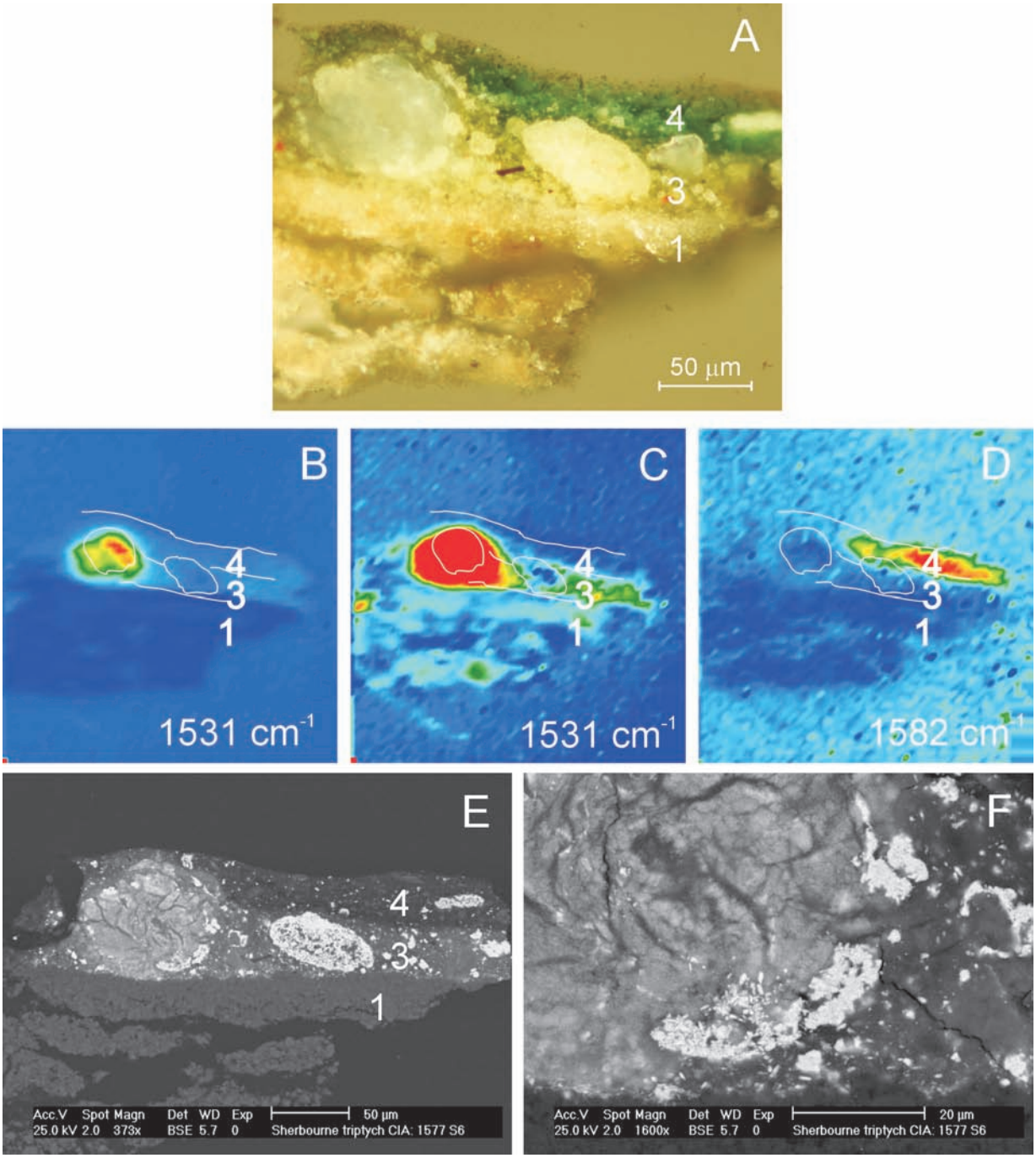

Fig. 5.6A-F The white light microscopic image (A) of the paint cross-section CIA 1577 RS06 derived from 'The Sherborne Triptych' (unknown northern painter 15th Century) elucidates a large lead soap aggregate and a porous residual lead-tin yellow particle in a lead-tin yellow-containing paint layer. FTIR images present lead carboxylate at 1531 cm^{-1} (B) (C, is overscaled) and copper carboxylate at 1582 cm^{-1} (D). An outline plotted over the FTIR image is deduced from the light microscopic image. BSE-images represent the paint cross-section (E) and a detail of the right part of the lead soap aggregate (F) (see coloured version at the end of this thesis).

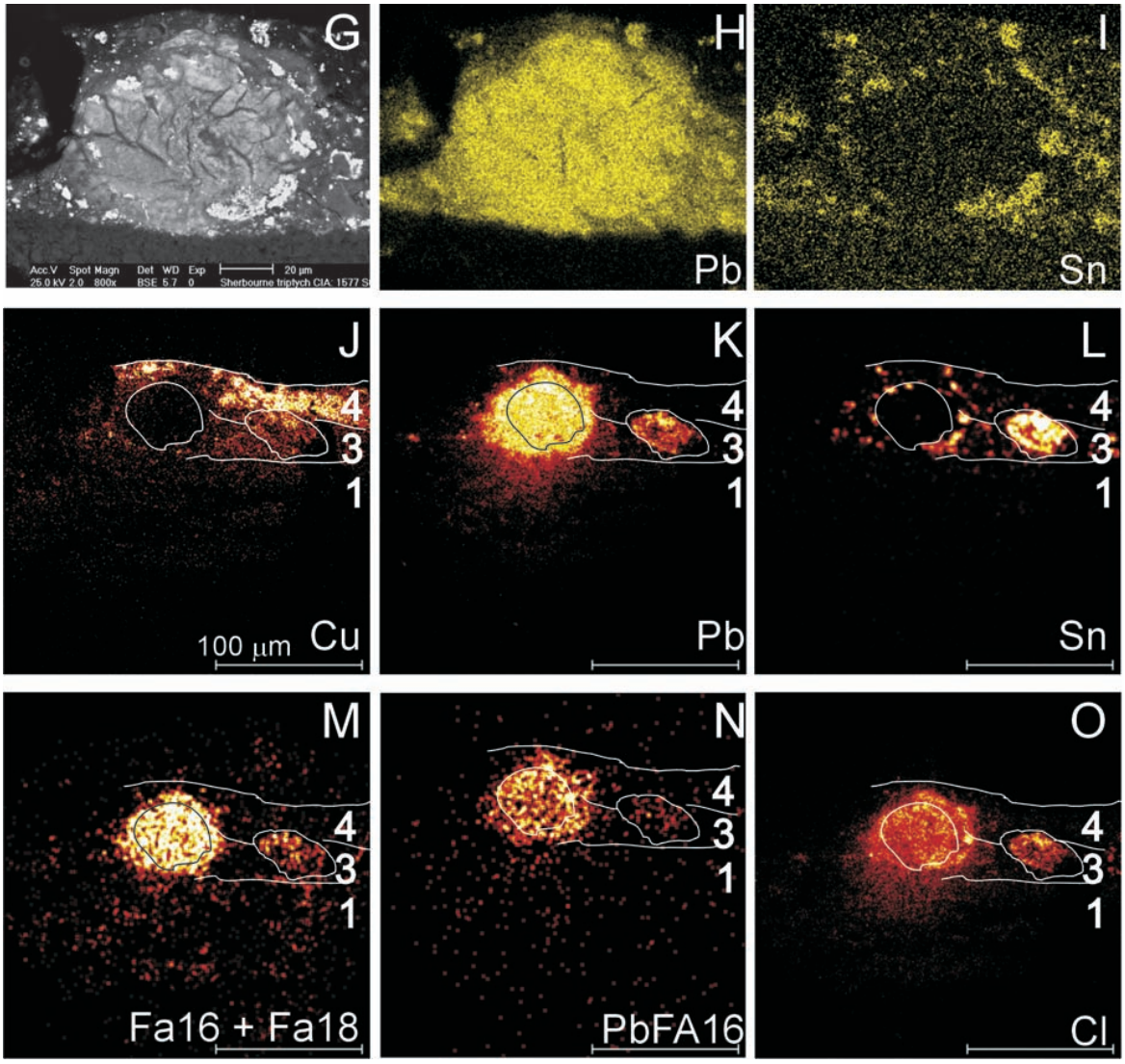

Fig. 5.6G-O BSE-image (G) and X-ray maps of lead (PbM) (H) and tin (SnL) (I) indicate the large lead soap aggregate. SIMS-images represent copper (+; m/z 63) (J), lead (+; m/z 208) (K), tin (+; m/z 52) (L), the sum of deprotonated palmitic and stearic acid (-; m/z 255 + m/z 283) (M), palmitic acid lead soap (+; m/z 461-463) (N) and chloride (-; m/z 35) (O) (see coloured version at the end of this thesis).

The backscatter image illustrates the lead soap mass, a large inhomogeneous light-greyish aggregate with dark grey "cracks" (Fig. 5.6e, f). Highly reflecting tiny particles are positioned around the soap mass. Lead and tin EDX maps of the aggregate illustrate tin and lead around the aggregate, but there is only lead inside the aggregate (Fig. 5.6g-i). The tin shows a spatial correlation with lead, indicative for lead-tin yellow pigment. The morphology of the lead soap aggregate and the lead-tin yellow particles positioned around the aggregate suggest that the growing lead soap aggregate has pushed residual lead-tin yellow particles aside (see detail in Fig. 5.6f). On the right side, an agglomerate of fine highly-reflecting particles matches the yellow area under

normal light. Lead and tin EDX maps of this yellow area overlap and the structure visualised in the backscatter image point to a porous lead-tin yellow particle (data not shown).

The paint cross-section was also analysed with static-SIMS. The Fig. 5.6j-o display the secondary ion images of copper (+; *m/z* 63), lead (+; *m/z* 208), tin (+; *m/z* 52), the sum of deprotonated palmitic and stearic acid (-; *m/z* 255 + *m/z* 283), palmitic acid lead soap (+; *m/z* 461-463) and chloride (-; *m/z* 35). The map of copper corresponds with the green glaze top layer. Note that this layer is pushed up due to the expanding lead soap aggregate. The lead ion yields are high inside the aggregate and the agglomerate. The monocarboxylic fatty acids are mainly located in the aggregate and in small yields in the intact porous lead-tin yellow particle. A similar distribution is found for the fatty acid lead soaps. Small spots of tin are positioned around the fatty acid lead soap mass, while a relatively high ion intensity of tin is observed in the lead-tin yellow pigment agglomerate. SIMS shows that fatty acids and lead soaps are present in the porous lead-tin yellow particle, but these lead soaps did not lead to destruction of the particle by expansion. Chloride is dominant in the lead soap aggregate and the intact porous lead-tin yellow particle.

5.3.4.2 Paint cross-section CIA 1577 RS06 – Discussion

The paint cross-section CIA 1577 RS06 contains a lead soap aggregate surrounded by intact lead-tin particles and a porous lead-tin yellow pigment particle. The various microscopic observations allow the proposal of a mechanism that correlates the degradation of the original lead-tin yellow pigment with the formation of lead soap aggregates. A hypothesis for the mechanism has been presented earlier and is reprinted in Scheme B.[13] An essential element in the formation of lead soaps is the existence of non-stoichiometric lead stannate phases in the lead-tin yellow type I pigment as a consequence of the production process of the pigment. The conditions in the melt and the cooling conditions are crucial for conversion of the lead and tin oxides to lead stannate.[32] The resulting mixed phases could be lead oxides co-crystallized with lead stannate or may be present as mixed crystals of lead stannate and lead plumbate which have a very similar crystal structure.[32] Free fatty acids that derive from outside the lead-tin yellow particles are proposed to react with reactive lead phases to form lead soaps next to the less reactive lead stannate. The local formation of a relatively high amount of lead soaps leads to volume expansion of the lead-tin yellow pigment particle and drives the residual lead stannate towards the periphery of the growing soap aggregate. The volume of the lead soap mass is much larger than the original lead-tin yellow particle(s), as can be deduced from the green glaze layer pushed upwards. The reactive lead fraction in the porous lead-tin yellow particle on the right in sample CIA 1577

RS06 was probably too low to result in sufficient lead soaps for fragmentation of the particle. The co-occurrence of a still intact conglomerate of lead-tin yellow pigment and a fully lead-saponified lead-tin yellow particle with remaining lead stannate on the borders gives a unique but illustrative view into the process that we propose.

5.3.5 'The Bad Chief' by Master of Flémalle (early 15th century)

The panel painting *The Bad Chief* (fragment) attributed to the 15th century Flemish artist the Master of Flémalle (who is probably the same as Robert Campin, 1378-1444) is displayed in the Städelsches Kunstinstitut in Frankfurt, Germany (Inv. nr. 886). The paint cross-section A342/18, yellow paint of the baldachin on the damaged reverse, originates from earlier studies by Prof. van Asperen de Boer. The sampled area showed tiny pits on the surface, a defect that was believed to be associated with proteinaceous globules from an emulsion paint.[33] However, staining tests with amido black provided negative results for protein.

The reverse of the panel painting 'The Bad Chief' (fragment) attributed to the 15th century Flemish artist the Master of Flémalle is displayed in the Städelsches Kunstinstitut in Frankfurt, Germany (Inv. nr. 886). photo: Prof. van Asperen de Boer (see coloured version at the end of this thesis).

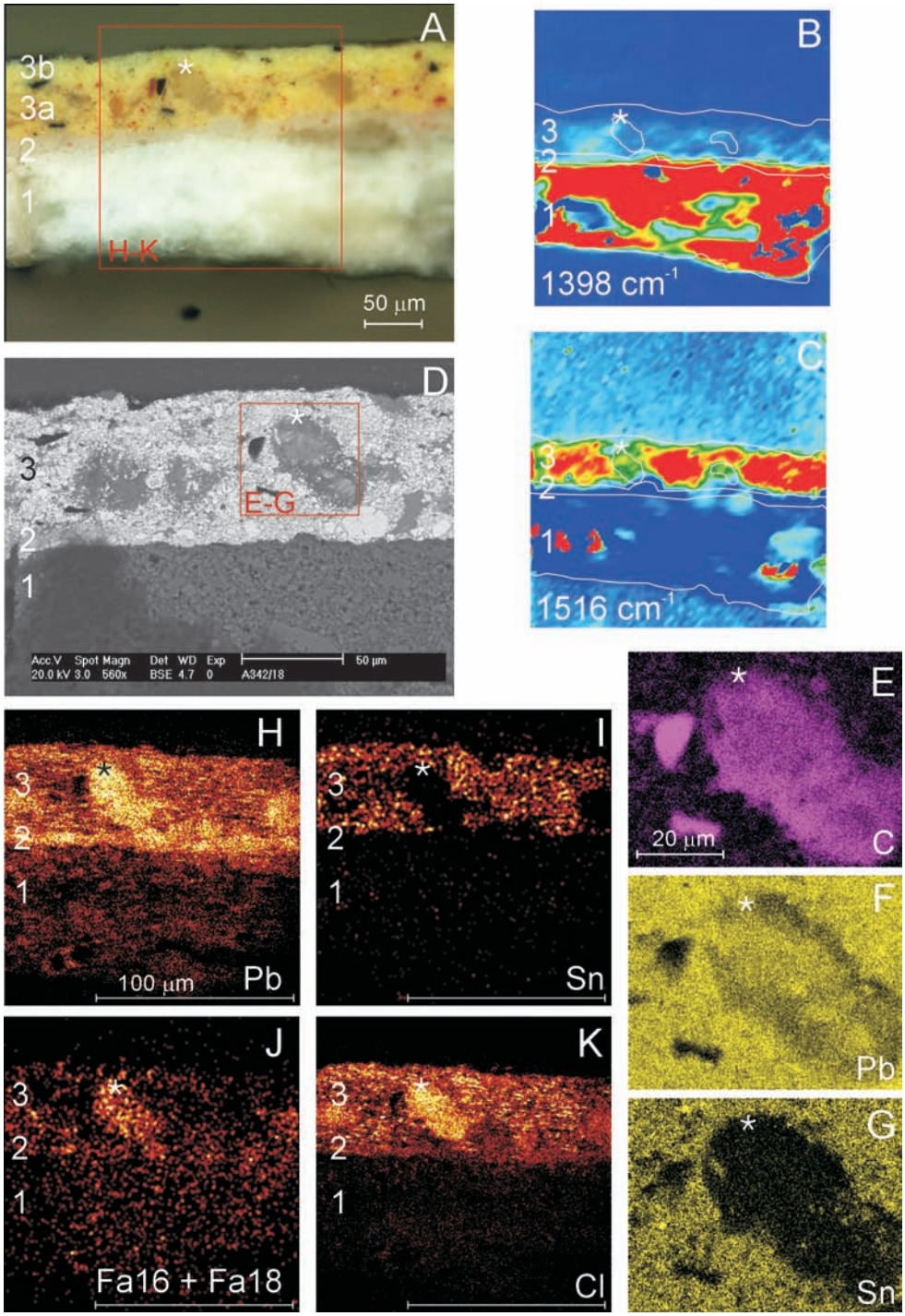

Fig. 5.7 Light microscopic image (A) elucidate paint cross-section A342/18. The asteriks in all images is indicative for the position of a large metal soap aggregate. FTIR images of carbonates at 1398 cm^{-1} (B) and lead carboxylates at 1516 cm^{-1} (C) reveal a saponified lead-tin yellow layer (3). An outline is plotted over the FTIR images; the two round features in layer 3 are indicative for two aggregates. The BSE-image (D) represents the paint cross-section. X-ray maps of carbon (CK) (E), lead (PbM) (F) and tin (SnL) (G) show details of a lead soap aggregate (square in Fig. 5.7B indicates the analysed area). SIMS-images represent lead (+; m/z 208) (H), tin (+; m/z 52) (I), the sum of deprotonated palmitic and stearic acid (-; m/z 255 + m/z 283) (J) and chloride (-; m/z 35) (K) (square in Fig. 5.7A illustrates the analysed area) (see coloured version at the end of this thesis).

5.3.5.1 Paint cross-section A342/18 – Results

Many transparent aggregates are dispersed in a lead-tin yellow paint layer (3a) in paint cross-section A342/18 (Fig. 5.7a). This yellow-orange layer containing also some carbon black and vermilion particles is positioned on a lead white-containing intermediate layer (2) with a calcium carbonate-containing ground (1) underneath. The top part of the lead-tin yellow layer is lighter in tone (3b). Specular reflection FTIR images of the carbonates (1398 cm^{-1}) and metal carboxylates (1516 cm^{-1}) are presented in Fig. 5.7b and c. The contours of the paint layers and aggregates are plotted over the FTIR maps to indicate their position. Lead carboxylates imaged with FTIR at 1516 cm^{-1} are homogenously dispersed in the lead-tin yellow layer. Due to incomplete carbon coating removal after SEM/EDX, lower intensities of lead carboxylates found in areas of the aggregates, but single point spectra taken from these areas still prove the presence of lead carboxylates. The carbonates are present in the ground layer (layer 1) and intermediate layer (layer 2). This implies that the lead white-containing layer 2 has been preserved and is not affected by lead soap formation.

The backscatter image in Fig. 5.7d reveals a homogenous densely packed layer of finely divided lead-tin yellow particles and some aggregates with a low electron backscattering intensity. The aggregates contain almost no pigment particles, but inside the aggregates cloudy areas with higher BSE reflectivity are visible. EDX maps of lead, carbon and tin illustrate a correspondence of lead and carbon inside the aggregate and demonstrate tin positioned around the aggregate (Fig. 5.7e-g). The few tin "hot" spots inside the aggregate are representative of lead-tin yellow particles that are also visible in the backscatter image. The higher BSE reflectivity in the aggregate refers to a higher lead and a lower carbon density. The stronger electron reflecting areas point to mineralisation. In one fully mineralised aggregate, FTIR and EDX (data not shown) point to the presence of lead and carbonates.

The secondary ion images corresponding to lead (+; *m/z* 208), tin (+; *m/z* 120), the sum of deprotonated palmitic and stearic acid (-; *m/z* 255 + *m/z* 283) and chloride (-; *m/z* 35) are presented in Fig. 5.7h-k. Lead is present in all the layers, however lead in the aggregates and in layer 2 have higher ion counts pointing to higher relative amounts. Tin is only present in layer 3 and is absent in the aggregates. The fatty acids are predominant in the aggregate and found in lower intensities in the other parts of layer 3 and in the layers 1 and 2. Chloride follows the lead map, but its intensity is low in layer 2.

5.3.5.2 Paint cross-section A342/18 – Discussion

In general, the lead soap aggregates are in the paint sample A342/18 much more dispersed and smaller in size compared to the lead soap aggregates found sample CIA

1577 RS06 of the Sherborne Triptych. The pigment particles in A342/18 are much more finely divided, which results in a higher availability of the reactive lead component in the lead-tin yellow pigment for free fatty acids. This can be concluded from the presence of lead soaps in the whole lead-tin yellow layer paint as visualised with imaging FTIR. The availability of fatty acids for reaction with lead into lead soaps must have been restricted to the lead-tin yellow layer itself, as the lead white-containing layer positioned lower is still unaffected.

5.3.6 'Impasse des deux frères and Moulin de Poivre' by Vincent van Gogh (1887)

Disfiguring drying cracks with soft underlying paint creeping to the surface and sharp stress cracks in the zinc white-containing film are observed in the *Impasse des deux frères and Moulin de Poivre* (F347) (canvas, wax lined) by Vincent van Gogh (March - mid April 1887). The phenomenon is associated with the underlying paint layer, which is affected by zinc soap formation. The same types of defects are also observed in other paintings by van Gogh that are painted in exactly the same period (*Montmartre; Mills and Vegetable Gardens* (F346) and *View from Theo's Apartment in the Rue Lepic* (F341)). These three paintings are in fact painted scenes painted on top of a first composition but separated by an artisit applied second ground that in each case consists of lead white, zinc white and ultramarine. The paint cross-section F347-1 originates from the sand path depicted at the right edge. The painting is in the collection of the Van Gogh Museum (Vincent van Gogh Foundation) in Amsterdam.

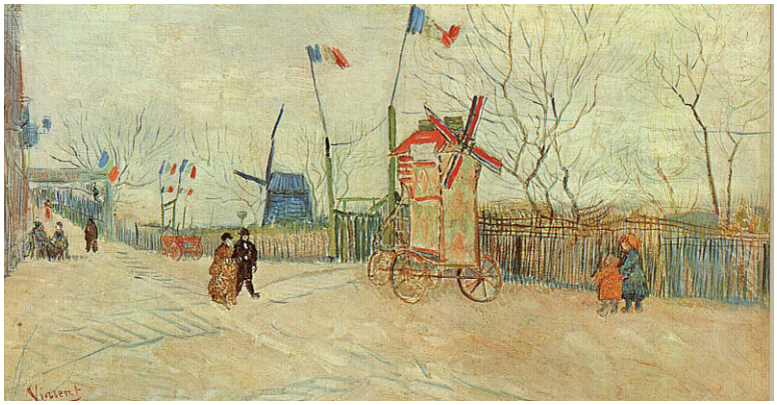

Impasse des deux frères and Moulin de Poivre (F347) (canvas, wax lined) by Vincent van Gogh (March - mid April 1887) The painting is in the collection of the Van Gogh Museum (Vincent van Gogh Foundation) in Amsterdam, The Netherlands (see coloured version at the end of this thesis).

5.3.6.1 Paint cross-section F347-1 - Results

The paint build-up illustrated in Fig. 5.8a consists of 5 layers. The first layer (1) is a red paint layer with red ochre, bone black and red lake, followed by a thick pink-coloured layer (2), which both belong to the first composition. This second layer contains a mixture of chrome orange pigments, red lake, zinc white, lead white, ultramarine, barite, gypsum, organic black and Schweinfurt green particles. Various tiny circular transparent areas varying between 5 and 10 μm are found in this layer. These circular areas are fluorescent under UV illumination (Fig. 5.8b). A large strongly blue-fluorescent transparent area is present on the left side. Layer 3 is a thin orange-yellow layer with vermilion and Schweinfurt green particles situated below the ground layer of the second composition (4). The second ground (4) is a white layer containing zinc oxide and lead white and some blue artificial ultramarine. The tiny bright fluorescent spots in layer 2 and in the upper layer 4 are indicative for zinc oxide. A very thin varnish layer (5) is visible on top.

Zinc oxide is transparent in the mid-infrared region. The FTIR spectrum from a spot in layer 2 proves the existence of metal soaps (see asymmetric stretch vibration of zinc carboxylate at 1535 cm^{-1}) (Fig. 5.8c). The peak at 1395 cm^{-1} is indicative of carbonate and predominates over the symmetric stretch vibration of zinc carboxylate band at 1403 cm^{-1} (Fig. 5.8c). FTIR spectrum derived from layer 4 shows an equal intensity of the peaks at 1535 and 1403 cm^{-1} in contrast to the spectrum derived from layer 2 (Fig. 5.8c). This points to a lower intensity of carbonates and higher intensity of zinc soaps in layer 4. The FTIR map at 1535 cm^{-1} reveals a dispersed existence of metal soaps in layer 2 (the contours of layer 4 and 2 are plotted over the images) (Fig. 5.8d). The zinc soap mass on the left in the FTIR image corresponds to the blue-fluorescent area in the UV light image of layer 2. Layer 4 is also affected by zinc soap formation. Carbonates at 1395 cm^{-1} are homogenously distributed in layer 2 (with the exception of the transparent particle) and are absent on the left side of the sample and in layer 4 (Fig. 5.8e).

Numerous dark circular areas in the finely pigmented matrix of layer 2 are observed in the backscatter image. These features are approximately 10 μm in size, but are towards the bottom of layer 2 more abundant with smaller sizes (Fig. 5.8f). The majority of the dark areas correspond with the transparent areas in the light microscopic images. The residual tiny dark circular areas correlate with the red and black coloured particles. A bright spot (> 1 μm) is found in the middle of some low BSE spots, which is mainly observed in the larger areas in the upper part of layer 2. The main elements in layer 2 determined by EDX analysis are carbon, oxygen, lead and zinc. The distribution of carbon, oxygen, lead and zinc and the corresponding backscatter image are displayed in Fig. 5.8h-k. Zinc and carbon are present in the low

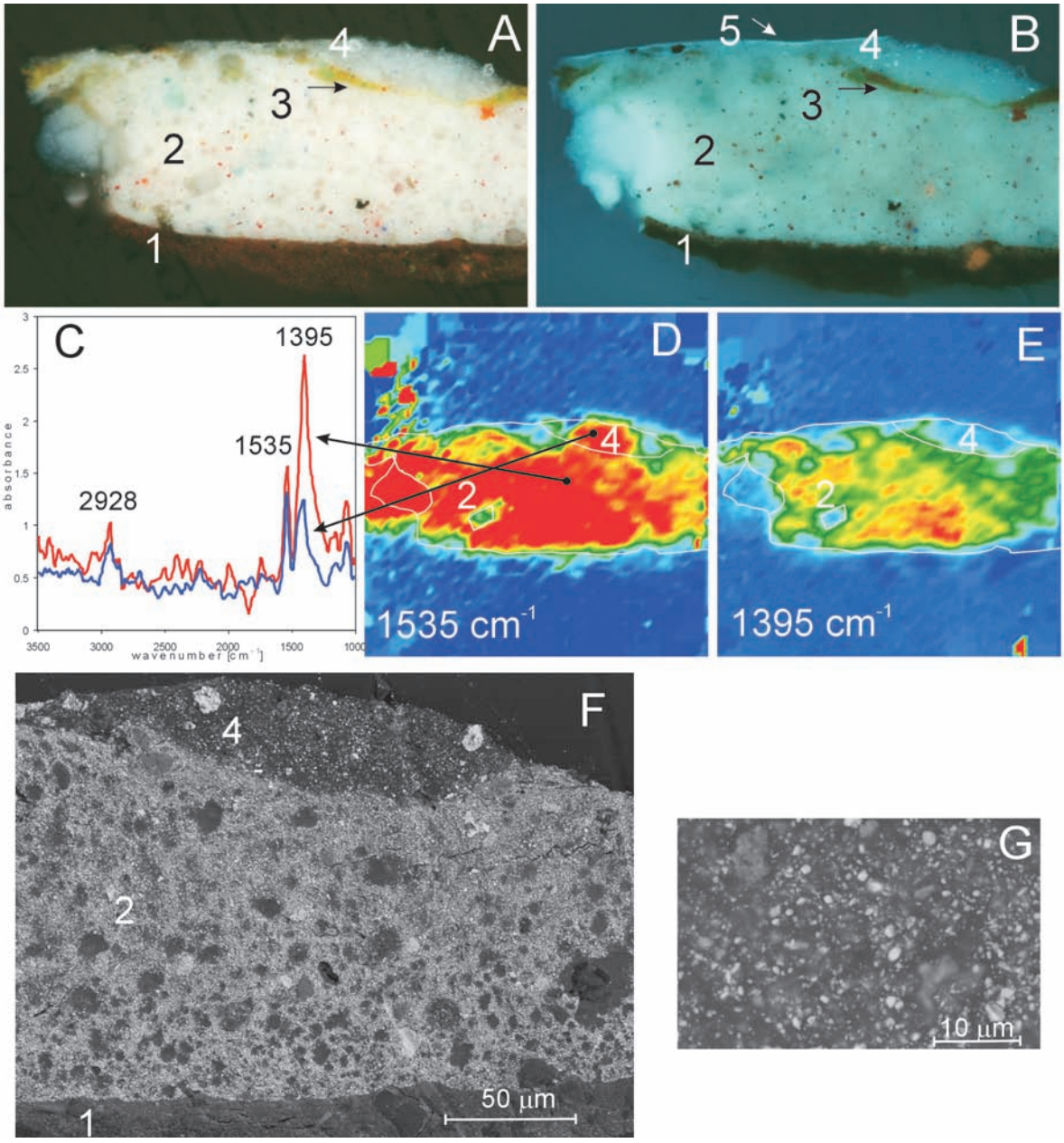

Fig. 5.8A-G Paint cross-section F347-1 originating from 'Impasse des deux frères and Moulin de Poivre' by Vincent van Gogh (1887) is depictured in the light microscopic images in white light (A) and UV (B). Two reflection FTIR spectra derived from a single point in layer 2 and layer 4 (C). FTIR images of metal carboxylates at 1535 cm^{-1} (D) and carbonates at 1395 cm^{-1} (E) reveal a saponified layer 2 and 4. BSE-image (F), (detail of layer 4 (G)) reveal the middle part of the paint cross-section (see coloured version at the end of this thesis).

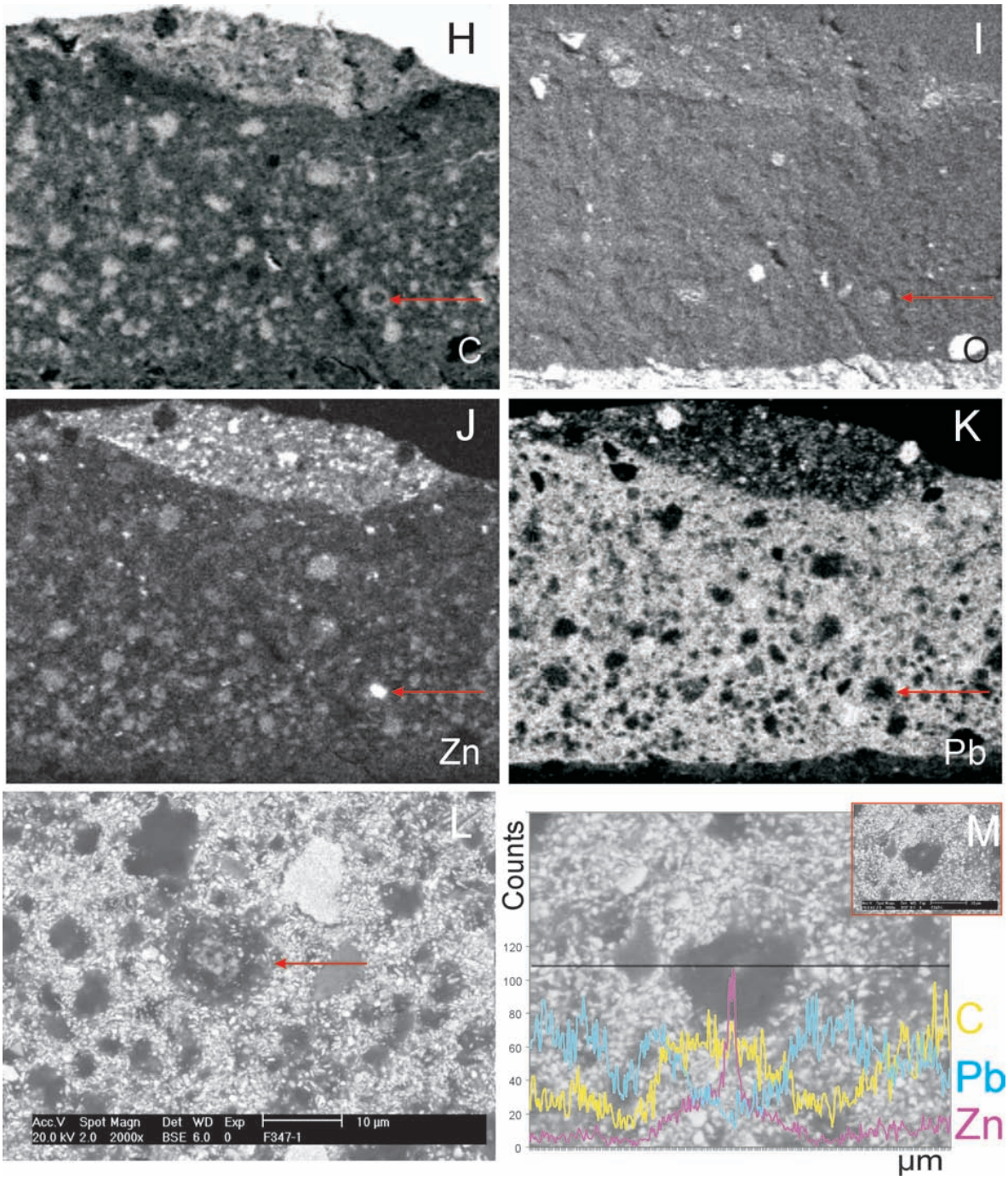

Fig. 5.8H-M BSE-image (F), (detail of layer 4 (G)) and corresponding X-ray maps of carbon (CK) (H), oxygen (OK) (I), zinc (ZnK) (J) and lead (PbM) (K) reveal the middle part of the paint cross-section. The BSE-image of a detail (indicated with an arrow in the X-ray maps) is depictured in Fig. 5.8L. Line scans (M) drawn over a zinc soap aggregate with a bright spot illustrate the distribution of carbon (yellow), zinc (purple) and lead (cyan) (see coloured version at the end of this thesis).

BSE spots and lead is detected outside these areas in the fine-pigmented matrix. The arrow in the EDX maps and in the backscatter image of the magnified area indicates a dark area with various bright spots inside (Fig. 5.8l). The rim of the area is carbon rich, while the centre is rich in zinc and oxygen. The lead is distributed around this area. The very small "hot" spots in the zinc map, *e.g.* in the upper part of layer 2 and layer 4, do not correlate directly with carbon "hot" spots and are considered indicative for zinc oxide (Fig. 5.8h and j). A line scan drawn over a low BSE circular area with high BSE core demonstrates the distribution of carbon, zinc and lead (Fig. 5.8m). The carbon counts increase in the circular area and towards the right indicative for organic rich regions. The finely pigmented matrix contains lead. The lead counts decrease inside the low BSE dark area and in the particle to the left of this area. Almost no counts are detected for zinc in the matrix, while the zinc counts increase in the circular area and zinc is most abundant in the central spot. The oxygen counts are also increased in the central spot (data not shown). The backscatter image shows a lower pigment concentration in layer 4 compared to layer 2 (Fig. 5.8f and g). The bright pigment particles in layer 4 in the backscatter image contain lead. Several dark areas (about 10 μm in size) are observed in the relatively organic-rich layer 4 (Fig. 5.8g). In the centre of these areas, cloudy areas with higher BSE reflectivity are visible. EDX analysis shows the presence of zinc, oxygen and carbon in these clouds (data not shown).

5.3.6.2 Paint cross-section F347-1 - Discussion

The dark circular low BSE areas observed in layer 2 and 4 in the backscatter image are interpreted as zinc soap aggregates. FTIR data supports this conclusion. Although the aggregates are too small in size to identify them with imaging FTIR (spatial resolution limit about 7 μm), the position of the asymmetric metal carboxylate vibration peak is very informative. The position of this absorption peak is dependent on the type of metal attached. Zinc carboxylate is positioned at 1540 cm^{-1} and lead carboxylates at 1513 cm^{-1}.[34] The peak at 1535 cm^{-1} in the spectrum of layer 2 and 4 is indicative for zinc carboxylates.

The mineralisation involving zinc inside the zinc soap aggregates is only observed in the larger aggregates, which means that the mineralised parts are formed after zinc soap aggregation. The zinc soap aggregates in layer 4 are in a more advanced state of development as the mineralised centres have "grown".

The zinc compound inside the large aggregates is believed to be zinc carbonate (and not zinc oxide as was proposed earlier), as a slight increase of carbon and oxygen is observed in the core. This hypothesis was further tested using paint cross-section KM224/2a from the *Les Alyscamps* by Vincent van Gogh (F486) investigated earlier by van der Weerd *et al*.[14] The paint cross-section contains two larger zinc soap aggre-

gates of which the one on the right side is partly mineralised (Fig 5.9a, b). EDX analysis reveals a higher intensity of zinc and oxygen in this mineralised area. A single point FTIR spectrum taken from the zinc soap aggregate on the left side shows carboxylate peaks at 1531, 1458 and 1403 cm^{-1} (representative for asymmetric metal carboxylate vibration, C-H bending vibration and symmetric metal carboxylate vibration, respectively) (Fig. 5.9c), while a FTIR spectrum taken from the mineralised aggregate reveals an extra peak in the carbonate region at 1368 cm^{-1} (Fig. 5.9c). Imaging of this peak reveals high intensities only in the mineralised aggregate (Fig. 5.9d). FTIR spectrum of the peaks at 1531 and 1403 cm^{-1} show that zinc soap are present in both aggregates (Fig. 5.9e, f). The FTIR data on the mineralised aggregate and the fact that zinc carbonate or basic zinc carbonate can precipitate from purified zinc salt solutions on contact with the atmosphere made us conclude that zinc carbonate is precipitating in zinc soap masses.[35] Atmospheric CO_2 is a potential carbonate source.

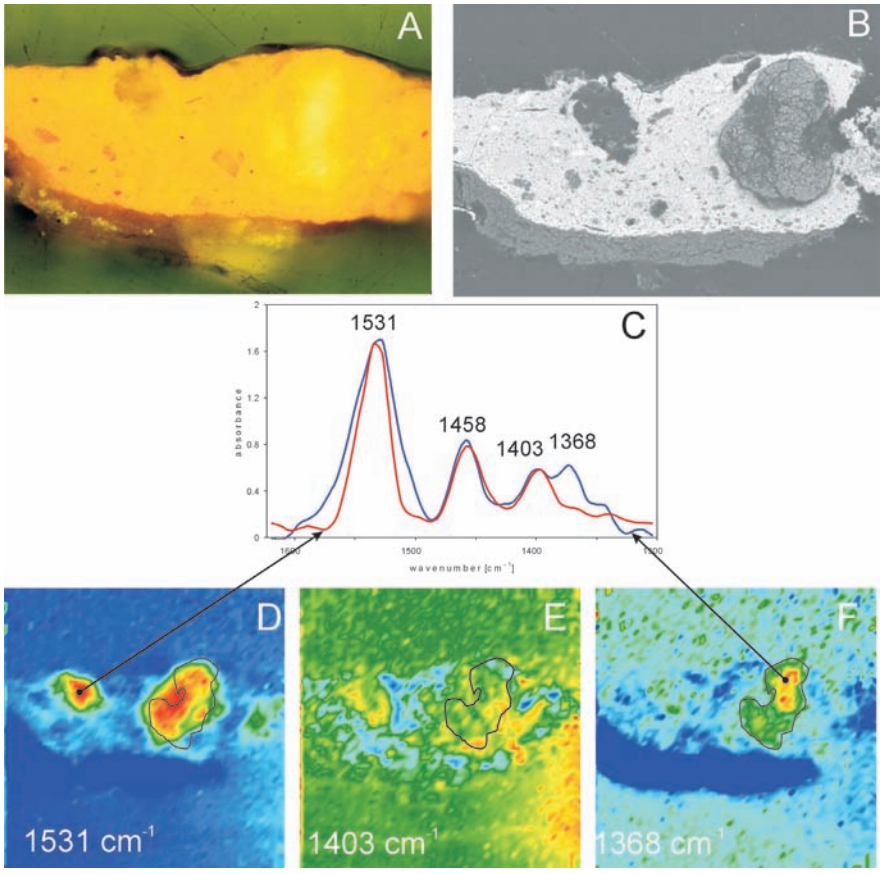

Fig. 5.9 White light microscopic image (A) and BSE-image (B) of paint cross-section KM224/2a from the 'Les Alyscamp' by Vincent van Gogh (F486) reveal two large zinc soap aggregates. A detail of the FTIR spectrum (C) derived from a spot on the left aggregate (red line) shows peaks at 1531, 1458 and 1403 cm^{-1}, FTIR spectrum derived from a spot on the right aggregate (blue line) shows peaks at 1531, 1458, 1403 and 1368 cm^{-1}. FTIR images of peaks at 1531, 1403 and 1368 cm^{-1} are depictured in Fig. 5.9D, E and F, respectively. The outline plotted on the FTIR image indicates the position of the mineralised matter (see coloured version at the end of this thesis).

The original source of the zinc in paint cross-section F347-1 is zinc oxide. A mixture of lead white and zinc oxide was used in the paints of layer 2 and 4. In layer 4, a few residual zinc oxide particles are still visible under UV illumination in the microscopic image. The lead white pigments are unaffected by metal soap formation, whereas the more reactive zinc oxide has reacted away. As the zinc soap aggregates are very abundant and finely dispersed in the layers, a local transition of zinc oxide into zinc soaps occurs and migration of zinc soaps is not expected to have taken place.

5.3.7 'Woolshed, New South Wales' by R. Godfrey Rivers (1890)

The painting *Woolshed, New South Wales* by the Australian artist R. Godfrey Rivers (1890, canvas) is affected by metal soap formation. Small transparent spots are distributed in some passages of the paint. A fine mechanical cracking is widespread, but also localised drying cracks are observed. The *Woolshed, New South Wales* is in the collection of the Queensland Art Gallery in Australia and was acquired by the Gallery within a few years after it was painted. The available paint cross-section originates from the iron roofing of the shearing shed.

'Woolshed, New South Wales' by the Australian artist R. Godfrey Rivers (1890, canvas) is in the collection of the Queensland Art Gallery, Brisbane, Australia.

5.3.7.1 Paint cross-section RWS5 - Results

The paint cross-section RWS5 reveals a build up of 5 layers: a white ground (1) (Note: SEM/EDX reveals a double ground), a light brown paint layer (2), a blue-grey layer (3), a purple-grey layer (with red and blue pigmentation) and finally a varnish layer in which three separate varnish layers can be distinguished (5) (Fig. 5.10a). Layer

3 and 4 are affected by metal soaps that appear as many small aggregates (around 10 μm) with a greenish core and a transparent halo, which are highly fluorescent under UV illumination (Fig. 5.10b). The small aggregates are finely distributed over the paint layers. FTIR detects metal soaps at 1542 cm^{-1} in the paint layers 3 and 4 and carbonates in layer 1 (Fig. 5.10c). The aggregates are clearly visible in the backscatter image: all aggregates consist of a brighter centre and a dark rim (Fig. 5.10d). Fine pigment particles are positioned around these aggregates. EDX analysis shows only the presence of carbon, oxygen, zinc and magnesium (low) inside the aggregates, while the EDX data of the paint matrix show many more elements like C, O, Zn, Mg, Al, Si, Pb, Cl, Fe and Co. The composition of the paint layer is not discussed further. Zinc is predominant in the core of the aggregate, while carbon is predominant in the rim. A very small amount of magnesium is found in the aggregate.

The paint cross-section was also analysed with static-SIMS. Fig. 5.10e-g show the positive secondary ion images of lead (*m/z* 208) and zinc (*m/z* 65) and the negative ion image of deprotonated palmitic acid (*m/z* 255). Lead is present in all the layers, but areas corresponding to the aggregates in layer 3 and 4, as observed with light microscopy, are free of lead. Zinc is present in these areas (mainly in layer 4) and in lower intensity in the other parts of layer 4. The deprotonated palmitic acid is present in all four paint layers, but the intensities are too low to correlate its distribution to the light microscopic or backscatter image. The P/S ratios of the layers differ pointing to the use of different types of oil: P/S ratio of layer 1 is 1.7, of layer 3 is 2 and of layer 4 is 3.

5.3.7.2 Paint cross-section RWS5 - Discussion

Paint layers 3 and 4 are affected by zinc soap formation. The paints are suspected to be commercially prepared paints. The source of zinc is not entirely clear, because the original zinc source has reacted away. The paint sample contains a mixtures including a white pigment, most likely zinc oxide. Besides zinc oxide, other zinc compounds could have been added to the tube paints in the 19th century to achieve a workable paint with good drying properties.[36] Possible zinc-containing compounds are lithopone, a mixture of barium sulphate and zinc sulphide, the white vitriol *i.e.* zinc sulphate and zinc stearate. Lithopone cannot be the zinc source in this sample as barium is not detected with EDX. No sulphur is detected in the EDX spectra of layer 3 and 4 either, so it is therefore not very likely that white vitriol was used. However, the sulphur could have been released as SO_2 and therefore no more detectable in the paint. Zinc stearate could have been added to the paint, but the P/S ratio detected in the layer 3 and 4 points to a normal P/S ratio and does not give any indications for a larger amount of stearic acid. On the other hand zinc stearate, in the 19th century is not a pure compound,

but more likely a mixture of stearic and palmitic acid.[37] So zinc soaps as an addition to the paint cannot be excluded.

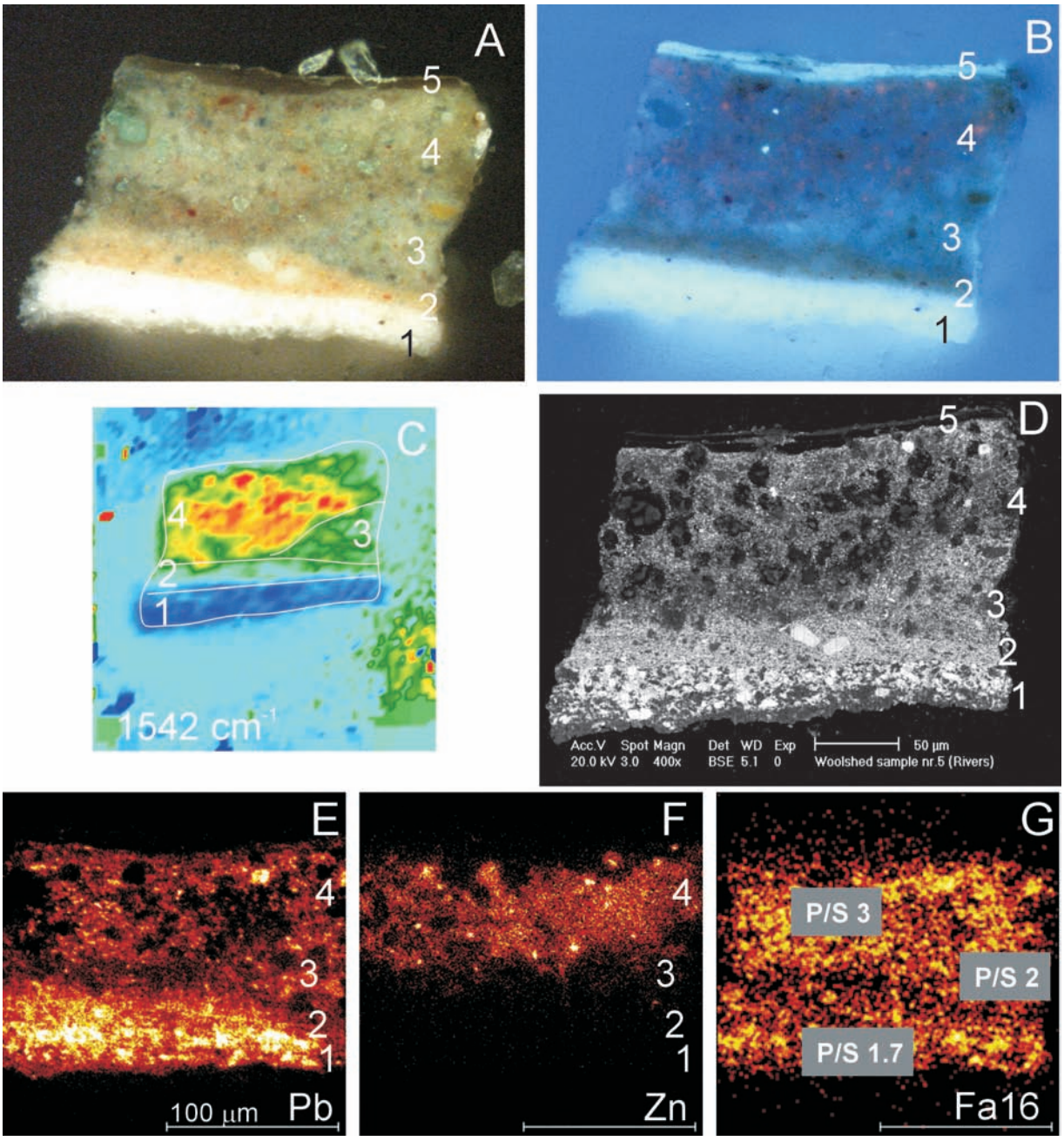

Fig. 5.10 Paint cross-section RWS5 originating from the painting 'Woolshed, New South Wales' by the Australian artist R. Godfrey Rivers (1890) is shown in the light microscopic images in white light (A) and UV (B). The FTIR image at 1542 cm^{-1} elucidates the presence of zinc carboxylates in the layers 3 and 4. BSE-image (D) visualises the aggregates that consist of a brighter centre and a dark rim. SIMS-images represent lead (+; m/z 208) (E), zinc (+; m/z 65) (F), deprotonated palmitic acid (-; m/z 255) (G). The three P /S ratios representative for layer 1 (P/S 1.7), 3 (P/S 2) and 4 (P/S 3) are shown in the ion image of deprotonated palmitic acid (see coloured version at the end of this thesis).

5.3.8 'Sydney Harbour, overlooking Taylor's Bay' by W. Lister Lister (c. 1912)

Sydney Harbour, overlooking Taylor's Bay by the Australian artist W. Lister Lister (canvas) is on display in the Queensland Art Gallery, Brisbane, Australia. The paint is thickly applied to obtain a textured surface. The painting has an overall crack pattern, but no obvious defects are seen with the naked eye on the surface of the painting. Surface investigation under high magnification has not been done. The precise position of the paint samples is uncertain.

'Sydney Harbour, overlooking Taylor's Bay' by the Australian artist W. Lister Lister (canvas, 1912) is on display in the Queensland Art Gallery, Brisbane, Australia (see coloured version at the end of this thesis).

5.3.8.1 Paint cross-section LLSH1 and LLSH2 - Results

The paint cross-section LLSH1 shows an extensive layer build-up of eight layers: a transparent white layer (1), a second white layer (2), a flesh coloured layer (3), a yellow layer (4), a green-brown layer (5), two purple-brown layer (6, 7) and varnish (8) (Fig. 5.11a). Layer 4 is affected by zinc soap formation, which was established by FTIR-imaging (data not shown). An extremely large amount of transparent aggregates is observed in layer 5 (Fig. 5.11a). Fig. 5.11b shows the backscatter image from an area of the saponified layer 5, which reveals lots of circular aggregates with a lighter grey material inside. In several cases the lighter centre emerges from the paint matrix and lays like toothpaste strings on top of the paint cross-section (arrow in Fig. 5.11b). The extrusion of the zinc soaps must have occurred during exposure of the cross-section to the electron beam under high vacuum conditions. In a few cases, a very bright small

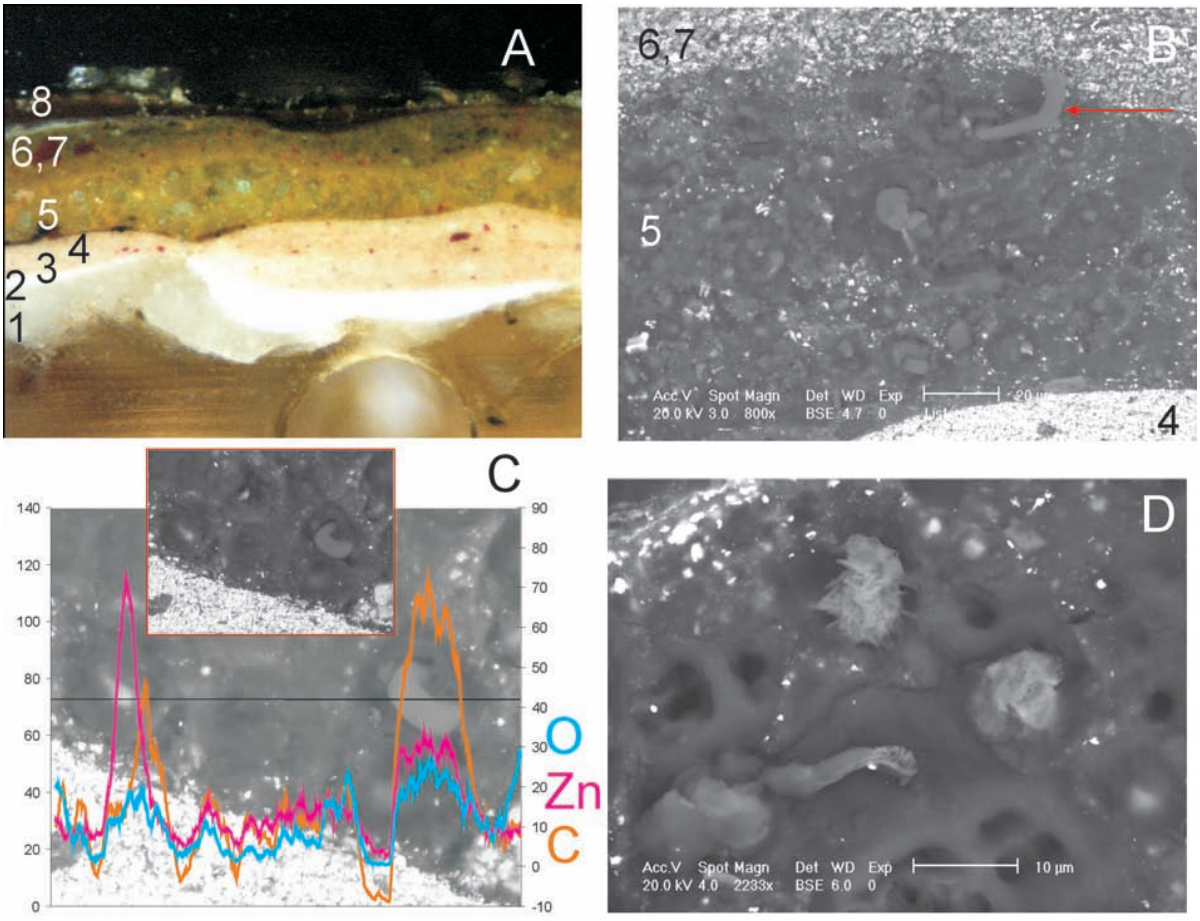

Fig. 5.11 The paint cross-section LLSH1 presented in the white light microscopic image (A) is taken from 'Sydney Harbour, overlooking Taylor's Bay' by the Australian artist W. Lister Lister (1912). BSE-image (B) visualises a detail of the zinc soap-containing layer 5; the arrow indicates a string of zinc soap emerges from the paint matrix. A line scan (C) elucidating the intensities of carbon (orange), oxygen (blue) and zinc (pink) was drawn over two aggregates, one with a bright spot in the centre (positioned left) and one where the central soap mass is emerging from of the paint matrix (positioned on the right). The BSE-image of LLSH2 in Fig. 5.11D illustrates zinc-containing nanocrystals in aggregates (see coloured version at the end of this thesis).

spot is found inside the aggregate. A line scan elucidating the intensities of carbon, oxygen and zinc was drawn over two aggregates, one with a bright spot in the centre (positioned left, Fig. 5.11c) and one where the central soap mass is emerging from of the paint matrix (positioned on the right). The aggregate on the left side shows predominantly zinc, while carbon is predominant and zinc is decreased in the rim (mainly on the right side). Oxygen follows in general the carbon line, though in the core of this aggregate, oxygen is increased again. Carbon predominates over zinc in the protruding mass that originates in the aggregate on the right side.

A zinc soap affected paint layer in paint cross-section LLSH2 derived from another position of the same painting has similar characteristics as the sample discussed above. Here, nanocrystal structures containing zinc are observed in several aggregates, which suggests mineralisation processes inside the aggregate (Fig. 5.11d).

5.3.8.2 Paint cross-section LLSH1 and LLSH2 - Discussion

The zinc soap aggregates in LLSH1 and LLSH2 have the same general appearance in the backscatter image as sample RWS5. The line scan shows the presence of two types of zinc compounds inside the aggregates. The aggregate with carbon, zinc and oxygen-containing material that extrudes from the paint matrix is believed to consist of zinc soaps, while another aggregate with a zinc, oxygen and carbon-containing centre is thought to be a combination of zinc soap and zinc carbonate. The phenomenon in the latter aggregate is comparable to the observations in sample F347-1, in which the precipitation of zinc carbonate in the zinc soap mass is proposed to take place. The sample LLSH2 illustrates the formation of zinc carbonate crystals. The zinc soaps are extremely soft and they easily extrude from the paint in the polished cross-section.

5.4 General discussion

5.4.1 Overall picture

The paint cross-sections presented in this chapter show different aspects of metal soap formation in multi-layered paint systems. Every example presented in this chapter shows specific characteristics of metal soap aggregates dependent on the paint composition. This implies that many aspects determine or influence the formation of metal soap aggregates. Therefore, one general mechanism describing the formation of metal soap aggregates cannot be proposed. On the other hand, relevant compounds and various processes that have played or play a role in metal soap formation can be deduced from the current material condition of the paint. The main differences between the case studies are the various reactive materials, the size and the distribution of the metal soap aggregates, the mineralised products and the role of other layers in the system.

The original metal source and its mineral form is diverse for the presented samples, *e.g.* lead white for MH146 and HSTB43/3, lead acetate for PCC01, lead-tin yellow for CIA 1577 RS6 and A342/18, zinc white for F347-1 and unidentified zinc source for RWS5 and LLSH1 and LLSH2. The lead white in MH146 and the zinc white in F347-1 have reacted away resulting in saponified regions in the case of the lead white and small zinc soap aggregates in the zinc white-containing sample. The lead white mineral matter in the layers affected by lead or zinc soaps remains present in the samples HSTB43/3, PCC01 and F347-1. In case of HSTB43/3 questions to be addressed are what the minimum amount of lead soap is needed to form an aggregate and what the role of chlorine is in relation to relatively intact lead white minerals. In PCC01 another lead source, lead acetate, is postulated to be present. The fatty acids are thought to preferentially react with the more reactive lead acetate to form lead soaps. In F347-1 the zinc white reacts away with the fatty acids and the lead white particles remain, as zinc oxide is more reactive than lead white.

In principal, the lead-tin yellow is unaffected by a reaction with fatty acids and another reactive lead compound - present as a residual product from its manufacture - inside the lead-tin yellow pigment is suggested to react with the fatty acids. The role and source of the fatty acids will be discussed in more detail in the section *Theoretical Concepts*.

The appearance of metal soap aggregates varies. Zinc soap aggregates derived from zinc white are approximately 10 μm in size whereas lead soap aggregates can become 100-200 μm in size. A direct correlation between the form of the aggregate and the type of pigment (and/or composition of the paint layer) is difficult to make and

more paint cross-sections will have to be studied. In general, the finer and more dispersed the pigment is in the paint layer, the more dispersed the metal soaps. In such paints, we have observed smaller aggregates that are more widely distributed over the layer.

Inside the aggregates lead or zinc carbonate can precipitate. The lead carbonate is detected in A342/18 and there is evidence for zinc carbonate in aggregates in F347-1, RWS5, LLSH1 and 2. Besides lead carbonate, minium is observed in the lead soap aggregates of MH146/B38 and HSTB 43/3.

The lead soap formation is not always restricted to a single layer. The samples MH146/B37 and /B39 are showing us that bordering layers are partially affected by lead soap formation, albeit only the contact side. In HSTB 43/3 the first lead white-containing ground layer (1) and in A342/18 the thin lead white-containing layer (2) are unaffected by lead soap formation. The composition of the paint and paint build-up determines whether lead soap formation takes place and whether it is limited to a single layer or not.

5.4.1.1 Questions addressed

The different phenomena in the various case studies are used to gain better insight into the question why certain paint systems become unstable and lead to metal soap formation and aggregation. Most defects associated with metal soap aggregates are noticed after the paint has aged, which implies that these are forming in a mature paint system and to a less much degree during the drying process of the oil. For preventive conservation and prudent restoration treatment of paintings, it is important to understand why some paints develop metal soap aggregates while others do not. A further question is what the role is of reactive compounds and what the circumstances are that can lead to metal soap aggregation. These questions will be addressed in the next sections.

5.4.2 Theoretical concepts

5.4.2.1 Model of stable oil paint system

A mature oil paint can be described as an ionomeric network of metal carboxylates of mono- and dicarboxylic acids.[38] The polyunsaturated moieties in the triglycerides of the fresh oil are activated to radicals that react with oxygen to form a cross-linked network. As the three dimensional network ages hydrolysis of the ester bonds occurs leading to free fatty acids groups, dicarboxylic fatty acids (diacids) and acid-rich network oligomers. These acid groups are immobilised and stabilised by coordination to metals (such as lead), originating from pigment or drier, to form metal carboxylate bonds. This oil paint model is the basis for further discussion to address

the following topics: composition of metal soap aggregates, stable versus unstable network, interaction between fatty acids and lead or zinc pigments/driers, different reaction processes of lead soaps, composition of divalent metal soaps and mineralisation inside aggregates.

5.4.2.2 Composition of metal soap aggregates

The detectable components in the metal soap aggregates, besides mineralised products, are monocarboxylic fatty acid metal soaps. This is deduced from the FTIR spectra and SIMS data. Single point FTIR spectra from aggregates demonstrate only peaks for metal soaps, while peaks for free fatty acids are absent. The very sharp C-H vibration bands of these metal soaps, especially compared to the broad C-H vibration bands of the mature oil network, indicate non-oxidised saturated hydrocarbon chains.[39] SIMS detects deprotonated palmitic and stearic acids, and their corresponding soaps inside soap aggregates. The deprotonated fatty acid negative ions derive from a free, metal- or ester-bound fatty acids. With the help of the FTIR spectra, free and ester-bound fatty acids inside aggregates can be excluded.

In the aggregate of sample PCC01 monocarboxylate fatty acids are detected in the core of the aggregate, while dicarboxylate acids are detected in the rim. DTMS analyses of the efflorescence and a manually separated aggregate from the preprimed canvas used by Church reveal free and lead bound monocarboxylate fatty acids (palmitic and stearic acid), and a small amount of free dicarboxylate fatty acids.[16] The GC/MS analyses performed by the scientific department of the National Gallery London on manually separated metal soap aggregates have revealed the presence of palmitic and stearic acid and generally very little azelaic acid.[4] Transmission FTIR diamond cell analysis done by the NG-group shows the absence of diacids in an isolated lead soap aggregate from a lead-tin yellow paint.[4]

Fatty diacids in contrast to monocarboxylic acids are present in significant amounts in mature oil paints. Approximately 7% of the fatty acid moieties in fresh linseed oil is monocarboxylic acids, while the diacid oxidation products are derived from the 93% of unsaturated fatty acid moieties. It seems that diacids are not significant in metal soap aggregates as small quantities of diacids in free form (and not metal bound) are detected in the aggregates. Specular reflection FTIR spectra are not able to distinguish mono- and diacids. SIMS on a gold-coated sample was able to detect diacids, but this method was not applied to all samples presented here. Free diacids are detected with electron impact DTMS analysis, but the spectrum of lead bound diacid is currently unknown. Preliminary results on the analysis of reference materials by on-column GC/MS (BF_3 derivatised) show that lead bound diacids have approximately 80% lower response than monoacids and therefore diacids in paint samples can be

underestimated.[40] The presence of monocarboxylic fatty acids in aggregates is proven, while dicarboxylic fatty acids are difficult to detect and therefore it is difficult to confirm their absence. In general, the monocarboxylic fatty acid lead soaps appear to be the major components in the aggregates and therefore will be the focus of our further discussion.

5.4.2.3 Stable versus unstable oil network

The composition of metal soap aggregates (and efflorescence) implies that monocarboxylic fatty acids are separated from the mature oil network. Theoretically separation would be possible by degrouping of the stable anionic network under some hypothetical environmental conditions. The existing metal-bound mono- and diacids would be released resulting in a destabilised network. By a later regrouping into a metal coordinated network it might not be energetically favourable to incorporate the monoacids in the newly formed network, while the diacids are bifunctional, more polar and are thought to form a new anionic network more easily. What the condition should be to induce an destabilised network is not known, but this type of mechanism, *i.e.* grouping and regrouping, is expected to take place in all mature oil paint systems. As metal soap aggregates are generally not present in all paint systems, it is difficult to understand via this model alone how aggregates of monoacid metal soaps are formed. The relative concentrations of the reactive components could play a very important role. In a medium poor layer (*i.e.* excess of metal and lack of fatty acids) the paint remains unaffected, while with an excess of reactive monocarboxylic acids, *i.e.* medium-rich, a metal soap aggregate-forming paint system develops, *e.g.* layer 3 in MH146/B37 and MH146/B39. In the latter situation, the monoacids cannot directly be incorporated into the stable network when an excess of free monocarboxylic fatty acids is introduced into the existing anionic mature network. In the case that free diacids are introduced in the anionic network, the diacids are thought to be incorporated easier into the mature network because diacids are chain building elements with two reactive acid groups while monoacids only have one and are end capping.

Possible sources of monoacids can be external or internal. An external source is seen in the samples MH146/B37 and MH146/B39, where the fatty acids migrate from underlying layers into upper lead white layer. In the case of an internal source, the free monocarboxylic fatty acids must be derived from hydrolysis of remaining ester-bound saturated fatty acids. Hydrolysis of the ester bonds is a normal process in an aged oil paint, but the degree of hydrolysis is not the same for every paint layer. Further progression of the hydrolysis of a paint film makes more free fatty acids available. Higher temperatures and humidity promote hydrolysis in the paint film, but the role of the

metal is probably also important. It is known that pigments like lead oxide, lead white and zinc oxide promote the de-esterification of the paint, which can explain why metal soap inclusions are seen in these type of layers.[41, 42] Ester-bound diacids are also released by de-esterification, but they are much better incorporated in the network as they are bifunctional and can be seen as bipolar building elements. This may be the reason why they are detected in low amounts in aggregates.

5.4.2.4 Interaction between fatty acids and reactive lead- or zinc-containing pigments/driers

Free fatty acids from external or internal sources that diffuse into the mature, fully metal-coordinated oil network cannot be directly incorporated in the mature oil network. We propose that free monocarboxylic fatty acids will interact with the surface of lead- or zinc-containing particles in the paint to form a lead or zinc soap. The fatty acid can be released from the surface as a metal soap or remain attached to the crystal surface. The release of metal soaps from the mineral surface should be in equilibrium with the supply of free fatty acids. When more free fatty acids are supplied, more metal soaps are being released and a saponified region around the metal-containing pigment particle develops (as is seen for the MH146 samples). An apolar shield of long chain monocarboxylic fatty acids that surrounds a pigment particle might facilitate the attraction of more long chain free fatty acids from the more polar ionomeric network. The end result is that lead- or zinc-containing pigment particles have reacted away and are replaced by lead or zinc soaps, as is observed in MH146, CIA 1577 RS6 and F347-1. The mechanism is slightly different when metal soaps migrate. In that case we propose that there is no further interaction with the mineral matter. Under these conditions metal soaps will eventually aggregate as is thought to be happening in samples HSTB 43/3 and PCC01. These proposed mechanisms will be discussed based on the case studies in the next section.

5.4.2.5 Different reaction processes of lead soap formation

The MH146 samples discussed illustrate many saponified regions, which are particle free or contain a small number of tiny lead white particles. The saponified regions as transparent areas in the paint layer or around larger lead white particles. The small particles are reacting away while the large ones are still present. Eventually all lead white particles will react away resulting in particle free saponified regions, which can grow further, swell and finally protrude through the paint surface. Homogeneous saponification of a layer is observed when the lead white in the layer is fine and evenly distributed (layer 3 of MH146/B37 and /B39). The aggregate in sample MH146/B37 illustrates a conversion of the lead white particles in layer 2 and 3 into lead soaps

without expansion. In the rim of the aggregate small lead white particles are still visible, which indicates that they are not completely converted yet.

The total conversion of the smaller lead white particles and the saponified 'halo' around larger particles leads to the conclusion that the fatty acids migrate to the surface of the lead white particle to react with the lead white under formation of lead soaps. The lead white particles finally disappear, which implies that free fatty acids must have been transported towards surface of the lead white and the lead bound fatty acids formed must be transported away from the now degraded surface. This results in a saponified hydrophobic regions around the dissolving particles. These fatty acid-rich hydrophobic regions are a potential sink for more free fatty acids that separate out of the less hydrophobic anionic oil network

Diffusion of fatty acids towards a reactive lead compound can also be deduced from the CIA 1557 RS06 sample. The lead-tin yellow particle did fall apart due to the increased volume of the lead soap forming inside while the residual lead-tin yellow particles collect around the aggregate. The lead soaps are formed inside the particle by reaction with a reactive lead component, in the lead-tin yellow particle. This implies that the fatty acids migrated towards the lead-tin yellow particle. A similar situation develops as with the lead white pigment discussed above, lead soaps inside the lead-tin yellow particle act as a hydrophobic sink to attract more free fatty acids, until eventually all reactive lead will have reacted away.

Lead soap aggregates are not always correlated with dissolution of the lead white particles in the layers. In sample HSTB 43/3 a large aggregate is present in a relatively intact, densely packed lead white matrix, with a relative low concentration of lead soaps. A similar phenomenon of an aggregate in a relative compact matrix is observed in paint cross-section MH928/2 originating from *Portrait of a Man* by F. van Hals (Mauritshuis, inv. no. 928) described by van der Weerd *et al.*[39] The lead soaps in these layers suggest that lead white is the reactive compound. These layers seem to be relatively medium poor. However, fatty acids must have become available to form lead soaps and are thought to derive from within the layers itself. It might be possible that the amount of lead soaps formed was sufficient to start the aggregation process. What the critical concentration is of lead soaps in a mineral matrix to form aggregates requires further investigation.

The exact role of chlorine and its relevance is currently unknown. Chlorine may play a role in this metal soap formation process, as it is found in high abundance in the aggregates. It is possible that chlorine-containing lead soaps are formed, in which the chloride is the counter ion for the lead fatty acid salt. To obtain a mobile lead soap one fatty acid must bind to the lead instead of two, which implies that a lower amount of fatty acids is needed for aggregation of lead soaps (see also section 5.4.2.6 on the

composition of divalent metal soaps).

In the PCC01 sample the lead white mineral fraction is unaffected so the lead acetate most likely present in the paint medium is supposed to be the reactive metal source. The lead acetate can react with an excess of free fatty acids (or when ester bound).[43] Such lead soaps formed are dispersed as separate entities in the paint system and are not incorporated into the oil network. As lead soap aggregation and efflorescence are observed in/on the primed canvas, migration directly to the surface or aggregation is more likely to occur. Local high concentrations of lead soap in the paint film may act as a nucleation point for an aggregate. If the free and lead bound fatty acids are not trapped to form an aggregate they would be free to migrate to the surface of the painting. The defects present in this preprimed canvas and also in paintings by F.E. Church were already observed by Church himself.[30] This indicates that these phenomena in this case have occurred in a relatively short period of time. We argue that due to the composition of the ground the mono- and diacids are released in an early stage of ageing by *e.g.* de-esterification promoted by lead acetate. This creates an unstable network where even diacids are not able to become incorporated into the network. In the aggregates, metal soaps of mono- and diacids have been detected.

5.4.2.6 Composition of divalent metal soaps

The metals lead and zinc are divalent and their metal soaps exist as $M(FA)_2$ (FA stands for monocarboxylic fatty acid) or as a basic metal soap M(FA)(OH). The basic metal soap is formed when more metal ions are available, and it is assumed to be more mobile than $M(FA)_2$.[44] FTIR or SIMS data however, provide no direct evidence for the presence of M(FA) (OH) in aggregates. We also propose that M(FA)Cl is formed, which requires one monoacid to obtain a mobile metal soap. Chloride and lead-chloride complexes were detected with SIMS inside the aggregate of HSTB 43/3, where chloride can be introduced into the aggregate via M(FA)Cl. The lead white itself could be indirectly the source of the chloride. The production of lead white is known to involve different procedures and purification methods. Raw lead whites still contain lead acetate and water washing reduces the acetates.[45] It is possible that chloride containing water was used. The questionable water quality in the 17th century might have introduced this impurity into the pigment only to affect the paint later on. On the other hand, salt-containing water has also been used for purification of drying oil. So there are several potential sources of chlorides. No direct evidence for M(FA)Cl as a molecular entity has been found however in the data presented in this chapter.

It would be interesting to know in what chemical form metal soaps are present inside the aggregates, ignoring the coordination chemistry of lead in this discussion. Such knowledge could be informative about the process of formation of the metal

soaps. The overall reaction for metal oxide and fatty acids is:[46]

$$M(OH)_2 + (HFA)_2 \rightarrow M(FA)_2 + 2H_2O$$

This means that two fatty acids are required to release the metal ion from the surface of the pigment particle. This implies that the reactive surface of the pigment particle must be rich in fatty acids. These fatty acids are presumably monocarboxylic fatty acids as these are the fatty acids that are mainly detected in the aggregates. An organic ´halo` of metal soaps is observed in the MH146 samples, in which the lead white particles are reacting away.

For the formation of basic metal soaps (M(FA)(OH)) only one monocarboxylic acid is required to create a mobile metal soap.

$$M(OH)_2 + HFA \rightarrow M(FA)(OH) + H_2O$$

In this scenario, a fatty acid rich shield around the pigment particle is really a requirement. Similarly, the absence of a fatty acid rich 'halo' can also be valid for metal soaps with chlorine as the counter ion (M(FA)Cl).

5.4.2.7 Mineralisation inside aggregates

Mineralisation processes are observed inside the lead- and zinc soap aggregates. The compound precipitating in lead and zinc soap aggregates is a lead- or zinc carbonate respectively. We assume that the carbonate source is atmospheric CO_2. The mineralisation in the various aggregates shows different phenomena. Lamellar bands are often observed in large lead soap aggregates, for example in *The Anatomy Lesson of Dr. Nicolaes Tulp* by Rembrandt van Rijn or *Diana and her companions* by Johannes Vermeer.[7] In the latter two cases the aggregates are fully mineralised, while in the lead-tin yellow sample A342/18 an earlier state is observed, in which precipitation of the metal carbonates occurs as a cloudy mass in the lead soap environment. In the core of zinc soap aggregates in LLSH2 a small circular centre with small crystals are observed, which might grow further to affect the whole zinc soap aggregate. In many examples orange particles, identified as minium, are found to be associated with lead soap aggregates, as is visible in MH146/B38 and HSTB43/3. The minium particles are only observed in or around an aggregate and not in the rest of the layer. We argue that these particles are formed in the aggregates during their development and were not added to the lead white ground to improve the chemical drying (see section 5.3.2.2 paint cross-section HSTB 43/3 – discussion).[8] The fact that metal soaps mineralise into metal

carbonates might be a way to stabilise metal soap affected paintings by incubation in an atmosphere with a high CO_2 content.

5.5 Conclusions

This work has shown that many aspects determine the formation of metal soap aggregates and therefore a single mechanism cannot be proposed. The analytical imaging results of the case studies are used as starting point for the discussion why certain paint layers are affected with an excess of metal soaps. Metal soap aggregates are formed from lead- or zinc-containing pigments (and driers) and mainly free monocarboxylic fatty acids. An excess of monoacids introduced in a mature oil network can lead to a saponified paint layer. The monoacids are derived from external sources, *i.e.* layers positioned above and below or within sources, *i.e.* de-esterification of a medium rich layer. The monoacids cannot directly be incorporated in the mature network. They migrate to the surface of pigment particles where they react with the metal ion into metal soaps. Depending on the amount of monoacids the pigment particles react away leading to metal soap aggregates. Inside the metal soap aggregates, lead or zinc carboxylate precipitates and minium particles can be formed in the lead soap aggregates.

5.6 Acknowledgements

We are very grateful to P. Noble (Royal Picture Gallery Mauritshuis, The Hague), J. Zucker (New York State Bureau of Historic Sites at Peebles Island), L. Speleers (AMOLF, Amsterdam), A. Burnstock (Courtauld Institute of Art, London), Prof. J.R.J. van Asperen de Boer, E. Hendriks (Van Gogh museum, Amsterdam) and G. Osmond (Queensland Art Gallery, Australia) for providing the paint cross-sections and for their fruitful discussions. Heleen Zuurendonk is thanked for the imaging-FTIR work on the zinc soap-containing samples. Maartje Witlox and Karin Groen are thanked for providing information on grounds used in the 17th century.

5.7 References

1 N. Middelkoop, P. Noble, J. Wadum and B. Broos, *Rembrandt under the scalpel The Anatomy Lesson of Dr Nicolaes Tulp Dissected*, Amsterdam/The Hague, 1998.

2 P. Noble, J. Wadum, K. Groen, R. Heeren and K.J. van den Berg, *Aspects of 17th century*

binding medium: inclusions in Rembrandt's 'Anatomy lesson of Nicolaes Tulp' In: Art et chimie, La couleur, Paris, Actes du Congrès (1998), 2000, p. 126-129.
3 U. Plather, *Baburen re-examined*, Conservare necesse est. Festskrift til Leif Einar Plather, IIC Nordic Group, Oslo, 1999, p. 65-67.
4 C. Higgitt, M. Spring and D. Saunders, *Pigment-medium interactions in oil paint films containing red lead or lead-tin yellow*, National Gallery Technical Bulletin, 24, 2003, p. 75-96.
5 P. Noble, J.J. Boon and J. Wadum, *Dissolution, Aggregation and Protrusion. Lead soap formation in 17th century grounds and paint layers*, ArtMatters, 1, 2003, p. 46-61.
6 R.M.A. Heeren, J.J. Boon, P. Noble and J. Wadum, *Integrating imaging FTIR and secondary ion mass spectrometry for the analysis of embedded paint cross-sections*, In: ICOM-CC Preprints of the 12th Triennial Meeting, J. Bridgland (Ed.), Lyon, 1, 1999, p. 228-233.
7 J. van der Weerd, J.J. Boon, M. Geldof, R.M.A. Heeren, P. Noble, *Chemical changes in old master paintings: dissolution, metal soap formation and remineralization processes in lead pigmented paint layers of 17th century paintings*, Zeitschrift für Kunsttechnologie und Konservierung, 16, 2002, p. 36-51.
8 K. Keune, P. Noble, J.J. Boon, *Chemical changes in lead-pigmented oil paints: on the early stage of formation of protrusions*, In: Proceedings of ART 2002, the 7th International Conference on Non-destructive Testing and Microanalysis for the Diagnostics and Conservation of the Cultural and Environmental Heritage, R. van Grieken, K. Janssens, L. Van' t dack, G. Meersman (Eds.), Antwerp, Belgium, 2002, 9 pages.
9 J. Boon, J. van der Weerd, K. Keune, P. Noble, *Chemical changes in Old Master paintings: dissolution, metal soap formation and remineralization processes in lead pigmented paint layers of 17th century painting*, ICOM-CC Working Groups Painting 1 & 2 and Painting section, UKIC, Deterioration of Artists Paints: Effects and Analysis Extended abstracts, September, 2001, p. 19-20.
10 J. Boon, J. van der Weerd, K. Keune, P. Noble, J. Wadum, *Mechanical and chemical changes in Old Master paintings: dissolution, metal soap formation and remineralization processes in lead pigmented ground/intermediate paint layers of 17th century paintings,* In: ICOM-CC Preprints of the 13th Triennial Meeting, R. Vontobel (Ed.), Rio de Janeiro, 1, James and James, London, 2002, p. 401-406.
11 C. Higgitt, M. Spring and D. Saunders, *Pigment medium interactions in oil paint films containing red lead or lead-tin yellow*, ICOM-CC Working Groups Painting 1 & 2 and Painting section, UKIC, Deterioration of Artists Paints: Effects and Analysis Extended abstracts, September, 2001, p. 21-25.
12 M.J. Plater, B. De Silva, T. Gelbrich, M.B. Hursthouse, C.L. Higgitt, D.R. Saunders, *The char acterisation of lead fatty acid soaps in 'protrusions' in aged traditional oil paint*, Polyhydron, 22, 2003, p. 3171-3179.
13 J.J. Boon, E. Gore, K. Keune and A. Burnstock, *Image analytical studies of lead soap aggre gates and their relationship to lead and tin in 15th century lead tin yellow paints from the S herbourne Triptych*, Infrared and Raman Users Group (IRUG) meeting, 29 March – 1 April, M. Picollo (Ed.), Il Prato, Padova, Florence, Italy, 2004, p. 66-74.
14 J. van der Weerd, M. Gelddof, L. Struik van der Loeff, R. Heeren and J. Boon, *Zinc soap aggregate formation in 'Falling leaves (Les Alyscamps)' by Vincent van Gogh*, Zeitschrift für Kunsttechnologie und Konservierung, 17, 2003, p. 407-416.
15 Personal communication with G. Osmond, the Queensland Art Gallery, Australia.
16 J.D.J. van den Berg, *Analytical chemical studies on traditional linseed oil paints,* PhD Thesis, University of Amsterdam, 2002 (http//www.amolf.nl/publications/theses/), Chapter 7.
17 J. van der Weerd, *Microspectroscopic analysis of traditional oil paint*, PhD Thesis, University

of Amsterdam, 2002 (http//www.amolf.nl/publications/theses/), Chapter 7.
18 A. Eisenberg, *Clustering of ions in organic polymers*. a *theoretical approach*, Macromolecules, 3, 1970, p. 147-154.
19 U.K. Mandal, *Ionic elastomer based on carboxylated nitrile rubber: infrared spectral analysis*, Polymer international, 49, 2000, p. 1653-1657.
20 A.D. Wilson, H.J. Prosser (Eds.), *Developments in Ionic Polymers-1*, Applied Science Publishers LTD, Essex, 1983.
21 A. Eisenberg, B. Hird, R.B. Moore, *A new multiplet-cluster model for the morphology of random ionomers*, Macromolecules, 23, 1990, p. 4098-4107.
22 U.K. Mandel, *Effect of zinc stearate on the rheology of ionic elastomer based on carboxylated nitrile rubber*, Polymer Engineering and Science, 36, 1996, p. 283-287.
23 C.M. Groen, *Grounds in Rembrandt's workshop and in paintings by his contemporaries*, In: E. van de Wetering, A Corpus of Rembrandt Paintings, Vol. IV (forthcoming), Chapter IV and tables.
24 T T. de Mayerne, Pictoria, Sculptoria et quae subalternarum artium, Manuscript Sloane 2052, British Museum, London, fol. 93v:
25 K. Groen, *Investigation of the use of the binding medium by Rembrandt*, Zeitschrift für Kunsttechnologie und Konservierung, 11, 1997, p. 207-227.
26 see Chapter 3.2
27 Forthcoming book on Oranjezaal. The RKD (Rijksbureau voor Kunsthistorische Documentatie/ Netherlands Institute for Art History) is preparing a book on the Oranjezaal. Chief editor is Dr. R. E. O. Ekkart.
28 D. Saunders, M. Spring, C. Higgitt, *Colour change in red-lead containing paint film*, In: ICOM-CC Preprints of the 13th Triennial Meeting, R. Vontobel (Ed.), Rio de Janeiro, 1, James and James, London, 2002, p. 455-463.
29 K. Keune, J.J. Boon, *Enhancement of the static-SIMS secondary ion yields of lipid moieties by ultrathin gold coating of aged oil paint surfaces*, Surface and Interface Analysis, 36, 2004, p. 1620-1628.
30 J. Zucker, *From the ground up: the ground in 19th-centruy American pictures*, Journal of American Institute of Conservation, 38, 1999, p. 3-20.
31 E. Gore, *A study of the interaction between oil and pigment through the analysis of cross-sections from paintings*, Postgraduate diploma thesis in the conservation of easel painting. Final year project, Courtauld Institute of Art, London, 2003.
32 N.J. Eastaugh, *Lead tin yellow: its history, manufacture, colour and structure*, PhD thesis, University of London, Courtauld Institute of Arts, 1988.
33 L. Kockaert, *Note sur les emulsions des Primitifs flamands*, Institut Royal du Patrimoine Artistque Bulletin, XIV, 1973/74, p. 133-139.
34 L. Robinet, M.C. Corbeil, *The characterization of metal soaps*, Studies in Conservation, 48, 2003, p. 23-40.
35 A.F. Holleman, E. Wilberg, In: Inorganic Chemistry; Academic Press, San Diego, 2001, p. 1298.
36 L. Carlyle, *The artist's assistant: oil painting instruction manuals and handbooks in Britain 1800-1900 with reference to selected eighteenth century sources*, Archetype Publications, London, 2001.
37 R. Mayer, The artist's handbook of materials & techniques, fifth Ed., Faber and Faber Limited, 1951, p. 184-185.
38 J.D.J. van den Berg, *Analytical chemical studies on traditional linseed oil paints*, PhD Thesis, University of Amsterdam, 2002 (http//www.amolf.nl/publications/theses/).

39 J. van der Weerd, *Microspectroscopic analysis of traditional oil paint*, PhD Thesis, University of Amsterdam, 2002 (http//www.amolf.nl/publications/theses/), p. 116-118.
40 Personal communication with Dr. Ester Ferreira (AMOLF/The Netherlands).
41 S.B. Elliott, In: The alkaline-earth and heavy-metal soap, Reinhold Publishing Corporation, New York, 1964, p. 25.
42 H. Kühn, *Zinc white* In: Artists' Pigments, vol. 1, R. L. Feller (Ed.), National Gallery of Art, Washington, 1986, p. 175.
43 Personal communication with Drs. Frank Hoogland (AMOLF/The Netherlands).
44 S.B. Elliott, In: The alkaline-earth and heavy-metal soap, Reinhold Publishing Corporation, New York, 1964, p. 99.
45 L. Carlyle (ICN, The Netherlands) and K. Keune, unpublished SIMS studies.
46 S.B. Elliott, In: The alkaline-earth and heavy-metal soap, Reinhold Publishing Corporation, New York, 1964, Chapter 5 and 6.

Appendix I

The appendix presents a table of paintings that are affected by metal soap formation. These are the results of a detailed questionnaire send out by Noble in 2002. In this table only the artist, the title of the painting, the owner and dating are given: for more detailed information regarding the questionnaire and the results of the questionnaire contact P. Noble, Mauritshuis, The Hague, The Netherlands (Noble.P@mauritshuis.nl).

Artist	**Painting title**	**Owner**	**Dating**
Master of Flemalle	The Bad Chief	Stadelsches Kunstinstituut Frankfurt	early 15th c
Bouts, Albrecht	Man of Sorrows	Fogg Art Museum, Boston	1490s
Anon. 15th c.	Sherborne Retable	National Trust, UK (from Sherborne Chapel, Dorset)	c.1480-1500
Mansueti (loosely attributed)	Double Portrait	Private Collection, UK	late 15thc.
Anon. 15thc - 16thc.	St James Panels	National Trust, UK (from Knole House, Kent)	late 15thc.-early 16thc.
Predis, Ambrogio de	Bianca Maria Sforza	National Gallery Washington	1493
Van Oostsanen, Jacob Cornelisz (group)	Virgin and Child with angel musicians	Boymans-van Beuningen Museum, Rotterdam	1510
Lotti, Lorenzo	Portrait of a Young Man	Staatliche Gemäldegalerie, Berlin	c. 1526
Ravesteyn, Jan van	Portrait of Hugo Grotius	Lugt Collection, Fondation Custodia, Paris	1599
Anon. (Southern Germany)	Holy Barbara	RijksmuseumTwente	15th c
Savery, Roelandt, (attrib.)	Venus und Amor vor der Liebesburg	Kunsthistorisches Museum, Vienna	c. 1605
Francesco Albani (workshop)	The Last Supper	Private Collection, UK	c. 1610
Anon.	Portrait of man	Tate Britain	c. 1610
Circle of Breughel	Paradise	Royal Picture Gallery Mauritshuis, The Hague	1620s?

Artist	Painting title	Owner	Dating
Baburen, Teodoer	The Young Christ among the Doctors	National Gallery, Oslo	1622
Salvator Rosa (attrib.)	Landscape	Courtauld Galleries, London	mid 17thc.
Savery, Roelandt	Flower Still life	Private Coll., The Netherlands	c. 1627
Savery, Roelandt	Orpheous enchanting the animals with his music	Royal Picture Gallery Mauritshuis, The Hague	1627
Rembrandt	The Anatomy Lesson of Dr Nicolaes Tulp	Royal Picture Gallery Mauritshuis, The Hague	1632
Rembrandt, attributed to	Laughing Man	Rijksmuseum Amsterdam	1630s
Van Dyck, Anthony	Portrait of W. Fielding, Ist Earl of Denbigh	National Gallery London	c.1633-34
Kalf, Willem	Still life	Wallraf-Richartz-Museum, Cologne	1643
Seghers, Daniel / Bosschaert, Willeboits	Garland of Flowers around an image of the Madonna	Royal Picture Gallery Mauritshuis, The Hague	1645
Weenix, Jan Baptist	Tobias sleeping under the Vine	Boymans-van Beuningen Museum, Rotterdam	1642?
Fabritius, Carel (circle of)	Man with helmet	Groningen Museum, Groningen	1640s
Soutman, Pieter	Triomfstoet met veroverde wapenen	Oranjezaal, Huis ten Bosch, The Hague	1648
Couwenbergh, C. van	Heraut zuidoost	Oranjezaal, Huis ten Bosch, The Hague	1649
Honthorst, Gerard van	Frederik Hendriks standvastigheid	Oranjezaal, Huis en Bosch, The Hague	circa 1650
Campen, Jacob van	Apollo op de zonnewagen	Oranjezaal, Huis ten Bosch, The Hague	circa 1650
Lievens, Jan	Five Muses	Oranjezaal, Huis ten Bosch, The Hague	1650
Couwenbergh, C. van	Herald southwest	Oranjezaal, Huis ten Bosch, The Hague	1651
Thulden, Theodoor van	Triomfstoet met olifant en schilderijen	Oranjezaal, Huis ten Bosch, The Hague	1651
Campen, Jacob van	triofstoet met geschenken...	Oranjezaal, Huis ten Bosch	before end of 1651
Potter, Paulus	Cattle in the Meadow	Royal Picture Gallery Mauritshuis, The Hague	1652
Potter, Paulus	A Farriers Shop	National Gallery Washington?	
Gysels, Pieter (1621-1690)	River Landscape with Villages and Travelers	National Gallery Washington	
Vermeer, Johannes	Diana and her Companions	Royal Picture Gallery Mauritshuis, The Hague	c. 1655
Cuyp, Albert	Girl with Peaches	Royal Picture Gallery Mauritshuis, The Hague	c. 1660
Hals. Frans	Portrait of a man	Royal Picture Gallery Mauritshuis, The Hague	c. 1660
Steen, Jan, attributed to	The Christening	Finnish National Museum, Helsinki	c. 1660
Steen, Jan	Twelfth Night	Staatliche Museen Kassel	1668
Backer, Adriaen	Anatomy Lesson of Professor Ruysch	Amsterdams Historisch Museum	1670
Torenvliet, J.	Portrait of Willem van der Goes	Musée des Beaux-Arts, Liege	c. 1670
Berchem, Nicolaes	Allegory of Summer	Royal Picture Gallery Mauritshuis, The Hague	1677-78
Gelder, Aert de	King David	Rijksmuseum Amsterdam	late 1600s
Coorte, Adrien	Still Life with Asparagus	Rijksmuseum Amsterdam	1697
Anon.	Portrait of a Lady	North Carolina Museum of	17th C.

Artist	Painting title	Owner	Dating
	View of Sunbury Hall from the North	Hamilton Kerr Institute, UK	18th C.
Romney, George	Portrait of Thomas Rakett	Private Collection, UK	early 1770s
Aide-Crequy, Jean-Antoine	The Annunciation	Ottawa	1776
Harris, W	Portrait of Surgeon James Heron Conroy	PEI Museum and Heritage Foundation	c. 1810
Eastlake, Charles, attributed to	Portrait of Admiral Sir J. Ross	Artic Institute of North America, Calgary	
Verboeckhoven, Louis (1802 - 1889)	Shipwreck	Maritiem Museum Rotterdam	
Unknown 19th c.	Portrait of a man	Rijksmuseum Amsterdam	1825
Courbet, Gustave	L'Immensité	Victoria & Albert Museum, London	1869
Rousseau, Theodoré	Pont de Batignies	Victoria & Albert Museum, London	
Church, Frederic	numerous canvasses and panels (approx. 100)	Olana State Historic Site	1870-1890
Van Gogh, Vincent	Portrait of an old woman	Van Gogh Museum, Amsterdam	1869
Van Gogh, Vincent	Vase with Gladioli and Chinese Asters	Van Gogh Museum, Amsterdam	1886
Van Gogh, Vincent	Impasse des deux frères and Moulin de Poivre	Van Gogh Museum, Amsterdam	1887
Van Gogh, Vincent	Still Life with Grapes, Pears and Lemons	Van Gogh Museum, Amsterdam	Dated 1887
Van Gogh, Vincent	Les Alycamps	Stichting Kröller-Müller Museum	1888
Van Gogh, Vincent	The enclosed field	Stichting Kröller-Müller Museum	1890
Bosch Reitz, Sigisbert Chrétien	The Sick Child	Private Collection	1889
Bosch-Reitz, Sigisbert Chrétien	Portrait P. J. Teding van Berkhout	Private Collection	1891 or 1894
Redon, Odilion	Fleurs dans une coupe	Van Gogh Museum, Amsterdam	c. 1900
Redon, Odilion	Bouquet in green vase	Van Gogh Museum, Amsterdam	c. 1900
John, Augustus	W. B. Yeats	Tate Gallery, London	1907
Rivers, Godfrey	Under the Jacaranda	Queensland Art Gallery, Australia	1890
Rivers, Godfrey	Woolshed, New South Wales	Queensland Art Gallery, Australia	1903
Rivers, Godfrey	An Alien in Australia	Queensland Art Gallery, Australia	1904
Svarstad, Anders Castus	Portrait of Sigrid Undset	Bergen Kunstmuseum	1911
Rivers, Godfrey	Florence	Queensland Art Gallery	c. 1913
Lister Lister, W	Sydney Harbour, Taylor bay	Queensland Art Gallery, Australia	early 20th C.
Hodler, Ferdinand	Lake Thun with Stockhorn Range	Private Collection	1905
Hodler, Ferdinand	Portrait of Berthe Hodler	Private Collection	1916
Hodler, Ferdinand	Dents du Midi and Mont-Blanc in the morning	Private Collection	1916
Corinth, Louis	Self-portrait	Art Institute of Chicago	1917
Toorop, Charlie	Portrait of Two Brothers	Stichting Kröller-Müller Museum	1926
Tamayo, Rufino	Woman with watermelon	Fine Arts Museum of San Francisco, USA	1931
Poliakoff, Serge	Composition Without Title		
Mitchell, Joan	Ste Hiliare	Art Institute of Chicago	c. 1958

Summary

Paintings are complex systems that continuously undergo chemical and physical alterations. The analytical studies of paintings reported in this thesis are performed on the microscopic and molecular level with the ultimate aim to utilise the acquired knowledge of the alteration processes to improve display and storage conditions, suggest suitable restoration treatments and address art historical issues.

The microscopic and molecular studies are carried out on tiny paint samples derived from paintings. Paint samples are embedded in resin and polished until a flat cross-section of the layer system, the so-called paint cross-section, is visible at the surface. By preserving the layer structure of the sample, the distribution of pigment, binding medium components and their aging and degradation products can be charted. The analysis of paint cross-sections with spatially resolving analytical imaging techniques facilitates the identification and localisation of the molecular and elemental composition in the paint sample.

Different non-destructive analytical imaging techniques applied to the same paint cross-section result in a combined set of data that gives a more complete impression of the chemical composition of the paint sample. The following techniques have been applied: light microscopy, imaging Fourier Transform Infrared spectroscopy (imaging-FTIR), scanning electron microscopy combined with energy dispersive X-ray analysis (SEM/EDX) and imaging static secondary ion mass spectrometry (SIMS).

SIMS applied to paint cross-sections from Old Master paintings is a relatively novel approach. SIMS is introduced as an analytical technique for the examination of paint cross-sections in **chapter 2**. The paint cross-section discussed in this chapter was taken from the blue robe of Maria in the panel painting *The Descent from the Cross* (Museo del Prado, Madrid) of the Early Netherlandish artist Rogier van der Weyden (1399/1400-1464). This 15th-century panel painting is in a very good condition, which makes the paint cross-section a suitable example of pigments and binding media in oil paintings. The identification of the pigments in the paint cross-section is based on the elemental composition. The shape and position of the sodium and aluminium in the SIMS image corresponds exactly with form and position of the ultramarine particles and the copper SIMS image matches the azurite particles observed by the light microscopy. The elemental composition and distribution is in agreement with the SEM/EDX results. The molecular information obtained with SIMS is representative for oleaginous binding media. The interpretation of the ion

peaks characteristic for binding medium constituents in the SIMS spectra is supported by spectral data from reference materials. SIMS fragment ions characteristic for drying oil are found in the upper three paint layers while the ratio of palmitic and stearic acid derived from the negative ion distribution pattern in each of the upper three paint layers is indicative of linseed oil. SIMS also detects lead soaps in the paint layers, which is indicative for a mature aged oil paint. The presence of lead soaps in these paint layers is confirmed by the results of imaging FTIR. SIMS is considered to be a very suitable analytical tool for the identification and localisation of the binding medium and pigment present in paint cross-sections.

The following chapters (3, 4 and 5) present different aspects of the paint (binding medium, pigment and their interaction products) studied with the various analytical imaging techniques mentioned above.

SIMS is one of the few non-destructive techniques that yields detailed spatially resolved molecular information on the micrometer scale. SIMS is therefore suitable for the study of binding medium in paint cross-sections. The scope of this technique for the localisation and identification of the oil binding medium is discussed in **chapter 3** which is divided in three separate sections: the interpretation of the SIMS spectra, the localisation of oil paint constituents, and enhancement of the yield of organic ion.

A natural and accelerated aged linseed oil paint reconstruction is analysed as model system by SIMS, DTMS and GC/MS as three different mass spectrometric techniques. Comparison of these data gives a good impression of the value of the molecular information on the oil medium obtained with SIMS. SIMS provides important combined information on the organic and inorganic components of the upper atomic layers of the analysed surface of the paint film. Characteristic peaks representative for the fatty acids as important oil paint constituents are detected as negative ions. Positive ion spectra provide detailed chemical information on the condition of the oil paint by distinguishing the speciation of the fatty acids in free, ester-bound or metal carboxylate form. SIMS does not produce significant yields of diacids and little relevant information concerning the polymeric network. GC/MS results on the other hand show that diacids are dominantly present and DTMS is more informative about polymeric network. Despite these limitations, I conclude that SIMS is a valid and important analytical method for the study the oil binding medium of paint samples.

The localisation of characteristic peak representative for fatty acids and their ratio in paint cross-section in the topic in the second section of chapter 3. SIMS studies of pure fatty acids mixed in a chalk matrix show that the response of the negative ions from the various fatty acids tested is identical under the SIMS ionisation conditions. Hence, the determination of the P/S ratio by SIMS is a valid method for

the identification of the type of oil in a paint layer. P/S ratios were determined in individual layers from 15th- to 19th-century paintings using paint cross-sections. Studies on non-fully dried multi-layered test oil paint systems of linseed and poppy oil by SIMS demonstrate P/S ratios that suggest a rapid exchange of oil triacylglycerols between the layers, which has relevance for the interpretation of paint systems made with the wet-in-wet technique. Positive ion SIMS mass spectral data presents information on the distribution of the free, ester bound or metal carboxylate the fatty acids in the paint layers.

In the last section of chapter 3 data are presented on the surface of a cross-section that is coated with a 20Å thick gold layer to improve the yield of secondary ions from organic fractions in the paint. The improvement is shown using a chalk tablet with 1% stearic acid of which one half of the surface is gold coated. A comparative study of a gold-coated native and aged surface of a linseed oil paint reconstruction further demonstrates the enhancement of the organic ion yields on this sample relevant for painting studies. The yield of oil paint derived negative ions increases by a factor of 3 whereas the yield of positive ions increases by a factor of 2 to 4. Gold coating improves the ionisation process of the fatty acids and does not influence their fragmentation. The gold coating method is applied to one paint cross-section presented in chapter 5 illustrating the improved quality of the data on the distribution of the different organic constituents of the oil medium (mono- and as well as dicarboxylic acids) in the paint sample.

Chapter 4 illustrates the different imaging analytical techniques applied to a paint cross-section complement each other in the description of pigment degradation phenomena. The light induced blackening of the traditional red pigment vermilion (mercury sulphide) is a century old problem. The blackening of vermilion is a phenomenon on the surface of paintings, which is illustrated in the paint cross-section as degraded pigment on top of intact vermilion. Detailed light microscopic images of a paint cross-section originating from a painting by Rubens (17th century) reveal a black and a white coloured reaction product. The position of the black and white products in the paint cross-section and the presence of partially degraded vermilion suggest that the white coloured products are formed after the black reaction product. SEM/EDX as well as SIMS data visualise the elementary and molecular composition and their distribution in the paint sample. Both techniques detect a high relative concentration of chloride in the degraded vermilion, while SIMS is sensitive enough to map chlorides in the intact vermilion. In contrast to SEM/EDX, SIMS can detect inorganic molecules and is able to identify the white product as mercuric chloride ($HgCl_2$). The distribution of atomic and molecular species in the paint cross-section leads to the formulation of a new hypothesis on the photo-degradation mechanism of

vermilion. We propose that traces of chloride catalyse a light-induced electrochemical reaction that converts red vermilion into a black product. The current interpretation that the black product is metacinnabar form of HgS is not supported by our investigation. The black product is proposed to be composed of residual vermilion with nanodroplets of metallic mercury that absorb the light. We observe that a relatively high amount of chloride is accumulating in the black product, which reacts with the mercury to white mercury chlorides. This mercury complex is described in paintings for the first time. The blackening of vermilion is an irreversible process, in which chlorides play an important role. For preventive conservation of vermilion containing works of art, exposure to chloride-containing compounds should be prevented.

Chapter 5 illustrates that binding medium and pigment cannot be seen as separated entities in paints because numerous paintings from the 15th to the 20th century are affected by metal soap aggregate formation. Ten paint cross-section that contain paints with lead or zinc soap aggregates were selected for investigation with the different imaging analytical techniques. Lead and zinc soap aggregates have a negative effect on the stability of the painting and as they can protrude through the surface they affect the appearance of the painting. Metal soap is formed in a chemical reaction between a fatty acid, derived from the oil medium, and a metal ion originating from pigment or drier. Metal soaps are normally formed in oil paintings, but many examples are found with an excess of metal soaps, which can lead to aggregation. Imaging analytical studies on the selected paint cross-sections derived from paintings by e.g. Rembrandt van Rijn (17th century) or Vincent van Gogh (19th century), have shown that in some cases the pigment completely reacts away. The reactive fatty acids are released during ageing of the oil, but in certain cases these fatty acids presumably cannot be directly incorporated in the oil network but migrate to the pigment surface. The reactive fatty acids can derive from the saponified paint layer or from other paint layers in the multi-layered paint system. Formation of mineralised matter is observed inside the aggregates, identified as lead carbonate in lead soaps or zinc carbonate in zinc soaps. In some cases, tiny orange minium (lead plumbate) crystals are seen on the inside of the edge of the lead soap aggregates. Metal soap aggregate formation is an irreversible process, the imaging studies however lead to better insight into some of the parameters which play a significant role in the formation of an excess of metal soap in paintings. Moisture and high temperature are two of these factors, which not only promote the hydrolysis during ageing of the oil paint, but also increase the reactivity of fatty acid and pigment. Reduction of the mobilisation of fatty acids in paintings by *e.g.* avoiding moisture and heat during restoration treatments and the optimizing storage conditions might reduce the risk of metal soap aggregation formation.

Samenvatting

Schilderijen zijn complexe systemen die continu aan chemische en fysische veranderingen onderhevig zijn. In dit proefschrift worden schilderijen op een microscopisch en moleculair niveau onderzocht. Dit type onderzoek is nodig om beter inzicht te krijgen in optimale bewaarcondities, passende restauratiebehandelingen en kunsthistorische vraagstukken van schilderijen.

Het onderzoek wordt verricht aan verfdwarsdoorsneden, een minuscuul verfmonster wat ingebed is in een polymeerblokje en zodanig geslepen is dat de laagopbouw van het schilderij zichtbaar is aan het oppervlak van dit blokje. De meerwaarde van onderzoek aan verfdwarsdoorsneden is dat precieze verdeling van pigment, bindmiddel en hun verouderings- of degradatieproducten in en tussen verflagen op deze manier in kaart gebracht kan worden. Met plaatsopgeloste technieken kan de elementaire en moleculaire samenstelling in een verfdwarsdoorsnede geïdentificeerd en gelokaliseerd worden.

De combinatie van verschillende niet destructieve plaatsopgeloste analytische technieken toegepast op dezelfde verfdwarsdoorsnede resulteert in complementaire informatie wat leidt tot een completer beeld over de samenstelling van het verfmonster. De volgende technieken zijn hier toegepast: lichtmicroscopie, plaatsopgeloste infraroodmicroscopie (imaging fourier transform Infrared spectroscopy, imaging-FTIR), rasterelektronenmicroscopie (scanning electron microscopy combined with energy dispersive X-ray analysis, SEM/EDX) en plaatsopgeloste massaspectrometrie (secondary ion mass spectrometry, SIMS).

De toepassing van SIMS op verfdwarsdoorsneden afkomstig uit schilderijen is relatief nieuw. In **hoofdstuk 2** wordt deze techniek geïntroduceerd als onderzoekstechniek voor verfdwarsdoorsneden. De verfdwarsdoorsnede besproken in dit hoofdstuk is afkomstig uit de blauwe mantel van de Maria in de *De Kruisafneming* (Museo del Prado, Madrid) van de vroeg Nederlandse kunstenaar Rogier van der Weyden (1399/1400-1464). Dit 15de eeuwse schilderij op paneel is in zeer goede conditie, wat de verfdwarsdoorsnede geschikt maakt voor onderzoek naar bindmiddel en pigmentsamenstelling in olieverfschilderijen. De identificatie van de pigmenten in de verfdwarsdoorsnede wordt gedaan op basis van de elementaire samenstelling. Zo komt de vorm en locatie van het natrium en het aluminium SIMS beeld precies overeen met die van de ultramarijn deeltjes in het lichtmicroscopisch plaatje en het koper SIMS beeld met de azuriet deeltjes. De elementaire verdeling verkregen met SIMS is in overeenstemming met die van SEM/EDX. De moleculaire informatie

verkregen met SIMS is representatief voor een oliehoudend bindmiddel. De interpretatie van de SIMS spectra is onderbouwd met spectra van referentiematerialen. De karakteristieke fragmenten voor olie worden gevonden in de bovenste drie verflagen. Op basis van de verhouding tussen de vetzuren palmitine- and stearinezuur kan afgeleid worden welk type olie gebruikt is. Deze verhouding is afzonderlijk berekend voor de bovenste drie verflagen en de waarde is in alle drie de gevallen indicatief voor lijnzaadolie. SIMS detecteert ook loodzepen in deze lagen, wat ondersteund wordt door de infrarood resultaten. De aanwezigheid van loodzepen wijst op een verouderd stabiel olieverfsysteem. SIMS is derhalve een zeer geschikte onderzoekstechniek om de samenstelling in verfdwarsdoorsneden, bindmiddel en pigment, te identificeren en te lokaliseren.

In de volgende hoofdstukken (3 t/m 5) komt de analyse van verschillende aspecten van de verf (bindmiddel, pigment en hun interactie) met de diverse plaatsopgeloste technieken aan bod.

SIMS is een van de weinige niet destructieve technieken die plaatsopgelost zeer gedetailleerde moleculaire informatie kan geven. SIMS is daarom een geschikte techniek om het bindmiddel in verfdwarsdoorsneden te bestuderen. De mogelijkheden van deze techniek voor de identificatie en lokalisatie van een olie medium wordt bediscussieerd in **hoofdstuk 3**. Het hoofdstuk is opgesplitst in drie afzonderlijke gedeelten, de interpretatie van de SIMS spectra, de lokalisatie van karakteristieke olieverfcomponenten en het verhogen van de opbrengst van karakteristieke olieverfcomponenten.

Een oliehoudend model systeem (loodwit in lijnzaadolie), dat natuurlijk en versneld verouderd werd, is geanalyseerd en vergeleken met verschillende massaspectrometrische technieken, nl. SIMS, DTMS and GC/MS. Door de verschillende massaspectrometrische resultaten van het modelsysteem te vergelijken is een goed beeld gekregen over de mogelijkheden van olie identificatie met SIMS. Een sterk punt van SIMS is de gecombineerde organische en anorganische informatie afkomstig van de bovenste atomaire lagen. Karakteristieke pieken representatief voor de vetzuren (een belangrijke olieverf componenten) worden gedetecteerd in het negatieve ionenspectrum. De wijze van coördinatie van het vetzuur (vrij, ester of metaal gebonden) kan worden afgeleid uit het positieve ionenspectrum. Dizuren worden nauwelijks gedetecteerd met SIMS, terwijl GC/MS aantoont dat de dizuren een dominant bestandsdeel zijn in een verouderd olieverfsysteem. In tegenstelling tot DTMS geeft SIMS geen duidelijke informatie over het olieverfnetwerk. Ondanks deze beperkingen is SIMS een informatieve en waardevolle analytische techniek voor de studie naar oliebindmiddel in verfmonsters.

De lokalisatie van karakteristieke pieken representatief voor de vetzuren en hun onderlinge verhouding wordt in het tweede gedeelte van hoofdstuk 3 besproken. SIMS studies aan zuivere vetzuren gemengd in een kalktablet laten zien dat de respons van de verschillende vetzuren onder de SIMS condities identiek is. De bepaling van de verhouding tussen palmitine- and stearinezuur met SIMS is betrouwbaar en kan gebruikt worden voor de identificatie van het type olie. In individuele verflagen van verfdwarsdoorsneden afkomstig van de 15de tot en met de 19de eeuw wordt deze verhouding bepaald. De verhouding verandert wanneer verflagen met verschillende type oliën nat op elkaar aangebracht worden. Dit wijst op een migratie van oliecomponenten tussen de lagen. De bepaling van het bindingstype van vetzuren (dwz. vrije, ester of metaal gebonden) m.b.v. het positieve ionen spectrum wordt in dit gedeelte wederom bediscussieerd.

In het laatste gedeelte van hoofdstuk 3 wordt een ultra dunne goudlaag op het oppervlak gedampt om zo een hogere opbrengst van de organische ionfragmenten te krijgen. Dit wordt bewezen met een testsysteem. Een hogere opbrengst van deze fragmenten leidt tot betere beeldkwaliteit wanneer naar de verdeling van dit fragment gekeken wordt. Een met goud bedekt modelsysteem resulteert in een verhoogde opbrengst met een factor 3 voor karakteristieke negatieve ionen van de olieverf componenten, terwijl de positieve ionen een factor 2-4 verbeteren. Deze methode is toegepast op een van de verfdwarsdoorsneden besproken in hoofdstuk 5 en leidt tot duidelijker beeld van de verdeling van de verschillende organische olieverfcomponenten in het verfmonster.

Hoofdstuk 4 laat zien dat door het gebruik van verschillende plaatsopgeloste technieken een beter inzicht gekregen wordt in de degradatieprocessen van pigmenten. Het zwart worden van het rode traditionele pigment vermiljoen (kwiksulfide) door licht is een eeuwenoud probleem. Het zwart worden van vermiljoen gebeurd aan het schilderijoppervlak waardoor in dwarsdoorsnede gedegradeerde en intacte vermiljoenverf zichtbaar is. Gedetailleerde lichtmicroscopie beelden van een verfdwarsdoorsnede met gedegradeerd vermiljoen afkomstig van een schilderij van Rubens (17de eeuw) laat twee producten, een zwart en wit product, zien. Op basis van hun onderlinge positie en de aanwezigheid van half gedegradeerde vermiljoen deeltjes concluderen we dat eerst het zwarte en daarna het witte product gevormd is. SIMS en SEM/EDX studies visualiseren de elementaire en moleculaire samenstelling en verdeling in het verfmonster. In het gedegradeerde vermiljoen wordt zowel met SEM/EDX als SIMS relatief hoge concentratie chloride aangetroffen, terwijl SIMS sporen van chloride in het intact vermiljoen detecteert. In tegenstelling tot SEM/EDX detecteert SIMS anorganische complexen en identificeert het witte product als een

kwikchloride complex. De plaatsopgeloste analytische resultaten leiden tot de vorming van een hypothese over het degradatiemechanisme van vermiljoen. De sporen van chloride in het intacte vermiljoen, katalyseren de lichtgedreven omzetting van rood naar zwart. De aloude opvatting dat het zwarte product de zwarte vorm van kwiksulfide is, wordt in dit onderzoek verworpen. We suggereren dat het zwarte product bestaat uit vermiljoenrestanten met nanobolletjes van metallisch kwik die het licht absorberen. Wij stelden vast dat een hoge concentratie chloride accumuleert in het zwarte product dat vervolgens met het kwik reageert tot een wit kwikchloride complex. Dit kwikcomplex is voor het eerst gevonden in schilderijen. Het 'zwart' worden van vermiljoen is een irreversibel proces, maar het is wel duidelijk dat chloriden een belangrijke rol spelen. Voor preventieve conservering van vermiljoenhoudende kunst objecten zou blootstelling aan chloridenbevattende middelen voorkomen moet worden.

Dat bindmiddel en pigment niet als twee afzonderlijke componenten in een verfsysteem kunnen worden gezien blijkt uit de aantasting van talloze schilderijen van de 15de tot en met de 20ste eeuw door metaalzeepaggregaten, het onderwerp van **hoofdstuk 5**. Tien verfdwarsdoorsneden die lood- of zinkzeep aggregaten bevatten worden bestudeerd met verschillende plaatsopgeloste technieken. De lood- en zinkzeep aggregaten hebben negatieve effecten op de stabiliteit van het schilderij en doordat ze aan het oppervlak van het schilderij verschijnen, tasten ze de afbeelding op het schilderij aan. Lood- en zinkzepen ontstaan door de reactie van een vetzuur, afkomstig uit de olieverf, met een metaal, afkomstig van het pigment. Metaalzepen worden in de olieverf gevormd, maar in veel schilderijen wordt een overmaat metaalzepen geproduceerd wat uiteindelijk leidt tot aggregatie. De plaatsopgeloste analytische studies aan de geselecteerde verfdwarsdoorsneden, bijvoorbeeld verfdwarsdoorsneden afkomstig uit schilderijen van Rembrandt van Rijn (17de eeuw) en Vincent van Gogh (19de eeuw), laten zien dat in sommige gevallen het pigment geheel is weg gereageerd. De reactieve vetzuren komen vrij door verouderingsprocessen van de olieverf. Vermoedelijk kunnen ze niet direct opgenomen worden in het olienetwerk en migreren ze naar het pigmentoppervlak. In dit hoofdstuk worden voorbeelden besproken waar de overmaat aan vrije vetzuren afkomstig is uit de verzeepte verflaag, of uit verflagen. In de metaalzeepaggregaten vinden mineralisaties plaats. In de loodzeepaggregaten wordt loodcarbonaat gevormd en in de zinkzeepaggregaten zinkcarbonaat. Een ander gevormd product, minium, een loodplumbaat, wordt meestal aan de binnenrand van de loodzeep aggregaten gevonden. Metaalzeepaggregaten zijn irreversibel, maar het plaatsopgeloste analytisch onderzoek leidt tot beter inzicht in belangrijke factoren die bij de formatie van metaalzeepaggregaten een rol spelen. Vocht en

warmte zijn twee factoren die veroudering van de olieverf, maar ook de reactie tussen vetzuur en pigment bevorderen. Een vermindering van het mobiliseren van vetzuren door o.a. het vermijden van de introduktie van vocht en warmte gedurende de restauratie van schilderijen en het optimaliseren van de bewaaromstandigheden zou van het risico van metaalzeepaggregaatvorming kunnen verlagen.

Dankwoord

Het is een kunst om in de wetenschap verschijnselen te verklaren, maar het is de wetenschap die de kunst moet helpen behouden. Het is echt uiterst interessant en uitdagend om op dit grensgebied werkzaam te zijn. Ik heb daarom ook vierenhalf jaar lang altijd met veel plezier aan mijn onderzoek gewerkt. Daarnaast is AMOLF echt een fantastische plek om je promotieonderzoek uit te voeren.

Natuurlijk heb ik veel te danken aan mijn promotor Jaap Boon. Beste Jaap, het staat mij nog goed bij dat ik bij ons eerste gesprek je duidelijk maakte dat ik toch eigenlijk geen massaspectrometrie wilde doen. Ik moet zeggen dat ik daar helemaal op terug ben gekomen. Op een gegeven moment begon ik zelfs lopend door een straat huisnummers te associëren met karakteristieke fragment pieken van de olie. De vrijheid en het vertrouwen dat je me gegeven hebt tijdens mijn onderzoek heb ik zeer gewaardeerd. Het feit dat je altijd zomaar bij je binnen kon lopen heb ik als zeer prettig ervaren. Jouw grote gedrevenheid voor de wetenschap en jouw brede interesses zorgden ervoor dat de besprekingen zeer intensief en niet kort van stof waren. Ik heb het plezierig gevonden altijd vrijuit met je te hebben kunnen discussiëren.

Collega´s zijn onmisbaar! Het hebben van goede collega´s leidt absoluut tot een beter resultaat. Ik heb in mijn tijd op AMOLF veel geleerd van de mensen om mij heen, zowel wetenschappelijk als daar buiten. Annelies van Loon, jij bent zeker zo´n collega. Onze dagelijkse discussies over het werk resulteerden altijd in een verdieping van de zojuist verkregen resultaten of in nieuwe ideeën voor onderzoek, die we in de meeste gevallen ook (tussen de bedrijven door) uitvoerden. En als er geen tijd van ´komen en gaan´ was, dan weet ik zeker dat we minstens nog zo´n twintig jaar met veel enthousiasme door waren gegaan. Jaap van der Weerd, ik had me geen betere start van mijn promotie kunnen bedenken. Je hebt me echt fantastisch goed wegwijs gemaakt in het onderzoek. Je wist altijd met alle geduld en duidelijkheid mijn vragen te beantwoorden. Alleen de pogingen om me enthousiast te maken voor het gebruik van Matlab waren tevergeefs… Ester Ferreira, I really enjoyed working with you. Your broad interest, critical mind and relativism made collaboration very fruitful. I hope we can work together again once in the future. Nicole de Waal, ik wil jouw zeker bedanken voor alles wat je om het schrijven heen voor mij geregeld en gedaan hebt. Zonder jouw goede zorgen en grote creativiteit had het boekje er zeker niet zo af uitgezien.

Er zijn er te velen voor wie ik graag een persoonlijk woordje zou willen doen, maar ik hou het beperkt hoewel ik weet dat ik nu echt een hoop mensen te kort doe. Ik

wil graag mijn huidige en oude groepsgenoten in willekeurig volgorde bedanken voor hun gezelligheid en collegialiteit: Lidwien Speleers, Beatrice Marino, Jerre van der Horst, Marc Duursma, Frank Hoogland, Gert Eijkel, Olga Katsibiri, Frans Giskes, Annebeth Kraij-Kerkhoff, Gisela van der Doelen, Tania Oudemans, Jorrit van den Berg, Oscar van den Brink, Nicolas Wyplosz, Donna Mehos, Georgiana Languri, Piet Kistemaker, Sander Koster, Mark Clarke, Rimco Geels, Anne Kleinijenhuis, Romulus Mihalca, Ioana Taban, Bas Ponsioen, Erika Amstalden, Andreas Römpp, the many guests who joined our group for a long period of time: Emily Gore, Stephan Schäfer, Ana Pecoraro Schäfer, Ilaria Bonaduce, Petra Novotna, Dominique Scalarone, Dorrit Nötzel. Mijn speciale dank gaat uit naar *´de mannen van de SIMS´*: Stefan Luxembourg, Liam McDonnell, Maarten Altelaar, Todd Mize, Sander Piersma en Ron Heeren. Heleen Zuurendonk bedankt voor jouw bijdrage aan het onderzoek, zoals je ziet is een gedeelte van jouw afstudeerwerk verwerkt in het laatste gedeelte van hoofdstuk 5.

Naast de groepsgenoten wil ik van AMOLF, Teun van Dillen en Hans Zeijlemakers bedanken voor het samenwerken met de SEM. Teun, de vele keren dat je enthousiast onze kamer binnen kwam stormen met de mededeling dat je weer een fout(je) in het programma of de microscoop had ontdekt waren ontelbaar, maar altijd erg gezellig en nuttig. Gelukkig is er naast de wetenschap ruimte voor ontspanning (onder werktijd…), daarom wil ik mijn collega´s uit de personeelsvereniging (de PV) 2001 t/m 2003 bedanken voor hun gezelligheid en creativiteit.

The interdisciplinary character of the research makes this work very dynamic. The collaboration with external institutes and people is really an added value to my research performed at AMOLF. I would like to thank a few people outside AMOLF for sharing their experience, knowledge and samples with me. Petria Noble (*Mauritshuis*) and Leslie Carlyle (*Instituut Collectie Nederland*, *ICN*) thanks for your great enthusiasm, interest in and direct assistence with my research. Leslie, for me is white no longer just *a* white. You showed me that it is much more complex than one might think. Petria, I will not forget the adventures in Rio, the peaceful evening walk in a favela. I am very grateful to Aviva Burnstock (*Courtauld Institute of Art*), after all what is life without questions…Thanks to: Prof. van Asperen de Boer, Maartje Witlox (*ICN*), Linnaea Saunders (*Kress Fellow 2003-2004, Mauritshuis*), Margriet van Eikema Hommes, Gillian Osmond (*Queensland Art Gallery*), Ella Hendriks (*Van Gogh museum*), Klaas-Jan van den Berg (*ICN*), Michiel Verhoeve (*Universiteit Leiden, UL*), Jaap Haasnoot (*UL*), Prof. Jan Reedijk (*UL*), the members of the ´pigment group` and of course I would like to add Pieter Keune, my father, (*Reinwardt Academie*) to this list.

Tot slot wil ik natuurlijk mijn vrienden en familie bedanken voor gewoon alles! Allereerst mijn oma met wie ik nooit uitgepraat raak, mijn moeder voor wat ze me heeft meegegeven, mijn vader en Marie-Thérèse, mijn lieve zusjes Hilde en Françoise, Wilfred, mijn nichtje Marike en de familie van den Berg.

Jorrit, ik ben jou ook zeker dank verschuldigd voor de tijd die je altijd nam om over mijn werk te discussiëren. Jouw kritische blik, gedrevenheid en enthousiasme waren (en zijn) zeker een toevoegende waarde. Ook je goeie zorgen en je vrolijke noot maakte mijn schrijfperiode zeer aangenaam. Jouw laatste zin in jouw proefschrift heb je dubbel en dwars waargemaakt!

Bedankt,

Katrien

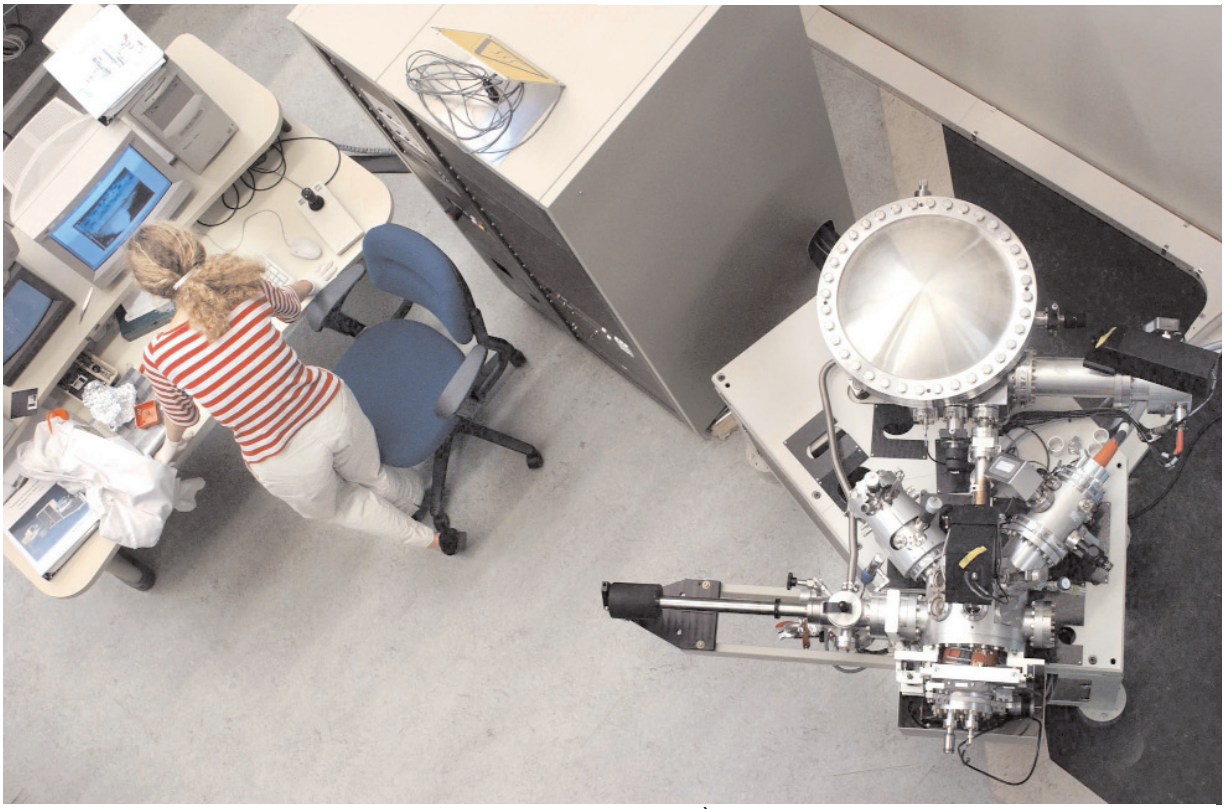

de Volkskrant, zaterdag 4 september 2004 (foto: R. Rutting)

Figures in colour

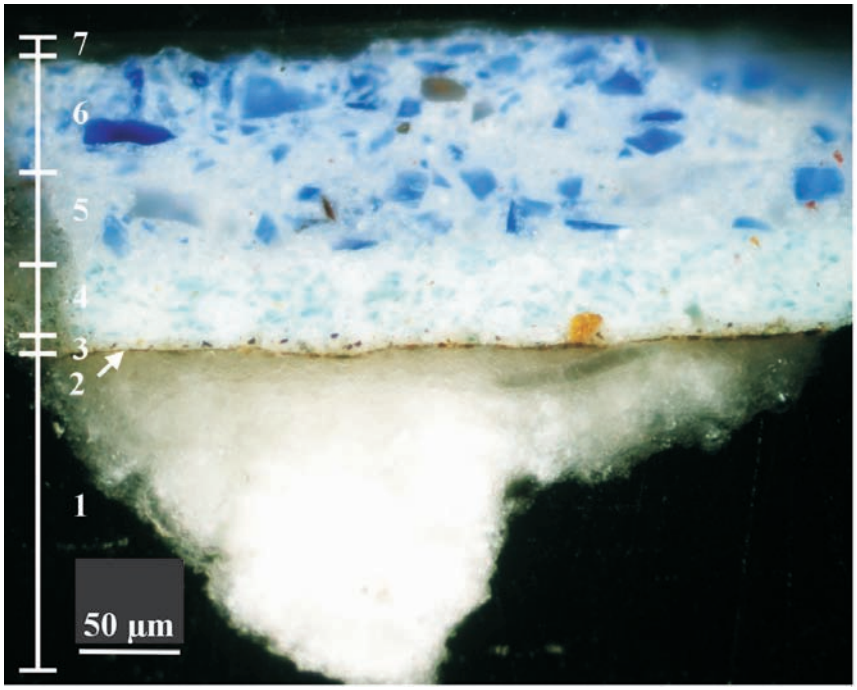

Fig. 2.1 Light microscopic image of paint cross-section van der Weyden (A166/1b); seven layers in this paint cross-section can be distinguished and are numbered from top to bottom (layers 1-7).

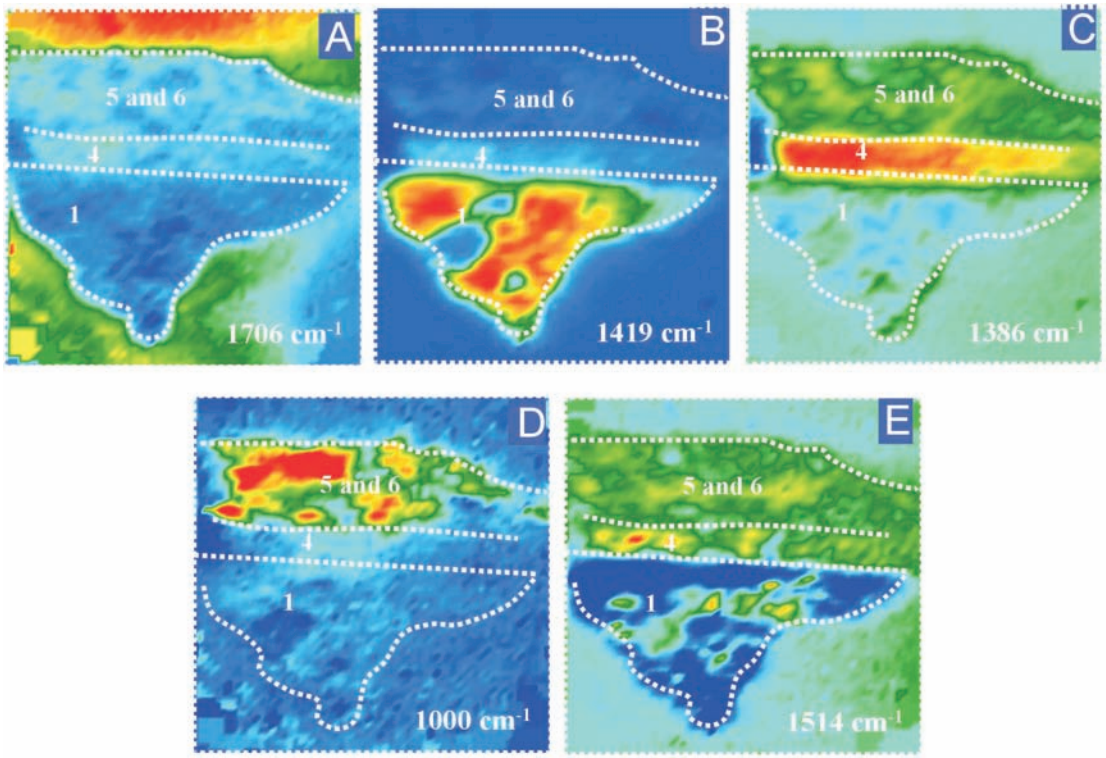

Fig. 2.2 Reflection FTIR-images; false colour images. Red represents a high absorption; FTIR-image (a) at 1706 cm^{-1} represents the embedding medium, (b) at 1419 cm^{-1} and (c) at 1382 cm^{-1} show the presence of carbonates. The FTIR-image (d) at 1000 cm^{-1} images the silicon-oxygen vibration and (e) at 1514 cm^{-1} the asymmetric vibration of lead carboxylate. The layers (1, 4, 5 and 6), which can be discerned, are indicated in the images.

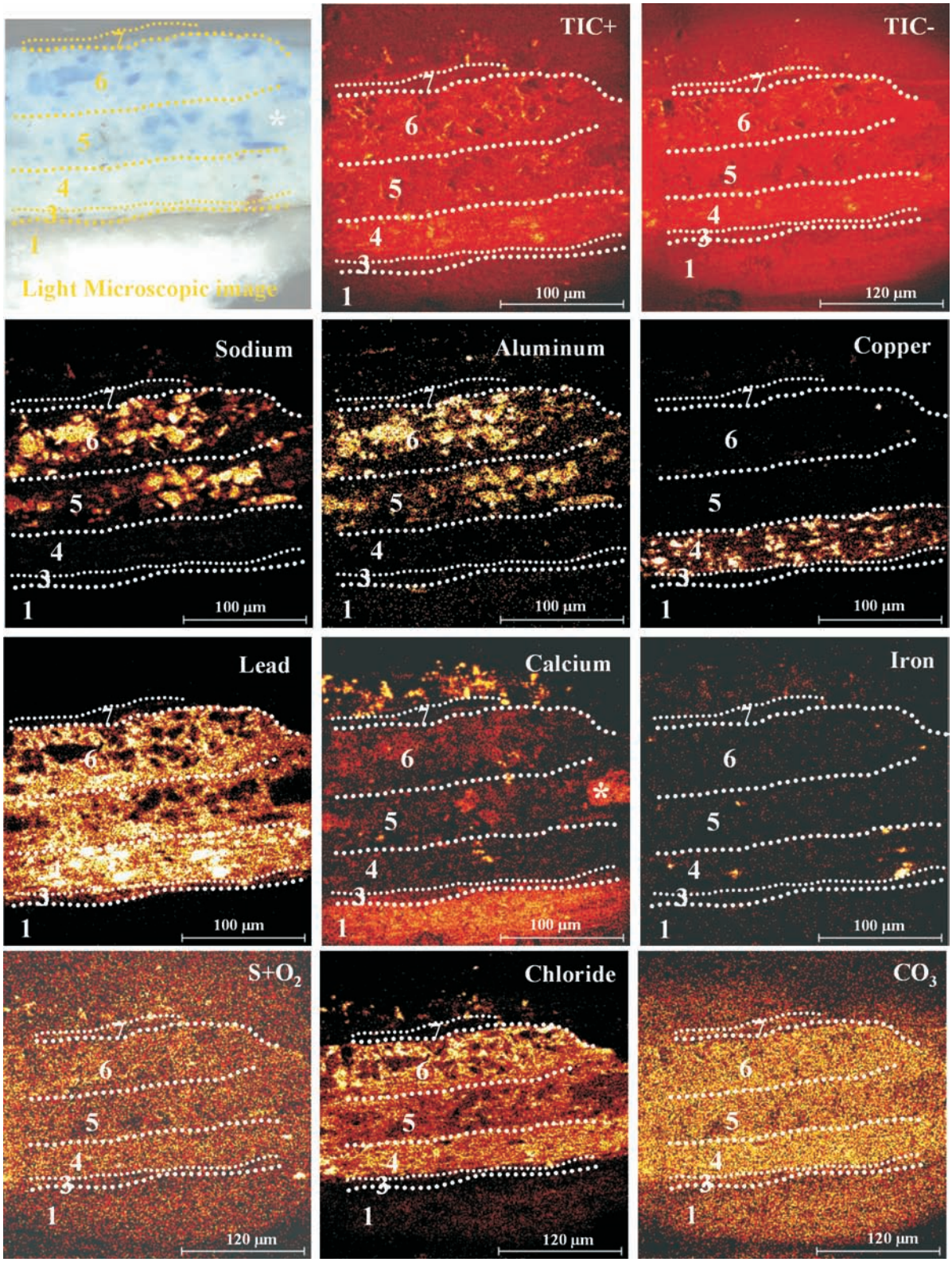

Fig. 2.7 SIMS images showing the spatial distribution of the total ion counts (TIC+ and TIC-), sodium, aluminium, copper, lead, calcium, iron, sulphur, chloride and carbonate detected in the SIMS spectra of the paint cross-section van der Weyden in positive (250 x 250 µm²) and negative mode (300 x 300 µm²). The layers (1, 3-7) detectable with SIMS are indicated in the images. Yellow represents high intensity and black low yields.

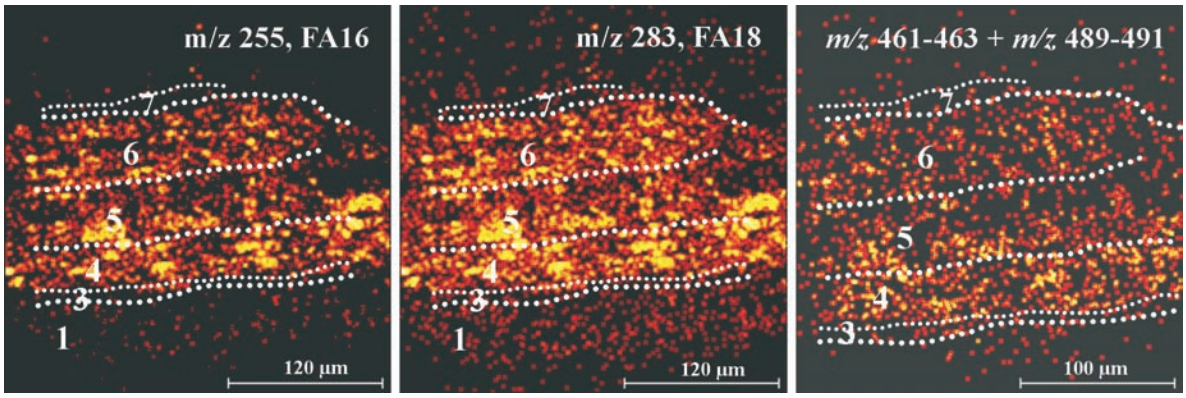

Fig. 2.8 SIMS images showing the spatial distribution of deprotonated palmitic acid (m/z 255) and stearic acid (m/z 283) and a sum image of palmitic and stearic acid lead soap (m/z 461-463, 489-491).

Fig. 4.1 Detail of 'Triumphal Procession with Sacrificial Bull' by P. de Grebber (1650) (Oranjezaal, Huis Ten Bosch Palace, The Hague, The Netherlands) showing grayish strokes on top of the red dress. These highlights consist of blackened vermilion. Photo: L. Speleers, Stichting Restauratie Atelier Limburg (SRAL), Maastricht, The Netherlands.

Portrait of a Young Woman by Peter Paul Rubens (1620s) displayed in Royal Picture Gallery Mauritshuis, The Hague (inv. no. 251).

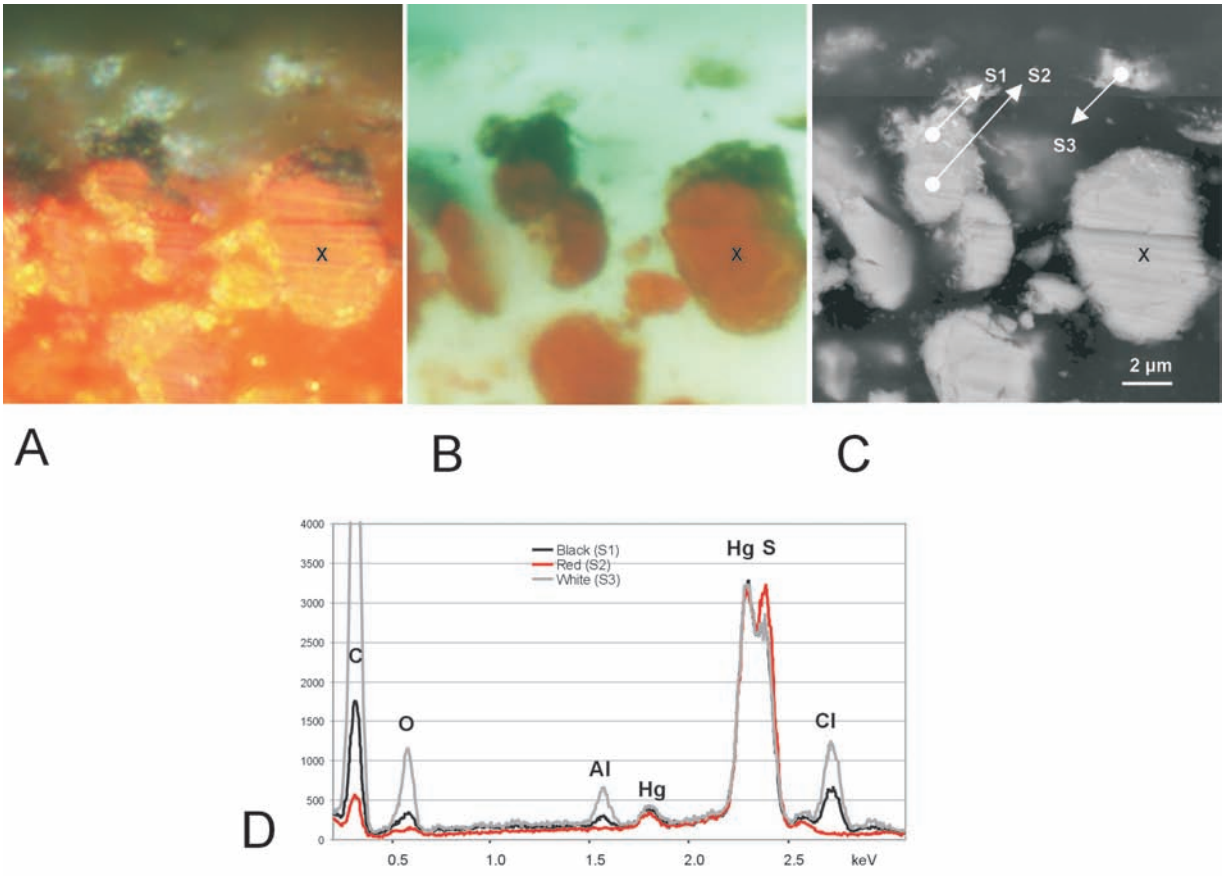

Fig. 4.2 Light microscopic image under white light (A) and UV illumination (B) illustrating the partial photodegradation of a vermilion particle. The backscattered electron image (BSE) (C) shows the structural difference between the red and the black area. The horizontal lines are due to polishing, the text refers to the particle marked X. EDX spectra of spot analyses (D) in black (S1), red (S2) and white (S3) area demonstrate the different elementary compositions of the native material and the reaction products.

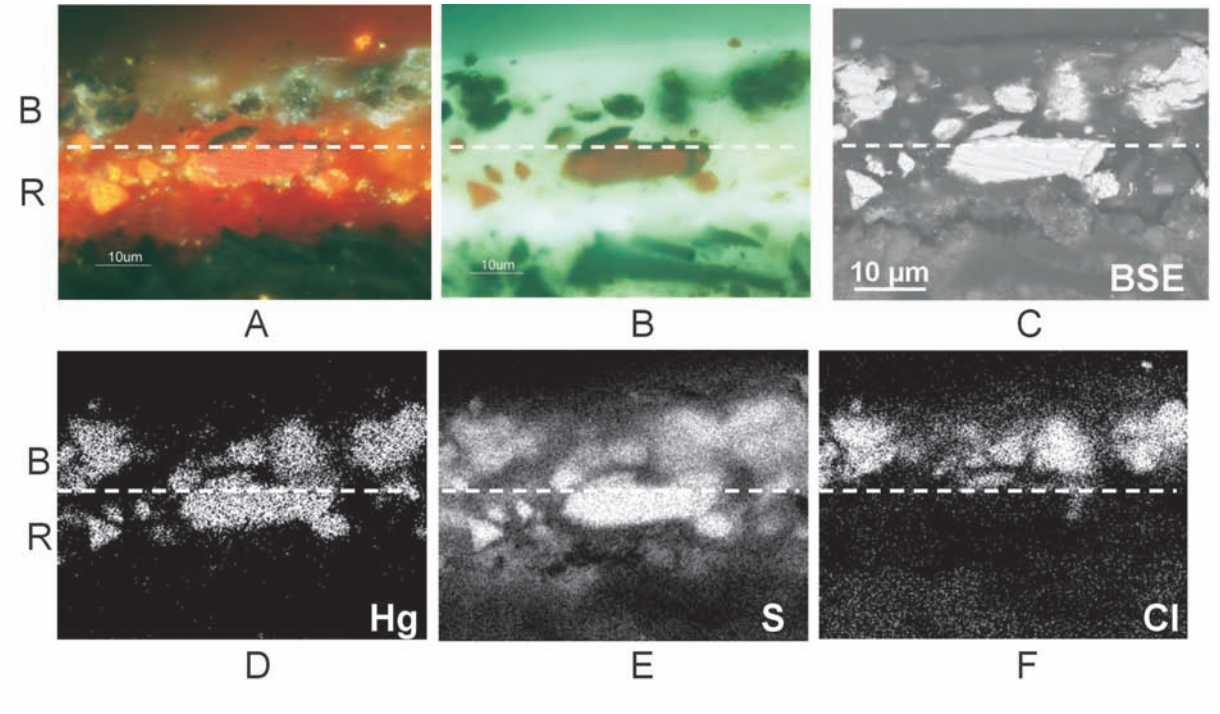

Fig. 4.3 The light microscopic images under white light (A) and UV light (B) illumination and backscattered electron image (BSE)(C) of the partially degraded vermilion paint in paint cross-section MH251/26 corresponding with the area analysed by EDX imaging. X-ray maps of intact (R) and blackened (B) vermilion in the layer reveals the spatial distribution of mercury (Hg L)(D), sulphur (S K)(E) and chlorine (Cl K)(F).

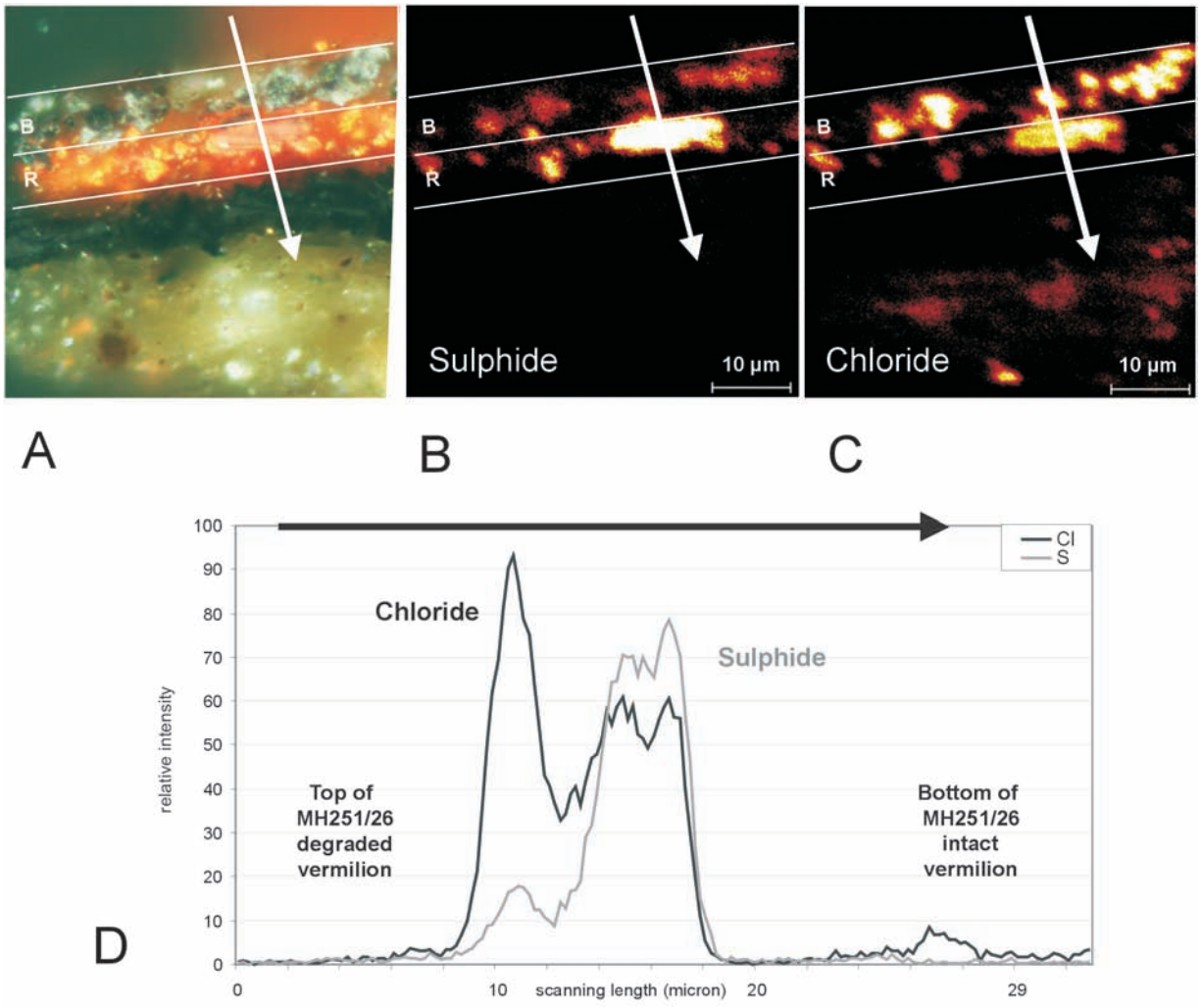

Fig. 4.4 The arrow in the light microscopic image (A), which is representing the scanned SIMS area of the partially degraded vermilion paint in MH251/26, indicates the direction of the line scan. SIMS images of the sulphide (B) and chloride (C) represent the distribution of these ions over the partially degraded vermilion paint layer. The line scan (D), illustrates the distribution of chlorine and sulphur from top to bottom in the paint cross-section.

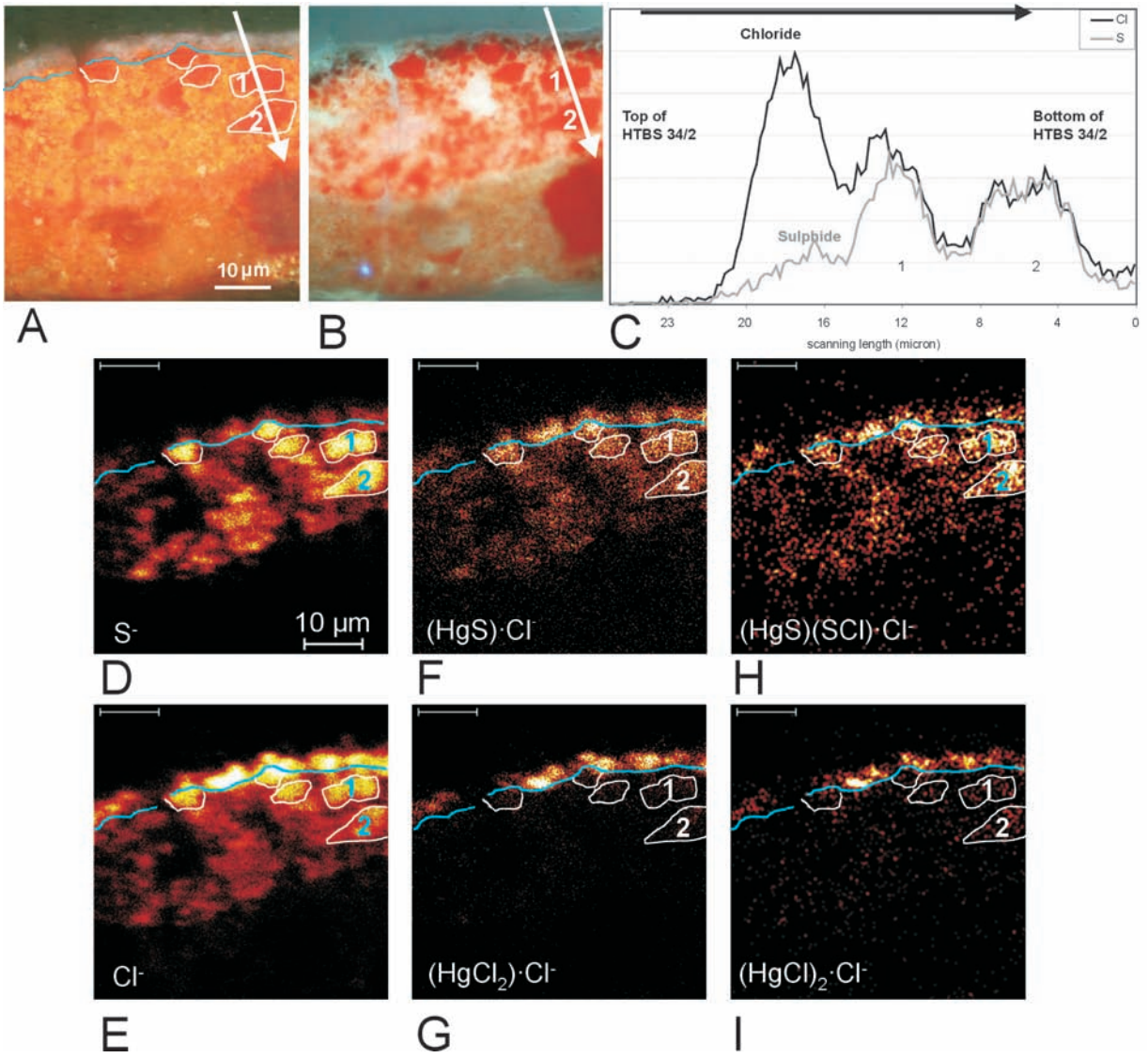

Fig. 4.5 Distribution of sulphur and chloride and the molecular distribution in a partially degraded vermilion paint; the arrow in the light microscopic image (A) and UV-light image (B), which is representing the scanned SIMS area, indicates the direction of the line scan (C). The negative SIMS image of mercury-halogen cluster ions elucidates the position of S^- (D), Cl^- (E), $(HgS)Cl^-$ (F), $(HgCl_2)Cl^-$ (G), $(HgS)(SCl)Cl^-$ (H), $(HgCl)_2Cl^-$ (I) in the partially degraded vermilion paint. The numbers 1-4 in the SIMS images refer to vermilion particles in the corresponding light microscopic images.

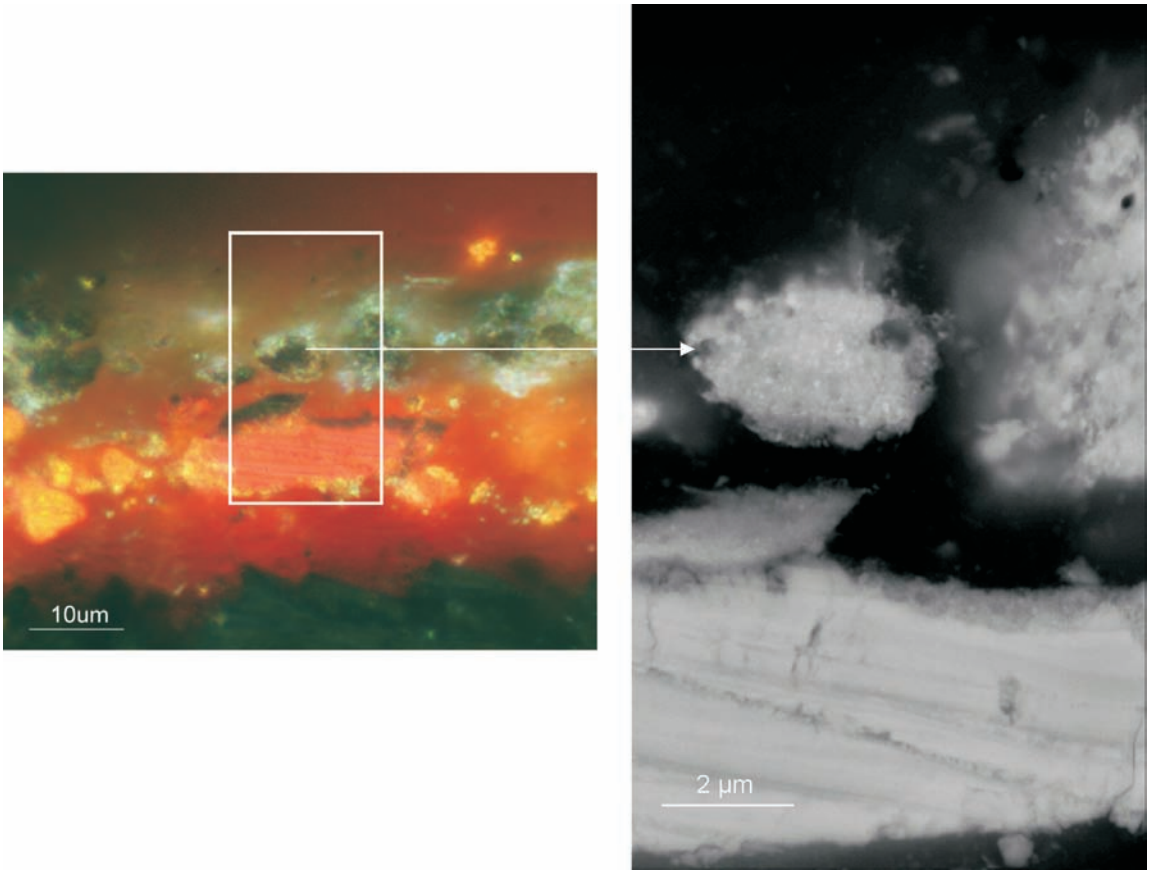

Supplementary Fig. 4.1 The BSE-image visualises a black particle containing hotspots of smaller than 100 nm. These hotspots are nanoparticles of metallic mercury.

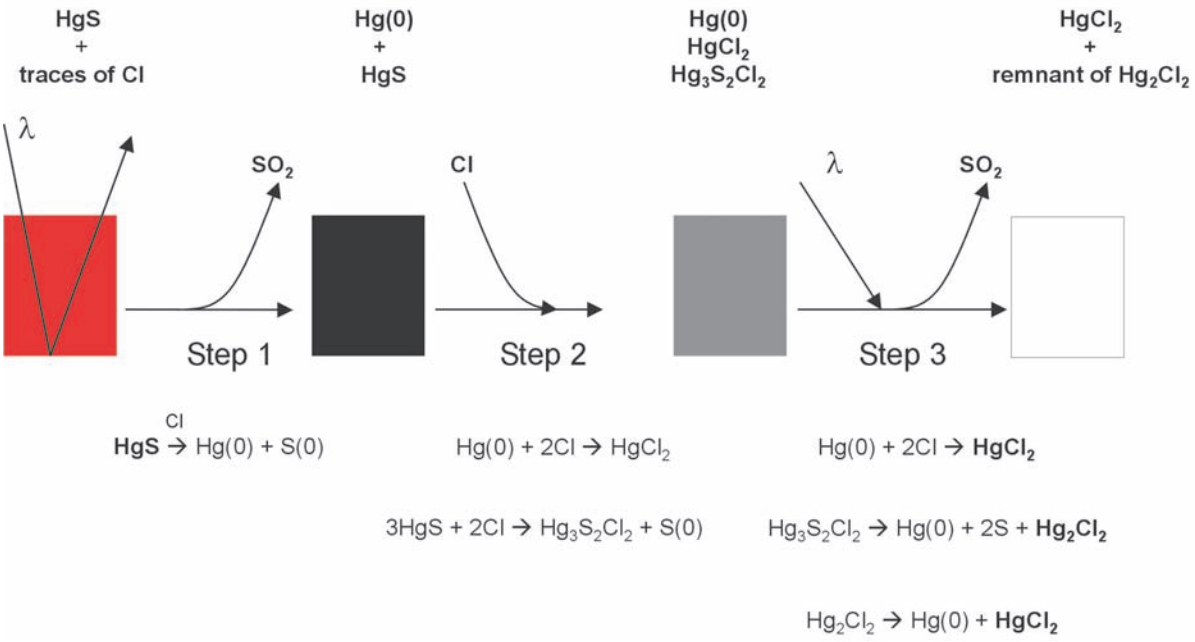

Fig. 4.7 Scheme of the proposed mechanisms of the degradation process of the red vermilion into a black and finally a white product.

'The Anatomy Lesson of Dr. Nicolaes Tulp' by Rembrandt van Rijn (canvas, lined) displayed in Royal Picture Gallery Mauritshuis, The Hague, The Netherlands (inv. no. 146).

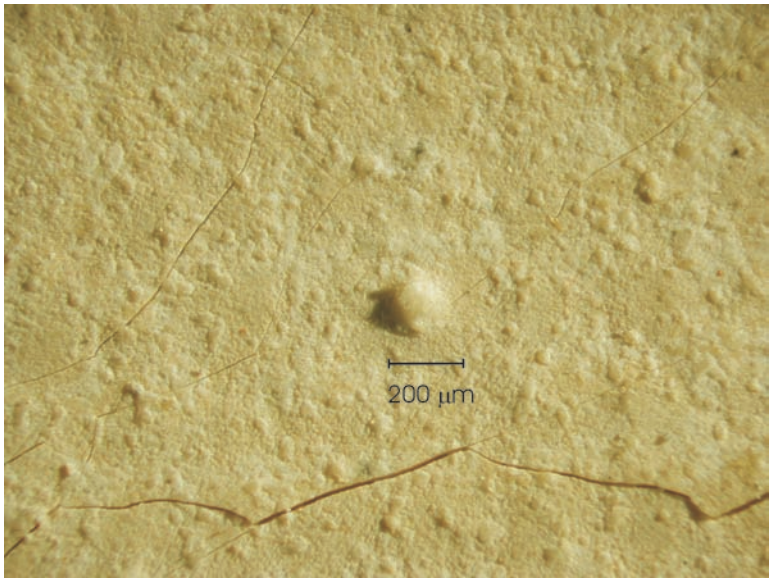

Detail of a residual piece of commercial preprimed canvas used by F.E. Church in the middle a large aggregate protruding through the paint surface. The canvas is part of the F.E. Church estate in Olana (near Hudson, New York)(photo: Dr. E. Ferreira, AMOLF).

'Herald with trophy, medallion and cartouche containing pictures of the triumph of Frederik Hendrik at Breda (1637) and at Gennep (1641)' painted by Christiaen van Couwenbergh (1651, canvas) is part of the paintings ensemble in the Oranjezaal of the Royal Palace Huis ten Bosch, The Hague, The Netherlands (inv. no. SC/1307).

The triptych (oak panel) by unknown nothern painter is displayed in Sherborne Abbey Almshouse (Dorset, UK) and owned by the National Trust.

The reverse of the panel painting 'The Bad Chief' (fragment) attributed to the 15th century Flemish artist the Master of Flémalle is displayed in the Städelsches Kunstinstitut in Frankfurt, Germany (Inv. nr. 886) (photo: Prof. van Asperen de Boer).

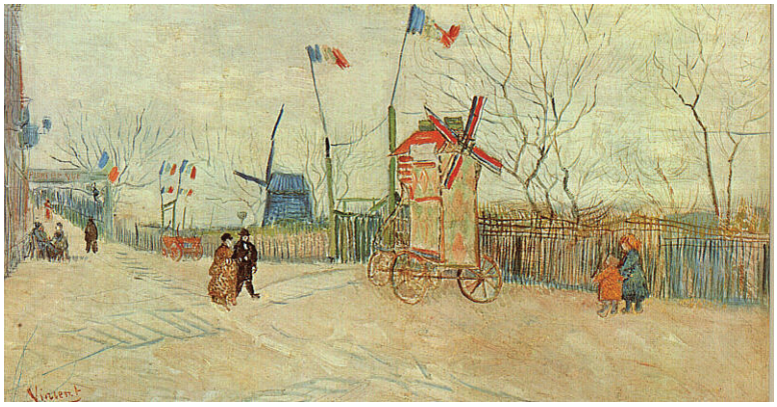

Impasse des deux frères and Moulin de Poivre (F347) (canvas, wax lined) by Vincent van Gogh (March - mid April 1887) The painting is in the collection of the Van Gogh Museum (Vincent van Gogh Foundation) in Amsterdam, The Netherlands

'Sydney Harbour, overlooking Taylor's Bay' by the Australian artist W. Lister Lister (canvas, 1912) is on display in the Queensland Art Gallery, Brisbane, Australia

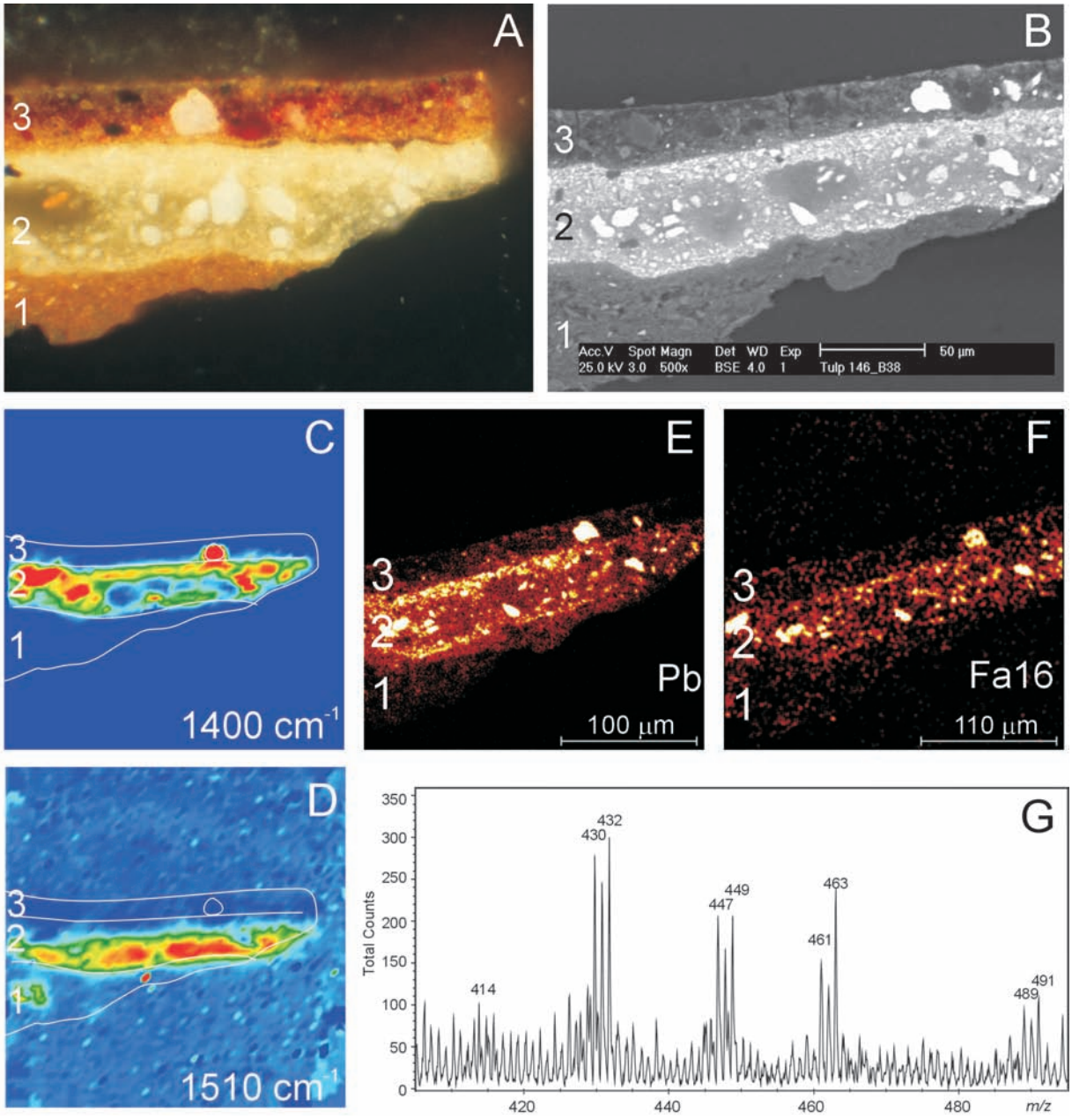

Fig. 5.1 Analytical imaging studies of paint cross-section MH146/B38 taken from 'The Anatomy Lesson of Dr. Nicolaes Tulp' by Rembrandt van Rijn (1632). White light microscopic image (A) and backscattered electron image (BSE-image) (B) reveal the layer buildup and granulometry. FTIR images represent carbonate carbonyl groups at 1400 cm^{-1} (C) and lead carboxylates at 1510 cm^{-1} (D) (red represents high and blue low intensity). An outline illustrates the three layers and the circle in layer 3 is indicative for the large lead white particle in this layer. SIMS-images represent lead (+; m/z 206-208) (E) and deprotonated palmitic acid (-; m/z 255) (F). A part of the positive SIMS spectrum presents Pb_2O at m/z 426-432, Pb_2O_2H at m/z 443-449, $PbOOC(CH_2)_{14}CH_3$ at m/z 461-463 and $PbOOC(CH_2)_{16}CH_3$ at m/z 489-491 (G).

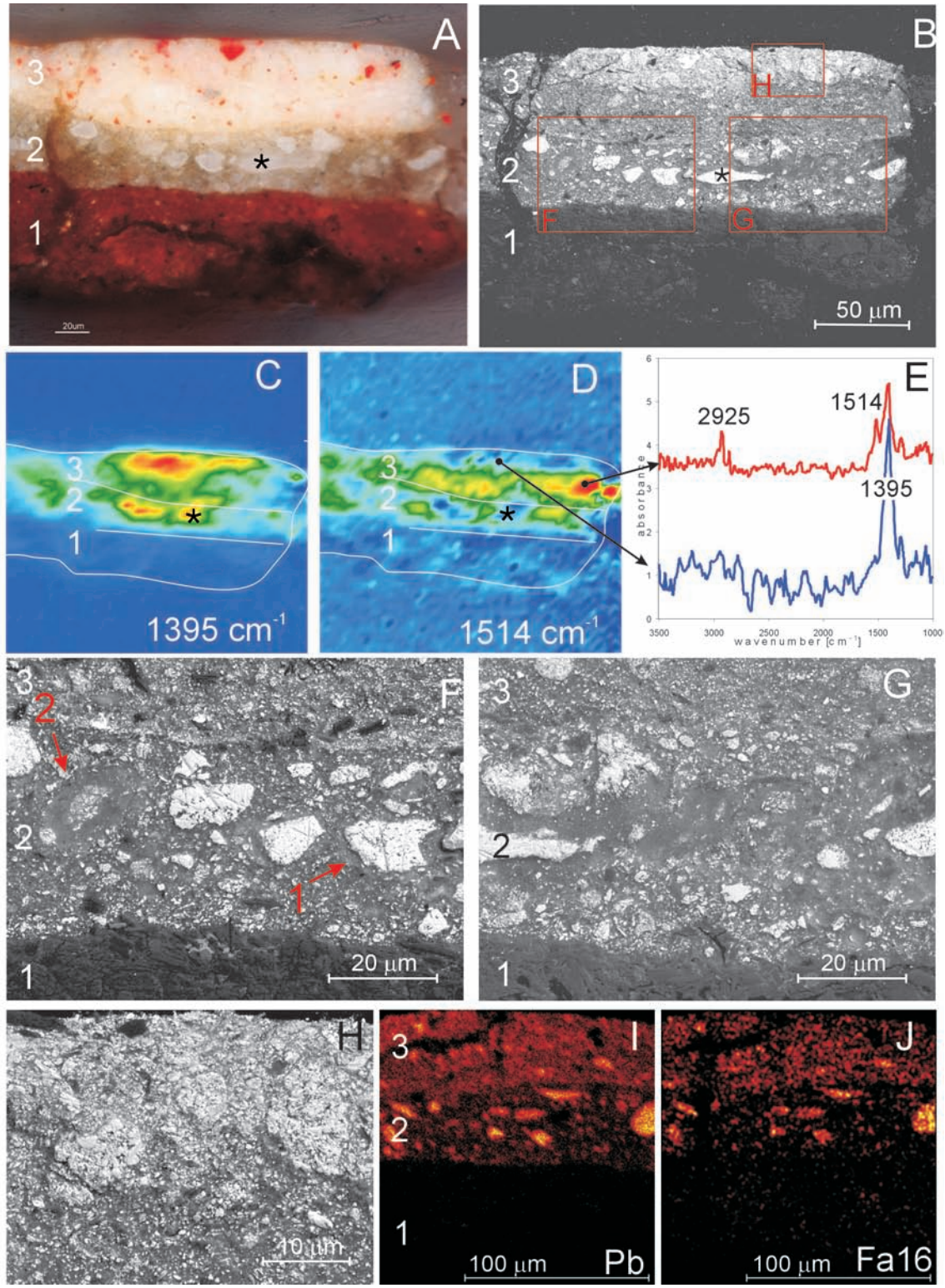

Fig. 5.2 Light microscopic image (A) and corresponding BSE-image (B) elucidates paint cross-section MH146/B39. FTIR images of carbonates at 1395 cm^{-1} (C) and lead carboxylates at 1514 cm^{-1} (D) reveal a partially saponified layer 3. Two FTIR spectra (E) derive each from a pixel in the FTIR image, indicated with an arrow. The asteriks indicates a large lead white particle in layer 2. BSE-images represent detailed areas of layer 2 (F, G) and layer 3 (H) (detail of layer 3 is indicated with a square in fig. 5.2b). SIMS image of lead (+; m/z 208) and deprotonated palmitic acids (-; m/z 255) are depicted in Fig. 5.2I and J, respectively.

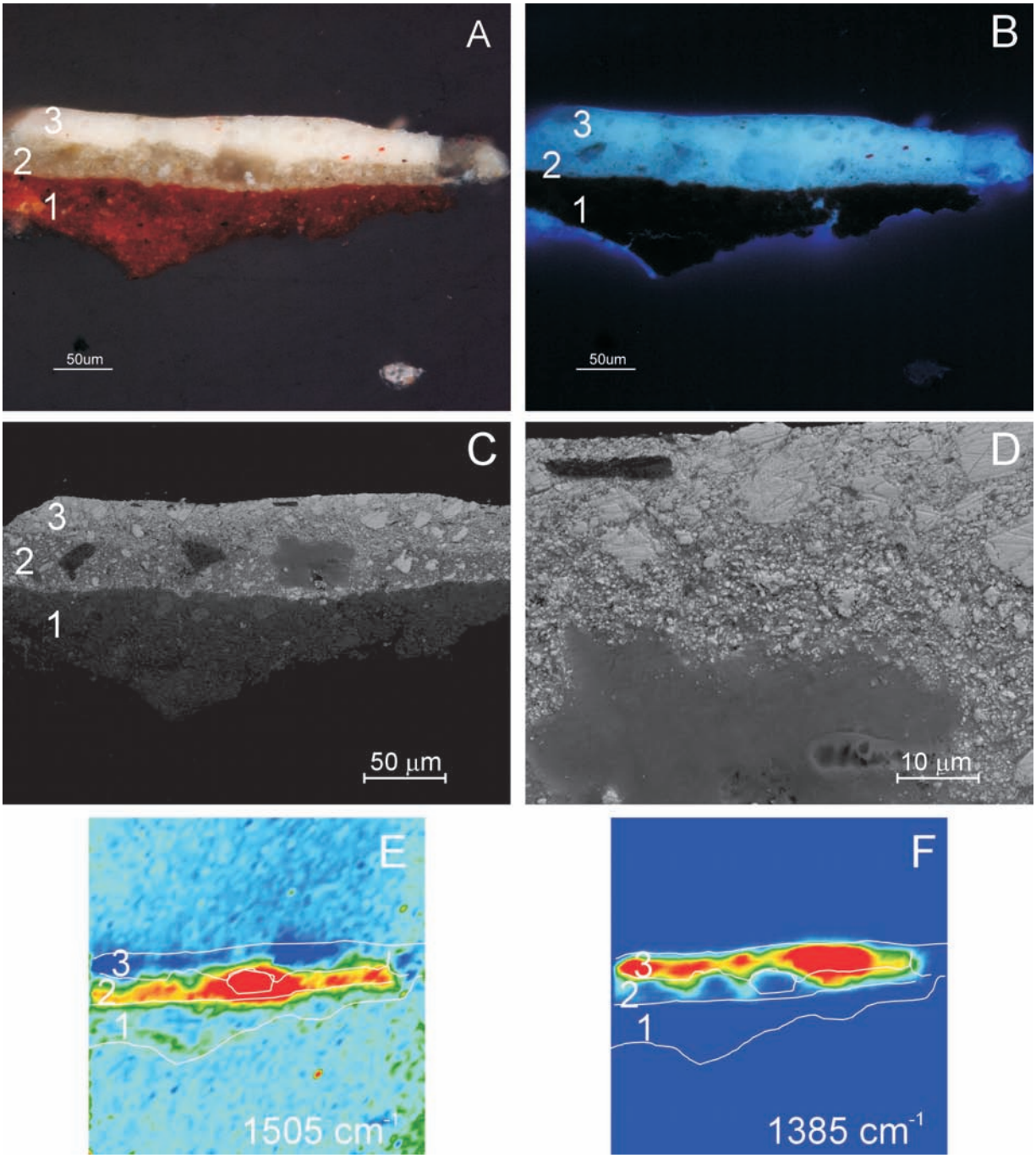

Fig. 5.3 Paint cross-section MH146/B37 contains a lead soap aggregate in the layer 2 and in layer 3, which is visible in the white light (A) and UV microscopic image (B). BSE-image (C) reveals different granulometry in the two lead white-containing layers 2 and 3. BSE-image (D) of a magnified area elucidates the top side of the aggregate positioned in layer 3. Fig. 5.3E and F represent the FTIR images of lead carboxylate at 1505 cm^{-1} (E) and carbonates at 1385 cm^{-1} (F). The loop in the outline indicates the position of the aggregate.

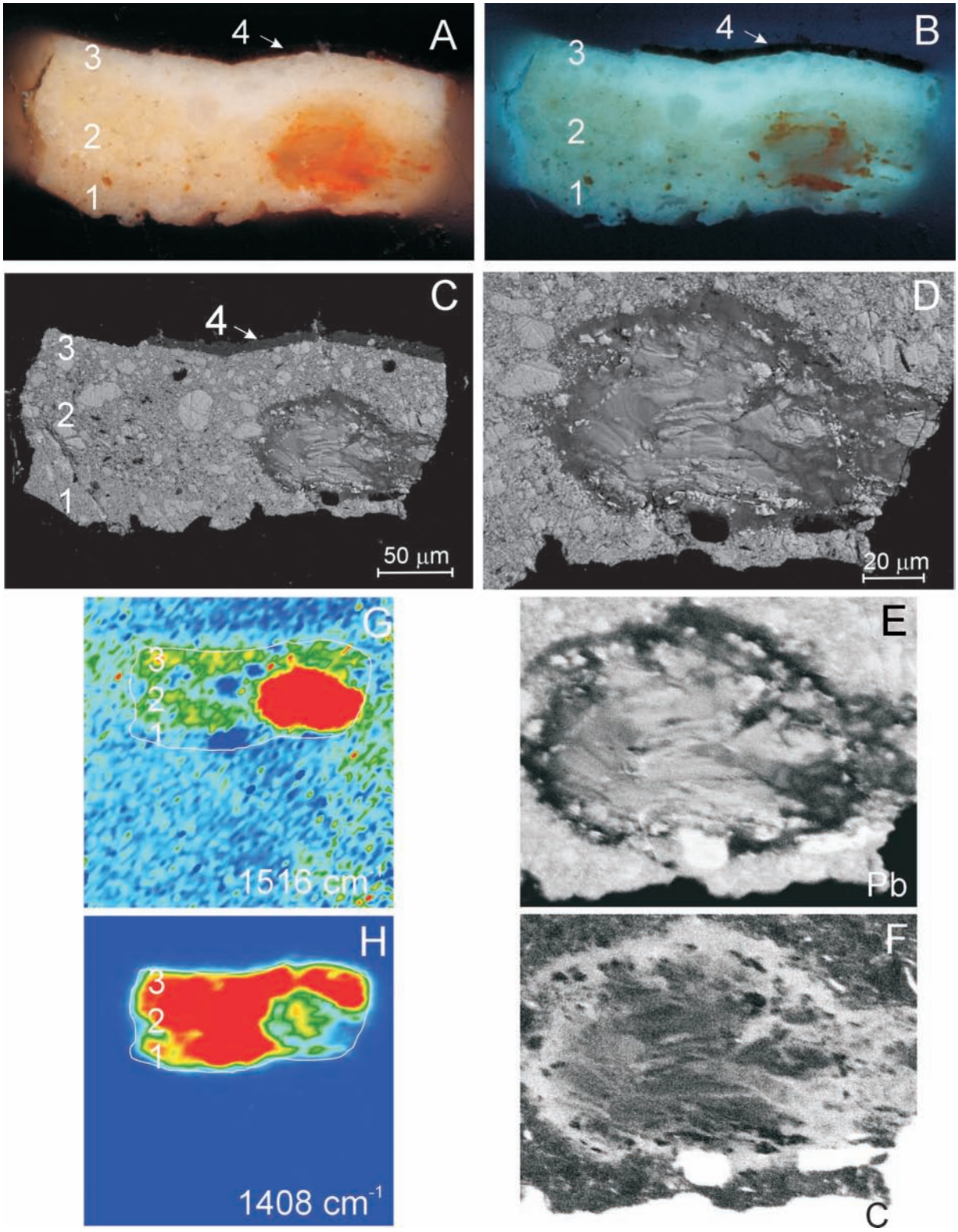

Fig. 5.4A-H Paint cross-section HSTB43/3 originating from 'Herald' (south-west) by Christiaen van Couwenbergh (1651) is depictured in the light microscopic images, white light (A) and UV (B), and in the corresponding BSE-image (C). BSE-image (D) and X-ray maps of lead (PbM) (E) and carbon (CK) (F) reveal the large lead soap aggregate. Lead carboxylates are detected and imaged with FTIR at 1516 cm^{-1} (G) and carbonates at 1408 cm^{-1} (H).

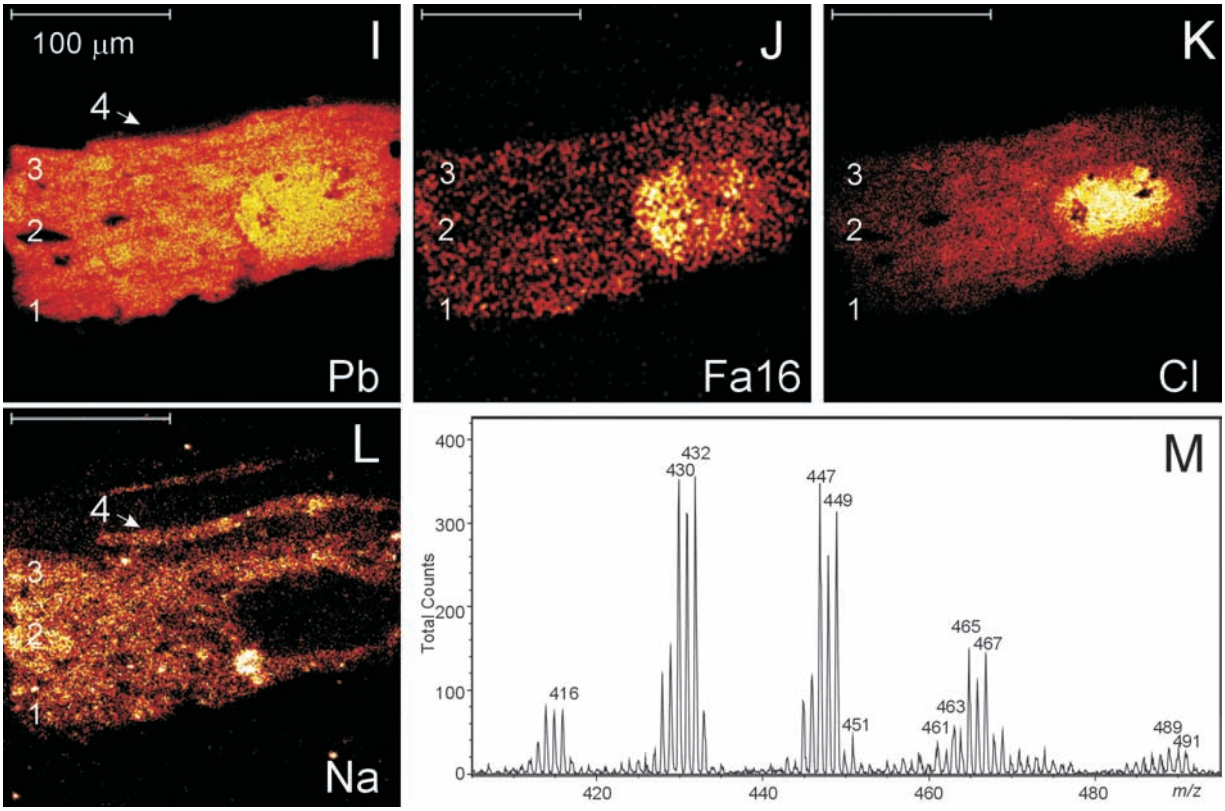

Fig. 5.4I-M SIMS images show the distribution of lead (+; m/z 208)(I), deprotonated palmitic acids (-; m/z 255)(J), chloride (-; m/z 35)(K) and sodium (+; m/z 23)(L). A partial positive SIMS spectrum presents Pb_2 at m/z 410-416, Pb_2O at m/z 426-432, Pb_2O_2H at m/z 443-449, Pb_2ClO (m/z 461-469), which overlaps with $PbOOC(CH_2)14CH_3$ at m/z 461-463 (M).

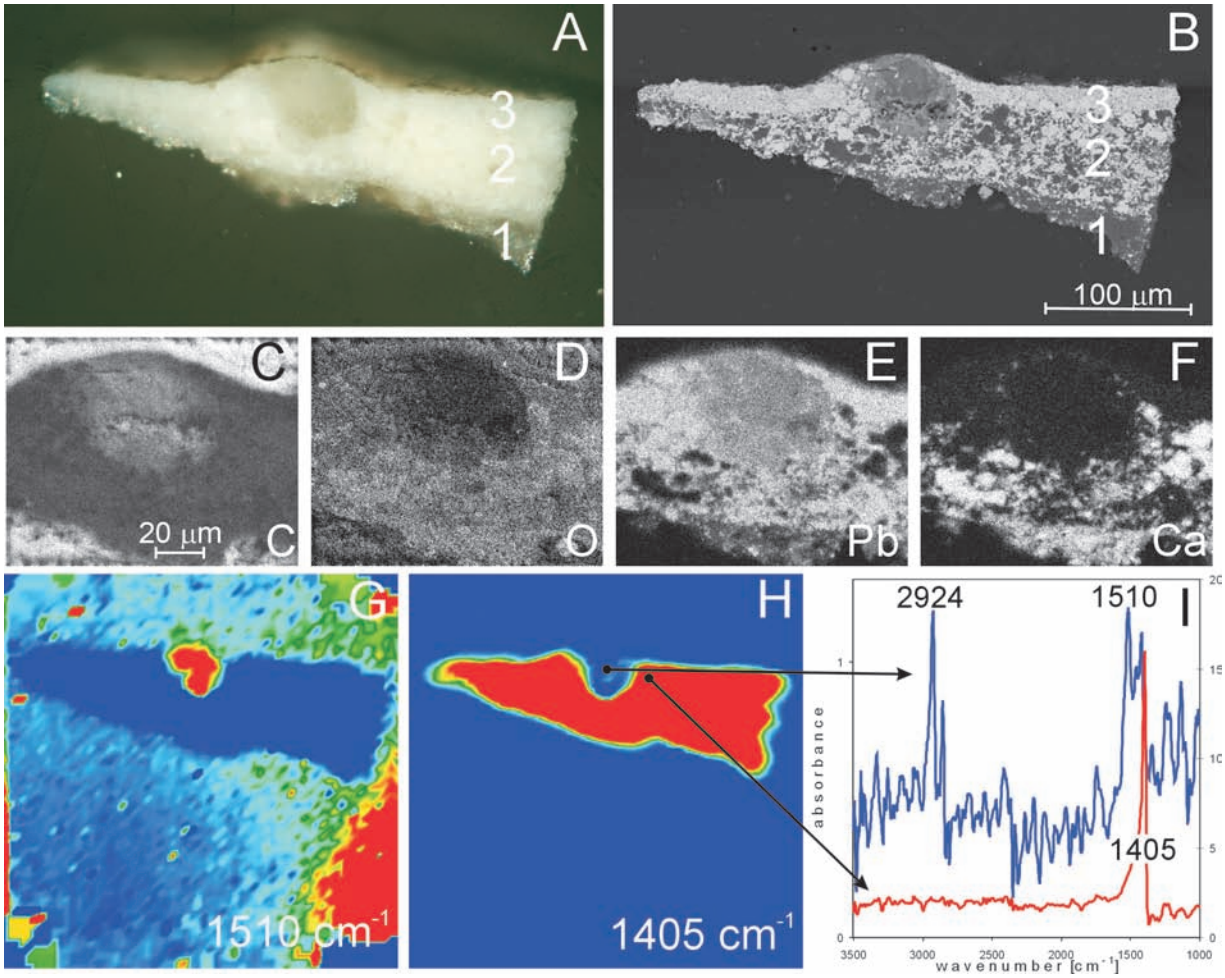

Fig. 5.5A-I A large lead soap aggregate is visible in the white light microscopic image (A) of a paint cross-section originating from the preprimed canvas used by Frederic E. Church (1826-1900). The BSE-image and X-ray maps of carbon (CK) (C), Oxygen (OK) (D), lead (PbM) (E) and calcium (CaK) (F) expose the particle and elemental distribution. FTIR images show lead carboxylates (G) in the aggregate and carbonates (H) in the rest of the paint sample. Two FTIR spectra derived from a single point in the aggregate and in the paint matrix (I).

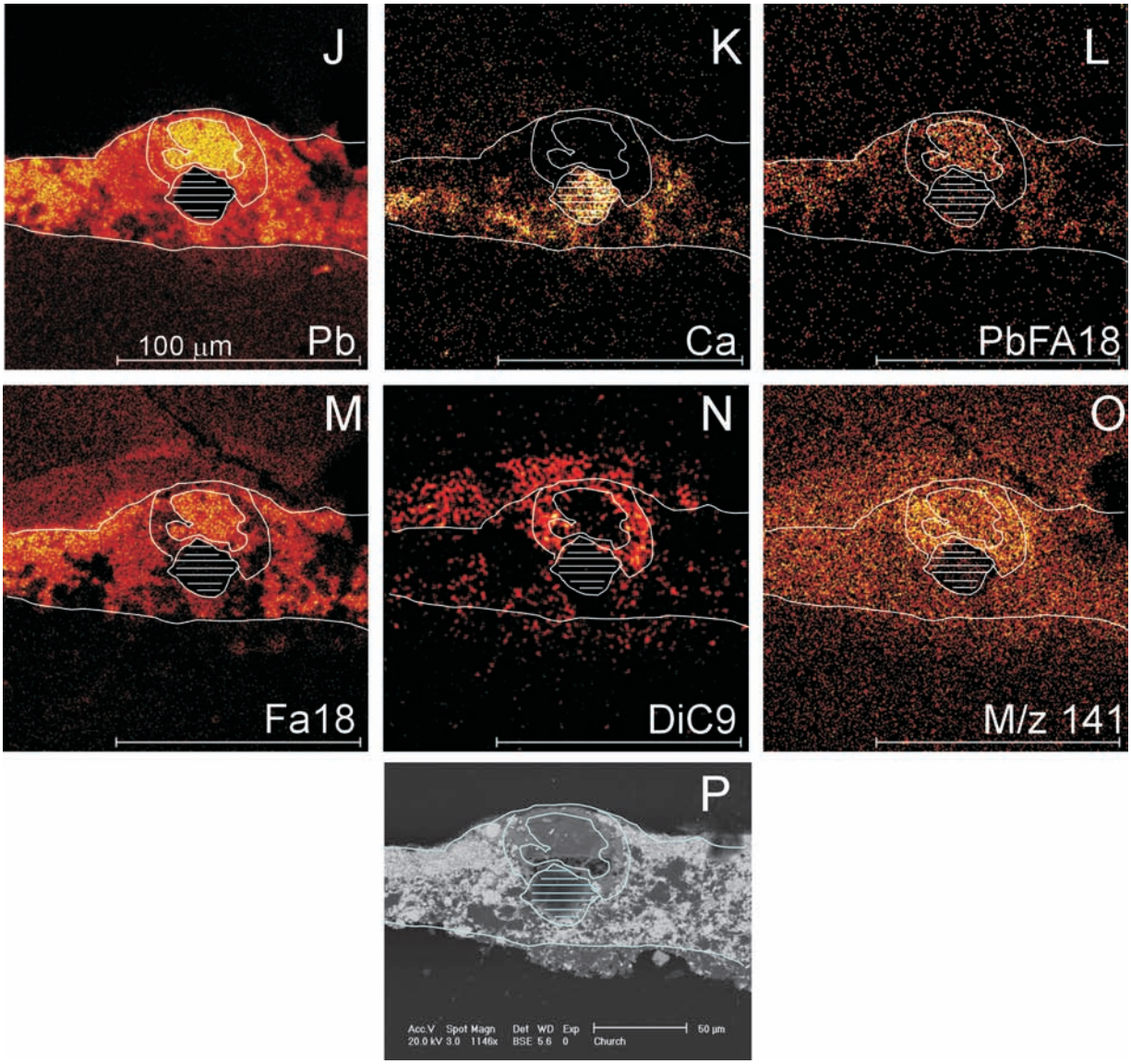

Fig 5.5J-P SIMS images of the gold-coated paint cross-section (2 nm) depicture lead (+; m/z 206-208) (J), calcium (+; m/z 40) (K) and lead stearic acid salt (+; m/z 489-491) (L), deprotonated stearic acid (-; m/z 283) (M), deprotonated azelaic acid (-; m/z 187) (N) and the $C_2H_3(CH_2)_5COO^-$ fragment ion of fatty acids (-; m/z 141) (O). An overlay derived from the corresponding BSE-image (P) is plotted over the SIMS images. The circular feature in the centre of the paint sample (indicated with the dashed area), an area on the right covering some of layer 3 and a scratch leading from middle top to middle right centre are sample preparation artefacts.

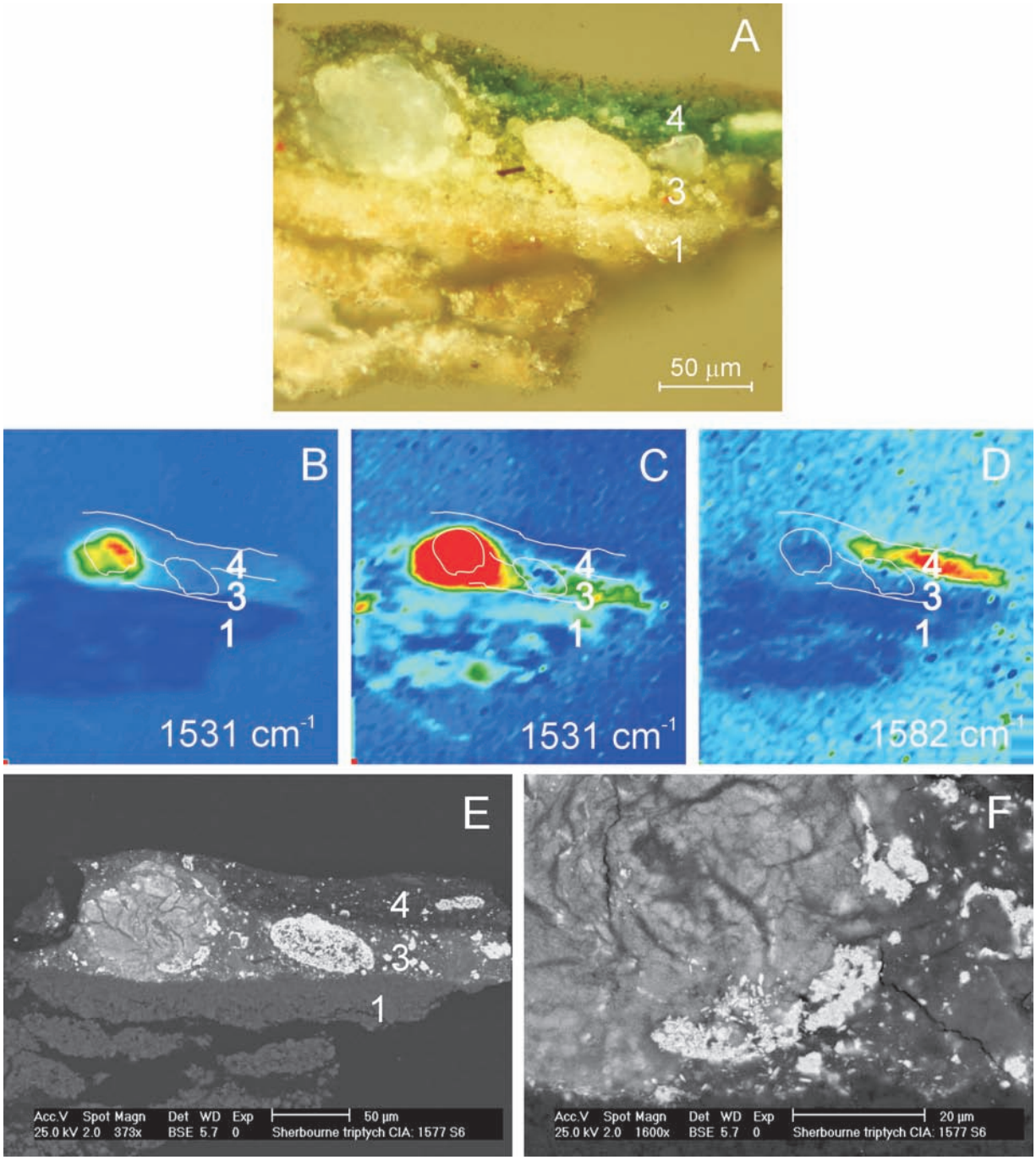

Fig. 5.6A-F The white light microscopic image (A) of the paint cross-section CIA 1577 RS06 derived from 'The Sherborne Triptych' (unknown northern painter 15th Century) elucidates a large lead soap aggregate and a porous residual lead-tin yellow particle in a lead-tin yellow-containing paint layer. FTIR images present lead carboxylate at 1531 cm^{-1} (B) (C, is overscaled) and copper carboxylate at 1582 cm^{-1} (D). An outline plotted over the FTIR image is deduced from the light microscopic image. BSE-images represent the paint cross-section (E) and a detail of the right part of the lead soap aggregate (F).

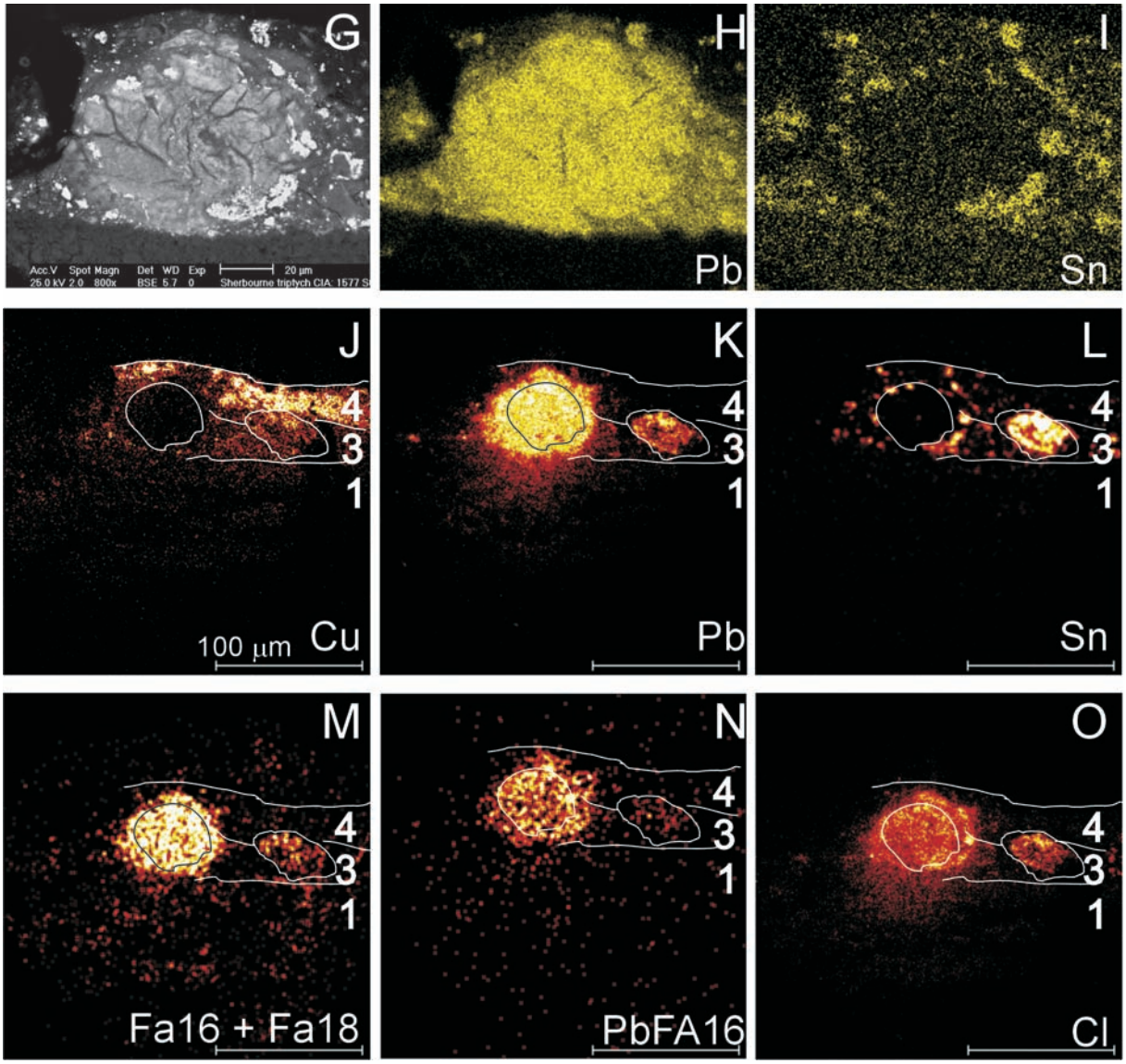

Fig. 5.6G-O BSE-image (G) and X-ray maps of lead (PbM) (H) and tin (SnL) (I) indicate the large lead soap aggregate. SIMS-images represent copper (+; m/z 63) (J), lead (+; m/z 208) (K), tin (+; m/z 52) (L), the sum of deprotonated palmitic and stearic acid (-; m/z 255 + m/z 283) (M), palmitic acid lead soap (+; m/z 461-463) (N) and chloride (-; m/z 35) (O).

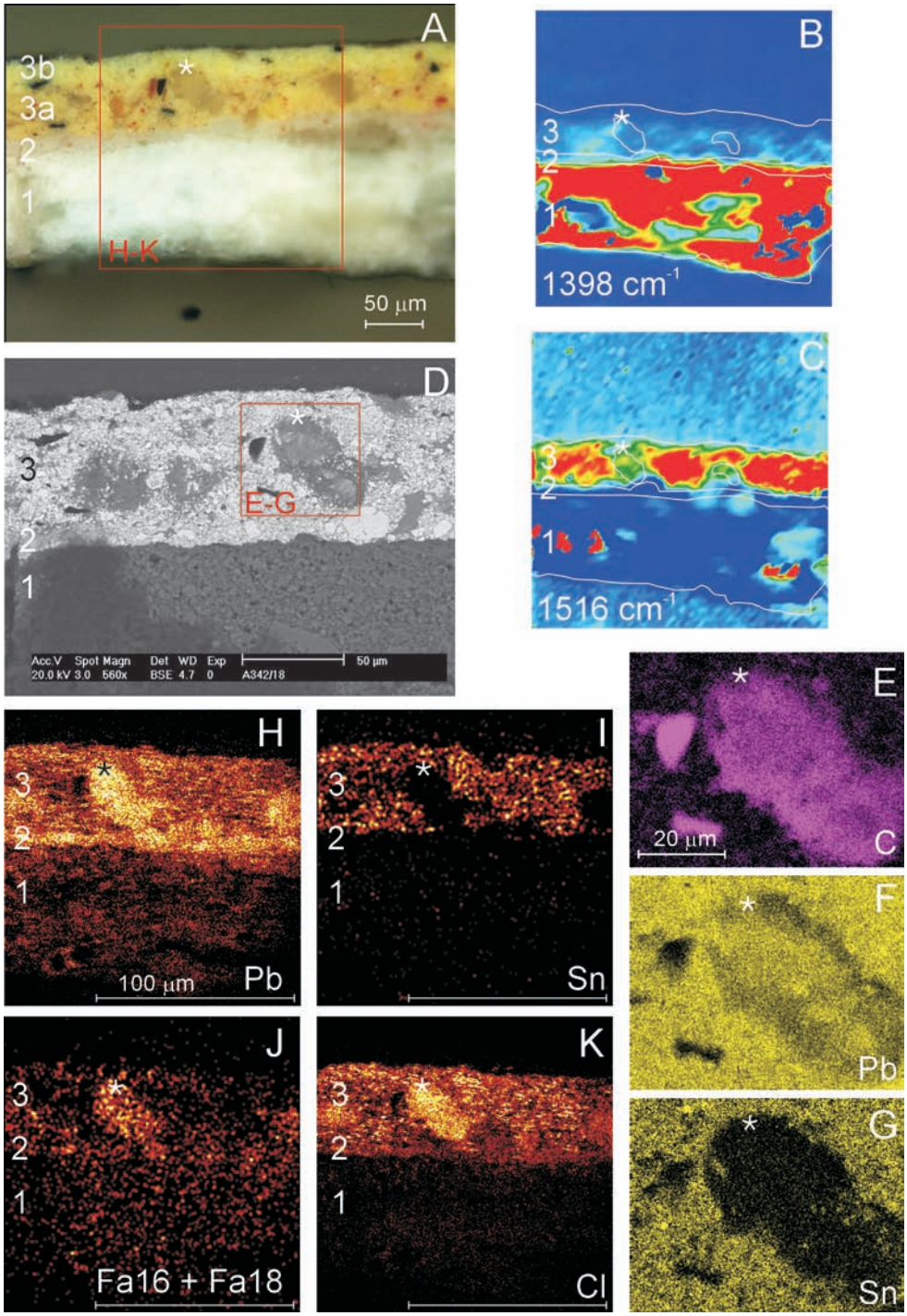

Fig. 5.7 Light microscopic image (A) elucidate paint cross-section A342/18. The asteriks in all images is indicative for the position of a large metal soap aggregate. FTIR images of carbonates at 1398 cm^{-1} (B) and lead carboxylates at 1516 cm^{-1} (C) reveal a saponified lead-tin yellow layer (3). An outline is plotted over the FTIR images; the two round features in layer 3 are indicative for two aggregates. The BSE-image (D) represents the paint cross-section. X-ray maps of carbon (CK) (E), lead (PbM) (F) and tin (SnL) (G) show details of a lead soap aggregate (square in Fig. 5.7B indicates the analysed area). SIMS-images represent lead (+; m/z 208) (H), tin (+; m/z 52) (I), the sum of deprotonated palmitic and stearic acid (-; m/z 255 + m/z 283) (J) and chloride (-; m/z 35) (K) (square in Fig. 5.7A illustrates the analysed area).

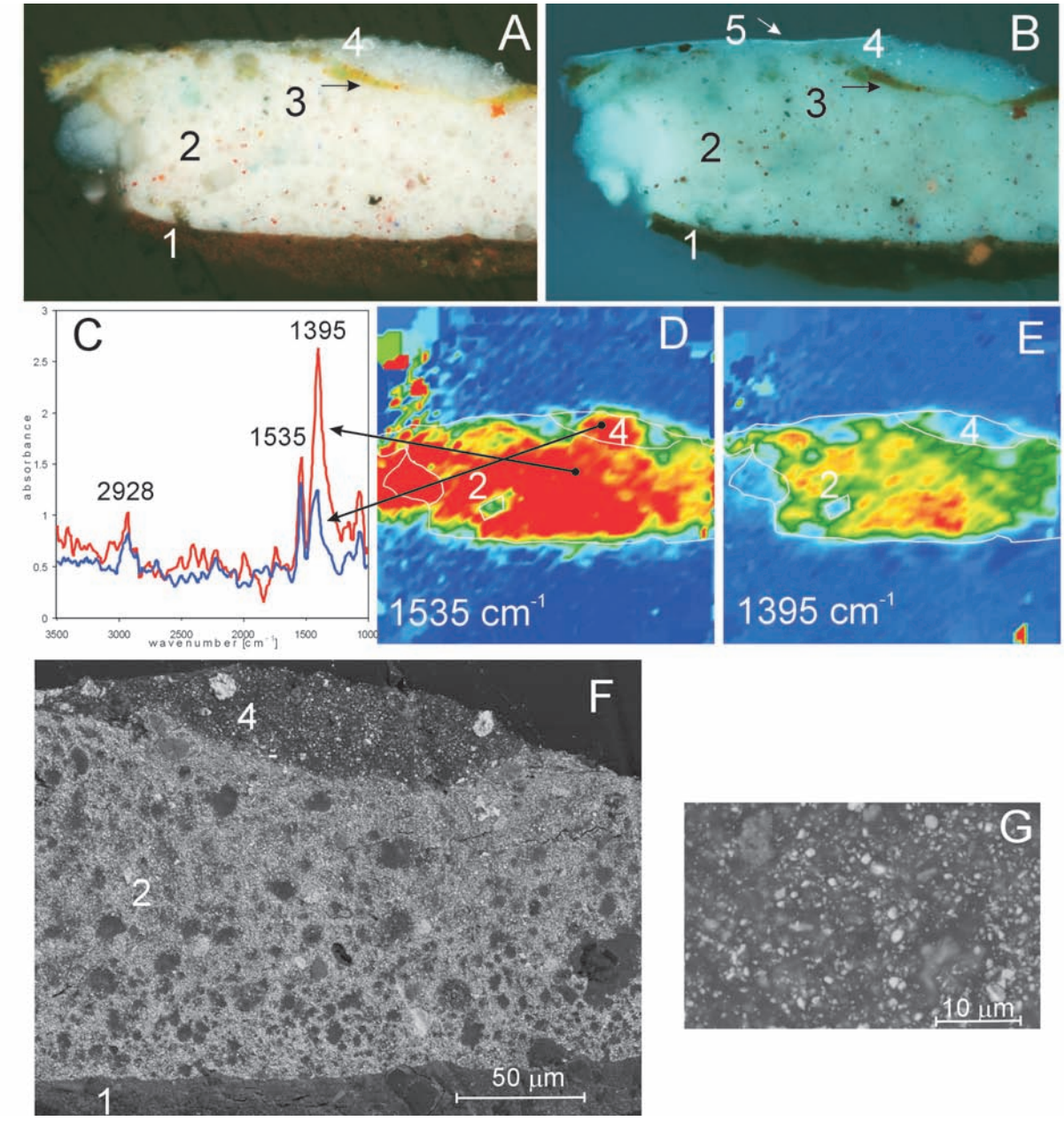

Fig. 5.8A-G Paint cross-section F347-1 originating from 'Impasse des deux frères and Moulin de Poivre' by Vincent van Gogh (1887) is depictured in the light microscopic images in white light (A) and UV (B). Two reflection FTIR spectra derived from a single point in layer 2 and layer 4 (C). FTIR images of metal carboxylates at 1535 cm^{-1} (D) and carbonates at 1395 cm^{-1} (E) reveal a saponified layer 2 and 4. BSE-image (F), (detail of layer 4 (G)) reveal the middle part of the paint cross-section.

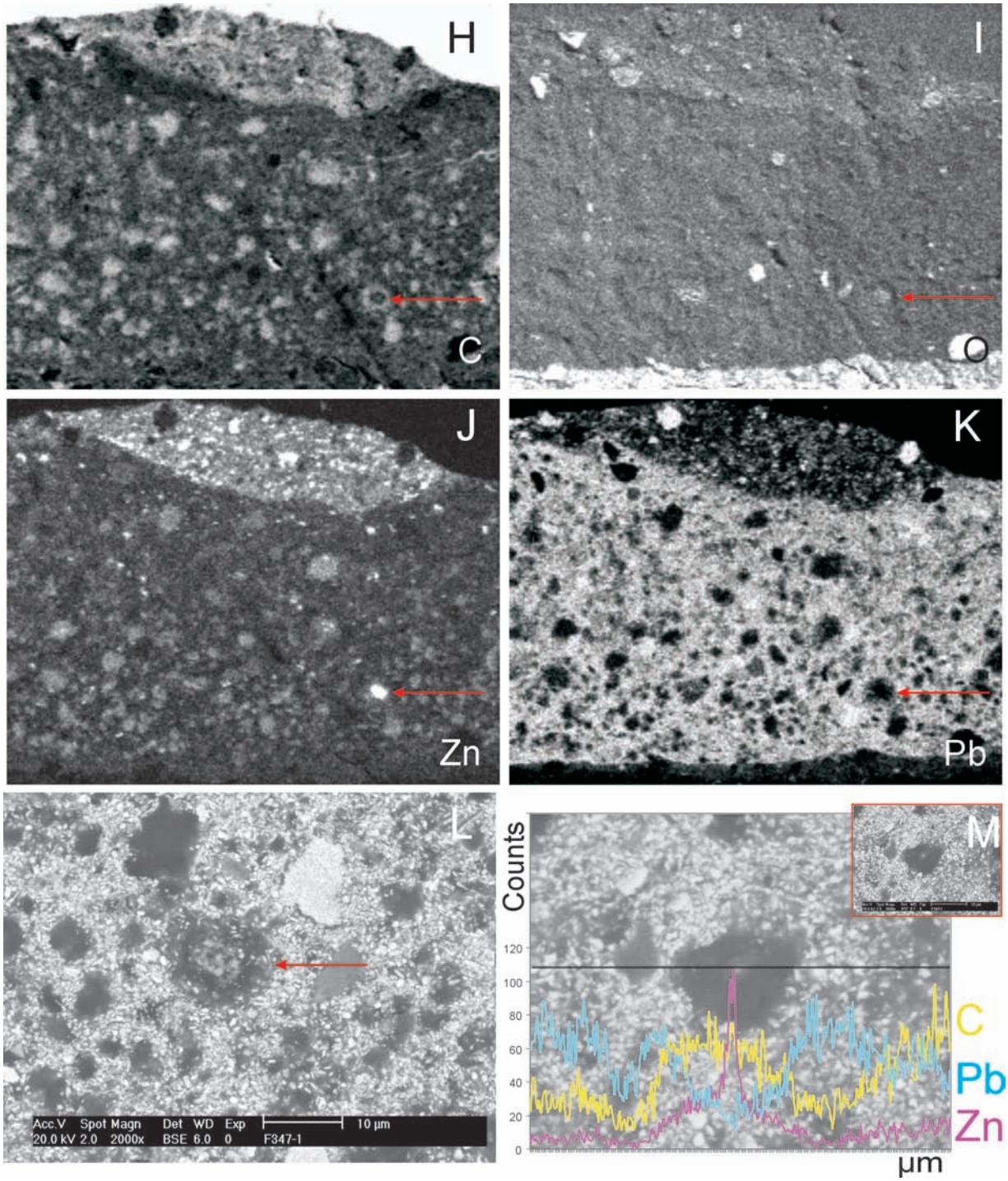

Fig. 5.8H-M BSE-image (F), (detail of layer 4 (G)) and corresponding X-ray maps of carbon (CK) (H), oxygen (OK) (I), zinc (ZnK) (J) and lead (PbM) (K) reveal the middle part of the paint cross-section. The BSE-image of a detail (indicated with an arrow in the X-ray maps) is depictured in Fig. 5.8L. Line scans (M) drawn over a zinc soap aggregate with a bright spot illustrate the distribution of carbon (yellow), zinc (purple) and lead (cyan).

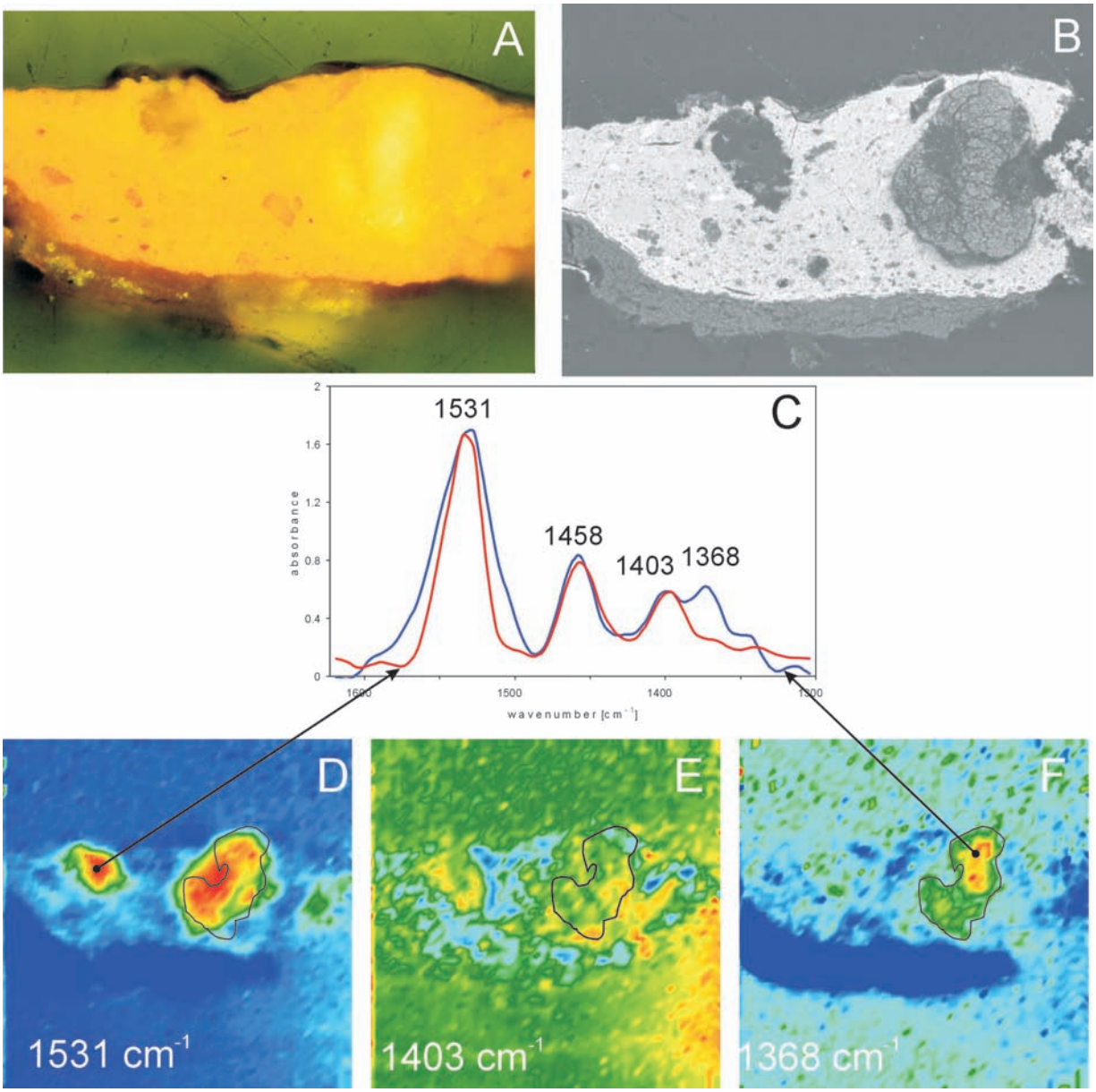

Fig. 5.9 White light microscopic image (A) and BSE-image (B) of paint cross-section KM224/2a from the 'Les Alyscamp' by Vincent van Gogh (F486) reveal two large zinc soap aggregates. A detail of the FTIR spectrum (C) derived from a spot on the left aggregate (red line) shows peaks at 1531, 1458 and 1403 cm^{-1}, FTIR spectrum derived from a spot on the right aggregate (blue line) shows peaks at 1531, 1458, 1403 and 1368 cm^{-1}. FTIR images of peaks at 1531, 1403 and 1368 cm^{-1} are depictured in Fig. 5.9D, E and F, respectively. The outline plotted on the FTIR image indicates the position of the mineralised matter.

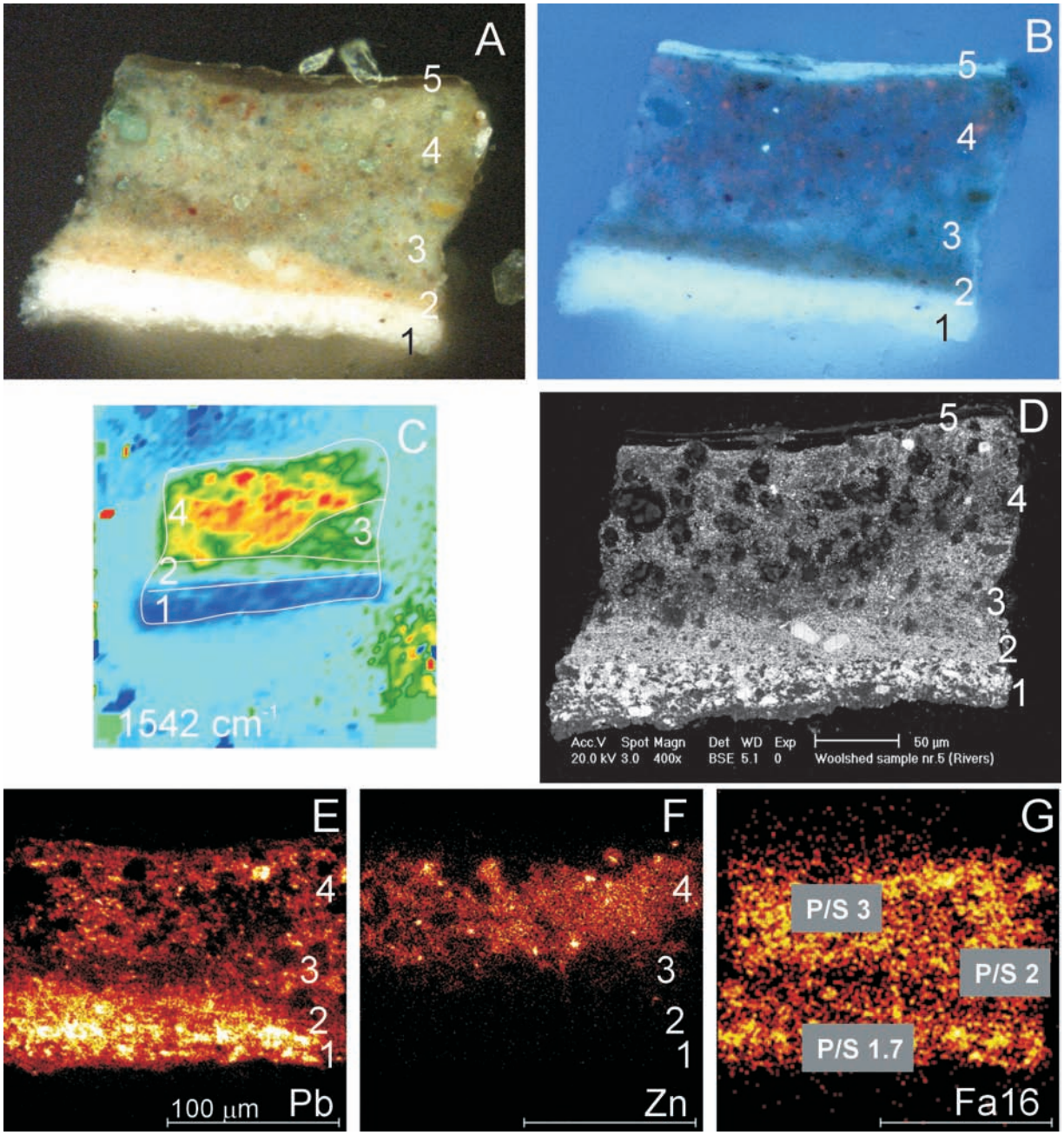

Fig. 5.10 Paint cross-section RWS5 originating from the painting 'Woolshed, New South Wales' by the Australian artist R. Godfrey Rivers (1890) is shown in the light microscopic images in white light (A) and UV (B). The FTIR image at 1542 cm^{-1} elucidates the presence of zinc carboxylates in the layers 3 and 4. BSE-image (D) visualises the aggregates that consist of a brighter centre and a dark rim. SIMS-images represent lead (+; m/z 208) (E), zinc (+; m/z 65) (F), deprotonated palmitic acid (-; m/z 255) (G). The three P /S ratios representative for layer 1 (P/S 1.7), 3 (P/S 2) and 4 (P/S 3) are shown in the ion image of deprotonated palmitic acid.

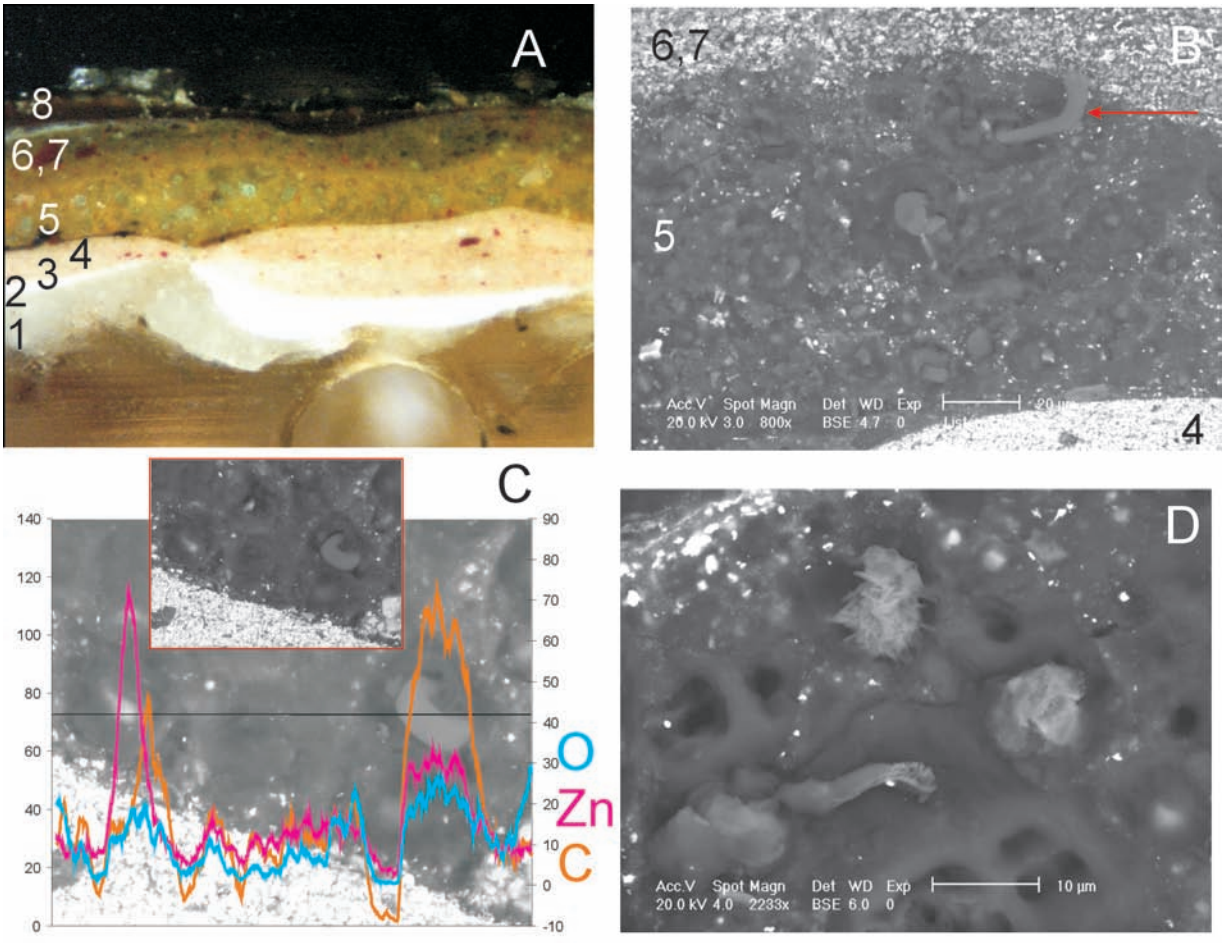

Fig. 5.11 The paint cross-section LLSH1 presented in the white light microscopic image (A) is taken from 'Sydney Harbour, overlooking Taylor's Bay' by the Australian artist W. Lister Lister (1912). BSE-image (B) visualises a detail of the zinc soap-containing layer 5; the arrow indicates a string of zinc soap emerges from the paint matrix. A line scan (C) elucidating the intensities of carbon (orange), oxygen (blue) and zinc (pink) was drawn over two aggregates, one with a bright spot in the centre (positioned left) and one where the central soap mass is emerging from of the paint matrix (positioned on the right). The BSE-image of LLSH2 in Fig. 5.11D illustrates zinc-containing nanocrystals in aggregates.